(2)

FACULTY OF TECHNOLOGY

ACOUSTIC SCATTERING BY NEAR-SURFACE INHOMOGENEITIES IN POROUS MEDIA

(2)

ACOUSTIC SCATTERING BY NEAR-SURFACE INHOMOGENEITIES IN POROUS MEDIA

Final Report on Contract DAJA 45-86-C-0012

Keith Attenborough
David L Berry
Yu Chen

Engineering Mechanics Discipline
Faculty of Technology
The Open University
Milton Keynes
MK7 6AA
England.

Unclassified
SECURITY CLASSIFICATION OF THIS PAGE

REPORT DOCUMENTATION PAGE

Form Approved
OMB No 0704-0188
Exp Date Jun 30, 1986

1a REPORT SECURITY CLASSIFICATION
Unclassified

1b. RESTRICTIVE MARKINGS

2a SECURITY CLASSIFICATION AUTHORITY

2b. DECLASSIFICATION / DOWNGRADING SCHEDULE

3. DISTRIBUTION / AVAILABILITY OF REPORT
Approved for public release; distribution unlimited.

4. PERFORMING ORGANIZATION REPORT NUMBER(S)
ACOUSTICS RESEARCH REPORT 1/90

5. MONITORING ORGANIZATION REPORT NUMBER(S)
R&D 5260-EN-01

6a. NAME OF PERFORMING ORGANIZATION
The Open University

6b. OFFICE SYMBOL (If applicable)

7a. NAME OF MONITORING ORGANIZATION
USARDSG-UK

6c. ADDRESS (City, State, and ZIP Code)
Faculty of Technology
Milton Keynes MK7 6AA, UK

7b. ADDRESS (City, State, and ZIP Code)
Box 65
FPO NY 09510-1500

8a. NAME OF FUNDING / SPONSORING ORGANIZATION
USAE Waterways Experiment Station

8b. OFFICE SYMBOL (If applicable)

9. PROCUREMENT INSTRUMENT IDENTIFICATION NUMBER
DAJA45-86-C-0012

8c. ADDRESS (City, State, and ZIP Code)
PO Box 631
Vicksburg, MS 39180-0631

10. SOURCE OF FUNDING NUMBERS

PROGRAM ELEMENT NO.	PROJECT NO.	TASK NO.	WORK UNIT ACCESSION NO
61102A	1L161102BH57	01	

11. TITLE (Include Security Classification) See Cover

(U) ~~Transmission and Scattering of Small Amplitude Mechanical Waves in Weathered Porous Soils~~

12 PERSONAL AUTHOR(S)
Attenborough, Keith and Berry, David

13a. TYPE OF REPORT	13b. TIME COVERED	14. DATE OF REPORT (Year, Month, Day)	15. PAGE COUNT
Final	FROM Mar 86 TO May 89	1990, 2, 21	

16. SUPPLEMENTARY NOTATION

17. COSATI CODES		
FIELD	GROUP	SUB-GROUP
17	04	

18. SUBJECT TERMS (Continue on reverse if necessary and identify by block number)
Acoustic scattering, boundary elements, surface waves, reflection and transmission. Add

19 ABSTRACT (Continue on reverse if necessary and identify by block number)

A theoretical and experimental investigation into the influence of near-surface buried inhomogeneities on the reflection of air-borne acoustic fields at a porous ground surface has been conducted based on the assumption that the ground supports only one wave type. Two theoretical treatments of this problem are presented, both involving reformulations of initial boundary value problems as boundary integral equations. Predictions of these formulations are compared with each other and with experimental data. The theoretical models enable constraints and possibilities to be discussed in the context of use of level difference spectra for acoustic detection of surface and sub-surface inhomogeneities. A final appendix is concerned with a theoretical study of surface waves on poroelastic surfaces.

Keywords:

20 DISTRIBUTION / AVAILABILITY OF ABSTRACT
☐ UNCLASSIFIED/UNLIMITED ☒ SAME AS RPT ☐ DTIC USERS

21 ABSTRACT SECURITY CLASSIFICATION
Unclassified

22a NAME OF RESPONSIBLE INDIVIDUAL	22b TELEPHONE (Include Area Code)	22c. OFFICE SYMBOL
Jerry C. Comati	+441-402-7331	AMXSN-UK-RE

DD FORM 1473, 84 MAR 83 APR edition may be used until exhausted
All other editions are obsolete

SECURITY CLASSIFICATION OF THIS PAGE
Unclassified

EXECUTIVE SUMMARY

1. It has been shown both theoretically and experimentally that surface and sub-surface inhomogeneities have a measurable influence the spectrum of the difference in signals received by vertically-separated microphones as a consequence of insonification by a point source positioned so that the point of specular reflection for the ground reflected path to the upper microphone is close the (horizontal plane) location of the inhomogeneity.

2. The extent of the influence has been found to depend on the shape and size of the scatterer, the depth of the upper scatterer surface below the ground surface the embedding medium and the geometry of the level difference measurements. Spheres, spheroids and discs have been considered. In particular flat-shapes produce a greater effect than spherical shapes for a given depth and cross-sectional area. The limited experimental and theoretical evidence here suggests that the minimum detectable scatterer dimension is approximately one quarter of the source-receiver separation for a surface scatterer.

3. The theoretical analysis developed is capable of extension to take account of more complicated circumstances than those so far considered including poroelasticity of the embedding medium and penetrable scatterers.

Abstract

A theoretical and experimental investigation into the influence of near-surface inhomogeneities on the reflection of air-borne acoustic fields at a porous ground surface is conducted. Two theoretical approaches to the three-dimensional physical problem are presented, both being initially formulated as boundary value problems but with subsequent reformulation as boundary integral equations via Green's Second Theorem. In the first *near-surface inhomogeneity* approach, a rigid inhomogeneity is embedded within the porous medium and the initial boundary value problem is formulated by assuming continuity of pressure and normal velocity at the ground surface, Sommerfeld's radiation conditions, and the Neumann boundary condition on the surface of the inhomogeneity. In the second *surface inhomogeneity* approach, the initial boundary value problem is formulated by assuming an impedance boundary condition on the plane boundary. Any near-surface inhomogeneities are assumed to induce a local variation of surface impedance within the boundary, and analytical expressions for such induced variations in surface impedance are presented. The resultant integral equations require knowledge of the Green's function for acoustic propagation in the presence of a plane boundary but in the absence of the inhomogeneity, and methods for calculating these Green's function are discussed.

The numerical solution of the boundary integral equations by a simple boundary element method is described. The solution, which reduces to a system of linear equations with a *block circulant* coefficient matrix, is applicable to any inhomogeneity which is axisymmetric about a vertical axis; and for the near-surface inhomogeneity approach, the inhomogeneity must also be smooth. The numerical solutions have shown good agreement with classical results. The experimental measurements, presented in the form of spectra of the difference in sound pressure levels received at vertically separated points above surfaces of different media containing various scatterers, are in good agreement with the theoretical predictions.

Contents

List of Figures

List of Tables

Chapter 1

Introduction

1.1 Background

When a porous ground surface is insonified by an air-borne acoustic field, the air in the pores near the surface, and consequently, through viscous drag, the porous skeletal frame, are excited. Three different wave types then propagate in the medium, two dilatational and one shear [1,2]. It has been shown, for air-filled porous soils, that one of the dilatational wave types is associated with a propagation mode in which the air and the porous skeletal frame are in phase and is called the *fast* wave [3]; it corresponds to the P-wave of seismology. In the second type of dilatational wave motion, the air and porous skeletal frame are out of phase. This propagates primarily through the air-filled connected pores and is called the *slow* or *acoustic* wave. These wave types have interested geophysicists since the 1950's. The recent work concerned with this acoustic-to-seismic and acoustic-to-acoustic coupling has involved the analysis of air-borne signals detected by microphones and geophones buried close to a porous ground surface. These results show that the fast wave, to which a sub-surface geophone responds, suffers relatively little attenuation with depth, and is non-dispersive [4]. Furthermore, the structure of the coupled spectrum is dependent upon the seismic structure of the ground [4], for example, any surficial layering. The spectrum contains peaks, the magnitude and frequency location of which depend upon the seismic characteristics of the surficial layer. In contrast to the fast wave,

the slow wave, to which a sub-surface microphone responds, is highly attenuating both with increasing frequency and depth [5].

For many purposes, most porous ground surfaces (grassland, forest floor, bare soil, snow, etc.) can be modelled as modified fluids consistent with the characteristics of rigid porous media, *i.e.* where the medium consists of a rigid porous skeletal frame containing air in the pores. For example, Attenborough [6], has shown that, for frequencies above 200Hz, the only wave possible in a rigid porous material is nearly identical to the slow wave predicted in a poro-elastic medium with the same pore characteristics. Various theories are available which predict the acoustical characteristics of rigid porous media. Delany and Bazley [7] deduced empirical relationships for the acoustical properties of fibrous absorbent materials and these have been used successfully in predicting the characteristics of outdoor ground surfaces [8]. Recently, this *empirical* model has been replaced by a more rigorous *microstructural* model [9]. Here, the acoustical characteristics of rigid porous media are predicted from four parameters: *porosity*, *flow resistivity*, *grain shape factor* and *pore shape factor ratio*. The use of these four parameters for the prediction of the medium characteristics is rather impractical. However, various approximations to this rigorous theory are available, including, one, two and three parameter approximations [9]. The justification for the extensive modelling of a porous ground as a rigid porous medium has been verified experimentally by measuring the acoustic field within a porous ground using a purpose built probe microphone, [10,11,12,13]. The existence of the seismic wave types has been verified experimentally by measuring time of flight data from above-ground impulsive acoustic sources to sub-surface geophones, [4,10,14].

The wave type that has the most influence on the reflection of air-borne acoustic fields at a porous ground surface is the slow wave. The high attenuation associated with this wave type within the porous ground means that only *near-surface* layering has an influence on the surface-reflected fields, and that there is a critical depth from the surface, below which such layering has little effect on the sound field. Consequently, a ground that has near-surface

layering at a depth greater than this critical depth appears acoustically to be homogeneous. Seismically, as a consequence of the relatively small attenuation of the fast wave, any near-surface layering has an influence on the surface reflected fields. These effects are seen in natural soils typically at low frequencies [15], less than 200Hz.

It has been stated above that the reflection of air-borne acoustic fields at the porous ground surface is influenced by the slow wave type and, to a limited extent, by the fast wave type, and hence by the variation of the porous ground structure with depth. Consequently, it is possible that any *inhomogeneities* on or beneath the porous surface, may also have an influence on the surface reflected acoustic fields. If such an influence exists, how can it be studied and, to what extent is this influence dependent upon the nature of the inhomogeneity? Such a problem is considered in this study both theoretically and experimentally. Similar problems have been considered before in the literature, and are summarised in the following sections.

1.2 Previous theoretical work

There is considerable literature that considers similar theoretical *scattering* problems, using a variety of techniques for solution. Most of this work, however, has been concerned with the scattering problem from bodies in a homogeneous fluid medium. This work includes the early work of Faran [16], Junger [17], Hickling [18], and others [19,20,21,22] and more recent studies using the T-matrix method [23,24,25,26,27,28], and resonance scattering theory [29,30,31,32,33,34]. This work involves scatterers that are spherical or spheroidal in shape. When the obstacle has an arbitrary shape, numerical methods have been used as opposed to approximate analytical methods. Such work has involved the use of the T-matrix method, boundary element methods, and hybrid methods such as the finite element/boundary element method.

The T-matrix method has been used only to obtain farfield data if the shape of the obstacle does not deviate substantially from the basic geomet-

rical shape (*e.g.* a sphere) used and cannot be used to obtain data near the surface of the scatterer. This situation may be contrasted with integral equation methods, where there has been a greater degree of flexibility in its use both in the near- and far-field and in the shape of the scatterers. Previous work has involved solving problems of scattering from rigid bodies [35,36,37,38,39,40,41,42] and elastic bodies [43]. Indeed, most of the applications of integral equation methods to acoustic scattering has been concerned with such scattering problems by finite objects in free space. Survey monographs and articles include Colton and Kress [44], Filippi [45], and Shaw [46]. Recently, these methods have been extended to consider acoustic scattering by a half space containing some form of local disturbance, for example, a noise barrier [47,48,49]. Others [50,51,52] have considered the application of integral equation methods to the case of a *surface impedance* variation on a flat boundary.

There are few references that consider the solution of the scattering of sound waves due to a source in one medium (air) by an inhomogeneity in another medium. Kristensson and Ström [53] consider this problem using the T-matrix method. However, their method still requires further development, in particular, with respect to the numerical integration problems. The method requires the numerical calculation of $O(n^2)$ integrals (see [53], equations (60) and (65)), where n is the degree of the expansion in spherical harmonics used to approximate the anomalous scattered field, and the rapid oscillations of the integrands of these integrals cause difficulties in numerical evaluation. These problems have only been partly solved by Kristensson and Ström, for the special case when source and receiver lie on the plane boundary between the two media.

1.3 Previous experimental work

Essentially, there are two techniques for analysing the influence of near-surface inhomogeneities on the reflection of air-borne acoustic fields at the porous ground surface. The first method involves analysing the acoustic

field reflected from the ground surface and the surface of the inhomogeneity separately. This has been considered before by Bass, Bolen *et al* [54], and involve the use of a pulsed acoustic source to enable the separation of the two reflected signals. The method, although satisfactory under certain conditions, did not overcome adequately the major problem of separating the pulses reflected from the ground surface and the surface of the inhomogeneity.

The second method considers the analysis of the acoustic fields associated with the *layer* between the surface of the inhomogeneity and the ground surface (*i.e.* the acoustic fields reflected from the ground surface and the surface of the inhomogeneity are considered together). This method has only been considered previously in the context of determining sub-surface ground layering for agricultural purposes [11]. It involves measuring directly the acoustic field due to a source obliquely incident on the ground surface by a microphone placed at a horizontal distance from the source. The direct and ground surface reflected contributions to the received signal will interfere [8]. The resulting spectrum, of the attenuation in excess of that due to spherical spreading, (*i.e.* the *excess attenuation spectra*), after taking account of the free-field spectrum and directivity of the source, shows one or more minima depending upon the source and microphone configuration above the ground surface, the frequency range, and the acoustic characteristics of the ground considered. Over acoustically hard ground with zero phase change on reflection, the frequency locations of the minima are determined entirely by the source-microphone configuration. Over finite impedance ground, the location and shape of the first minimum is determined both by the configuration and the acoustical nature of the ground including its sub-surface structure. The free-field spectrum and directivity of the source can be either measured in an anechoic chamber [55] or over a perfectly reflecting plane [56,57].

A refinement of this method is that proposed by Glaretas [58]. Instead of using one microphone, two vertically separated microphones are used to receive the acoustic field and the difference in the sound pressure levels (*i.e.* the *Level Difference* between the two microphones is calculated. The re-

sulting spectra produce maxima and minima similar to those of the excess attenuation spectra. However, if the vertical separation of the two microphones is sufficiently small such that the directivity of the source can be neglected, then the free-field spectrum of the source is directly cancelled in the calculation of the level difference. The main advantage of measuring excess attenuation and level difference is that spectra for a broad-band of frequencies are obtained simultaneously. Further, except for the requirement on the bandwidth of the measurement to include at least the first minimum, there is no restriction on the source-microphone(s) configuration. For small source-microphone(s) configurations, meteorological effects are unimportant, but for large geometries, measurements can be taken only under calm conditions (a wind speed of less than $2m.s^{-1}$) and with a frequency range of up to 5kHz [59]. For all geometries, the received signals must be at least 10dB above background noise [60].

1.4 The present work

The purpose of this study is to develop a theoretical description of the influence of near-surface inhomogeneities on the reflection of air-borne acoustic fields at a porous ground surface. The frequency range to be considered is 200Hz to 5kHz, for which seismic effects may safely be ignored and the porous ground is modelled as rigid porous with only the slow wave considered within the porous medium. The inhomogeneities that will be investigated will have a smooth, rigid surface and will be typically $\sim$ 0.25m in dimension. This theoretical description is then compared with experimental results.

Two mathematical approaches to this scattering problem are considered and chapter 2 deals with their mathematical formulation as *Boundary Value Problems* and subsequent reformulation as *Boundary Integral Equations*. The first approach considers the scattering by a near-surface inhomogeneity embedded within a rigid porous medium directly, the second approach assumes the *surface impedance* of the porous ground surface is modified locally in a region directly above the inhomogeneity.

The boundary integral equations formulated in chapter 2 require expressions for the Green's function which is the solution to the simple problem of acoustic propagation in the presence of a plane boundary separating two semi-infinite media of different properties with various configurations of source and receiver. There have been many papers concerned with this problem, an exact solution of which, for wave propagation between source and receiver, above a plane boundary was first given by Sommerfeld [61,62]. Later, further advances were made by Van der Pol [63], Norton [64,65], Rudnick [66], and others [67,68,69,70,71]. The exact solution for the corresponding problem with a locally reacting boundary has been given by Ingard [72], Thomasson [73], and Wenzel [74]. Ingard [72] and Lawhead and Rudnick [75] have given approximate solutions, whereas Thomasson [76], Chien and Soroka [77,78] and others [79,80,81,82] have given asymptotic solutions. An exact solution for the transmission of sound across a plane boundary with extended reaction has been given by Richards *et al* [5]. The theory is based on the earlier work of Paul [69] and Brekhovskikh [83]. These various solutions are discussed in chapter 3. Finally, modelling the effect of the rigid porous ground is discussed and reviewed.

The expressions for the induced surface impedance required for the second approach are derived in chapter 4. It will be seen that this second approach gives more flexibility to the shapes of the scattering surfaces; indeed scattering by local surface impedance discontinuities caused by circumstances other than the presence of an embedded inhomogeneity, may be considered.

Chapter 5 considers the numerical solution of the boundary integral equations developed in chapter 2, and presents numerical tests and comparisons of the solutions with standard results.

The experimental investigation of this study is introduced in chapter 6, which details the experimental procedure, apparatus, test scatterers and media. The experimental results are then presented in chapter 7. The object of these experiments was to confirm the main qualitative features of the models developed. The chapter also details a series of theoretical results.

In the concluding chapter, chapter 8, a review of the study is presented, together with limitations and recommendations for future work, and finally, some concluding remarks.

Chapter 2

Mathematical formulation

The theoretical problem of determining the influence of near-surface inhomogeneities on the reflection of air-borne acoustic fields at the porous ground surface is described in this chapter. Section 2.1 briefly summarises some basic acoustic theory relevant to the theoretical problem. The basic theoretical problem to be considered is then described in section 2.2, where two treatments are formulated mathematically as boundary value problems and subsequently reformulated as boundary integral equations by standard arguments using Green's second theorem. The final section then briefly summarises these treatments.

2.1 Basic theory of sound propagation

This study is basically concerned with sound propagation in a fluid medium above an absorbing boundary. It is assumed that the fluid medium is homogeneous and, in the absence of the sound field, is at rest; this means that the prediction of outdoor sound propagation, in situations where wind and temperature gradients have a significant effect, cannot be considered. Further, the flow induced by the sound wave in the fluid medium is assumed to be inviscid and isentropic, which means that internal energy loss and slight energy losses due to viscosity and heat conduction associated with boundary layer effects can be neglected [84]. If the above conditions are satisfied and the perturbations due to the sound field are small, then the theory of

linear sound propagation applies [45], and the perturbation in the pressure P, satisfies the homogeneous wave equation,

$$\nabla^2 P = \frac{1}{c^2}\frac{\partial^2 P}{\partial t^2}, \tag{2.1}$$

where c is the wave propagation velocity. The sound pressure, in a fluid of unperturbed density ρ, is related to the velocity potential Φ by

$$P = -\rho\frac{\partial \Phi}{\partial t}, \tag{2.2}$$

and the particle velocity is related to velocity potential by,

$$\mathbf{V} = \nabla\Phi. \tag{2.3}$$

The assumption is made throughout this thesis that the sources of sound are single frequency (though, of course, by Fourier analysis an arbitrary transient wave can be built up by superposing monofrequency waves) with wavelength λ, corresponding to a frequency $f = c/\lambda$. With this assumption, P can be written as

$$P = Re(pe^{-i\omega t}), \tag{2.4}$$

where $\omega = 2\pi f/c$, $i = \sqrt{-1}$ and the complex acoustic pressure p, which is independent of t, satisfies the Helmholtz equation

$$(\nabla^2 + k^2)p = 0, \tag{2.5}$$

where $k = 2\pi/\lambda$ is the wave number. Similarly to equation (2.4), it is possible to write

$$\Phi = Re(\phi e^{-i\omega t}), \tag{2.6}$$

and

$$\mathbf{V} = Re(\mathbf{v}e^{-i\omega t}) \tag{2.7}$$

and equations (2.2) and (2.3) are satisfied provided the complex-valued functions ϕ and $\mathbf{v}$ satisfy

$$p = i\omega\rho\phi, \tag{2.8}$$

and,

$$\mathbf{v} = \nabla\phi. \tag{2.9}$$

The theoretical content of this study is concerned with the solution of equation (2.5), subject to just sufficient boundary conditions so as to permit equation (2.5) to have exactly one solution. The appropriate boundary condition at a rigid surface, for example, is that

$$\mathbf{v}.\mathbf{n} = \frac{\partial \phi}{\partial n} = 0, \tag{2.10}$$

where $\mathbf{n}$, the unit normal to the boundary directed out of the fluid medium. On boundaries between two different fluid media, two conditions must be satisfied: the acoustic pressures on both sides of the boundary *and* the normal component of particle velocity, must be equal. The first *continuity of pressure* condition, is required so that there can be no *net* force on the boundary separating the fluids. The second *continuity of normal velocity* condition is required so that the fluids remain in contact. In certain circumstances, these two conditions combined imply that the fluid satisfies approximately the *locally reacting* boundary condition, *i.e.* the pressure in the boundary is proportional to the normal velocity,

$$p = \frac{\partial \phi}{\partial n} Z_s, \tag{2.11}$$

where the value of the constant Z_s, the *surface impedance* is dependent only on local surface properties. Z_s may vary from point to point on the boundary, but at each point, Z_s is independent of the acoustic field above the boundary. Any boundary to which the boundary condition (2.11) does not apply (*i.e.* the surface is not locally reacting) is said to be *externally reacting*. Equation (2.11) can be written as the Robin or impedance boundary condition

$$\frac{\partial \phi}{\partial n} = ik\beta\phi, \tag{2.12}$$

or,

$$\frac{\partial p}{\partial n} = ik\beta p, \tag{2.13}$$

where, $\beta = 1/\zeta_s$, is the normalised surface admittance and ζ_s is the relative surface impedance, defined by $\zeta_s = Z_s/\rho c$.

In addition to boundary conditions on physical boundaries, a boundary condition in the far-field must be specified, and this *Sommerfeld radiation*

condition is

$$\left.\begin{array}{rcl} \frac{\partial p}{\partial r} - ikp & = & o(r^{-1}) \\ p & = & O(r^{-1}) \end{array}\right\} \tag{2.14}$$

where r is the distance from a fixed origin.

Sound propagation in a homogeneous porous medium has been reviewed by Attenborough [85], who considers the case of a rigid matrix and that of an elastic matrix. For the case of the rigid matrix, the acoustic pressure within the porous medium is shown to satisfy the Helmholtz equation,

$$(\nabla^2 + k_p^2)p = 0, \tag{2.15}$$

where k_p is a complex function of ω, with $Re(k_p)$, $Im(k_p) > 0$ and $k_p = \omega/c_p$, c_p being a complex wave propagation velocity. Also,

$$p = i\omega\rho_p\phi, \tag{2.16}$$

ρ_p being an effective fluid density, also a complex function of ω.

Consider now a plane wave travelling within a fluid medium, incident upon a plane boundary between the fluid and a porous medium. Let the boundary have the equation $z = 0$ (Cartesian coordinates), and assume that the plane incident wave makes the angle θ with the z-axis and that the upper fluid half-space ($z > 0$) be characterised by characteristic impedance Z_1 and wavenumber k_1 and the lower porous medium half-space ($z < 0$) be characterised by characteristic impedance Z_2 and wavenumber k_2. For oblique incidence, the incident acoustic field at $\mathbf{r} = (x, y, z)$ is given by

$$p_i(\mathbf{r}) = e^{i(k_{1,x}x - k_{1,z}z)}, \tag{2.17}$$

for $z \geq 0$, where $k_{1,x} = k_1 sin\theta$, $k_{1,z} = k_1 cos\theta$, so that p_i satisfies

$$(\nabla^2 + k_1^2)p_i(\mathbf{r}) = 0. \tag{2.18}$$

The reflected wave is given by

$$p_r(\mathbf{r}) = R_p e^{i(k_{1,x}x + k_{1,z}z)}, \tag{2.19}$$

for $z \geq 0$, where R_p is a plane wave reflection coefficient, and where p_r satisfies

$$(\nabla^2 + k_1^2)p_r = 0. \tag{2.20}$$

The transmitted wave is given by

$$p_t(\mathbf{r}) = T_p e^{i(k_{2,x}x - k_{2,z}z)}, \tag{2.21}$$

for $z \leq 0$, where T_p is the plane wave transmission coefficient, and,

$$k_2 = (k_{2,x}^2 + k_{2,z}^2)^{\frac{1}{2}}, \tag{2.22}$$

so that p_t satisfies

$$(\nabla^2 + k_2^2)p_t = 0. \tag{2.23}$$

Continuity of pressure at the plane boundary requires,

$$(1 + R_p)e^{ik_{1,x}x} = T_p e^{ik_{2,x}x}, \tag{2.24}$$

which implies that,

$$k_{2,x} = k_{1,x} \tag{2.25}$$

and,

$$1 + R_p = T_p. \tag{2.26}$$

Continuity of normal velocity requires,

$$\frac{1}{i\omega\rho_1} \lim_{z\to 0+} \left(\frac{\partial p}{\partial z}\right) = \frac{1}{i\omega\rho_2} \lim_{z\to 0-} \left(\frac{\partial p}{\partial z}\right) \tag{2.27}$$

using equations (2.3) and (2.8) and where ρ_1 and ρ_2 are the unperturbed densities, in $z > 0$ and $z < 0$, respectively. This gives expressions for T_p and R_p as,

$$T_p = (1 - R_p)\frac{k_{1,z}\rho_2}{k_{2,z}\rho_1} \tag{2.28}$$

and

$$R_p = \frac{k_{1,z}\rho_2 - k_{2,z}\rho_1}{k_{1,z}\rho_2 + k_{2,z}\rho_1}. \tag{2.29}$$

Equation (2.29) can be written as,

$$R_p = \frac{cos\theta - \beta(\theta)}{cos\theta + \beta(\theta)}, \tag{2.30}$$

where,

$$\beta(\theta) = \frac{1}{\zeta}(1 - sin^2\theta/n^2)^{\frac{1}{2}}, \tag{2.31}$$

$\zeta = \rho_1 c_1/\rho_2 c_2$ and $n = k_2/k_1$. If $|n^2| \gg 1$, then $\beta(\theta)$ is approximately independent of θ and

$$\beta(\theta) \approx \beta(0). \tag{2.32}$$

In this case, the boundary is approximately *locally* reacting with surface admittance

$$\beta = \beta(0). \tag{2.33}$$

2.2 The theoretical approaches

The previous section has summarised the basic mathematical concepts behind the theoretical study to be discussed in this section, and it is the purpose of this section to define the mathematical problem of determining the influence of near-surface inhomogeneities on the reflection of acoustic fields at the surface of a porous medium. Two approaches to this problem will be considered. In the first approach, the acoustic fields transmitted through the plane boundary are incident on the inhomogeneity and scattered, and through the various boundary conditions, the acoustic field at a receiver in the upper medium will be calculated. In the second approach, any near-surface inhomogeneity is assumed to induce a local surface impedance variation at the boundary above the inhomogeneity. In both approaches, the complex acoustic pressure at a point in the upper half-space is to be determined when the plane boundary is insonified by a monofrequency point source at a point also in the upper half-space. It will be seen that the first approach is sufficiently general that the acoustic pressure in the lower half-space may be calculated also. These approaches are first stated as boundary value problems with subsequent reformulation as boundary integral equations by a standard procedure via Green's second theorem.

To formulate the boundary integral equations, the solution to much simpler but related problems are required. These are the determination of

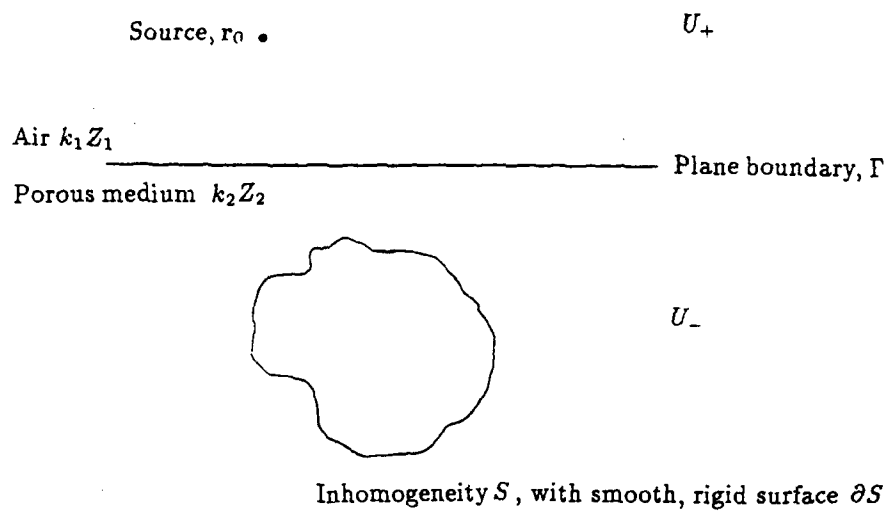

Figure 2.1 Geometry for scattering by a near-surface rigid inhomogeneity

Green's functions for sound propagation in two half-spaces, separated by the plane boundary, and these are discussed in the next chapter.

2.2.1 The first approach

The geometry for this first approach is shown in figure 2.1. An inhomogeneity, labelled S, with a smooth (Lyapunov), rigid surface ∂S, is embedded in a porous half-space, characterised by a complex characteristic impedance Z_2, and a complex wavenumber, k_2. The upper half-space, denoted U_+, contains air, and is assumed to be characterised by real characteristic impedance and wavenumber, Z_1 and k_1, respectively. To define the other notation in figure 2.1, $U_- := \mathbf{R}^3 \backslash (\overline{S \bigcup U_+})$ denotes the porous medium, and $\Gamma = \{(x, y, z) \in \mathbf{R}^3 | z = 0\}$, the boundary between the two half spaces. The complex acoustic pressure is assumed to satisfy the following boundary value problem:
an inhomogeneous Helmholtz equation for $\mathbf{r} \in U_+$,

$$(\nabla^2 + k_1^2) p(\mathbf{r}, \mathbf{r}_0) = \delta(\mathbf{r} - \mathbf{r}_0); \tag{2.34}$$

the Helmholtz equation for $\mathbf{r} \in U_-$,

$$(\nabla^2 + k_2^2)p(\mathbf{r}, \mathbf{r}_0) = 0; \tag{2.35}$$

the Neumann boundary condition for $\mathbf{r} \in \partial S$, for a rigid surface on the inhomogeneity,

$$\frac{\partial p(\mathbf{r}, \mathbf{r}_0)}{\partial n(\mathbf{r})} = 0; \tag{2.36}$$

continuity of complex acoustic pressure, for $\mathbf{r} \in \Gamma$,

$$p_+(\mathbf{r}, \mathbf{r}_0) = p_-(\mathbf{r}, \mathbf{r}_0); \tag{2.37}$$

continuity of normal velocity, for $\mathbf{r} \in \Gamma$,

$$\alpha \frac{\partial p_+(\mathbf{r}, \mathbf{r}_0)}{\partial z} = \frac{\partial p_-(\mathbf{r}, \mathbf{r}_0)}{\partial z}; \tag{2.38}$$

where $\alpha = k_2 Z_2 / k_1 Z_1$, and Sommerfeld's radiation conditions for $\mathbf{r} \in U_+$ uniformly in $\mathbf{r}$ as $r := |\mathbf{r}| \to \infty$,

$$\left.\begin{aligned} \tfrac{\partial p(\mathbf{r}, \mathbf{r}_0)}{\partial r} - ik_1 p(\mathbf{r}, \mathbf{r}_0) &= o(r^{-1}), \\ p(\mathbf{r}, \mathbf{r}_0) &= O(r^{-1}), \end{aligned}\right\} \tag{2.39}$$

and for $\mathbf{r} \in U_-$ uniformly in $\mathbf{r}$ as $r := |\mathbf{r}| \to \infty$,

$$\left.\begin{aligned} \tfrac{\partial p(\mathbf{r}, \mathbf{r}_0)}{\partial r} - ik_2 p(\mathbf{r}, \mathbf{r}_0) &= o(r^{-1}), \\ p(\mathbf{r}, \mathbf{r}_0) &= O(r^{-1}). \end{aligned}\right\} \tag{2.40}$$

In the above, the subscripts $+/-$ denote the limiting values of a function as Γ is approached from the U_+/U_- side and $n(\mathbf{r})$ denotes the normal to the surface ∂S at point $\mathbf{r}$.

Two integral equation formulations of the above boundary value problem shall now be considered. It will be seen that the first reformulation requires Green's functions in the presence of plane boundaries, and this reformulation is quite general. The second reformulation, involving *Free-Field* Green's functions, uses some of the results of the first approach and thus, is less exhaustive.

First integral equation formulation

The first integral equation reformulation of the boundary value problem, involves letting the Green's function $G(\mathbf{r}, \mathbf{r}_0)$, satisfy the following boundary value problem, for each $\mathbf{r}_0 \in \mathbf{R}^3 \backslash \Gamma$:
an inhomogeneous Helmholtz equation for $\mathbf{r} \in U_+$,

$$(\nabla^2 + k_1^2) G(\mathbf{r}, \mathbf{r}_0) = \delta(\mathbf{r} - \mathbf{r}_0); \tag{2.41}$$

the Helmholtz equation for $\mathbf{r} \in U_-$,

$$(\nabla^2 + k_2^2) G(\mathbf{r}, \mathbf{r}_0) = \alpha \delta(\mathbf{r} - \mathbf{r}_0); \tag{2.42}$$

the following jump conditions for $\mathbf{r} \in \Gamma$, the boundary between the two half-spaces,

$$G_+(\mathbf{r}, \mathbf{r}_0) = G_-(\mathbf{r}, \mathbf{r}_0); \tag{2.43}$$

and

$$\alpha \frac{\partial G_+(\mathbf{r}, \mathbf{r}_0)}{\partial z} = \frac{\partial G_-(\mathbf{r}, \mathbf{r}_0)}{\partial z}; \tag{2.44}$$

and Sommerfeld's radiation conditions for $\mathbf{r} \in U_+$, uniformly in $\mathbf{r}$ as $r := |\mathbf{r}| \to \infty$,

$$\left.\begin{array}{rcl} \frac{\partial G(\mathbf{r}, \mathbf{r}_0)}{\partial r} - ik_1 G(\mathbf{r}, \mathbf{r}_0) & = & o(r^{-1}), \\ G(\mathbf{r}, \mathbf{r}_0) & = & O(r^{-1}), \end{array}\right\} \tag{2.45}$$

and for $\mathbf{r} \in U_-$, uniformly in $\mathbf{r}$ as $r := |\mathbf{r}| \to \infty$,

$$\left.\begin{array}{rcl} \frac{\partial G(\mathbf{r}, \mathbf{r}_0)}{\partial r} - ik_2 G(\mathbf{r}, \mathbf{r}_0) & = & o(r^{-1}), \\ G(\mathbf{r}, \mathbf{r}_0) & = & O(r^{-1}). \end{array}\right\} \tag{2.46}$$

Note that in the case when no inhomogeneity is present

$$p(\mathbf{r}, \mathbf{r}_0) = G(\mathbf{r}, \mathbf{r}_0) \tag{2.47}$$

for $\mathbf{r} \in \mathbf{R}^3$ and $\mathbf{r}_0 \in U_+$; but $G(\mathbf{r}, \mathbf{r}_0)$ is defined also when $\mathbf{r}_0 \in U_-$. In physical terms, and for this integral equation reformulation, $G(\mathbf{r}, \mathbf{r}_0)$ is the complex acoustic pressure at point $\mathbf{r}$ in a medium consisting of two half spaces of different characteristic impedances and/or propagation constants

due to a simple point source at point $\mathbf{r}_0$ of unit volume flux strength; the point $\mathbf{r}_0$ may lie in either half space.

The integral equation for this first reformulation may be obtained by considering regions V_1 and V_2, V_1/V_2 consisting of that part of U_+/U_- contained within a large hemisphere of surface, Σ and radius R, centred on the origin, and the boundary, Γ, but excluding small spheres, σ_r and σ_{r_0} of radii ε, centred on $\mathbf{r}$ and $\mathbf{r}_0$. The interiors of the spheres σ_r and σ_{r_0} are excluded so that the conditions of Green's second theorem are satisfied by p and G in regions V_1 and V_2. Applying Green's second theorem to regions V_1 and V_2, the following two equations are obtained:

$$\int_{\partial V_1}(p(\mathbf{r}_s,\mathbf{r}_0)\frac{\partial G(\mathbf{r}_s,\mathbf{r})}{\partial n(\mathbf{r}_s)} - G(\mathbf{r}_s,\mathbf{r})\frac{\partial p(\mathbf{r}_s,\mathbf{r}_0)}{\partial n(\mathbf{r}_s)})ds(\mathbf{r}_s) = \int_{V_1}(p(\mathbf{r}_s,\mathbf{r}_0)\nabla^2_{\mathbf{r}_s}G(\mathbf{r}_s,\mathbf{r}) - G(\mathbf{r}_s,\mathbf{r})\nabla^2_{\mathbf{r}_s}p(\mathbf{r}_s,\mathbf{r}_0))dV(\mathbf{r}_s) \quad (2.48)$$

and

$$\int_{\partial V_2}(p(\mathbf{r}_s,\mathbf{r}_0)\frac{\partial G(\mathbf{r}_s,\mathbf{r})}{\partial n(\mathbf{r}_s)} - G(\mathbf{r}_s,\mathbf{r})\frac{\partial p(\mathbf{r}_s,\mathbf{r}_0)}{\partial n(\mathbf{r}_s)})ds(\mathbf{r}_s) = \int_{V_2}(p(\mathbf{r}_s,\mathbf{r}_0)\nabla^2_{\mathbf{r}_s}G(\mathbf{r}_s,\mathbf{r}) - G(\mathbf{r}_s,\mathbf{r})\nabla^2_{\mathbf{r}_s}p(\mathbf{r}_s,\mathbf{r}_0))dV(\mathbf{r}_s), \quad (2.49)$$

for $\mathbf{r}_0 \in U_+$ and $\mathbf{r} \in \mathbf{R}^3$ and where $\nabla^2_{\mathbf{r}_s} = \partial^2/\partial x_s^2 + \partial^2/\partial y_s^2 + \partial^2/\partial z_s^2$, $ds(\mathbf{r}_s)$ denotes an element of surface area at the point $\mathbf{r}_s$ on ∂V_1 and ∂V_2, and $dV(\mathbf{r}_s)$ denotes an element of volume at the point $\mathbf{r}_s$. (In each equation, the normal n is directed out of V_1/V_2).

Since $p(\mathbf{r}_s,\mathbf{r}_0)$ and $G(\mathbf{r}_s,\mathbf{r})$, both considered as functions of $\mathbf{r}_s$, satisfy Helmholtz's equation in V_1 and V_2, the integrals over volumes V_1 and V_2 in equations (2.48) and (2.49) are equal to zero. Thus, equations (2.48) and (2.49) reduce to

$$\int_{\partial V_1}(p(\mathbf{r}_s,\mathbf{r}_0)\frac{\partial G(\mathbf{r}_s,\mathbf{r})}{\partial n(\mathbf{r}_s)} - G(\mathbf{r}_s,\mathbf{r})\frac{\partial p(\mathbf{r}_s,\mathbf{r}_0)}{\partial n(\mathbf{r}_s)})ds(\mathbf{r}_s) = 0 \quad (2.50)$$

and

$$\int_{\partial V_2}(p(\mathbf{r}_s,\mathbf{r}_0)\frac{\partial G(\mathbf{r}_s,\mathbf{r})}{\partial n(\mathbf{r}_s)} - G(\mathbf{r}_s,\mathbf{r})\frac{\partial p(\mathbf{r}_s,\mathbf{r}_0)}{\partial n(\mathbf{r}_s)})ds(\mathbf{r}_s) = 0, \quad (2.51)$$

for $\mathbf{r}_0 \in U_+$ and $\mathbf{r} \in \mathbf{R}^3$. These two integrals are now considered in turn.

Integral over ∂V_1 Equation (2.50) is considered for three different cases: $\mathbf{r} \in U_+$, $\mathbf{r} \in \Gamma$, and $\mathbf{r} \in U_-$.

For $\mathbf{r} \in U_+$ the region V_1 is bounded by the hemispherical surface Σ, of radius R, the plane boundary Γ, and the surfaces of the spheres $\sigma_{\mathbf{r}}$ and $\sigma_{\mathbf{r}_0}$ of radii ϵ. The integral (2.50) is now evaluated with the radius of the surface Σ taken to the limit $R \to \infty$, and the radii of the surfaces $\sigma_{\mathbf{r}}$ and $\sigma_{\mathbf{r}_0}$ taken to the limit $\epsilon \to 0$. The integral (2.50) can now be written as

$$I^{1U_+} + I_{\Sigma}^{1U_+} + I_{\sigma_{\mathbf{r}_0}}^{1U_+} + I_{\sigma_{\mathbf{r}}}^{1U_+} = 0, \tag{2.52}$$

where I represents the limiting values of the integral (2.50) over the surfaces Γ, Σ, $\sigma_{\mathbf{r}_0}$, and $\sigma_{\mathbf{r}}$ respectively. The superscripts denote the integrating volume and the position of $\mathbf{r}$. It is assumed that these limits exist, which will be shown to be the case. The contributions $I_{\Sigma}^{1U_+}$, $I_{\sigma_{\mathbf{r}_0}}^{1U_+}$, and $I_{\sigma_{\mathbf{r}}}^{1U_+}$ to equation (2.52) will now be evaluated.

The limit $I_{\Sigma}^{1U_+}$ is given by

$$I_{\Sigma}^{1U_+} = \lim_{R\to\infty} \int_{\Sigma} (p(\mathbf{r}_s, \mathbf{r}_0) \frac{\partial G(\mathbf{r}_s, \mathbf{r})}{\partial n(\mathbf{r}_s)} - G(\mathbf{r}_s, \mathbf{r}) \frac{\partial p(\mathbf{r}_s, \mathbf{r}_0)}{\partial n(\mathbf{r}_s)}) ds(\mathbf{r}_s). \tag{2.53}$$

and may be written as

$$\begin{aligned} I_{\Sigma}^{1U_+} &= \lim_{R\to\infty} \int_{\Sigma} p(\mathbf{r}_s, \mathbf{r}_0) \left(\frac{\partial G(\mathbf{r}_s, \mathbf{r})}{\partial r_s} - ik_1 G(\mathbf{r}_s, \mathbf{r}) \right) \\ &\quad - G(\mathbf{r}_s, \mathbf{r}) \left(\frac{\partial p(\mathbf{r}_s, \mathbf{r}_0)}{\partial r_s} - ik_1 p(\mathbf{r}_s, \mathbf{r}_0) \right) ds(\mathbf{r}_s), \end{aligned} \tag{2.54}$$

since $\partial G(\mathbf{r}_s, \mathbf{r})/\partial n(\mathbf{r}_s) = \partial G(\mathbf{r}_s, \mathbf{r})/\partial r_s$ on Σ. This may now be evaluated by utilising the Sommerfeld radiation conditions for G with $\mathbf{r}_s \in U_+$ uniformly in $\mathbf{r}_s$ as $r_s := |\mathbf{r}_s| \to \infty$

$$\left.\begin{aligned} \tfrac{\partial G(\mathbf{r}_s, \mathbf{r})}{\partial r_s} - ik_1 G(\mathbf{r}_s, \mathbf{r}) &= o(r_s^{-1}), \\ G(\mathbf{r}_s, \mathbf{r}) &= O(r_s^{-1}), \end{aligned}\right\} \tag{2.55}$$

and p with $\mathbf{r}_s \in U_+$, uniformly in $\mathbf{r}_s$ as $r_s := |\mathbf{r}_s| \to \infty$

$$\left.\begin{aligned} \tfrac{\partial p(\mathbf{r}_s, \mathbf{r}_0)}{\partial r_s} - ik_1 p(\mathbf{r}_s, \mathbf{r}_0) &= o(r_s^{-1}), \\ p(\mathbf{r}_s, \mathbf{r}_0) &= O(r_s^{-1}). \end{aligned}\right\} \tag{2.56}$$

These conditions imply that there exist constants C_{SG} and C_{SP} and functions $c_{SG}(r_s)$ and $c_{SP}(r_s)$ defined for $r_s > 0$ and such that $c_{SG}(r_s)$ and $c_{SP}(r_s) \to 0$ as $r_s \to \infty$ giving

$$\left.\begin{aligned} r_s\left|\tfrac{\partial G(\mathbf{r}_s,\mathbf{r})}{\partial r_s} - ik_1 G(\mathbf{r}_s,\mathbf{r})\right| &\leq c_{SG}(r_s), \\ r_s|G(\mathbf{r}_s,\mathbf{r})| &\leq C_{SG}, \end{aligned}\right\} \tag{2.57}$$

and

$$\left.\begin{aligned} r_s\left|\tfrac{\partial p(\mathbf{r}_s,\mathbf{r}_0)}{\partial r_s} - ik_1 p(\mathbf{r}_s,\mathbf{r}_0)\right| &\leq c_{SP}(r_s), \\ r_s|p(\mathbf{r}_s,\mathbf{r}_0)| &\leq D_{SP}. \end{aligned}\right\} \tag{2.58}$$

Utilising these inequalities in equation (2.54) gives

$$\begin{aligned} |I_\Sigma^{1U_+}| &\leq \lim_{R\to\infty}\int_\Sigma (C_{SP}c_{SG}(R) + C_{SG}c_{SP}(R))/R^2 ds(\mathbf{r}_s), \\ &\leq \lim_{R\to\infty}\{2\pi(C_{SP}c_{SG}(R) + C_{SG}c_{SP}(R))\}, \\ &= 0. \end{aligned} \tag{2.59}$$

The limit $I_{\sigma_{\mathbf{r}_0}}^{1U_+}$ is given by

$$I_{\sigma_{\mathbf{r}_0}}^{1U_+} = \lim_{\epsilon\to 0}\int_{\sigma_{\mathbf{r}_0}} (p(\mathbf{r}_s,\mathbf{r}_0)\frac{\partial G(\mathbf{r}_s,\mathbf{r})}{\partial n(\mathbf{r}_s)} - G(\mathbf{r}_s,\mathbf{r})\frac{\partial p(\mathbf{r}_s,\mathbf{r}_0)}{\partial n(\mathbf{r}_s)})ds(\mathbf{r}_s). \tag{2.60}$$

This may be evaluated by writing $p(\mathbf{r}_s,\mathbf{r}_0)$ as the sum of the free-field Green's function,

$$G_F(\mathbf{r}_s,\mathbf{r}_0) = \frac{-e^{ik_1|\mathbf{r}_s-\mathbf{r}_0|}}{4\pi|\mathbf{r}_s-\mathbf{r}_0|}, \tag{2.61}$$

plus a correction term, $g_F(\mathbf{r}_s,\mathbf{r}_0)$, *i.e.*,

$$p(\mathbf{r}_s,\mathbf{r}_0) = G_F(\mathbf{r}_s,\mathbf{r}_0) + g_F(\mathbf{r}_s,\mathbf{r}_0), \tag{2.62}$$

where $g_F(\mathbf{r}_s,\mathbf{r}_0)$, considered as a function of $\mathbf{r}_s$, is continuous and has continuous partial derivatives of all orders in U_+, so that, for small enough ϵ, and for all $\mathbf{r}_s$ on $\sigma_{\mathbf{r}_0}$,

$$|g_F(\mathbf{r}_s,\mathbf{r}_0)| \leq C_F, \tag{2.63}$$

and,

$$|\frac{\partial g_F(\mathbf{r}_s,\mathbf{r}_0)}{\partial n(\mathbf{r}_s)}| \leq C_F, \tag{2.64}$$

where C_F is a constant. Also, for $\mathbf{r}_s$ on $\sigma_{\mathbf{r}_0}$,

$$|G_F(\mathbf{r}_s, \mathbf{r}_0)| = \frac{1}{4\pi\varepsilon}, \tag{2.65}$$

and

$$\frac{\partial G_F(\mathbf{r}_s, \mathbf{r}_0)}{\partial n(\mathbf{r}_s)} = -\frac{1}{4\pi\varepsilon^2} + g^*(\mathbf{r}_s, \mathbf{r}_0), \tag{2.66}$$

where

$$|g^*(\mathbf{r}_s, \mathbf{r}_0)| \leq \frac{C^*}{\varepsilon}, \tag{2.67}$$

C^* being a constant. Further, $G(\mathbf{r}_s, \mathbf{r})$ and $\nabla_{\mathbf{r}_s} G(\mathbf{r}_s, \mathbf{r})$ are continuous functions of $\mathbf{r}_s$ in a neighbourhood of $\mathbf{r}_0$. Thus, there exists a constant C_G such that, for all small enough ε, and all $\mathbf{r}_s$ on $\sigma_{\mathbf{r}_0}$,

$$|G(\mathbf{r}_s, \mathbf{r})| \leq C_G, \tag{2.68}$$

and,

$$\left|\frac{\partial G(\mathbf{r}_s, \mathbf{r})}{\partial n(\mathbf{r}_s)}\right| \leq |\nabla_{\mathbf{r}_s} G(\mathbf{r}_s, \mathbf{r})| \leq C_G. \tag{2.69}$$

Substituting equation (2.62) into (2.60) gives

$$I^{1U_+}_{\sigma_{\mathbf{r}_0}} = \lim_{\varepsilon \to 0}(I_1 + I_2 + I_3 + I_4), \tag{2.70}$$

where

$$I_1 = \int_{\sigma_{\mathbf{r}_0}} G_F(\mathbf{r}_s, \mathbf{r}_0) \frac{\partial G(\mathbf{r}_s, \mathbf{r})}{\partial n(\mathbf{r}_s)} ds(\mathbf{r}_s), \tag{2.71}$$

$$I_2 = \int_{\sigma_{\mathbf{r}_0}} g_F(\mathbf{r}_s, \mathbf{r}_0) \frac{\partial G(\mathbf{r}_s, \mathbf{r})}{\partial n(\mathbf{r}_s)} ds(\mathbf{r}_s), \tag{2.72}$$

$$I_3 = -\int_{\sigma_{\mathbf{r}_0}} G(\mathbf{r}_s, \mathbf{r}) \frac{\partial G_F(\mathbf{r}_s, \mathbf{r}_0)}{\partial n(\mathbf{r}_s)} ds(\mathbf{r}_s), \tag{2.73}$$

and,

$$I_4 = -\int_{\sigma_{\mathbf{r}_0}} G(\mathbf{r}_s, \mathbf{r}) \frac{\partial g_F(\mathbf{r}_s, \mathbf{r}_0)}{\partial n(\mathbf{r}_s)} ds(\mathbf{r}_s). \tag{2.74}$$

Now,

$$\begin{aligned} |I_1| &\leq \int_{\sigma_{\mathbf{r}_0}} |G_F(\mathbf{r}_s, \mathbf{r}_0)| \left|\frac{\partial G(\mathbf{r}_s, \mathbf{r})}{\partial n(\mathbf{r}_s)}\right| ds(\mathbf{r}_s), \\ &\leq C_G \varepsilon, \end{aligned} \tag{2.75}$$

using inequalities (2.65) and (2.69). Also,

$$\begin{aligned} |I_2| &\leq \int_{\sigma_{\mathbf{r}_0}} |g_F(\mathbf{r}_s, \mathbf{r}_0)| \left| \frac{\partial G(\mathbf{r}_s, \mathbf{r})}{\partial n(\mathbf{r}_s)} \right| ds(\mathbf{r}_s), \\ &\leq C_F C_G 4\pi\varepsilon^2, \end{aligned} \tag{2.76}$$

using inequalities (2.63) and (2.69). And

$$\begin{aligned} |I_4| &= \int_{\sigma_{\mathbf{r}_0}} |G(\mathbf{r}_s, \mathbf{r})| \left| \frac{\partial g_F(\mathbf{r}_s, \mathbf{r}_0)}{\partial n(\mathbf{r}_s)} \right| ds(\mathbf{r}_s) \\ &\leq C_G C_F 4\pi\varepsilon^2 \end{aligned} \tag{2.77}$$

using inequalities (2.64) and (2.68). Thus, $|I_1|$, $|I_2|$, and $|I_4| \rightarrow 0$ as $\varepsilon \rightarrow 0$. Finally, I_3 can be expanded to give,

$$\begin{aligned} I_3 &= \int_{\sigma_{\mathbf{r}_0}} G(\mathbf{r}_s, \mathbf{r})/4\pi\varepsilon^2 ds(\mathbf{r}_s) \\ &\quad + \int_{\sigma_{\mathbf{r}_0}} G(\mathbf{r}_s, \mathbf{r}) g^*(\mathbf{r}_s, \mathbf{r}_0) ds(\mathbf{r}_s), \end{aligned} \tag{2.78}$$

using equation (2.66).The magnitude of the second integral of equation (2.78) is given by

$$\int_{\sigma_{\mathbf{r}_0}} |G(\mathbf{r}_s, \mathbf{r})||g^*(\mathbf{r}_s, \mathbf{r}_0)| ds(\mathbf{r}_s) \leq 4\pi C_G C^* \varepsilon. \tag{2.79}$$

Now,

$$\lim_{\varepsilon \rightarrow 0} \int_{\sigma_{\mathbf{r}_0}} G(\mathbf{r}_s, \mathbf{r})/4\pi\varepsilon^2 ds(\mathbf{r}_s) = G(\mathbf{r}_0, \mathbf{r}). \tag{2.80}$$

Thus, the limit $I^{1U_+}_{\sigma_{\mathbf{r}_0}}$ is given by

$$I^{1U_+}_{\sigma_{\mathbf{r}_0}} = G(\mathbf{r}_0, \mathbf{r}). \tag{2.81}$$

The limit $I^{1U_+}_{\sigma_{\mathbf{r}}}$ is given by,

$$I^{1U_+}_{\sigma_{\mathbf{r}}} = \lim_{\varepsilon \rightarrow 0} \int_{\sigma_{\mathbf{r}}} (p(\mathbf{r}_s, \mathbf{r}) \frac{\partial G(\mathbf{r}_s, \mathbf{r})}{\partial n(\mathbf{r}_s)} - G(\mathbf{r}_s, \mathbf{r}) \frac{\partial p(\mathbf{r}_s, \mathbf{r}_0)}{\partial n(\mathbf{r}_s)}) ds(\mathbf{r}_s). \tag{2.82}$$

and is evaluated in the same manner as $I^{1U_+}_{\sigma_{\mathbf{r}_0}}$. $G(\mathbf{r}_s, \mathbf{r})$ may be written as the sum of the free-field Green's function

$$G_F(\mathbf{r}_s, \mathbf{r}) = \frac{-e^{ik_1|\mathbf{r}_s - \mathbf{r}|}}{4\pi |\mathbf{r}_s - \mathbf{r}|}, \tag{2.83}$$

plus a correction term, $g_F(\mathbf{r}_s, \mathbf{r})$,

$$G(\mathbf{r}_s, \mathbf{r}) = G_F(\mathbf{r}_s, \mathbf{r}) + g_F(\mathbf{r}_s, \mathbf{r}), \tag{2.84}$$

where $g_F(\mathbf{r}_s, \mathbf{r})$, considered as a function of $\mathbf{r}_s$, is continuous and has continuous partial derivatives of all orders in U_+. Also, $p(\mathbf{r}_s, \mathbf{r}_0)$ and $\nabla_{\mathbf{r}_s} p(\mathbf{r}_s, \mathbf{r}_0)$ are continuous functions of $\mathbf{r}_s$ in a neighbourhood of $\mathbf{r}$. Thus, it can be shown that

$$I^{1U_+}_{\sigma_\mathbf{r}} = -p(\mathbf{r}_0, \mathbf{r}). \tag{2.85}$$

By applying equations (2.59), (2.81), (2.85), equation (2.52) reduces to,

$$\begin{aligned} p(\mathbf{r}_0, \mathbf{r}) &= G(\mathbf{r}_0, \mathbf{r}) + \int_\Gamma p_+(\mathbf{r}_s, \mathbf{r}_0) \frac{\partial G_+(\mathbf{r}_s, \mathbf{r})}{\partial n(\mathbf{r}_s)} \\ &\quad - G_+(\mathbf{r}_s, \mathbf{r}) \frac{\partial p_+(\mathbf{r}_s, \mathbf{r}_0)}{\partial n(\mathbf{r}_s)} ds(\mathbf{r}_s) \end{aligned} \tag{2.86}$$

for $\mathbf{r}_0 \in U_+$ and $\mathbf{r} \in U_+$.

For $\mathbf{r} \in \Gamma$ the region V_1 is again bounded by the hemispherical surface Σ, of radius R, the plane boundary Γ, the surface of the sphere $\sigma_{\mathbf{r}_0}$, of radius ε and, in this case, the *hemispherical* surface $\sigma_\mathbf{r}$ of radius ε, as $\mathbf{r} \in \Gamma$. Again, as for the case with $\mathbf{r} \in U_+$, integral (2.50) is evaluated with the radius of the surface Σ taken to the limit $R \to \infty$ and the radii of the surfaces $\sigma_\mathbf{r}$ and $\sigma_{\mathbf{r}_0}$ taken to the limit $\varepsilon \to 0$. Integral (2.50) can now be written as,

$$I^{1\Gamma} + I^{1\Gamma}_\Sigma + I^{1\Gamma}_{\sigma_{\mathbf{r}_0}} + I^{1\Gamma}_{\sigma_\mathbf{r}} = 0, \tag{2.87}$$

with the similar notation of I as previously. The contributions $I^{1\Gamma}_\Sigma$, and $I^{1\Gamma}_{\sigma_{\mathbf{r}_0}}$ to equation (2.87) will be identical to those of $I^{1U_+}_\Sigma$ and $I^{1U_+}_{\sigma_{\mathbf{r}_0}}$, obtained previously. However, it is found that the contribution $I^{1\Gamma}_{\sigma_\mathbf{r}}$ is

$$I^{1\Gamma}_{\sigma_\mathbf{r}} = -\frac{1}{2} p(\mathbf{r}_0, \mathbf{r}), \tag{2.88}$$

and equation (2.87) reduces to

$$\begin{aligned} \frac{1}{2} p(\mathbf{r}_0, \mathbf{r}) &= G(\mathbf{r}_0, \mathbf{r}) + \int_\Gamma p_+(\mathbf{r}_s, \mathbf{r}_0) \frac{\partial G_+(\mathbf{r}_s, \mathbf{r})}{\partial n(\mathbf{r}_s)}, \\ &\quad - G_+(\mathbf{r}_s, \mathbf{r}) \frac{\partial p_+(\mathbf{r}_s, \mathbf{r}_0)}{\partial n(\mathbf{r}_s)} ds(\mathbf{r}_s) \end{aligned} \tag{2.89}$$

for $\mathbf{r}_0 \in U_+$ and $\mathbf{r} \in \Gamma$.

For $\mathbf{r} \in U_-$ the region V_1 is again bounded by the hemispherical surface Σ, of radius R, the plane boundary Γ, and the surface of the sphere $\sigma_{\mathbf{r}_0}$ of radius ε. As $\mathbf{r} \in U_-$, a surface $\sigma_{\mathbf{r}}$ is absent. Again, as for the cases with $\mathbf{r} \in U_+$ and $\mathbf{r} \in \Gamma$, equation (2.50) is evaluated with the radius of the surface Σ taken to the limit $R \to \infty$, and the radius of the surface $\sigma_{\mathbf{r}_0}$ taken to the limit $\varepsilon \to 0$. The integral (2.50) can now be written as

$$I^{1U_-} + I_{\Sigma}^{1U_-} + I_{\sigma_{\mathbf{r}_0}}^{1U_-} = 0, \tag{2.90}$$

with the similar notation for I as previously. The contributions $I_{\Sigma}^{1U_-}$ and $I_{\sigma_{\mathbf{r}_0}}^{1U_-}$ to equation (2.90) will be identical to those of $I_{\Sigma}^{1U_+}$, $I_{\sigma_{\mathbf{r}_0}}^{1U_+}$ and equation (2.90) reduces to

$$0 = G(\mathbf{r}_0, \mathbf{r}) + \int_{\Gamma} p_+(\mathbf{r}_s, \mathbf{r}_0) \frac{\partial G_+(\mathbf{r}_s, \mathbf{r})}{\partial n(\mathbf{r}_s)} - G_+(\mathbf{r}_s, \mathbf{r}) \frac{\partial p_+(\mathbf{r}_s, \mathbf{r}_0)}{\partial n(\mathbf{r}_s)} ds(\mathbf{r}_s), \tag{2.91}$$

for $\mathbf{r}_0 \in U_+$ and $\mathbf{r} \in U_-$.

The results of evaluating equation (2.50) for the three different cases, $\mathbf{r} \in U_+$, $\mathbf{r} \in \Gamma$, and $\mathbf{r} \in U_-$, *i.e.*, equations (2.86), (2.89) and (2.91) may now be combined to give the following integral equation for for $\mathbf{r}_0 \in U_+$ and $\mathbf{r} \in \mathbf{R}^3$,

$$\begin{aligned} \kappa_1(\mathbf{r}) p(\mathbf{r}, \mathbf{r}_0) &= G(\mathbf{r}_0, \mathbf{r}) + \int_{\Gamma} p_+(\mathbf{r}_s, \mathbf{r}_0) \frac{\partial G_+(\mathbf{r}_s, \mathbf{r})}{\partial z_s} \\ &\quad - G_+(\mathbf{r}_s, \mathbf{r}) \frac{\partial p_+(\mathbf{r}_s, \mathbf{r}_0)}{\partial z_s} ds(\mathbf{r}_s), \end{aligned} \tag{2.92}$$

where $\kappa_1(\mathbf{r}) := 1$ for $\mathbf{r} \in U_+$, $1/2$ for $\mathbf{r} \in \Gamma$, 0 for $\mathbf{r} \in U_-$. In the above equations (2.86), (2.89), (2.91) and (2.92), the subscript $+$ implies that p and G are calculated on the U_+ side of the boundary Γ, for $\mathbf{r}_s \in \Gamma$.

Integral over ∂V_2 Equation (2.51) is considered for the three different cases, $\mathbf{r} \in U_-$, $\mathbf{r} \in \Gamma \bigcup \partial S$, and $\mathbf{r} \in U_+$.

For $\mathbf{r} \in U_-$ the region V_2 is bounded by the hemispherical surface Σ of radius R, the plane boundary Γ, the surface of the sphere $\sigma_{\mathbf{r}}$ of radius ε and the surface of the rigid inhomogeneity, ∂S. As $\mathbf{r}_0 \in U_+$, a surface $\sigma_{\mathbf{r}_0}$

is absent. The integral (2.51) is evaluated with the radius of the surface Σ taken to the limit $R \to \infty$, and the radius of the surface $\sigma_{\mathbf{r}}$ taken to the limit $\varepsilon \to 0$. Equation (2.51) can now be written as

$$I^{2U-} + I^{2U-}_{\Sigma} + I^{2U-}_{\sigma_{\mathbf{r}}} + I^{2U-}_{\partial S} = 0, \tag{2.93}$$

with the similar notation for I as previously and $I^{2U-}_{\partial S}$ represents the integral in (2.51) over the surface ∂S. The contribution I^{2U-}_{Σ} to equation (2.93) will be identical to that of I^{1U+}_{Σ} obtained previously. The evaluation of $I^{2U-}_{\sigma_{\mathbf{r}}}$ follows that of $I^{1U+}_{\sigma_{\mathbf{r}_0}}$ except here, the Green's function $G(\mathbf{r}_s, \mathbf{r})$ can be written as

$$G(\mathbf{r}_s, \mathbf{r}) = \alpha G_F(\mathbf{r}_s, \mathbf{r}) + g_F(\mathbf{r}_s, \mathbf{r}), \tag{2.94}$$

where $G_F(\mathbf{r}_s, \mathbf{r})$ is the free-field Green's function, and $g_F(\mathbf{r}_s, \mathbf{r})$ is a correction term, which considered as a function of $\mathbf{r}_s$ is continuous and has continuous partial derivatives of all orders in U_-. Thus, it is found that

$$I^{2U-}_{\sigma_{\mathbf{r}}} = -\alpha p(\mathbf{r}_0, \mathbf{r}). \tag{2.95}$$

The limit $I^{2U-}_{\partial S}$ is given by

$$\begin{aligned} I^{2U-}_{\partial S} &= \int_{\partial S} (p(\mathbf{r}_s, \mathbf{r}_0) \frac{\partial G(\mathbf{r}_s, \mathbf{r})}{\partial n(\mathbf{r}_s)} - G(\mathbf{r}_s, \mathbf{r}) \frac{\partial p(\mathbf{r}_s, \mathbf{r}_0)}{\partial n(\mathbf{r}_s)}) ds(\mathbf{r}_s) \\ &= \int_{\partial S} p(\mathbf{r}_s, \mathbf{r}_0) \frac{\partial G(\mathbf{r}_s, \mathbf{r})}{\partial n(\mathbf{r}_s)} ds(\mathbf{r}_s), \end{aligned} \tag{2.96}$$

using the boundary condition, equation (2.36), on ∂S.

So, equation (2.93) reduces to

$$\begin{aligned} \alpha p(\mathbf{r}_0, \mathbf{r}) &= \int_{\Gamma} p_-(\mathbf{r}_s, \mathbf{r}_0) \frac{\partial G_-(\mathbf{r}_s, \mathbf{r})}{\partial n(\mathbf{r}_s)} - G_-(\mathbf{r}_s, \mathbf{r}) \frac{\partial p_-(\mathbf{r}_s, \mathbf{r}_0)}{\partial n(\mathbf{r}_s)} ds(\mathbf{r}_s) \\ &\quad + \int_{\partial S} p(\mathbf{r}_s, \mathbf{r}_0) \frac{\partial G(\mathbf{r}_s, \mathbf{r})}{\partial n(\mathbf{r}_s)} ds(\mathbf{r}_s), \end{aligned} \tag{2.97}$$

for $\mathbf{r}_0 \in U_+$ and $\mathbf{r} \in U_-$.

For $\underline{\mathbf{r} \in \Gamma \bigcup \partial S}$, the region V_2 is bounded by the hemispherical surface Σ of radius R, the plane boundary Γ, the surface of the rigid inhomogeneity ∂S and the hemispherical surface $\sigma_{\mathbf{r}}$ of radius ε.The integral (2.51) is evaluated with the radius of the surface Σ taken to the limit $R \to \infty$, and the radius of

the surface $\sigma_{\mathbf{r}}$ taken to the limit $\varepsilon \to 0$. Equation (2.51) can now be written as

$$I^{2\Gamma} + I_{\Sigma}^{2\Gamma} + I_{\sigma_{\mathbf{r}}}^{2\Gamma} + I_{\partial S}^{2\Gamma} = 0, \tag{2.98}$$

with the similar notation for I as used previously. The only contribution that will be affected by imposing $\mathbf{r} \in \Gamma \bigcup \partial S$, is $I_{\sigma_{\mathbf{r}}}^{2\Gamma}$, for which the integrating surface is a hemisphere, and it is found that,

$$I_{\sigma_{\mathbf{r}}}^{2\Gamma} = -\frac{1}{2}\alpha p(\mathbf{r}_0, \mathbf{r}). \tag{2.99}$$

So, equation (2.98) reduces to,

$$\begin{aligned} \frac{1}{2}\alpha p(\mathbf{r}_0, \mathbf{r}) &= \int_{\Gamma} p_-(\mathbf{r}_s, \mathbf{r}_0)\frac{\partial G_-(\mathbf{r}_s, \mathbf{r})}{\partial n(\mathbf{r}_s)} - G_-(\mathbf{r}_s, \mathbf{r})\frac{\partial p_-(\mathbf{r}_s, \mathbf{r}_0)}{\partial n(\mathbf{r}_s)} ds(\mathbf{r}_s) \\ &\quad + \int_{\partial S} p(\mathbf{r}_s, \mathbf{r}_0)\frac{\partial G(\mathbf{r}_s, \mathbf{r})}{\partial n(\mathbf{r}_s)} ds(\mathbf{r}_s), \end{aligned} \tag{2.100}$$

for $\mathbf{r}_0 \in U_+$ and $\mathbf{r} \in \Gamma \bigcup \partial S$.

For $\mathbf{r} \in U_+$ the region V_2 is bounded by the surface Σ, of radius R, the plane boundary Γ and the surface of the rigid inhomogeneity S. As $\mathbf{r} \in U_+$, a surface $\sigma_{\mathbf{r}}$ is absent. The integral (2.51) is evaluated with the radius of the surface Σ taken to the limit $R \to \infty$. Equation (2.51) can now be written as

$$I^{2U_+} + I_{\Sigma}^{2U_+} + I_{\partial S}^{2U_+} = 0, \tag{2.101}$$

with the similar notation for I as used previously. The contributions $I_{\Sigma}^{2U_+}$ and $I_{\partial S}^{2U_+}$ to equation (2.101) will be identical to those of $I_{\Sigma}^{2U_-}$, $I_{\partial S}^{2U_-}$. So equation (2.101) reduces to

$$\begin{aligned} 0 &= \int_{\Gamma} p_-(\mathbf{r}_s, \mathbf{r}_0)\frac{\partial G_-(\mathbf{r}_s, \mathbf{r})}{\partial n(\mathbf{r}_s)} - G_-(\mathbf{r}_s, \mathbf{r})\frac{\partial p_-(\mathbf{r}_s, \mathbf{r}_0)}{\partial n(\mathbf{r}_s)} ds(\mathbf{r}_s) \\ &\quad + \int_{\partial S} p(\mathbf{r}_s, \mathbf{r}_0)\frac{\partial G(\mathbf{r}_s, \mathbf{r})}{\partial n(\mathbf{r}_s)} ds(\mathbf{r}_s), \end{aligned} \tag{2.102}$$

for $\mathbf{r}_0 \in U_+$ and $\mathbf{r} \in \Gamma \bigcup U_+$.

The results of evaluating equation (2.51), *i.e.* equations (2.97), (2.100) and (2.102) for the three different cases $\mathbf{r} \in U_-$, $\mathbf{r} \in \Gamma \bigcup \partial S$ and $\mathbf{r} \in U_+$ may

be combined to give the following integral equation for ∂V_2, for $\mathbf{r}_0 \in U_+$ and $\mathbf{r} \in \mathbb{R}^3$,

$$\begin{aligned}\alpha\kappa_2(\mathbf{r})p(\mathbf{r},\mathbf{r}_0) &= \int_\Gamma (p_-(\mathbf{r}_s,\mathbf{r}_0)\frac{\partial G_-(\mathbf{r}_s,\mathbf{r})}{\partial z_s} - G_-(\mathbf{r}_s,\mathbf{r})\frac{\partial p_-(\mathbf{r}_s,\mathbf{r}_0)}{\partial z_s})ds(\mathbf{r}_s) \\ &\quad + \int_{\partial S}(p(\mathbf{r}_s,\mathbf{r}_0)\frac{\partial G(\mathbf{r}_s,\mathbf{r})}{\partial n(\mathbf{r}_s)})ds(\mathbf{r}_s), \qquad (2.103)\end{aligned}$$

where $\kappa_2(\mathbf{r}) := 1$ for $\mathbf{r} \in U_-$, $1/2$ for $\mathbf{r} \in \Gamma \bigcup \partial S$, 0 for $\mathbf{r} \in U_+$. In the above equations (2.97), (2.100), (2.102) and (2.103), the subscript $-$ implies that p and G are calculated on the U_- side of the boundary Γ for $\mathbf{r}_s \in \Gamma$.

The final integral equation Equations (2.92) and (2.103) can now be combined to give a single integral equation. Multiplying equation (2.92) by α, and subtracting equation (2.103) from this, and making use of the conditions on Γ satisfied by p and G (equations (2.37), (2.38), (2.42) and (2.43)), gives, for $\mathbf{r}_0 \in U_+$ and $\mathbf{r} \in \mathbb{R}^3$,

$$\alpha\kappa(\mathbf{r})p(\mathbf{r},\mathbf{r}_0) = \alpha G(\mathbf{r}_0,\mathbf{r}) + \int_{\partial S} p(\mathbf{r}_s,\mathbf{r}_0)\frac{\partial G(\mathbf{r}_s,\mathbf{r})}{\partial n(\mathbf{r}_s)}ds(\mathbf{r}_s) \qquad (2.104)$$

where $\kappa(\mathbf{r}) := 1$ for $\mathbf{r} \in \mathbb{R}^3\backslash S$, $1/2$ for $\mathbf{r} \in \partial S$. This integral equation is completely equivalent to the original boundary value problem, *i.e.* the integral equation has exactly one solution, and the solution satisfies the original boundary value problem. This equation has been presented previously in [86] though without such a thorough derivation.

Reciprocity of the Green's function The arguments to derive equation (2.104) via equations (2.92) and (2.103), can be used to show that G satisfies reciprocity, *i.e.* $G(\mathbf{r},\mathbf{r}_0) = G(\mathbf{r}_0,\mathbf{r})$. Equations (2.50) and (2.51) hold good with $p(\mathbf{r}_s,\mathbf{r}_0)$ replaced by $G(\mathbf{r}_s,\mathbf{r}_0)$. Thus, and by letting the surface of the inhomogeneity S become negligibly small,

$$\int_{\partial V_i}(G(\mathbf{r}_s,\mathbf{r}_0)\frac{\partial G(\mathbf{r}_s,\mathbf{r})}{\partial n(\mathbf{r}_s)} - G(\mathbf{r}_s,\mathbf{r})\frac{\partial p(\mathbf{r}_s,\mathbf{r}_0)}{\partial n(\mathbf{r}_s)})ds(\mathbf{r}_s) = 0, \qquad (2.105)$$

for $i = 1,2$ and $\mathbf{r}, \mathbf{r}_0 \in \mathbb{R}^3\backslash\Gamma$. V_2 is now defined to be that part of $\mathbb{R}^3\backslash(U_+ \bigcup \Gamma)$ contained within a large sphere, excluding small spheres about

$\mathbf{r}$ and $\mathbf{r}_0$. Following the procedure which gave equation (2.92), gives

$$\begin{aligned}\epsilon_1(\mathbf{r})G(\mathbf{r},\mathbf{r}_0) &= \epsilon_1(\mathbf{r})G(\mathbf{r}_0,\mathbf{r}) - \int_\Gamma (G_+(\mathbf{r}_s,\mathbf{r}_0)\frac{\partial G_+(\mathbf{r}_s,\mathbf{r})}{\partial z_s} \\ &\quad -G_+(\mathbf{r}_s,\mathbf{r})\frac{\partial G_+(\mathbf{r}_s,\mathbf{r}_0)}{\partial z_s})ds(\mathbf{r}_s), \end{aligned} \tag{2.106}$$

for $\mathbf{r}$, $\mathbf{r}_0 \in \mathbf{R}^3\backslash\Gamma$ and $\epsilon_1(\mathbf{r}) = 1$ for $\mathbf{r} \in U_+$, 0 for $\mathbf{r} \in U_-$. Similarly, following the procedure which gave equation (2.103), gives,

$$\begin{aligned}\alpha\epsilon_2(\mathbf{r})G(\mathbf{r},\mathbf{r}_0) &= \alpha\epsilon_2(\mathbf{r})G(\mathbf{r}_0,\mathbf{r}) + \int_\Gamma (G_-(\mathbf{r}_s,\mathbf{r}_0)\frac{\partial G_-(\mathbf{r}_s,\mathbf{r})}{\partial z_s} \\ &\quad -G_-(\mathbf{r}_s,\mathbf{r})\frac{\partial G_-(\mathbf{r}_s,\mathbf{r}_0)}{\partial z_s})ds(\mathbf{r}_s), \end{aligned} \tag{2.107}$$

for $\mathbf{r}$, $\mathbf{r}_0 \in \mathbf{R}^3\backslash\Gamma$ and $\epsilon_1(\mathbf{r}) = 1$ for $\mathbf{r} \in U_-$, 0 for $\mathbf{r} \in U_+$. Multiplying equation (2.106) by α and adding to equation (2.107), and making use of the boundary conditions on Γ, equations (2.42) and (2.43), gives,

$$\alpha G(\mathbf{r},\mathbf{r}_0) = \alpha G(\mathbf{r}_0,\mathbf{r}), \tag{2.108}$$

a statement of reciprocity.

Second integral equation reformulation

The second integral equation formulation of the boundary value problem has been proposed by Chandler-Wilde, [87], and will be presented here for completeness. This makes use of the Green's functions, G_1 and G_2, given by,

$$G_j(\mathbf{r},\mathbf{r}_0) = -\frac{e^{(ik_j|\mathbf{r}-\mathbf{r}_0|)}}{4\pi|\mathbf{r}-\mathbf{r}_0|}, \tag{2.109}$$

where $\mathbf{r}, \mathbf{r}_0 \in \mathbf{R}^3$ for $j = 1, 2$. These functions satisfy the inhomogeneous Helmholtz equation,

$$(\nabla^2 + k_j^2)G_j(\mathbf{r},\mathbf{r}_0) = \delta(\mathbf{r}-\mathbf{r}_0), \tag{2.110}$$

for $j = 1, 2$, and also the Sommerfeld radiation conditions, with $\mathbf{r} \in U_+$, uniformly in $\mathbf{r}$ as $r := |\mathbf{r}| \to \infty$,

$$\left.\begin{aligned}\tfrac{\partial G(\mathbf{r},\mathbf{r}_0)}{\partial r} - ik_1G(\mathbf{r},\mathbf{r}_0) &= o(r^{-1}), \\ G(\mathbf{r},\mathbf{r}_0) &= O(r^{-1}),\end{aligned}\right\} \tag{2.111}$$

The same procedure as in the first formulation, is now followed, *i.e.* consider regions V_1 and V_2, V_1/V_2 consisting of that part of U_+/U_- contained within a large sphere of radius R, centred on the origin, but excluding small spheres of radius ϵ, centred on r and r_0. Applying Green's second theorem to regions V_1 and V_2 and using the Helmholtz equations satisfied by p and G_i , equations similar to equations (2.50) and (2.51) are obtained,

$$\int_{\partial V_1} (p(\mathrm{r}_s,\mathrm{r}_0)\frac{\partial G_1(\mathrm{r}_s,\mathrm{r})}{\partial n(\mathrm{r}_s)} - G_1(\mathrm{r}_s,\mathrm{r})\frac{\partial p(\mathrm{r}_s,\mathrm{r}_0)}{\partial n(\mathrm{r}_s)})ds(\mathrm{r}_s) = 0, \qquad (2.112)$$

and,

$$\int_{\partial V_2} (p(\mathrm{r}_s,\mathrm{r}_0)\frac{\partial G_2(\mathrm{r}_s,\mathrm{r})}{\partial n(\mathrm{r}_s)} - G_2(\mathrm{r}_s,\mathrm{r})\frac{\partial p(\mathrm{r}_s,\mathrm{r}_0)}{\partial n(\mathrm{r}_s)})ds(\mathrm{r}_s) = 0, \qquad (2.113)$$

for $\mathrm{r}_0 \in U_+$ and $\mathrm{r} \in \mathbb{R}^3$. Letting the radius of the small spheres, $\epsilon \to 0$, and the radius of the large sphere, $R \to \infty$, and using the Sommerfeld radiation conditions satisfied by p and G_i, in a similar manner to the first formulation, the following pair of equations is obtained,

$$\begin{aligned}\kappa_1(\mathrm{r})p(\mathrm{r},\mathrm{r}_0) &= G_1(\mathrm{r}_0,\mathrm{r}) - \int_\Gamma p_+(\mathrm{r}_s,\mathrm{r}_0)\frac{\partial G_1(\mathrm{r}_s,\mathrm{r})}{\partial z_s} \\ &\quad -G_1(\mathrm{r}_s,\mathrm{r})\frac{\partial p_+(\mathrm{r}_s,\mathrm{r}_0)}{\partial z_s}ds(\mathrm{r}_s), \qquad (2.114)\end{aligned}$$

and

$$\begin{aligned}\kappa_2(\mathrm{r})p(\mathrm{r},\mathrm{r}_0) &= \int_\Gamma p_-(\mathrm{r}_s,\mathrm{r}_0)\frac{\partial G_2(\mathrm{r}_s,\mathrm{r})}{\partial z_s} - G_2(\mathrm{r}_s,\mathrm{r})\frac{\partial p_-(\mathrm{r}_s,\mathrm{r}_0)}{\partial z_s}ds(\mathrm{r}_s) \\ &\quad + \int_{\partial S} p(\mathrm{r}_s,\mathrm{r}_0)\frac{\partial G_2(\mathrm{r}_s,\mathrm{r})}{\partial n(\mathrm{r}_s)}ds(\mathrm{r}_s), \qquad (2.115)\end{aligned}$$

for $\mathrm{r}_0 \in U_+$ and $\mathrm{r} \in \mathbb{R}^3$, where the normal, n on ∂S is directed into S, κ_1 and κ_2 being defined previously as $\kappa_1(\mathrm{r}) := 1$ for $\mathrm{r} \in U_+$, 1/2 for $\mathrm{r} \in \Gamma$, 0 for $\mathrm{r} \in U_-$ and $\kappa_2(\mathrm{r}) := 1$ for $\mathrm{r} \in U_-$, 1/2 for $\mathrm{r} \in \Gamma \bigcup \partial S$ and 0 for $\mathrm{r} \in U_+$. A further equation is obtained by adding equations (2.114) and (2.115) and using the boundary conditions (2.37) and (2.38) on Γ, giving,

$$\begin{aligned}\kappa(\mathrm{r})p(\mathrm{r},\mathrm{r}_0) &= G_1(\mathrm{r}_0,\mathrm{r}) + \int_\Gamma p_+(\mathrm{r}_s,\mathrm{r}_0)\left(\frac{\partial G_2(\mathrm{r}_s,\mathrm{r})}{\partial z_s} - \frac{\partial G_1(\mathrm{r}_s,\mathrm{r})}{\partial z_s}\right) \\ &\quad + \frac{\partial p_+(\mathrm{r}_s,\mathrm{r}_0)}{\partial z_s}\left(G_1(\mathrm{r}_s,\mathrm{r}) - \alpha G_2(\mathrm{r}_s,\mathrm{r})\right)ds(\mathrm{r}_s) \\ &\quad + \int_{\partial S} p(\mathrm{r}_s,\mathrm{r}_0)\frac{\partial G_2(\mathrm{r}_s,\mathrm{r})}{\partial n(\mathrm{r}_s)}ds(\mathrm{r}_s), \qquad (2.116)\end{aligned}$$

for $\mathbf{r}_0 \in U_+$, $\mathbf{r} \in \mathbf{R}^3 \backslash S$, again, $\kappa(\mathbf{r})$ has been defined previously as $\kappa(\mathbf{r}) := 1$ for $\mathbf{r} \in \mathbf{R}^3 \backslash \bar{S}$, $1/2$ for $\mathbf{r} \in \partial S$. Note that the derivatives $\partial G_i / \partial z_s$, $i = 1, 2$ in equation (2.116) vanish when $\mathbf{r} \in \Gamma$. Taking the derivative with respect to z of equation 2.116, gives,

$$\begin{aligned} \kappa(\mathbf{r}) \frac{\partial p(\mathbf{r}, \mathbf{r}_0)}{\partial z} &= \frac{\partial G_1(\mathbf{r}_0, \mathbf{r})}{\partial z} + \int_\Gamma p_+(\mathbf{r}_s, \mathbf{r}_0) \frac{\partial}{\partial z} \left(\frac{\partial G_2(\mathbf{r}_s, \mathbf{r})}{\partial z_s} - \frac{\partial G_1(\mathbf{r}_s, \mathbf{r})}{\partial z_s} \right) ds(\mathbf{r}_s) \\ &\quad + \int_\Gamma \frac{\partial p_+(\mathbf{r}_s, \mathbf{r}_0)}{\partial z_s} \left(\frac{\partial G_1(\mathbf{r}_s, \mathbf{r})}{\partial z} - \alpha \frac{\partial G_2(\mathbf{r}_s, \mathbf{r})}{\partial z_s} \right) ds(\mathbf{r}_s) \\ &\quad + \int_{\partial S} p(\mathbf{r}_s, \mathbf{r}_0) \frac{\partial^2 G_2(\mathbf{r}_s, \mathbf{r})}{\partial z \partial n(\mathbf{r}_s)} ds(\mathbf{r}_s) \end{aligned} \tag{2.117}$$

for $\mathbf{r}_0 \in U_+$, $\mathbf{r} \in \mathbf{R}^3 \backslash (\bar{S} \bigcup \Gamma)$. Letting $z \to 0_+$ in equation 2.116, gives,

$$\begin{aligned} \frac{1}{2}(1+\alpha) \frac{\partial p_+(\mathbf{r}, \mathbf{r}_0)}{\partial z} &= \frac{\partial G_1(\mathbf{r}_0, \mathbf{r})}{\partial z} \\ &\quad + \int_\Gamma p_+(\mathbf{r}_s, \mathbf{r}_0) \frac{\partial}{\partial z} \left(\frac{\partial G_2(\mathbf{r}_s, \mathbf{r})}{\partial z_s} - \frac{\partial G_1(\mathbf{r}_s, \mathbf{r})}{\partial z_s} \right) ds(\mathbf{r}_s) \\ &\quad + \int_{\partial S} p(\mathbf{r}_s, \mathbf{r}_0) \frac{\partial^2 G_2(\mathbf{r}_s, \mathbf{r})}{\partial z \partial n(\mathbf{r}_s)} ds(\mathbf{r}_s) \end{aligned} \tag{2.118}$$

for $\mathbf{r} \in \Gamma$, $\mathbf{r}_0 \in U_+$. A system of three equations has been obtained, in which the unknown functions are p and $\partial p / \partial z$ on Γ, and p on ∂S. These equations are (2.116) restricted to Γ, and (2.118) and (2.116) restricted on ∂S, and as for the first integral equation formulation, they are completely equivalent to the original boundary value problem, *i.e.* the combined integral equations have exactly one solution, and the solution satisfies the original boundary value problem.

Comparison of formulations

It is quite apparent that when the integral equations from the two formulations are considered, the solution of the system of three integral equations from the second formulation will be seen to have several disadvantages in comparison to the single integral equation of the first. Firstly, having a system of coupled equations to solve in contrast to the single equation of the first formulation will tend to a more computationally expensive solution. Secondly, in all of the three coupled integral equations, there is an integral having an infinite region of integration, Γ, making, again, computation

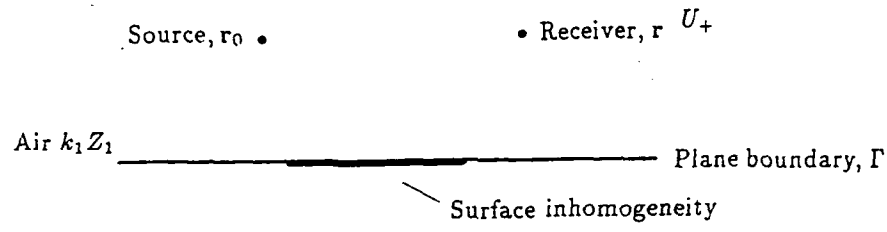

Figure 2.2 Geometry for scattering by a surface inhomogeneity

expensive. Nevertheless, the Green's function involved in the second formulation are straightforward conceptually, and easy to calculate. The Green's functions for the first formulation are less straightforward, since they involve the plane boundary, Γ. But, under certain circumstances (*e.g.* locally reacting conditions), they yield simple expressions. In view of this and the disadvantages associated with the second formulation, the second formulation shall be discarded in favour of the first formulation, in the present study.

2.2.2 The second approach

Here, the basic concept behind this second approach is that the embedded inhomogeneity is assumed to induce a variation in the surface admittance directly above it. This implies that knowledge of any sub-surface structuring is not required, and that all acoustic information in given by the surface impedance. This approach therefore gives more flexibility to the types of surface and near-surface inhomogeneities considered.

The geometry for this second approach is shown in figure 2.2. An irregular patch, S, of normalised surface admittance, β, is embedded in a plane of homogeneous admittance, characterised by a constant normalised surface admittance, β_c. As for the first case, the upper half-space is again denoted U_+, contains air, and is assumed to be characterised by real characteristic impedance and wavenumber, Z_1 and k_1, respectively; the boundary between the upper and lower half spaces is denoted by $\Gamma = \{(x, y, z) \in \mathbf{R}^3 | z = 0\}$.

The surface Γ is assumed to be locally reacting, i.e. $|n^2| \gg 1$. The complex acoustic pressure is assumed to satisfy the inhomogeneous Helmholtz equation,

$$(\nabla^2 + k_1^2)p(\mathbf{r}, \mathbf{r}_0) = \delta(\mathbf{r} - \mathbf{r}_0), \tag{2.119}$$

for $\mathbf{r}, \mathbf{r}_0 \in U_+$. This equation is to be satisfied subject to the impedance boundary condition, equation (2.13),

$$\frac{\partial p(\mathbf{r}, \mathbf{r}_0)}{\partial z} + ik_1\beta(\mathbf{r}_s)p(\mathbf{r}, \mathbf{r}_0) = 0, \tag{2.120}$$

for $\mathbf{r} \in \Gamma$, where $\beta(\mathbf{r}) = \beta$ for $\mathbf{r} \in \Gamma \backslash \overline{S}$, and Sommerfeld's radiation conditions with $\mathbf{r} \in U_+$, uniformly in $\mathbf{r}$ as $r := |\mathbf{r}| \to \infty$

$$\left.\begin{aligned} \tfrac{\partial p(\mathbf{r},\mathbf{r}_0)}{\partial r} - ik_1 p(\mathbf{r}, \mathbf{r}_0) &= o(r^{-1}), \\ p(\mathbf{r}, \mathbf{r}_0) &= O(r^{-1}). \end{aligned}\right\} \tag{2.121}$$

This boundary value problem is now reformulated in terms of an integral equation. As for the first approach, the formulation of an integral equation from the boundary value problem via Green's second theorem, involves letting the Green's function, $G(\mathbf{r}, \mathbf{r}_0)$, satisfy the following boundary value problem, for each $\mathbf{r}_0, \mathbf{r} \in U_+$: an inhomogeneous Helmholtz equation,

$$(\nabla^2 + k_1^2)G(\mathbf{r}, \mathbf{r}_0) = \delta(\mathbf{r} - \mathbf{r}_0), \tag{2.122}$$

subject to the impedance boundary condition,

$$\frac{\partial G(\mathbf{r}, \mathbf{r}_0)}{\partial z} + ik_1\beta G(\mathbf{r}, \mathbf{r}_0) = 0, \tag{2.123}$$

and Sommerfeld's radiation conditions with $\mathbf{r} \in U_+$, uniformly in $\mathbf{r}$ as $r := |\mathbf{r}| \to \infty$,

$$\left.\begin{aligned} \tfrac{\partial G(\mathbf{r},\mathbf{r}_0)}{\partial r} - ik_1 G(\mathbf{r}, \mathbf{r}_0) &= o(r^{-1}), \\ G(\mathbf{r}, \mathbf{r}_0) &= O(r^{-1}), \end{aligned}\right\} \tag{2.124}$$

Now consider the region V_1 consisting of that part of U_+ contained within a large hemisphere of surface Σ and radius R centred on the origin, and the boundary Γ, but excluding small spheres $\sigma_{\mathbf{r}}$ and $\sigma_{\mathbf{r}_0}$ of radii ϵ, centred on $\mathbf{r}$ and $\mathbf{r}_0$. Applying Green's second theorem to the region V_1, and noting that

$p(\mathbf{r}_s, \mathbf{r}_0)$ and $G(\mathbf{r}_s, \mathbf{r})$ satisfy the Helmholtz equation, the following equation is obtained for $\mathbf{r}, \mathbf{r}_0 \in U_+$,

$$p(\mathbf{r}, \mathbf{r}_0) = G(\mathbf{r}_0, \mathbf{r}) + \int_{\partial S} p(\mathbf{r}_s, \mathbf{r}_0) \frac{\partial G(\mathbf{r}_s, \mathbf{r})}{\partial n(\mathbf{r}_s)} - G(\mathbf{r}_s, \mathbf{r}) \frac{\partial p(\mathbf{r}_s, \mathbf{r}_0)}{\partial n(\mathbf{r}_s)} ds(\mathbf{r}_s). \tag{2.125}$$

Substituting the impedance boundary conditions (2.120) and (2.123) into equation (2.125) gives for $\mathbf{r}, \mathbf{r}_0 \in \overline{U}_+$,

$$p(\mathbf{r}, \mathbf{r}_0) = G(\mathbf{r}_0, \mathbf{r}) - ik_1 \int_S p(\mathbf{r}_s, \mathbf{r}_0) G(\mathbf{r}_s, \mathbf{r}) \left(\beta(\mathbf{r}_s) - \beta_c\right) ds(\mathbf{r}_s). \tag{2.126}$$

This integral equation is a completely equivalent to the original boundary value problem, *i.e.* the integral equation has exactly one solution, and the solution satisfies the original boundary value problem. This integral equation is, of course, not new, and is stated in [84] but without a rigorous derivation.

2.3 Summary

This chapter has been concerned with describing mathematically the influence of near-surface inhomogeneities on the reflection of air-borne acoustic fields at a rigid porous ground surface, and two approaches to the problem were considered. In both approaches, the complex acoustic pressure at a point in the upper half-space was determined when the plane boundary was insonified by a monofrequency point source at a point also in the upper half-space. In the first approach, the transmitted acoustic fields that become incident on the inhomogeneity are scattered, and the boundary value problem could be stated through the various boundary conditions on the inhomogeneity, the plane boundary and in the upper and lower media. The surface of the inhomogeneity was assumed smooth and rigid. Two integral equation reformulations of this boundary value problem were considered, but the second was discarded in favour of the first for the reasons mentioned in section 2.2.1.

In the second approach, any near-surface inhomogeneities were assumed to induce a surface impedance at the plane boundary above the inhomo-

geneity. With the condition of local reaction at the plane boundary, the boundary value problem could be stated through the boundary conditions at the plane boundary and in the upper medium. The reformulation of this boundary value problem in terms of an integral equation was straightforward.

It has been seen in these two approaches, that Green's functions are required for a various source and receiver configurations, and these are discussed in the next chapter.

Chapter 3

The Green's functions

It was seen in the previous chapter that Green's functions and their derivatives for sound propagation in the presence of two media for various source and receiver configurations were required. It is the purpose of this chapter to derive expressions for these, and the chapter begins with a formulation of the Green's functions in terms of a boundary value problem with subsequent reformulation as integral representations. Although this is quite standard material, it is instructive in that it explains the basis for the various starting points adopted by many of the authors. Irrespective of their manner of formulation, it turns out that the integrals cannot be expressed in terms of known functions, and approximate methods of evaluation have to be employed. The following two sections then derive approximate expressions for the reflected and transmitted fields in porous media respectively, considering both externally reacting and locally reacting boundaries. A discussion of how ground acoustic characteristics are modelled then follows, with the chapter being concluded by a brief summary.

3.1 Formulation of the Green's functions

Let U_+ be the upper half-space, characterised by real impedance and wave number, Z_1, k_1, respectively. Let $U_- := \mathbf{R}^3 \backslash \overline{U}_+$ denote the porous medium characterised by complex impedance and wavenumber, Z_2, k_2 respectively, and $\Gamma := \{(x, y, z) \in \mathbf{R}^3 | z = 0\}$, the boundary between the two half-spaces.

It is intended to determine the value of the complex acoustic pressure, $G(\mathbf{r}, \mathbf{r}_0)$ at the point $\mathbf{r} \in \mathbf{R}^3$, given a monofrequency point source at $\mathbf{r}_0 \in \mathbf{R}^3$. The complex acoustic pressure is assumed to satisfy the following boundary value problem:
an inhomogeneous Helmholtz equation for $\mathbf{r} \in U_+$,

$$(\nabla^2 + k_1^2)G(\mathbf{r}, \mathbf{r}_0) = \delta(\mathbf{r} - \mathbf{r}_0), \tag{3.1}$$

a homogeneous Helmholtz equation for $\mathbf{r} \in U_-$,

$$(\nabla^2 + k_2^2)G(\mathbf{r}, \mathbf{r}_0) = \alpha\delta(\mathbf{r} - \mathbf{r}_0), \tag{3.2}$$

where $\alpha = (Z_2 k_2)/(Z_1 k_1)$, and the boundary conditions of continuity of complex acoustic pressure for $\mathbf{r} \in \Gamma$,

$$G_+(\mathbf{r}, \mathbf{r}_0) = G_-(\mathbf{r}, \mathbf{r}_0), \tag{3.3}$$

continuity of normal velocity for $\mathbf{r} \in \Gamma$,

$$\alpha \frac{\partial G_+(\mathbf{r}, \mathbf{r}_0)}{\partial z} = \frac{\partial G_-(\mathbf{r}, \mathbf{r}_0)}{\partial z}. \tag{3.4}$$

Finally, the Sommerfeld radiation conditions, that, for $\mathbf{r} \in U_+$, uniformly in $\mathbf{r}$ as $r := |\mathbf{r}| \to \infty$,

$$\left.\begin{aligned} \tfrac{\partial G(\mathbf{r}, \mathbf{r}_0)}{\partial r} - ik_1 G(\mathbf{r}, \mathbf{r}_0) &= o(r^{-1}), \\ G(\mathbf{r}, \mathbf{r}_0) &= O(r^{-1}), \end{aligned}\right\} \tag{3.5}$$

and for $\mathbf{r} \in U_-$, uniformly in $\mathbf{r}$ as $r := |\mathbf{r}| \to \infty$,

$$\left.\begin{aligned} \tfrac{\partial G(\mathbf{r}, \mathbf{r}_0)}{\partial r} - ik_2 G(\mathbf{r}, \mathbf{r}_0) &= o(r^{-1}), \\ G(\mathbf{r}, \mathbf{r}_0) &= O(r^{-1}). \end{aligned}\right\} \tag{3.6}$$

The above boundary value problem completely defines $G(\mathbf{r}, \mathbf{r}_0)$ for all possible configurations of source and receiver.

Due to the cylindrical symmetry of this problem, the above equations can be re-expressed in terms of cylindrical coordinates, and the problem can then be reformulated as integrals by applying the Hankel transform. For brevity,

the reformulation is restricted here to the case when $\mathbf{r}_0 \in U_+$. Equations (3.1) and (3.2) can be written as, assuming, without loss of generality, that $\mathbf{r}_0 = (0, 0, z_0)$, and writing $G(r, z)$ for $G(\mathbf{r}, \mathbf{r}_0)$,

$$\left(\frac{\partial^2}{\partial z^2} + \frac{\partial^2}{\partial r^2} + \frac{1}{r}\frac{\partial}{\partial r} + k_1^2\right) G(r, z) = \delta(x)\delta(y)\delta(z - z_0), \tag{3.7}$$

for $z > 0$, and,

$$\left(\frac{\partial^2}{\partial z^2} + \frac{\partial^2}{\partial r^2} + \frac{1}{r}\frac{\partial}{\partial r} + k_2^2\right) G(r, z) = 0, \tag{3.8}$$

for $z < 0$, where the Laplacian has been written in cylindrical polar coordinates, in which there is no θ dependence due to the symmetry. Also, equations (3.2) and (3.3) can be written as,

$$G_+(r, 0) = \alpha G_-(r, 0), \tag{3.9}$$

and,

$$\frac{\partial G_+(r, 0)}{\partial z} = \frac{\partial G_-(r, 0)}{\partial z}. \tag{3.10}$$

Applying the Hankel transform to equation (3.8) gives,

$$\mathcal{F}\left\{\frac{\partial^2 G(r, z)}{\partial z^2} + k_2^2 G(r, z)\right\} + \mathcal{F}\left\{\frac{\partial^2 G(r, z)}{\partial r^2} + \frac{1}{r}\frac{\partial G(r, z)}{\partial r}\right\} = 0, \tag{3.11}$$

where the Hankel transform is defined as [88],

$$\hat{f}(K, z) = \mathcal{F}(f(r, z)) = \frac{1}{2\pi}\int_0^\infty r f(r, z) J_0(Kr) dr, \tag{3.12}$$

and the inverse Hankel transform as,

$$f(r, z) = \mathcal{F}^{-1}(\hat{f}(K, z)) = 2\pi \int_0^\infty K \hat{f}(K, z) J_0(Kr) dK. \tag{3.13}$$

Expanding the second term on the left hand side of equation (3.11) and making use of Bessel's equation which gives that,

$$K^2 r^2 J_0''(Kr) + Kr J_0'(Kr) + K^2 r^2 J_0(Kr) = 0, \tag{3.14}$$

reduces equation (3.11) to,

$$\frac{\partial^2 \hat{G}(r, z)}{\partial z^2} + (k_2^2 - K^2)\hat{G}(r, z) = 0, \tag{3.15}$$

for $z < 0$, and where $\hat{G}$ is the Hankel transform of G. From the standard solution for differential equations of this form,

$$\hat{G}(K,z) = A(K)e^{i\nu_2 z} + B(K)e^{-i\nu_2 z}, \tag{3.16}$$

where $\nu_2 = (k_2^2 - K^2)^{\frac{1}{2}}$. If ν_2 is defined so that $Im\nu_2 \geq 0$ and $Re\nu_2 \geq 0$, the Sommerfeld radiation condition is satisfied only if $A(K) = 0$, which gives for $z < 0$,

$$\hat{G}(K,z) = B(K)e^{-i\nu_2 z}. \tag{3.17}$$

Following a similar procedure, $\hat{G}(K,z)$, for $z > 0$, is given as,

$$\hat{G}(K,z) = A(K)e^{i\nu_1 z} + \frac{e^{i\nu_1|z-z_0|}}{2i\nu_1}, \tag{3.18}$$

where $\nu_1 = (k_1^2 - K^2)^{\frac{1}{2}}$, $Im\nu_1 \geq 0$ and $Re\nu_1 \geq 0$ The functions $A(K)$ and $B(K)$ in equations (3.17) and (3.18) are obtained through applying the Hankel transform to the boundary conditions, equations (3.9) and (3.10), on Γ. Applying the Hankel transform to these equations gives,

$$\hat{G}_+(K,0) = \alpha\hat{G}_-(K,0), \tag{3.19}$$

and,

$$\frac{\partial\hat{G}_+(K,0)}{\partial z} = \frac{\partial\hat{G}_-(K,0)}{\partial z}. \tag{3.20}$$

By substituting equations (3.17) and (3.18) into equations (3.19) and (3.20), $A(K)$ and $B(K)$ are determined to be,

$$A(K) = \frac{1}{2i}\frac{(\alpha - \nu_2/\nu_1)}{(\nu_2 + \nu_1\alpha)}e^{i\nu_1 z_0}, \tag{3.21}$$

and,

$$B(K) = \frac{1}{i(\nu_2 + \nu_1\alpha)}e^{i\nu_1 z_0}. \tag{3.22}$$

Equation (3.18) may now be written,

$$\hat{G}(K,z) = \frac{1}{2i}\frac{(\alpha - \nu_2/\nu_1)}{(\nu_2 + \nu_1\alpha)}e^{i\nu_1(z_0+z)} + \frac{e^{i\nu_1|z-z_0|}}{2i\nu_1}, \tag{3.23}$$

and applying the inverse Hankel transform gives,

$$G(r,z) = 2\pi \int_0^\infty K \left\{ \frac{1}{2i} \frac{(\alpha - \nu_2/\nu_1)}{(\nu_2 + \nu_1\alpha)} e^{i\nu_1(z_0+z)} + \frac{e^{i\nu_1|z-z_0|}}{2i\nu_1} \right\} J_0(Kr)dK; \tag{3.24}$$

for $z > 0$; also, equation (3.17) may be written,

$$\hat{G}(K,z) = \frac{e^{i(\nu_1 z_0 - \nu_2 z)}}{i(\nu_2 + \nu_1\alpha)}, \tag{3.25}$$

and again, applying the inverse Hankel transform gives,

$$G(r,z) = 2\pi \int_0^\infty K \frac{e^{i(\nu_1 z_0 - \nu_2 z)}}{i(\nu_2 + \nu_1\alpha)} J_0(Kr)dK. \tag{3.26}$$

for $z < 0$. Integral representations have thus been formulated for the Green's functions for the problem of sound propagation in two media, where the source is positioned in the upper medium. Approximations to equations (3.24) and (3.26) are now considered in detail.

3.2 The reflected wave field

This section considers the approximate solutions to equation (3.24) for the total field above the plane surface firstly, when it is externally reacting and secondly, when it is locally reacting. It will be seen that the result for a locally reacting boundary may be deduced, under the approximation $|n^2| \gg 1$, from that for a semi-infinite externally reacting half space.

Rewriting equation (3.23) slightly differently and then applying the inverse Hankel transform gives equations that have been obtained by Rudnick [66], and Briquet *et al* [67], and alternative forms have been used by other authors [69,73,74,77], where they have separated out reflected components either from a rigid boundary or a pressure release boundary. The method of ***subtraction of the pole*** has been used by several authors for solution of these equations [69,77]. Attenborough *et al* [71] have given expressions for the results of this procedure for a porous lower half space, and also, if $k_1 R_1 \gg 1$, then the results reduce to (see figure 3.1),

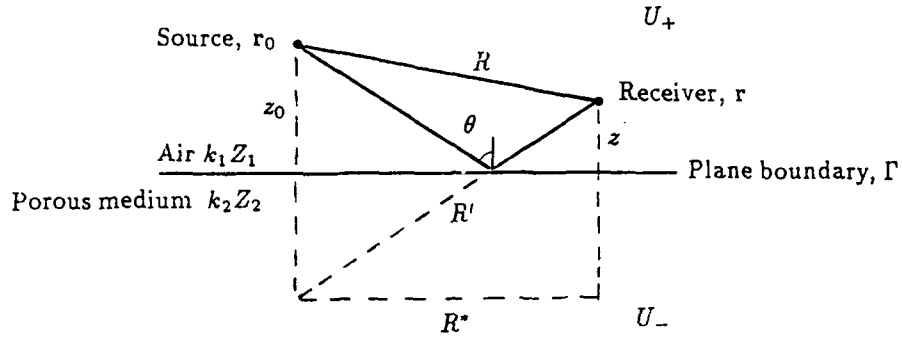

Figure 3.1 Geometry for propagation over a plane boundary

$$G(\mathbf{r},\mathbf{r}_0) = -\left(\frac{e^{ik_1R}}{4\pi R} + R_p\frac{e^{ik_1R'}}{4\pi R'} + B(1-R_p)F(w)\frac{e^{ik_1R'}}{4\pi R'}\right), \qquad (3.27)$$

where, R_p is the plane wave reflection coefficient defined by equation (2.29), $R = |\mathbf{r}-\mathbf{r}_0| = (R^{*2}+(z-z_0)^2)^{\frac{1}{2}}$, and $R' = |\mathbf{r}-\mathbf{r}_0'| = (R^{*2}+(z-z_0)^2)^{\frac{1}{2}}$, $\mathbf{r}_0'$ being the image of $\mathbf{r}_0$ in the boundary, and $R^* = ((x-x_0)^2+(y-y_0)^2)^{\frac{1}{2}}$,

$$B = \frac{B_N}{B_D}, \qquad (3.28)$$

where,

$$\begin{aligned} B_N &= (cos\theta+\beta)(1-n^{-2})^{\frac{1}{2}}\left[(1-\alpha^{-2})^{\frac{1}{2}}\right. \\ &\quad \left.+\alpha^{-1}n(1-n^{-2})^{\frac{1}{2}}cos\theta + sin\theta(1-\alpha^{-2}n^2)^{\frac{1}{2}}\right]^{\frac{1}{2}}, \qquad (3.29) \end{aligned}$$

and,

$$\begin{aligned} B_D &= (cos\theta+\alpha^{-2}((n^2-1)/(1-\alpha^{-2}))^{\frac{1}{2}}) \\ &\quad \times(1-sin^2\theta/n^2)^{\frac{1}{2}}(1-\alpha^2)^{\frac{3}{2}}(2sin\theta)^{\frac{1}{2}}(1-\alpha^{-2}n^2)^{\frac{1}{4}}, \qquad (3.30) \end{aligned}$$

$$F(w) = 1 + i\pi^{\frac{1}{2}}we^{-w^2}erfc(-iw) \qquad (3.31)$$

erfc being the error function, and the numerical distance w is defined by,

$$w^2 \approx \frac{ik_1R_2}{2}[cos\theta_0 + \beta_c(1-n^{-2})^{\frac{1}{2}}/(1-\alpha^{-2})^{\frac{1}{2}}]^2. \qquad (3.32)$$

Away from grazing incidence, the third term in equation (3.27) (the so-called *ground wave* term) is negligible, and a simple approximation to this equation is,

$$G(\mathbf{r},\mathbf{r}_0) = -\left(\frac{e^{ik_1R}}{4\pi R} + R_p\frac{e^{ik_1R'}}{4\pi R'}\right). \tag{3.33}$$

By a simple manipulation of equation (2.30), R_p is calculated by,

$$R_p = \frac{\alpha cos\theta - (n^2 - sin^2\theta)^{\frac{1}{2}}}{\alpha cos\theta + (n^2 - sin^2\theta)^{\frac{1}{2}}}, \tag{3.34}$$

where $cos\theta = (z + z_0)/R'$, $sin\theta = R^*/R'$. $G(\mathbf{r},\mathbf{r}_0)$ of equation (3.33) along with equation (3.34) for R_p is calculated by subroutine G11 found in appendix D. If both source and receiver are in the lower medium ($z, z_0 \leq 0$) then,

$$G(\mathbf{r},\mathbf{r}_0) = -\alpha\left(\frac{e^{ik_2R}}{4\pi R} + R_p\frac{e^{ik_2R'}}{4\pi R'}\right), \tag{3.35}$$

and in this case,R_p is calculated by,

$$R_p = \frac{\alpha^{-1}cos\theta - (n^{-2} - sin^2\theta)^{\frac{1}{2}}}{\alpha^{-1}cos\theta + (n^{-2} - sin^2\theta)^{\frac{1}{2}}}. \tag{3.36}$$

$G(\mathbf{r},\mathbf{r}_0)$ of equation (3.35) along with equation (3.36) for R_p is calculated by subroutine G22 found in appendix D.

The first derivative of $G(\mathbf{r},\mathbf{r}_0)$ for $\mathbf{r}_0, \mathbf{r} \in U_-$ as defined by equation (3.35) can be written as,

$$\nabla G(\mathbf{r},\mathbf{r}_0) = -\frac{\alpha}{4\pi}\left[\nabla\left(\frac{e^{ik_2R}}{R}\right) + \nabla\left(R_p\frac{e^{ik_2R'}}{R'}\right)\right]. \tag{3.37}$$

Writing,

$$f(\hat{R}) = \frac{e^{ik_2\hat{R}}}{\hat{R}}, \tag{3.38}$$

where, $\hat{R} = R$ or R',

$$\begin{aligned}\nabla f(R) &= \frac{\partial f(R)}{\partial R}\nabla R, \\ &= \left(\frac{ik_2R - 1}{R^3}\right)e^{ik_2R}[(x - x_0),(y - y_0),(z - z_0)]^T,\end{aligned} \tag{3.39}$$

where T is the transpose, and,

$$\begin{aligned}\nabla(R_p f(R')) &= R_p \nabla f(R') + f(R')\nabla R_p, \\ &= R_p \frac{\partial f(R')}{\partial R'}\nabla R' + f(R')\frac{dR_p}{d\theta}\nabla\theta, \end{aligned} \tag{3.40}$$

$$\frac{\partial f(R')}{\partial R'} = \frac{ik_2R' - 1}{sin^2\theta}e^{ik_2R'}, \tag{3.41}$$

$$\nabla R' = \frac{1}{R'}\left[(x - x_0),(y - y_0),(z - z_0)\right]^T, \tag{3.42}$$

$$\frac{dR_p}{d\theta} = -\frac{2\alpha sin\theta}{(cos\theta + \alpha(n^{-2} - sin^2\theta)^{\frac{1}{2}})^2}\left[(n^{-2} - sin^2\theta)^{\frac{1}{2}} - \frac{cos^2\theta}{(n^{-2} - sin^2\theta)^{\frac{1}{2}}}\right], \tag{3.43}$$

and,

$$\nabla\theta = \frac{1}{R'}\left[-\frac{cos\theta}{R^*}(x - x_0), -\frac{cos\theta}{R^*}(y - y_0), sin\theta\right]^T. \tag{3.44}$$

$\nabla G(\mathbf{r}, \mathbf{r}_0)$ of equation (3.37), along with the expression for R_p given by equation (3.36) is calculated using subroutine G22DER found in appendix D.

3.2.1 The locally reacting boundary

If $|n^2| \gg 1$ (so that as was seen in section 2.1, the boundary is locally reacting), and if $|n/\alpha| < 1$, $|\alpha| \gg$ ', then it is possible to obtain an expression similar to that of (3.48) of reference [89]. Further approximations for $|n/\alpha| \ll 1$ and $\theta \approx \pi/2$ gives,

$$G(\mathbf{r}, \mathbf{r}_0) \approx \frac{e^{ik_1R_1}}{4\pi R_1} + [R_p + (1 - R_p)F(p_e)]\frac{e^{ik_1R_2}}{4\pi R_2}, \tag{3.45}$$

where F is defined as above with p_e given by,

$$p_e^2 = \frac{ik_1R_2}{2}(cos\theta + \beta_c)^2 \tag{3.46}$$

replacing w and,

$$R_p = \frac{cos\theta - \beta_c}{cos\theta + \beta_c} \tag{3.47}$$

This form of solution is known as the Weyl-van der Pol solution. It was first suggested by Rudnick [66], based on the earlier work of Norton [64,65]

and others [90]. $G(\mathbf{r}_0, \mathbf{r})$ is calculated by equation (3.45) using subroutine G11WVDP found in appendix D.

Integral representations for the reflected wave field, similar to equation (3.24), may be obtained by applying a Hankel transform to the boundary value problem in the locally reacting case. Various authors have studied the reformulation of the inverse Hankel transform representation into a form where the integrand is more suitable for numerical integration, notably Thomasson [73]. Recently, Chandler-Wilde [91,92] has proposed a representation for grazing incidence which can be evaluated accurately, provided $kR \gg 0.5$, using numerical integration, *i.e.*,

$$\begin{aligned} G(\mathbf{r}, \mathbf{r}_0) &= -\frac{e^{ikR}}{2\pi R} + \frac{k\beta}{2\pi} e^{ikR} \int_0^\infty t^{-\frac{1}{2}} e^{-kRt} g(t) dt \\ &\quad + \frac{k\beta}{4} H_0^{(1)}(kR\sqrt{1-\beta^2}) erfc(e^{\frac{-i\pi}{4}} \sqrt{kR}\sqrt{a_+}), \end{aligned} \tag{3.48}$$

where,

$$g(t) = f(t) - \frac{\frac{1}{2} e^{-\frac{i\pi}{4}} \sqrt{a_+} e^{-ikR\sqrt{1-\beta^2}} H_0^{(1)}(kR\sqrt{1-\beta^2})}{(t - ia_+)}, \tag{3.49}$$

$$a_+ = 1 - \sqrt{1-\beta^2}, \tag{3.50}$$

and, $Re(\sqrt{a_+})$, $Re(\sqrt{1-\beta^2}) \gg 0$, and the integral in equation (3.48) is evaluated essentially by Gauss-Laguerre quadrature, by the subroutine PBETA3 [93].

3.3 The transmitted wave field

This section considers the approximate solutions to equation (3.26) for the total field beneath the plane surface.

Starting from the inverse Hankel transform given in equation (3.26), Richards *et al* [5] show, via a deformation of the path of integration to a steepest descent path, that if n has an appreciable imaginary component,

$$G(\mathbf{r}, \mathbf{r}_0) \approx exp\left[-ik_1 z(n^2 - sin^2\theta)^{\frac{1}{2}}\right] G(\mathbf{r}_\Gamma, \mathbf{r}_0) \tag{3.51}$$

where z is the depth beneath the plane boundary to the receiver point,

$$G(\mathbf{r}_\Gamma, \mathbf{r}_0) = -\frac{e^{ik_1 R^\Gamma}}{4\pi R^\Gamma} + R_p \frac{e^{ik_1 R^\Gamma}}{4\pi R^\Gamma}. \tag{3.52}$$

and,

$$R^\Gamma = \left((x - x_0)^2 + (y - y_0)^2 + z_0^2\right)^{\frac{1}{2}}, \tag{3.53}$$

R_p is defined as in equation (3.34).

The first derivative of $G(\mathbf{r}, \mathbf{r}_0)$ for $\mathbf{r}_0 \in U_+$, $\mathbf{r} \in U_-$ can be written as,

$$\nabla G(\mathbf{r}, \mathbf{r}_0) = \frac{\partial G}{\partial R^\gamma} \nabla R^\gamma - ik_1 (n^2 - sin^2\theta)^{\frac{1}{2}} G(\mathbf{r}_\Gamma, \mathbf{r}_0), \tag{3.54}$$

where,

$$\begin{aligned} \frac{\partial G(\mathbf{r}, \mathbf{r}_0)}{\partial R^\gamma} &= G(\mathbf{r}, \mathbf{r}_0)\Big(\frac{sin\theta}{R_\Gamma}(iK_1 R_\Gamma - 1) - \frac{1}{\alpha cos\theta + (n^2 - sin^2\theta)^{\frac{1}{2}}} \\ &\quad \times \left[\frac{sin\theta}{R_\Gamma}(n^2 - sin^2\theta)^{\frac{1}{2}} - \frac{1}{(n^2 - sin^2\theta)^{\frac{1}{2}}} sin\theta cos\theta \frac{cos\theta}{R_\Gamma}\right] \\ &\quad + \frac{1}{(n^2 - sin^2\theta)^{\frac{1}{2}}} ik_1 z sin\theta cos\theta \frac{cos\theta}{R_\Gamma}, \end{aligned} \tag{3.55}$$

$$\nabla R^\gamma = \frac{1}{R^\gamma}[(x - x_0), (y - y_0)], \tag{3.56}$$

and,

$$R^\gamma = \left((x - x_0)^2 + (y - y_0)^2\right)^{\frac{1}{2}}. \tag{3.57}$$

The calculation of $G(\mathbf{r}, \mathbf{r}_0)$ and $\nabla G(\mathbf{r}, \mathbf{r}_0)$ using equations (3.51) and (6.3) are carried out by subroutines G12 and G12DER respectively, found in appendix D.

3.4 The ground acoustic characteristics

The Green's functions derived in the previous section can only be calculated with knowledge of the propagation characteristics of the porous media. It is the purpose of this section to describe how the acoustical properties of such media may be modelled.

Delany and Bazley [94], by making measurements on many different fibrous sound absorbent materials whose porosities (Ω), were near unity, and

whose specific flow resistivities (σ) varied between 2000 and 80000 N.s.m^{-4}, were able to find a dependence of both the propagation constant and characteristic impedances of these materials on frequency, *i.e.*,

$$k_2 = 1 + 0.0978\left(\frac{f\rho}{\sigma}\right)^{-0.693} + 0.189\left(\frac{f}{\sigma}\right)^{-0.618} i, \qquad (3.58)$$

and,

$$Z_c = 1 + 0.0571\left(\frac{f\rho}{\sigma}\right)^{-0.754} + 0.087\left(\frac{f\rho}{\sigma}\right)^{-0.732} i. \qquad (3.59)$$

These relationships are semiempirical, in that power laws with $(f/\Omega\sigma)$ were expected from the theory for rigid porous media derived by Zwikker and Kosten [95]. Since $\Omega \approx 1$, for the fibrous materials under investigation, Delany and Bazley were able to replace the effective flow resistivity by the actual flow resistivity. The range of validity of equations (3.58) and (3.59) was stated originally as $0.01 < f\rho/\sigma < 1$. In a subsequent paper [96], Delany and Bazley proposed using equations (3.58) and (3.59) to model outdoor ground surfaces. In applying these equations, Delany and Bazely [7] and subsequent authors do not use the measured flow resistance, but rather a so-called effective flow resistance, σ_e. The effective flow resistivity may be quite different from the actual flow resistivity, and is estimated empirically from acoustical measurements. The effective flow resistivities of outdoor ground surfaces vary from 10000N.S.m^{-4} for loosely packed snow to over 25000000N.s.m^{-4} for Asphalt. A typical value of effective flow resistivity for grass covered ground might be 300000N.s.m^{-4}. For this value, the criterion $f/\sigma_e > 0.01$ would imply a lower limiting frequency for application of equations (3.58) and (3.59) of 2500 Hz.

The Delany and Bazley model has proved quite successful in describing the variation with frequency of the surface admittance of outdoor ground surfaces, see Chessell [35], Attenborough [97], and Embleton [98]. However, some surfaces are not modelled adequately by this model, and Attenborough [3] has proposed a *microstructural* model for ground surfaces. This study has taken the classical approach pioneered by Lord Rayleigh and by Zwikker and Kosten based upon a conceptual model of parallel cylindrical pores running normal to the surface of a rigid porous medium. Subsequent modifications

[3] have made possible inclusion of the effects of random pore orientation or deviations of the pore axes from straight lines along their lengths, (*i.e.* their *tortuosity*, q) and departures of the pore cross - section from that of a circular cylinder. The dependence of the characteristic impedance and propagation constant on frequency after these modifications are given as,

$$k_2^2 = \frac{q^2[1 + 2(\nu - 1)(N_{pr}^{\frac{1}{2}}\lambda\sqrt{i})^{-1}T(N_{pr}^{\frac{1}{2}}\lambda\sqrt{i})]}{[1 - 2(\lambda\sqrt{i})^{-1}T(\lambda\sqrt{i})]}, \tag{3.60}$$

and,

$$Z_2 = \frac{\omega\rho_2(\omega)}{k_2}, \tag{3.61}$$

where,

$$\rho_2(\omega) = \left(\frac{q^2}{\Omega}\right)\rho_0[1 - 2(\lambda\sqrt{i})^{-1}T(\lambda\sqrt{i})]^{-1}, \tag{3.62}$$

and $q^2 = \Omega^{-n'}$, n' being a grain shape factor, $T(x) = J_1(x)/J_0(x)$, J_0 and J_1 being cylindrical Bessel functions of the zeroth and first order respectively, $\nu(\approx 1.4)$ is the ratio of specific heats in air, $N_{pr}(\approx 0.72)$ is the Prandtl number, $\lambda = (1/s_f)(8\rho_0 q^2\omega/\Omega\sigma)^{\frac{1}{2}}$, s_f being the pore shape factor ratio. k_2, $\rho_2(\omega)$ and Z_2 are calculated by subroutines PC, CD and ZC found in appendix D.

Extreme pore shapes were considered to be those of a circular capillary and of a parallel - sided slit of infinite extent. Given those extremes, $1 > s_f > 0.6$. The lower limiting value has been found appropriate for lead shot and sand, where the grains are nearly spherical, whereas values from the mid range to the upper limiting value, together with $n' = 1$, model various soils, [9]. The equations (3.60) and (3.61) depend on four physical parameters which characterise the properties of the ground matrix, namely, Ω, n', s_f and σ. However, the use of four parameters is rather impractical for ground effect prediction, and Attenborough, [9], has deduced two pairs of simpler expressions, for $\lambda^2 \ll 1$. This condition corresponds to low frequency and/or high flow resistivity, and gives,

$$Z_2 \approx \frac{1}{k_2}\left[\frac{4q^2}{3\Omega} + \left(\frac{s_f^2\sigma}{\omega\rho_0}\right)i\right], \tag{3.63}$$

and,

$$k_2 \approx (\gamma\Omega)^{\frac{1}{2}} \left[\left(\frac{4}{3} - \left(\frac{\gamma - 1}{\gamma} \right) N_{pr} \right) \frac{q^2}{\Omega} + \frac{s_f^2 \sigma i}{\omega \rho_0} \right]^{\frac{1}{2}}. \tag{3.64}$$

Further approximations can be made for high flow resistivity and low frequency to these expressions, giving,

$$Z_2 = \frac{k_2}{\gamma\Omega} = (2\gamma\Omega)^{-\frac{1}{2}} s_f (\sigma/\omega\rho)^{\frac{1}{2}} (1+i). \tag{3.65}$$

If an effective flow resistivity $\sigma_e = s_f^2 \sigma/\Omega$ is introduced, equation (3.65) may be written as,

$$Z_2 = (4\pi\nu\rho)^{-\frac{1}{2}} (\sigma/f)^{-\frac{1}{2}} (1+i). \tag{3.66}$$

3.5 Summary

The Green's functions for propagation in the presence of a plane boundary have been presented, and table 3.1 is a summary of those derived , along with the names of the subroutines found in appendix D for their calculation.

r_0	r	$G(r_0, r)$	$\nabla G(r_0, r)$
U_+	U_+	(3.33) G11 (3.45) G11WVDP	Not required
U_+	U_-	(3.51) G12	(6.3) G12DER
U_-	U_+	(3.51) G12	(6.3) G12DER
U_-	U_-	(3.35) G22	(3.37) G22DER
Γ	Γ	(3.48) PBETA3	Not required

Table 3.1 The Green's functions and the subroutines for their calculation.

The Green's functions have all involved the plane wave reflection coefficient and for the case of the reflected wave, the ground wave term has been neglected. For the source/receiver geometries used in the numerical solution, this neglect is justified. This has resulted in simple expressions for the first derivatives of the Green's functions. An integral expression has been considered appropriate for the prediction of propagation from point to point on a locally reacting boundary.

Finally, this chapter considered the modelling of ground acoustic characteristics, with particular emphasis on the Four parameter model of Attenborough, that will be used extensively later.

Chapter 4

Induced surface impedance models

It was seen in chapter 2 that the second *surface inhomogeneity* approach to the theoretical problem regarded the near-surface inhomogeneity as inducing a variation in the surface impedance directly above it. The purpose of this chapter is to derive expressions for such induced surface impedance due to firstly, a layer, and secondly, due to an embedded sphere.

4.1 Rigidly backed layer

The simplest form of sub-surface structuring is that of a single layer above a semi-infinite medium. The surface impedance induced by such a layer can be deduced by following the analysis of Brekhovskikh [83], where plane waves are incident on a layer of thickness d, at an arbitrary angle of incidence. In the steady state, as a result of multiple reflections at the boundaries of the layer, two waves with different directions of propagation result in the layer. By considering the boundary conditions of continuity of pressure and normal particle velocity, and restricting analysis to normal incidence, the surface impedance can be shown to be given by,

$$Z = z_2 coth(-ik_2 d). \tag{4.1}$$

The induced surface impedance by a rigidly backed layer is calculated using subroutine ZL, found in appendix D.

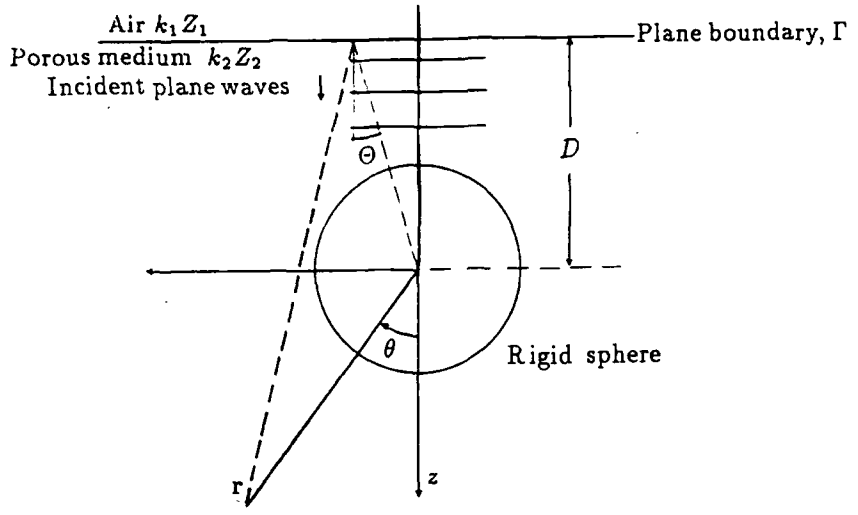

Figure 4.1 Reflection from the plane of a rigid porous half-space containing a rigid sphere

4.2 Medium containing a rigid sphere

Consider now the surface impedance induced by a near-surface rigid sphere. Figure 4.1 shows a rigid sphere labelled S, with surface ∂S, embedded in a porous half-space, characterised by a complex impedance Z_2 and a complex wavenumber, k_2.

The upper half-space, denoted U_+, contains air, and is assumed to be characterised by real impedance and wavenumber, Z_1 and k_1, respectively. The lower porous half-space, is denoted $U_- := \mathbf{R}^3 \backslash (\overline{S \bigcup U_+})$. The boundary between the upper and lower half spaces is denoted by: $\Gamma = \{(x, y, z) \in \mathbf{R}^3 | z = -D\}$, the sphere being centred on the origin. The boundary is assumed to have a sufficiently large complex refractive index such that the boundary is locally reacting.

Consider a plane wave incident on the plane boundary. The plane wave gives rise to a transmitted plane wave that propagates normal to the boundary with complex acoustic pressure $p_t(\mathbf{r})$ given by [84],

$$p_t(\mathbf{r}) = e^{ik_2 z}, \tag{4.2}$$

or, expressed in spherical coordinates (see figure 4.1),

$$\begin{aligned} p_t(\mathbf{r}) &= e^{ik_2 r cos\theta}, \\ &= \sum_{m=0}^{\infty} (2m+1) i^m P_m(cos\theta) j_m(k_2 r), \end{aligned} \tag{4.3}$$

where j_m denotes the spherical Bessel function of order m and $P_m(x)$ denotes the Legendre polynomial of degree m, as defined in Abramowitz and Stegun [99]. The corresponding velocity is given by,

$$\mathbf{v}_t(\mathbf{r}) = -\frac{i}{Z_2 k_2} \left[\hat{\mathbf{r}} \frac{\partial}{\partial r} + \hat{\theta} \frac{1}{r} \frac{\partial}{\partial \theta} + \hat{\phi} \frac{1}{r sin\theta} \frac{\partial}{\partial \phi} \right] p_t(\mathbf{r}), \tag{4.4}$$

where $\hat{\mathbf{r}}$, $\hat{\theta}$ and $\hat{\phi}$ are the unit vectors in the three axial directions. Due to the symmetry, $p_t(\mathbf{r})$ is independent of ϕ, and so,

$$\begin{aligned} \mathbf{v}_t(\mathbf{r}) &= -\frac{i}{Z_2 k_2} \sum_{m=0}^{\infty} (2m+1) i^m \left[\hat{\mathbf{r}} P_m(cos\theta) k_2 j'_m(k_2 r) \right. \\ &\quad \left. -\hat{\theta} P'_m(cos\theta) sin\theta j_m(k_2 r)/r \right], \end{aligned} \tag{4.5}$$

The field scattered from the sphere can be written in the form [84],

$$p_s(\mathbf{r}) = \sum_{m=0}^{\infty} a_m P_m(cos\theta) h_m^{(1)}(k_2 r), \tag{4.6}$$

where $h_m^{(1)}$ denotes the spherical Hankel function of the first kind of order m, and the corresponding velocity is,

$$\begin{aligned} \mathbf{v}_s(\mathbf{r}) &= -\frac{i}{Z_2 k_2} \sum_{m=0}^{\infty} a_m \left[\hat{\mathbf{r}} P_m(cos\theta) k_2 h_m^{(1)'}(k_2 r) \right. \\ &\quad \left. -\hat{\theta} P'_m(cos\theta) sin\theta h_m^{(1)}(k_2 r)/r \right]. \end{aligned} \tag{4.7}$$

The constants a_m can be determined by considering the boundary condition on the surface of the sphere. Insisting that the normal component of velocity is zero on the surface of the sphere, *i.e.*,

$$\hat{\mathbf{r}}.(\mathbf{v}_t(\mathbf{r}) + \mathbf{v}_s(\mathbf{r})) = 0, \tag{4.8}$$

for $\mathbf{r} \in \partial S$, gives,

$$\sum_{m=0}^{\infty} \left[(2m+1) i^m P_m(cos\theta) j'_m(k_2 R) + a_m P_m(cos\theta) h_m^{(1)'}(k_2 R) \right] = 0, \tag{4.9}$$

for $0 \leq \theta \leq \pi$, and thus,

$$a_m = -(2m+1)i^m \frac{j_m'(k_2R)}{h_m^{(1)'}(k_2R)}, \tag{4.10}$$

for $m = 0, 1, \ldots$. The induced surface impedance at the point $\mathbf{r} \in \Gamma$ is given by,

$$Z(\mathbf{r}) = \frac{p(\mathbf{r})}{\mathbf{n}.\mathbf{v}(\mathbf{r})}. \tag{4.11}$$

where $\mathbf{n}$ is the downward normal to the surface Γ, and, for $\mathbf{r} \in \Gamma$,

$$\begin{aligned} p(\mathbf{r}) &= p_t(\mathbf{r}) + p_s(\mathbf{r})(1+R_p) \\ &= e^{ik_2 z} + \sum_{m=0}^{\infty} P_m(cos\theta) a_m h_m^{(1)}(k_2 r)(1+R_p), \end{aligned} \tag{4.12}$$

and, for $\mathbf{r} \in U_-$,

$$\mathbf{n}.\mathbf{v}(\mathbf{r}) = -\frac{i}{k_2 Z_2} \mathbf{n}.\left[\nabla p_t(\mathbf{r}) + \nabla p_s(\mathbf{r}) + \nabla(R_p p_r(\mathbf{r}))\right], \tag{4.13}$$

where $p_r(\mathbf{r})$ denotes the wave that would be reflected back from the interaction of the scattered wave with the boundary if the boundary were perfectly rigid. Now, since for $\mathbf{r} \in \Gamma$,

$$\mathbf{n}.\nabla p_s(\mathbf{r}) = -\mathbf{n}.\nabla p_r(\mathbf{r}), \tag{4.14}$$

and,

$$p_s(\mathbf{r}) = p_r(\mathbf{r}), \tag{4.15}$$

$$\mathbf{n}.\mathbf{v}(\mathbf{r}) = -\frac{i}{Z_2 k_2} \mathbf{n}.\left[\nabla p_t(\mathbf{r}) + \nabla p_s(\mathbf{r})(1-R_p) + p_s(\mathbf{r})\nabla R_p\right]. \tag{4.16}$$

Now here, the plane wave reflection coefficient, R_p is defined as,

$$R_p = \frac{\alpha^{-1} cos\Theta - (n^{-2} - sin^2\Theta)^{\frac{1}{2}}}{\alpha^{-1} cos\Theta + (n^{-2} - sin^2\Theta)^{\frac{1}{2}}}, \tag{4.17}$$

where Θ is as defined in figure 4.1, so that,

$$\nabla R_p = \frac{dR_p}{d\Theta} \nabla\Theta. \tag{4.18}$$

Also, for $\mathbf{r} \in \Gamma$,

$$\Theta = \pi - \theta, \tag{4.19}$$

and,

$$\nabla\Theta = -\nabla\theta = -\frac{\hat{\theta}}{r}. \tag{4.20}$$

Thus, for $\mathbf{r} \in \Gamma$,

$$\begin{aligned}\mathbf{n}.\mathbf{v}(\mathbf{r}) &= -\frac{i}{Z_2}\left\{ie^{ik_2 z} + (1-R_p)\sum_{m=0}^{\infty} a_m \left[cos\theta P_m(cos\theta)k_2 h_m^{(1)\prime}(k_2 r)\right.\right. \\ &\quad \left. + P_m'(cos\theta)sin^2\theta h_m^{(1)}(k_2 r)/r\right] \\ &\quad \left.\times \frac{sin\theta}{r}\frac{dR_p}{d\Theta}\sum_{m=0}^{\infty} a_m P_m(cos\theta)h_m^{(1)}(k_2 r)\right\}. \end{aligned} \tag{4.21}$$

$Z(\mathbf{r})$, defined by equation (4.11), can be calculated using subroutines PLNSCATCOE and ZSPHERE found in appendix D.

Figure 4.2 shows the variation with radius of the surface impedance induced by an embedded rigid sphere, at the point directly above the sphere, where the depth (the closest point of the sphere to the plane boundary) is kept constant. Also shown is the surface impedance induced by a rigidly backed layer, and the impedance for a homogeneous medium. It can be seen that with increasing radius of the sphere, (for very small radii, the induced surface impedance in indestinguishable from that for the homogeneous medium), there is a gradual convergence to that for the rigidly backed layer case.

Figure 4.3 shows the variation with position of the surface impedance at 1kHz, induced by an embedded rigid sphere with different depths. It can be seen that the induced surface impedance due to the sphere is a very local effect, not surprisingly, at a position directly above the sphere.

4.3 Summary

Expressions for the induced surface impedance due to two different types of near-surface inhomogeneities have been presented. In the first section, the surface impedance induced by a rigidly backed layer of infinite extent was discussed and presented. The second section considered the surface impedance induced by an embedded finite sized inhomogeneity: a rigid

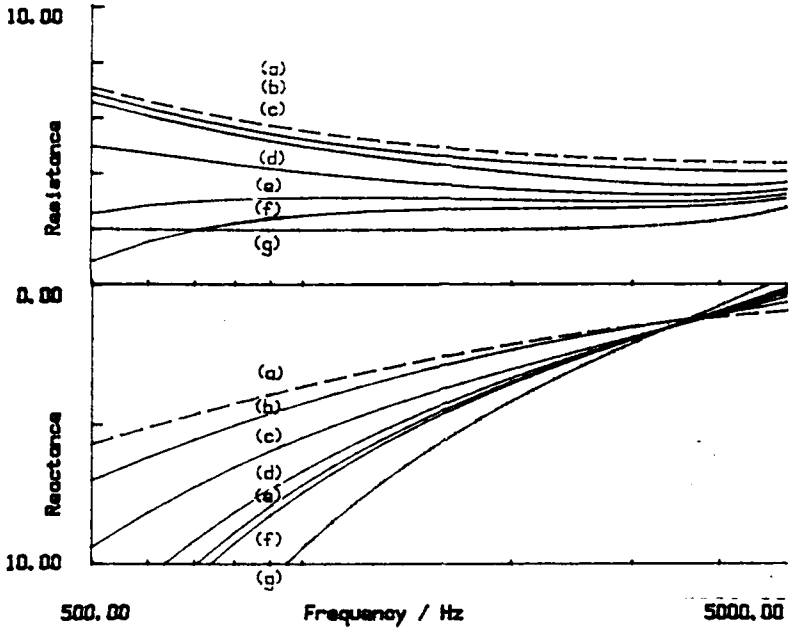

Figure 4.2 Variation with radius of the surface impedance induced by an embedded rigid sphere. The medium is characterised by the four parameters, $\sigma = 300,000\text{N.s.m}^{-4}$, $\Omega = 0.4$, $s_f = 0.75$ and $n' = 1$. Depth, d =0.01m. (a) Homogeneous (dashed), (b)radius=0.0125m, (c)radius=0.025m, (d)radius=0.05m, (e)radius=0.1m, (f)radius=0.2m, and (g)rigidly backed layer.

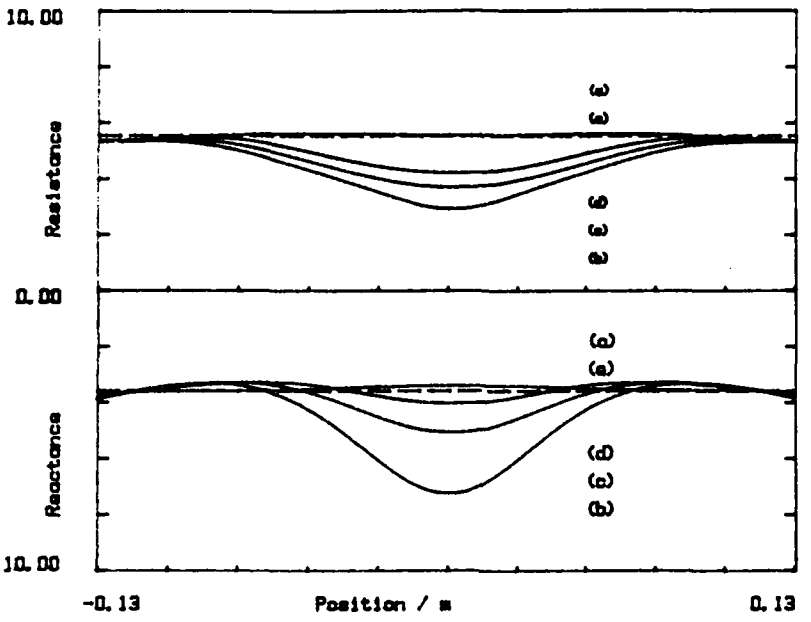

Figure 4.3 Variation with position of the surface impedance at 1kHz, induced by an embedded rigid sphere with different depths. Sphere radius = 0.125m. The medium is characterised by the four parameters, $\sigma = 300,000\text{N.s.m}^{-4}$,$\Omega = 0.4$, $s_f = 0.75$ and $n' = 1$. (a) Homogeneous (dashed), (b)depth, $d = 0.01$m, (c)depth, $d = 0.015$m, (d)depth, $d = 0.02$m, and (e)depth, $d = 0.04$m.

sphere. In both sections, the theory considered plane wave incidence with the first section considering the steady-state conditions; in the second, only the first interaction of the scattered wave from the rigid sphere with the plane boundary Γ was considered, and this interaction was approximated by using the plane wave reflection coefficient. Use of the more accurate spherical wave reflection coefficient would have resulted in some difficult algebra, and has not been pursued in this study.

Some results of calculating the surface impedance induced by a sphere were also presented. It was seen that there was convergence to the surface impedance induced by a rigidly backed layer, for increasing sphere radius.

Chapter 5

Solution of the boundary integral equations

In chapter 2, the mathematical formulation of the theoretical problem of acoustic scattering by a near-surface inhomogeneity was presented. The two treatments of the problem were first stated as boundary value problems, and then subsequently reformulated as boundary integral equations. The Green's functions and the models based on induced surface impedance arising from these formulations, were then presented in chapters 3 and 4. It is the purpose of this chapter to detail the solution of the boundary integral equations. The chapter considers the integral equations from the two approaches separately, including details of the scattering surfaces and the coefficient matrix structure and its solution. A section on the numerical tests and comparisons of the two approaches then follows with, finally, a brief summary of the chapter.

5.1 The numerical solution

Equations (2.104) and (2.126), restricted to $\mathbf{r} \in \mathbf{r}_s$ are particular examples of weakly singular Fredholm integral equations of the second kind. These equations are not, in general, amenable to analytic solution and numerical methods must be considered. A numerical solution, by a simple quadrature method as described by Mayers [100], can be obtained as follows. The range of integration is split into T sub-regions (*boundary elements*) , and

the values of the pressure field at the midpoints of these boundary elements are determined by producing and solving a set of linear equations obtained by making approximations for the acoustic field within each element in the integral equation, the number of linear equations being equal to the number of elements into which the integrating surface is split. The values of the pressure field on the integrating surface are then substituted back into the approximated integral equation to obtain values of the pressure field elsewhere.

For large problems, the major part of the computational labour required to calculate the solution is the solution of the linear equations, this stage becoming more labour intensive as the number of equations increases. The available solution techniques can be divided into two classes, 'direct' and 'iterative' methods. The iterative methods include Gauss-Seidel iteration and multigrid methods [101]. The direct methods can be divided into methods of general application (for example Gaussian elimination) and methods which use the structure of the coefficient matrix. It is this last category of methods of solution that is the most applicable to the sets of linear equations generated for axi-symmetric scattering surfaces.

The numerical solution of the integral equation for scattering by a near-surface rigid inhomogeneity has been confined here to inhomogeneities that are axisymmetric about an axis perpendicular to the plane boundary, and those considered in this study were *spheroids*. The advantage of choosing this shape was that its *ellipticity* or *flattening* could be varied while still, of course, maintaining its basic shape. Thus, the variation of the results for gradually flattening a sphere to the oblate spheroid shape could be obtained. Furthermore, results for oblate spheroids could be compared with other, more standard, results such as those for rigidly backed layers. The numerical solution of the integral equation for scattering by a surface inhomogeneity was confined to a finite *circular* surface inhomogeneity that were axisymmetric about an axis perpendicular to the plane boundary. The geometric restriction for both approaches simplified the numerical implementation and lead to structured matrices that were *block circulant*. Standard

packages are available for the solution of linear systems with this type of coefficient matrix as will be discussed later.

5.1.1 The first approach

The difficulty in the numerical solution of the integral equation (2.104) is that the kernel function tends to infinity as $\mathbf{r}$ approaches $\mathbf{r}_s$. This difficulty is resolved by applying the following modification of Burton [102]. For $\mathbf{r} \in \partial S$, equation (2.104) is written,

$$\begin{aligned}\alpha\frac{1}{2}p(\mathbf{r},\mathbf{r}_0) &= \alpha G(\mathbf{r}_0,\mathbf{r}) + \int_{\partial S} p(\mathbf{r}_s,\mathbf{r}_0)\frac{\partial G(\mathbf{r}_s,\mathbf{r})}{\partial n(\mathbf{r}_s)} - p(\mathbf{r},\mathbf{r}_0)\frac{\partial G_0(\mathbf{r}_s,\mathbf{r})}{\partial n(\mathbf{r}_s)}ds(\mathbf{r}_s) \\ &\quad + p(\mathbf{r},\mathbf{r}_0)\int_{\partial S}\frac{\partial G_0(\mathbf{r}_s,\mathbf{r})}{\partial n(\mathbf{r}_s)}ds(\mathbf{r}_s), \qquad (5.1)\end{aligned}$$

where $G_0(\mathbf{r}_1,\mathbf{r}_2) = -\alpha/(4\pi|\mathbf{r}_s - \mathbf{r}|)$ is the principal singularity of $G(\mathbf{r}_s,\mathbf{r})$. From Gauss' theorem, the last integral can be integrated exactly giving,

$$\int_{\partial S}\frac{\partial G_0(\mathbf{r}_s,\mathbf{r})}{\partial n(\mathbf{r}_s)}ds(\mathbf{r}_s) = -\frac{\alpha}{2}, \qquad (5.2)$$

for $\mathbf{r} \in \partial S$, and hence, equation (5.1) can be written as,

$$\alpha p(\mathbf{r},\mathbf{r}_0) = \alpha G(\mathbf{r}_0,\mathbf{r}) + \int_{\partial S} p(\mathbf{r}_s,\mathbf{r}_0)\frac{\partial G(\mathbf{r}_s,\mathbf{r})}{\partial n(\mathbf{r}_s)} - p(\mathbf{r},\mathbf{r}_0)\frac{\partial G_0(\mathbf{r}_s,\mathbf{r})}{\partial n(\mathbf{r}_s)}ds(\mathbf{r}_s). \qquad (5.3)$$

According to Burton [102], the new integrand, taken as a whole, remains finite as $\mathbf{r}$ approaches $\mathbf{r}_s$. Now, if the surface ∂S is split into T boundary elements, $\partial S_1, \partial S_2, \ldots, \partial S_T$, then from equation (5.3) it follows that,

$$\alpha p(\mathbf{r}_j,\mathbf{r}_0) = \alpha G(\mathbf{r}_0,\mathbf{r}_j) + \sum_{k=1}^{T} I_{jk}, \qquad (5.4)$$

for $j = 1(1)T$, where $\mathbf{r}_j$ is the midpoint of area element ∂S_j, and,

$$I_{jk} = \int_{\partial S_k} p(\mathbf{r}_s,\mathbf{r}_0)\frac{\partial G(\mathbf{r}_s,\mathbf{r}_j)}{\partial n(\mathbf{r}_s)} - p(\mathbf{r}_j,\mathbf{r}_0)\frac{\partial G_0(\mathbf{r}_s,\mathbf{r}_j)}{\partial n(\mathbf{r}_s)}ds(\mathbf{r}_s). \qquad (5.5)$$

For $j \neq k$, the approximation can be made that,

$$I_{jk} \approx A_k\left(p(\mathbf{r}_k,\mathbf{r}_0)\frac{\partial G(\mathbf{r}_k,\mathbf{r}_j)}{\partial n(\mathbf{r}_k)} - p(\mathbf{r}_j,\mathbf{r}_0)\frac{\partial G_0(\mathbf{r}_k,\mathbf{r}_j)}{\partial n(\mathbf{r}_k)}\right), \qquad (5.6)$$

where A_k is the area of ∂S_k, and for $j = k$,

$$I_{jk} \approx 0. \tag{5.7}$$

Thus the following linear equations are satisfied approximately by the unknown values $p(\mathbf{r}_j, \mathbf{r}_0)$:

$$\begin{aligned} \alpha p(\mathbf{r}_j, \mathbf{r}_0) &= \alpha G(\mathbf{r}_0, \mathbf{r}_j) + \sum_{k=1(k\neq j)}^{T} A_k \left(p(\mathbf{r}_k, \mathbf{r}_0) \frac{\partial G(\mathbf{r}_k, \mathbf{r}_j)}{\partial n(\mathbf{r}_k)} \right. \\ &\quad \left. - p(\mathbf{r}_j, \mathbf{r}_0) \frac{\partial G_0(\mathbf{r}_k, \mathbf{r}_j)}{\partial n(\mathbf{r}_k)} \right), \end{aligned} \tag{5.8}$$

for $j = 1(1)T$. These approximately satisfied set of T linear equations for the values of p at the midpoints $\mathbf{r}_k$ of ∂S_k can be written in the standard form,

$$\sum_{k=1}^{T} a_{jk} p(\mathbf{r}_k, \mathbf{r}_0) = \alpha G(\mathbf{r}_0, \mathbf{r}_j), \tag{5.9}$$

for $j = 1(1)T$ and where,

$$\begin{aligned} a_{jk} &= \left[\alpha + \sum_{i=1(i\neq j)}^{T} \frac{\partial G_0(\mathbf{r}_i, \mathbf{r}_j)}{\partial n(\mathbf{r}_i)} A_i \right] \delta_{jk} \\ &\quad - (1 - \delta_{jk}) \frac{\partial G(\mathbf{r}_k, \mathbf{r}_j)}{\partial n(\mathbf{r}_k)} A_k, \end{aligned} \tag{5.10}$$

where δ_{jk} is the Kronecker delta.

Once values of a_{jk} are determined, the values of p at the midpoints of the elements can be calculated. It is then a simple task to calculate values of $p(\mathbf{r}, \mathbf{r}_0)$ for $\mathbf{r} \in U_+$ by simple substitution into,

$$\alpha \kappa(\mathbf{r}) p(\mathbf{r}, \mathbf{r}_0) = \alpha G(\mathbf{r}_0, \mathbf{r}) + \sum_{j=1}^{T} p(\mathbf{r}_j, \mathbf{r}_0) \frac{\partial G(\mathbf{r}_j, \mathbf{r})}{\partial n(\mathbf{r}_j)} A_j. \tag{5.11}$$

The scattering surface

Here, only spheroidal scatterers are considered, and expressions for the area of each of the boundary elements along with expressions for the coordinates of the midpoints of these elements, and the inward normals at these midpoints are derived in this section.

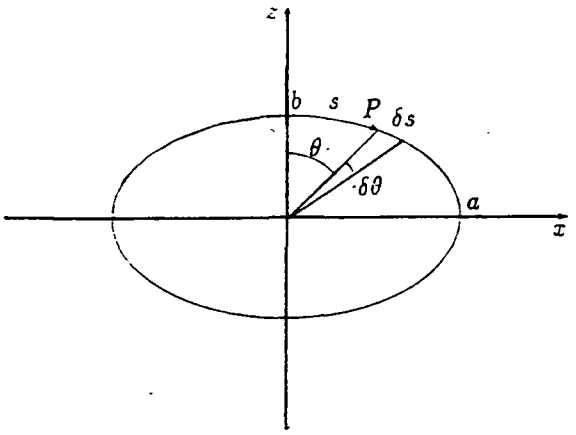

Figure 5.1 Section through an oblate spheroid scatterer

The mesh generation on the surface of the spheroid must be such that the maximum boundary element diameter is to be no greater than a value h, dependent upon the wavelength of the acoustic field. Consider the diagram in figure 5.1, which shows a section through the centre of an oblate spheroid. The spheroid is formed by rotating an ellipse about the z-axis, and the boundary elements are formed by first dividing the ellipse into elements, each of which subtending the same angle $\delta\theta$ at the origin. The arc length of ellipse corresponding to a typical element will be $\delta s \approx \delta\theta ds/d\theta$, where θ and s are the angle and arc length indicated in the figure. Thus, the maximum element length will be, approximately, $\delta\theta(ds/d\theta)_{max}$, and to ensure an element length no greater than h, the angle divisions must be no greater than,

$$\delta\theta = h/\left(\frac{ds}{d\theta}\right)_{max}. \tag{5.12}$$

To determine $ds/d\theta$ and $(ds/d\theta)_{max}$, consider the point P. $ds/d\theta$ is given by,

$$\frac{ds}{d\theta} = \frac{ds}{dx}/\frac{d\theta}{dx}. \tag{5.13}$$

From the defining equation for an ellipse,

$$\frac{x^2}{a^2} + \frac{z^2}{b^2} = 1, \tag{5.14}$$

$$\frac{dz}{dx} = -\frac{xb^2}{a^2 z}. \tag{5.15}$$

Now,

$$\frac{ds}{dx} = \pm\sqrt{1 + (\frac{dz}{dx})^2} = \pm\frac{1}{a^2 z}\sqrt{a^4 z^2 + b^4 x^2}. \tag{5.16}$$

Also,

$$\theta = tan^{-1}(z/x) + n\pi, \tag{5.17}$$

and, using equation (5.15),

$$\frac{d\theta}{dx} = -\frac{b^2}{z(x^2 + z^2)}. \tag{5.18}$$

Thus, since $ds/d\theta > 0$,

$$\frac{ds}{d\theta} = \frac{(x^2(a^2 - b^2) + b^2 a^2)}{a^4 b}\sqrt{a^4 + x^2(b^2 - a^2)}. \tag{5.19}$$

Letting $A = a^2$, $B = b^2$, and $X = x^2$, then,

$$\frac{d}{dX}\left(\frac{ds}{d\theta}\right) = \frac{(A - B)[A(2A - B) + 3X(B - A)]}{2A^2 b\sqrt{A^2 + X(B - A)}} \tag{5.20}$$

Clearly, this is continuous in the range $0 \leq X \leq A$, and,

$$\frac{d}{dX}\left(\frac{ds}{d\theta}\right) = 0, \tag{5.21}$$

in this range only possibly at $X = A(2A - B)/3(A - B)$. Also,

$$\frac{d}{dX}(\frac{ds}{d\theta}) = \frac{(A - B)(2A - B)}{2A^2 b} > 0, \tag{5.22}$$

at $X = 0$ and,

$$\frac{d}{dX}(\frac{ds}{d\theta}) = \frac{(A - B)(2B - A)}{2ABa} \tag{5.23}$$

at $X = A$. Now, if $2B \geq A > B$, then $ds/d\theta$ is strictly increasing as X increases from 0 to A, and thus $ds/d\theta$ achieves its maximum at $X = A$. If $A > 2B$ then,

$$\frac{d}{dX}(\frac{ds}{d\theta}) \begin{cases} > 0 & \text{for } 0 \leq X \leq A(2A - B)/3(A - B) \\ < 0 & \text{for } A \geq X > A(2A - B)/3(A - B) \end{cases} \tag{5.24}$$

where $A(2A - B)/3(A - B)$ lies in the range $[0, A]$, and thus, $ds/d\theta$ achieves its maximum value at $X = A(2A - B)/3(A - B)$. Thus, if $2B \geq A > B$ then,

$$\left(\frac{ds}{d\theta}\right)_{max} = a \tag{5.25}$$

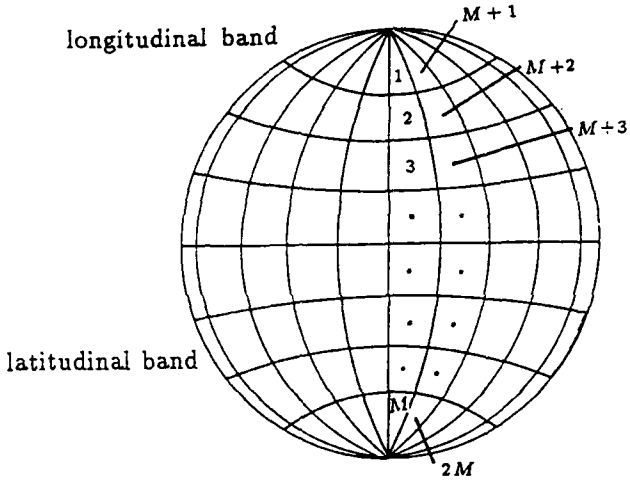

Figure 5.2 Element configuration for a sphere, including numbering system for the elements

and if $A > 2B$, then,

$$\left(\frac{ds}{d\theta}\right)_{max} = \frac{2}{3\sqrt{3}} \frac{(a^2 + b^2)^{3/2}}{ab} \tag{5.26}$$

Equation (5.12), along with equations (5.25) and (5.26) the values of h, can be used to calculate the maximum values of $\delta\theta$. The spheroid is now divided up into a number M, of *latitudinal bands*, and a number N, of longitudinal bands, see figure 5.2 for a sphere, $(A = B)$. The minimum number, M, of latitudinal bands running around the z-axis of the spheroid, for a given maximum value of h, *i.e.* in effect, the minimum number of arcs of length δs, will then be,

$$M = \left|\frac{\pi}{\delta\theta}\right|. \tag{5.27}$$

To have elements that have a diameter no bigger than h, the minimum number N , of longitudinal bands must be,

$$N = 2M. \tag{5.28}$$

The area of each boundary element, A_j, can be calculated by determining the total area of the latitudinal band it is in, and dividing by the total

number of longitudinal bands, N, *i.e.*,

$$A_j = \frac{2\pi}{N}\int_{\theta_1}^{\theta_2} Rsin\theta Rd\theta \approx 2\pi Rsin\theta\delta s, \tag{5.29}$$

where R in the distance from the centre of the spheroid to the midpoint of the boundary element. Thus, the area of each boundary element in any latitudinal band will be equal. Using the numbering system of the boundary elements as in figure 5.2, where the example in the figure is that of a sphere, the coordinates of the midpoint of element j (the mth latitudinal band crossed with the nth longitudinal band) is calculated by,

$$\begin{aligned} x_j &= Rsin\theta_m cos\phi_n, \\ y_j &= Rsin\theta_m sir\phi_n, \\ z_j &= Rcos\theta_m, \end{aligned} \tag{5.30}$$

for $m = 1(1)M$, $n = 1(1)N$ and where θ_m and ϕ_n are the angles subtended by the midpoint of the element from the z-axis and the x-axis in the xy plane, respectively, calculated by,

$$\theta_m = (\frac{1}{2} + (m-1))\delta\theta, \tag{5.31}$$

and,

$$\phi_n = ((n-1))\delta\phi. \tag{5.32}$$

Thus, the midpoints of the first longitudinal band are positioned along the xz plane. the first boundary element of this band being positioned at $\theta = \theta_1 = \delta\theta/2$. Furthermore, the components of the inward normal (*i.e.* the normal directed towards the centre of the spheroid) at these midpoints, are calculated by,

$$\begin{aligned} n_x &= -(1+(\nabla \mathbf{n})^2)^{-\frac{1}{2}} cos\phi_n \mathbf{i}, \\ n_y &= -(1+(\nabla \mathbf{n})^2)^{-\frac{1}{2}} sin\phi_n \mathbf{j}, \\ and, n_z &= -\nabla \mathbf{n}(1+(\nabla \mathbf{n})^2)^{-\frac{1}{2}} cos\phi_n \mathbf{i} \end{aligned} \tag{5.33}$$

where the gradient of the normal $\nabla \mathbf{n}$ is calculated by,

$$\nabla \mathbf{n} = \frac{z_{m,n} A^2}{B^2 (x_{m,n}^2 + y_{m,n}^2)^{\frac{1}{2}}}. \tag{5.34}$$

Subroutine GEOSPHEROID found in appendix D calculates values of area, the coordinates of the midpoints and normals at the midpoints for the boundary elements of a spheroid, of major axis radius A, and minor axis radius B.

5.1.2 The second approach

As for the previous section, the surface S is split into T boundary area elements, $S_1, S_2, \ldots, S_T$, and equation (2.126) can be written,

$$p(\mathbf{r}, \mathbf{r}_0) = G(\mathbf{r}_0, \mathbf{r}) - ik_1 \sum_{k=1}^{T} \int_{S_k} p(\mathbf{r}_s, \mathbf{r}_0) G(\mathbf{r}_s, \mathbf{r}) (\beta(\mathbf{r}_s) - \beta_c) ds(\mathbf{r}_s), \tag{5.35}$$

for $\mathbf{r} \in \overline{U_+}$. If the maximum dimension, h, of each boundary area element is small enough so that $p(\mathbf{r}, \mathbf{r}_0)$ and $\beta(\mathbf{r})$ are approximately constant over each element, then equation (5.35) can be approximated as,

$$p(\mathbf{r}, \mathbf{r}_0) = G(\mathbf{r}_0, \mathbf{r}) - ik_1 \sum_{k=1}^{T} p(\mathbf{r}_k, \mathbf{r}_0) (\beta(\mathbf{r}_k) - \beta_c) \int_{S_k} G(\mathbf{r}_s, \mathbf{r}) ds(\mathbf{r}_s). \tag{5.36}$$

Now, for $\mathbf{r} \neq \mathbf{r}_k$,

$$\int_{S_k} G(\mathbf{r}_s, \mathbf{r}) ds(\mathbf{r}_k) \approx A_k G(\mathbf{r}_k, \mathbf{r}), \tag{5.37}$$

where A_k is the area of element S_k. For $\mathbf{r} = \mathbf{r}_k$,

$$\int_{S_k} G(\mathbf{r}_s, \mathbf{r}) ds(\mathbf{r}_k) \approx -\frac{1}{2\pi} \int_{S_k} \frac{1}{|\mathbf{r}_s - \mathbf{r}_k|} ds(\mathbf{r}_s), \tag{5.38}$$

since,

$$G(\mathbf{r}_s, \mathbf{r}_k) \approx -\frac{1}{2\pi} \frac{1}{|\mathbf{r}_s - \mathbf{r}_k|} \tag{5.39}$$

for $\mathbf{r}_s \in S_k$. Analytical expressions for the integral (5.12) when S_k is a polygon have been given by Birtles [103] and Chandler-Wilde [91].

Thus, the following linear equations are satisfied approximately by the unknown values of $p(\mathbf{r}_l, \mathbf{r}_0)$,

$$\begin{aligned} p(\mathbf{r}_k, \mathbf{r}_0) &= G(\mathbf{r}_0, \mathbf{r}_k) + \frac{ik_1}{2\pi} p(\mathbf{r}_k, \mathbf{r}_0)(\beta(\mathbf{r}_k) - \beta_c) \int_{S_k} \frac{1}{|\mathbf{r}_s - \mathbf{r}_k|} ds(\mathbf{r}_s) \\ &\quad -ik_1 \sum_{k=1(k\neq j)}^{T} A_k p(\mathbf{r}_k, \mathbf{r}_0) G(\mathbf{r}_k, \mathbf{r}_j)(\beta(\mathbf{r}_k) - \beta_c), \end{aligned} \tag{5.40}$$

for $j = 1(1)T$. The values of p at the midpoints $\mathbf{r}_k$ of A_k are determined by solving the set of T linear equations,

$$\sum_{k=1}^{T} a_{jk} p(\mathbf{r}_k, \mathbf{r}_0) = G(\mathbf{r}_0, \mathbf{r}_j), \tag{5.41}$$

for $j = 1(1)N$ and where,

$$\begin{aligned} a_{jk} &= \left[1 - \frac{ik_1}{2\pi}(\beta(\mathbf{r}_k) - \beta_c) \int_{A_k} \frac{1}{|\mathbf{r}_s - \mathbf{r}_k|} ds(\mathbf{r}_s)\right] \delta_{jk} \\ &\quad +ik_1 A_k G(\mathbf{r}_k, \mathbf{r}_j)(\beta(\mathbf{r}_k) - \beta_c)(1 - \delta_{jk}). \end{aligned} \tag{5.42}$$

The integral over A_k in equation (5.42) is approximated as,

$$\begin{aligned} \int_{A_k} \frac{ds(\mathbf{r}_s)}{|\mathbf{r}_s - \mathbf{r}_k|} &\approx \int_{\tilde{A}} \frac{ds(\mathbf{r}_s)}{|\mathbf{r}_s - \mathbf{r}_j|} \\ &= \int_0^{2\pi} \int_0^{\tilde{R}} dr d\theta \\ &= 2\pi \tilde{R}, \end{aligned} \tag{5.43}$$

where $\tilde{A}_j$ is a circle centred on $\mathbf{r}_j$ of the same area as A_j, i.e. $\tilde{A}_j$ has radius $\tilde{R} = \sqrt{A_j/\pi}$.

Again, as for the previous section, once values of a_{jk} are determined, the values of p at the midpoints of the elements can be calculated. It is then a simple task to calculate values of p for $\mathbf{r} \in U_+$ by substitution into,

$$p(\mathbf{r}, \mathbf{r}_0) = G(\mathbf{r}_0, \mathbf{r}) - ik_1 \sum_{j=1}^{T} p(\mathbf{r}_j, \mathbf{r}_0) G(\mathbf{r}_j, \mathbf{r})(\beta(\mathbf{r}_j) - \beta_c) A_j. \tag{5.44}$$

The scattering surface

Here, only *circular* surface inhomogeneities are considered, and expressions for the area of each of the boundary elements along with expressions for the coordinates of the midpoints of these elements, are derived.

The mesh generation on the circular surface inhomogeneity must be such that the maximum boundary area element diameter is to be no greater than a value h, dependent upon the incident acoustic field; values of which shall be considered in chapter 6. Consider the diagram in figure 5.3. The mesh on the circular surface is formed by dividing the surface into circular bands and sectors. In cylindrical coordinates, where the origin is taken to be at

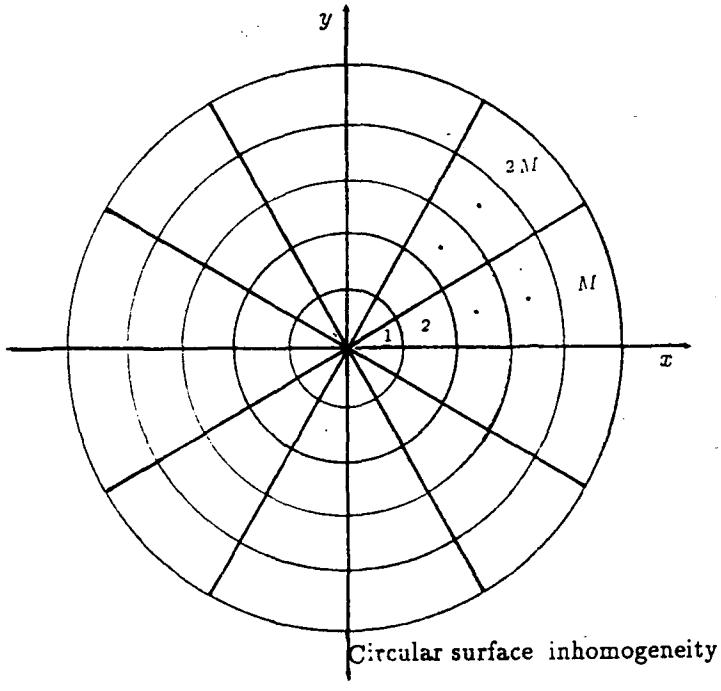

Figure 5.3 Element configuration for a circular surface inhomogeneity including numbering system for the elements

the centre of the circular patch, the circular bands are formed as follows. The interval $[0, r_C]$ is split into M subintervals, $I_1, I_2, \ldots, I_M$, where,

$$I_i = [(i-1)h, ih], \tag{5.45}$$

for $i = 1(1)M$ and $h = r_C/M$. The sectors are formed by dividing the interval $[0, 2\pi]$ into N subintervals $J_1, J_2, \ldots, J_N$, where,

$$J_j = [(j-1)\theta, j\theta], \tag{5.46}$$

for $j = 1(1)N$ and $\theta = 2\pi/N$. The area of each element is given by,

$$A_{i+(j-1)m} = \theta(i - \frac{1}{2})h^2, \tag{5.47}$$

for $i = 1(1)M, j = 1(1)N$. The coordinates of the midpoint of the boundary element j are,

$$x_j = Rcos\theta_m, \tag{5.48}$$

$$y_j = Rsin\theta_m, \tag{5.49}$$

and,

$$z_j = 0. \tag{5.50}$$

Subroutine GEOCIRCLE found in appendix D calculates values of area and the coordinates of the midpoints for the boundary elements of a circular surface inhomogeneity.

With the circular scattering surface used together with an induced surface impedance within this surface due to a rigidly backed layer, the boundary element method effectively calculates the scattered field due to a *disk* embedded within the porous medium. This type of scatterer will be used extensively later in this chapter and chapter 7.

5.1.3 Matrix structure and solution

With the numbering of the boundary elements of the spheroid as in figure 5.2, and that of the circular surface scatterer as in figure 5.3, then the matrices $[a_{jk}]$ for the solution of the two integral equations, have the same

structure, and are in fact block-circulant [104], *i.e.*, they are of the form,

$$[a_{jk}] = \begin{pmatrix} A_1 & A_2 & . & . & . & A_T \\ A_T & A_1 & . & . & . & A_{T-1} \\ . & . & . & . & . & . \\ . & . & . & . & . & . \\ . & . & . & . & . & . \\ A_2 & A_3 & . & . & . & A_1 \end{pmatrix} \tag{5.51}$$

where each entry of the matrix is itself a square matrix (of dimensions $M \times M$). It is easy to see that a necessary and sufficient condition for a matrix of order $T = M \times N$ to be block circulant, with block entries of order M, is that,

$$a_{jk} = a_{(j+M)_{mod_T},(k+M)_{mod_T}}, \tag{5.52}$$

for $j, k = 1(1)T$ and where,

$$mod_T i = \begin{cases} i & \text{for } i = 1(1)T \\ i - T & \text{for } i = T+1, \ldots, T+M \end{cases} \tag{5.53}$$

To show that a_{jk} of equation (5.10) satisfies this condition, consider the element $a_{(j+M)_{mod_T},(k+M)_{mod_T}}$ $(j, k = 1(1)T)$. For brevity, writing $(j+M)$ for $(j+M)_{mod_T}$, etc, and noting that $\delta_{(j+M),(k+M)} = \delta_{j,k}$,

$$\begin{aligned} a_{(j+M),(k+M)} &= \left[\alpha + \sum_{i=1(i\neq(j+M))}^{T} \frac{\partial G_0(\mathbf{r}_i, \mathbf{r}_{(j+M)})}{\partial n(\mathbf{r}_i)} A_i\right] \delta_{j,k} \\ &\quad -(1-\delta_{j,k}) \frac{\partial G(\mathbf{r}_{(k+M)}, \mathbf{r}_{(j+M)})}{\partial n(\mathbf{r}_{(k+M)})} A_{k+M}. \end{aligned} \tag{5.54}$$

Due to the axi-symmetry of the problem, and the ordering adopted by the elements,

$$A_{(i+M)} = A_i, \tag{5.55}$$

$$\frac{\partial G_0(\mathbf{r}_{(i+M)}, \mathbf{r}_{(j+M)})}{\partial n(\mathbf{r}_{(i+M)})} = \frac{\partial G_0(\mathbf{r}_i, \mathbf{r}_j)}{\partial n(\mathbf{r}_i)}, \tag{5.56}$$

for $i, j = 1(1)T$, so that,

$$\sum_{i=1(i\neq(j+M))}^{T} \frac{\partial G_0(\mathbf{r}_i, \mathbf{r}_{(j+M)})}{\partial n(\mathbf{r}_i)} = \sum_{i=1+M(i\neq(j+M))}^{T+M} \frac{\partial G_0(\mathbf{r}_i, \mathbf{r}_{(j+M)})}{\partial n(\mathbf{r}_i)} A_i$$

$$= \sum_{i=1(i\neq j)}^{T} \frac{\partial G_0(\mathbf{r}_i, \mathbf{r}_j)}{\partial n(\mathbf{r}_i)}. \qquad (5.57)$$

Thus,

$$a_{(j+M)_{mod_T},(k+M)_{mod_T}} = a_{j,k}. \qquad (5.58)$$

A similar argument shows that a_{jk} of equation (5.42) satisfies the condition for the block circulant structure.

The solution of this matrix type can be carried out using the subroutine CGSLC of the Toeplitz package, from the Argonne National Laboratory [105].

The boundary element methods detailed above are implemented in a set of subroutines in appendix D. For the first approach, subroutines FSURSPH and FRECSPH found in appendix D calculate values of pressure on the surface of a spheroid and at a receiver point in the upper medium, respectively. For the second approach, subroutines FSURCIR and FRECCIR calculate values of pressure on the surface of a circular surface inhomogeneity and at a receiver point in the upper medium, respectively.

5.2 Numerical tests and comparisons

5.2.1 Effect of element sizes

It has been seen that the boundary element methods for the solution of the boundary integral equations require that the scattering surfaces are divided into a number of elements, and that with correct numbering of these elements, matrices are produced that have a particular useful structure. The order of each matrix is equal to the number of elements on the scattering surface, and it will be seen that the number of elements in turn, is dependent upon the frequency of the acoustic field being considered. Thus, it is important to establish the element sizes on the scattering surfaces that allow accurate calculations to be made. Element sizes that are too small, although giving accurate results, would result in a large number of matrix elements, involving a large computational cost for solution; on the other hand, elements that are too large would give inaccurate results.

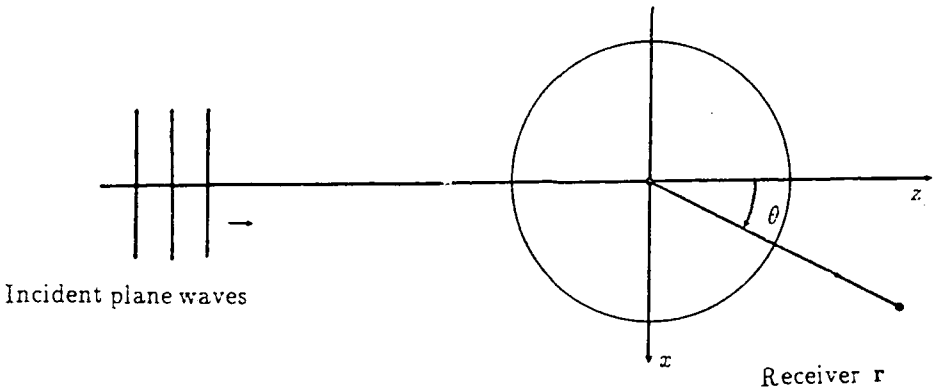

Figure 5.4 Theoretical source/receiver configuration for comparison of a boundary element method with classical scattering by a rigid sphere. The sphere has a radius of 0.5m, the propagating medium having a wavenumber $k = (5.0 + 0.05i)/m$.

The method used here, to establish *reasonable* element sizes, is to compare numerical results with classical theory; and here, the classical theory is that of scattering of an incident plane wave by a rigid sphere in an infinite homogeneous medium [84], expressions for which have been presented in appendix B. If, in equation (2.104), $k_1 = k_2$ and $Z_1 = Z_2$, *then this* equation predicts the scattering of an incident spherical wave by a rigid inhomogeneity in an infinite homogeneous medium (appendix A gives a full derivation of the boundary integral equation assuming at the start that the rigid inhomogeneity is in an infinite homogeneous medium). This means that if the source is positioned sufficiently far from the inhomogeneity, such that the incident field at the inhomogeneity is effectively plane, then a direct comparison with the results from classical theory can be made. Figure 5.4 shows the source/receiver configuration for a rigid sphere in an infinite homogeneous porous medium used, and table 5.1 shows values of the ratio of the scattered field to the direct field at several points close to a rigid sphere of radius 0.5m in an infinite absorbing medium having a propagation constant of $k = (5.0 + 0.05i)$/m, calculated by numerically solving the integral equation A.7. The coordinates of the source, in metres, is (-1000,0,0), where the centre of the sphere is taken as the origin. Also shown in this table

Receiver position / m		Boundary element method								Classical
		$h = 1, M = 1, N = 2$		$h = 0.5, M = 2, N = 4$		$h = 0.25, M = 5, N = 10$		$h = 0.125, M = 10, N = 20$		
x	y	p_s/p_d	E_{BC}	p_s/p_d	E_{BC}	p_s/p_d	E_{BC}	p_s/p_d	E_{BC}	p_s/p_d
1	0	1.7562 + 0.8736i	3.0730	0.1318 + 0.7407i	0.3518	−0.0003 + 0.5918i	0.0201	−0.0055 + 0.5838i	0.0055	−0.0045 + 0.5808i
$1/\sqrt{2}$	$1/\sqrt{2}$	−1.0853 + 0.4187i	4.7990	−0.4535 − 0.0795i	1.4256	−0.2108 − 0.0762i	0.0708	−0.2006 + 0.0804i	0.0195	−0.1965 + 0.0807i
0	1	−0.1830 − 0.8451i	5.8736	−0.0401 + 0.0202i	1.0095	0.0755 + 0.1657i	0.0794	0.0669 + 0.1617i	0.0247	0.0628 + 0.1606i
$-1/\sqrt{2}$	$1/\sqrt{2}$	−0.9435 − 0.3504i	2.9308	0.0291 − 0.0731i	1.0694	−0.2530 − 0.0940i	0.0792	−0.2470 − 0.0780i	0.0129	−0.2448 − 0.0755i
−1	0	1.4144 − 2.4971i	9.3618	0.3335 − 0.4379i	2.8937	−0.0246 − 0.2886i	0.0833	−0.0409 + 0.2779i	0.0133	−0.0437 − 0.2754i

Table 5.1 Comparison of the values of the scattered to the direct pressure field at various receiver positions using the boundary element method (with decreasing element sizes) with classical theory for a rigid sphere in an infinite absorbing medium. The propagation constant for the medium is $k = (5.0 + 0.05i)/\mathrm{m}$, and the sphere radius is 0.5m. For the boundary element method, the coordinates of the source, in metres,is (-1000,0,0). Also shown is the error, E_{BC}.

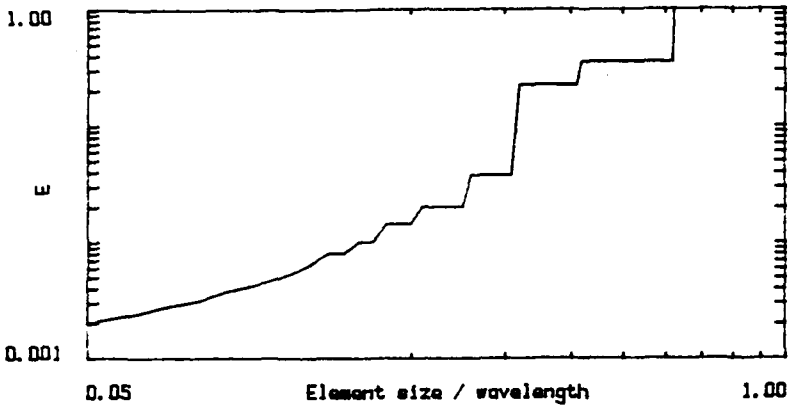

Figure 5.5 Error in the boundary element method versus element size for a rigid sphere in an infinite absorbing medium

is the *relative error*, E_{BC} in the scattered field calculated by the boundary element method, *i.e.*,

$$E_{BC} = \left| \frac{p_b^b - p_s^c}{p_s^c} \right| \tag{5.59}$$

where p_s^b and p_s^c are the scattered pressures calculated by the boundary element method and the classical theory respectively. The graph in figure 5.5 shows this error versus element size for the receiver position (1,0,0). It can be seen that the graph is not smooth. This is due to the fact that the number of elements M, is calculated by taking the modulus of a real number, giving the stepped feature of the graph.

It can be seen that as the element sizes are decreased, there is a gradual convergence of values to those calculated by the classical results, *i.e.* for small enough element sizes, the boundary element method compares favourably with the classical results. Furthermore, element sizes of the order 0.2λ have an error ≈ 0.01, sufficient to give reasonable results.

Now consider the source/receiver configuration of figure 5.6, which shows the side elevation and plan view of a sphere of radius 0.125m, embedded within a rigid porous medium characterised by the four parameters $\sigma =$

100000n.s.m^{-4}, $\Omega = 0.4$, $s_f = 0.75$ and $n' = 1$. At the frequency of 500Hz, the refractive index has a value of $n = 2.5703 + 1.6575i$. Table 5.2 shows the results of the ratio of the scattered field to the direct field p_s/p_d calculated at several points near to the plane boundary above the embedded sphere. Also shown is the relative error E_{BB} in the scattered field calculated by the boundary element method, *i.e.*,

$$E_{BB} = \left| \frac{p_s^b - p_s^{bf}}{p_s^{bf}} \right| \tag{5.60}$$

where p_s^{bf} is an accurate boundary element method calculation of the scattered pressure using a very small element size of $h = 0.0625\lambda$. (The comparison with this fine mesh boundary element method result is made in the absence of a comparable classical or analytical result.) It can be seen, in table 5.2 that the ratio p_s/p_d gradually converges with decreasing element size. Futhermore, as indicated by the initial test for scattering of plane waves by a sphere in an infinite medium, element sizes with $h \approx 0.2\lambda$ are adequate in terms of accuracy and computational time. Similar results can be obtained for a disk embedded within a rigid porous medium, giving similar conclusions. The suggestion that an element size of $h \approx 0.2\lambda$ is adequate has, of course, been made previously [91].

5.2.2 Validation of the boundary element methods

It was seen in the previous section that the numerical methods converged for decreasing element size. This does not mean necessarily that the methods are giving correct and meaningful results, and it is the purpose of this section to validate these methods.

Table 5.3 and 5.4 show the results of calculating the ratio of the total to the direct pressure field using the boundary element methods for a sphere and for a disk embedded within a rigid porous medium for various radii of both sphere and disk with a constant depth as shown in figure 5.7.

Ratios at two receiver positions are calculated, the first at a position of 0.2m above the plane boundary and the second at the midpoint of the

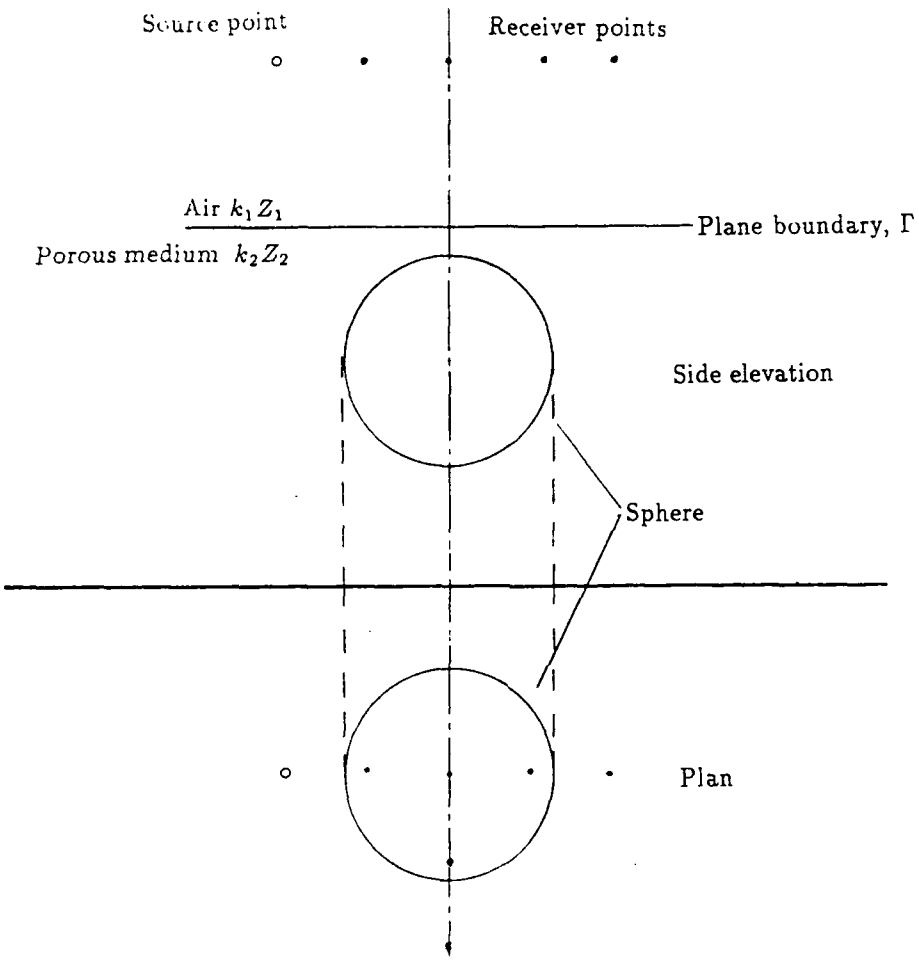

Figure 5.6 Theoretical source/receiver configuration for testing of convergence for the boundary element method for scattering by a sphere embedded within a rigid porous medium

Receiver positi n / m			$h = 1$ $M = 2, N = 4$		$h = 0.5$ $M = 4, N = 8$		$h = 0.25$ $M = 8, N = 16$		$h = 0.125$ $M = 15, N = 30$	
x	y	z	p_s/p_d	E_{BC}	p_s/p_d	E_{BC}	p_s/p_d	E_{BC}	p_s/p_d	E_{BC}
0.1	0	0.335	−0.0079 − 0.0067i	1.3015	−0.0077 + 0.0057i	0.5601	−0.0066 + 0.0021i	0.0254	−0.0066 + 0.0021i	0.0110
0	0	0.335	−0.0229 + 0.0044i	1.5230	0.0034 + 0.0220i	0.6942	−0.0030 + 0.0146i	0.0244	−0.0029 + 0.0144i	0.0115
0.1	0	0.335	−0.0228 + 0.0248i	1.6316	0.0221 + 0.0202i	0.7422	0.0083 + 0.0180i	0.0242	0.0082 + 0.0177i	0.0113
0.2	0	0.335	−0.0118 + 0.0350i	1.6193	0.0282 + 0.0111i	0.7183	0.0145 + 0.0149i	0.0242	0.0143 + 0.0147i	0.0108
0	0.1	0.335	−0.0234 + 0.0064i	1.4769	0.0036 + 0.0216i	0.6506	−0.0030 + 0.0149i	0.0247	0.0030 + 0.0147i	0.0111
0	0.2	0.335	−0.0227 + 0.0094i	1.3698	0.0033 + 0.0204i	0.5716	−0.0029 + 0.0149i	0.0249	−0.0029 + 0.0148i	0.0106

Table 5.2 Values of the scattered to the direct pressure field at various receiver positions with decreasing element size for a rigid sphere embedded within a rigid porous medium, with the source coordinates, in metres, at (-0.2,0,0.335); the sphere has a radius of 0.125m, and the medium is characterised by the four parameters $\sigma = 100000\text{N.s.m.}^{-4}$, $\Omega = 0.4$, $s_f = 0.75$ and $n' = 1$, and the frequency is 500Hz.

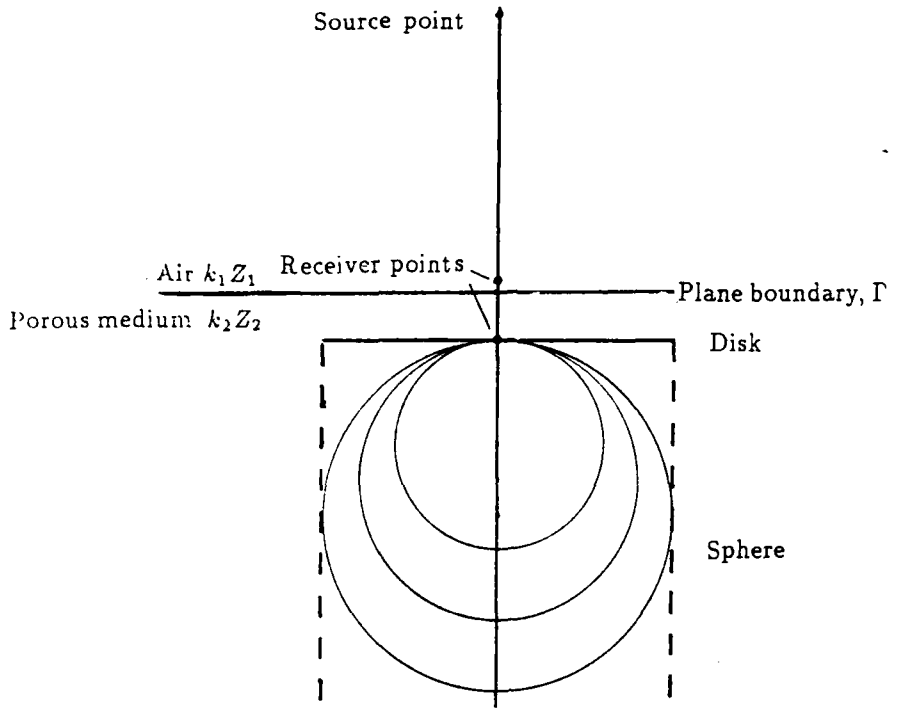

Figure 5.7 Theoretical source/receiver configuration for testing of convergence of the boundary element methods to simple results for increased scatterer radius

first element of the meshes used in both numerical solutions. This means that this second receiver point varies slightly with position according to the radius of the scatterer considered; however, initial tests have shown that this variation is small and can be ignored here. With the source positioned at z=100.0m, comparisons can be made with values of ratios calculated using a simple (plane wave) theory for transmission through a layer [106] (Approx.1 in the tables), and secondly, a theory which considers a boundary integral equation for scattering by an embedded sphere of infinite radius [107], which is summarised in appendix A.2 (Approx.2 in the tables).

Table 5.3 shows the results for the special case where the refractive index $n = 1$ and the relative impedance $\zeta = 1$. For comparison, equivalent results for a sphere in an infinite medium calculated by solving the integral equation (A.7) are shown. The calculation of pressure fields using this method involves using free-field Green's functions, whereas the method here involves the Green's function for transmission across a plane boundary. This approximation requires that $|n^2| \gg 1$, which, of course is not satisfied. It

Radius / m	Position (a)		Position (b)	
	Two media case	One medium case	Two media case	One medium case
1×10^{-5}	1.0000 + 0.0000i	1.0000 + 0.0000i	0.9999 + 0.0001i	1.0000 + 0.0000i
1×10^{-4}	1.0000 + 0.0000i	1.0000 + 0.0000i	0.9999 + 0.0001i	1.0000 + 0.0000i
1×10^{-3}	1.0000 + 0.0000i	1.0000 + 0.0000i	0.9999 + 0.0001i	1.0000 + 0.0000i
1×10^{-2}	0.9922 − 0.0020i	0.9920 − 0.0099i	0.9995 + 0.0001i	0.9997 − 0.0002i
1×10^{-1}	1.5104 − 0.4358i	1.5099 − 0.4358i	1.1325 + 0.0539i	1.1143 + 0.0833i
2×10^{-1}	1.7613 − 0.3367i	1.7594 − 0.3383i	1.2552 + 0.2863i	1.1493 + 0.2595i
4×10^{-1}	1.9196 − 0.2321i	1.9068 − 0.2315i	1.3454 + 0.3047i	1.1791 + 0.4218i
8×10^{-1}	1.9670 − 0.1683i	1.9520 − 0.1363i	1.3540 + 0.5914i	1.1822 + 0.6061i
Approx.1	2.0000-0.0000		1.6453+0.7640i	

Table 5.3 Variation of the ratio of the total to direct pressure field at two receiver positions. Position (a) is at the midpoint of the first element of the sphere; position (b) is at 0.2m above the plane boundary. For the two media case, the refractive index, $n = 1$, and the relative impedance $\zeta = 1$. For comparison, Approx.1 is a simple calculation for transmission through a layer assuming plane wave incidence.

Radius / m	Position (a)		Position (b)	
	Sphere	Disk	Sphere	Disk
1×10^{-5}	1.4471 + 0.3186i	–	0.4404 − 0.4658i	0.4404 − 0.4660i
1×10^{-4}	1.4447 + 0.3201i	–	0.4404 − 0.4658i	0.4404 − 0.4660i
1×10^{-3}	1.4214 + 0.3313i	–	0.4404 − 0.4658i	0.4404 − 0.4658i
1×10^{-2}	1.2115 + 0.4523i	–	0.4405 − 0.4658i	0.4402 − 0.4655i
1×10^{-1}	1.7600 + 0.0621i	–	0.4231 − 0.4599i	0.4193 − 0.4160i
2×10^{-1}	1.7269 + 0.0028i	–	0.4045 + 0.4587i	0.3135 − 0.3135i
4×10^{-1}	1.6897 − 0.0152i	–	0.3750 − 0.4594i	−0.0333 − 0.4402i
8×10^{-1}	1.6684 − 0.0175i	–	0.3359 − 0.4651i	0.4904 − 0.5594i
Approx.1	2.0189-0.0115i		0.1956-0.5767	
Approx.2	1.7870-0.0160i		–	

Table 5.4 Variation with radius of embedded scatterer of the values of the ratio of the total to direct field at two receiver positions. Position (a) is at the midpoint of the first element of the scatterer; position (b) is at 0.2m above the plane boundary of a rigid porous medium characterised by the four parameters $\sigma = 100,000\text{N.s.m}^{-4}$, $\Omega = 0.4$, $s_f = 0.75$ and $n' = 1$. Depth, $d = 0.01$m, frequency=500Hz. For comparison, Approx.1 is a simple calculation for transmission through a layer assuming plane wave incidence; Approx.2 is an approximation for an embedded sphere of infinite radius.

can be seen that with increasing sphere radius, there is gradual convergence of values to that for the simple plane wave theory.

Table 5.4 shows the results for a sphere and disk embedded within a rigid porous medium, characterised by the four parameters $\sigma = 100,000\text{N.s.m}^{-4}$, $\Omega = 0.4$, $s_f = 0.75$ and $n' = 1$, at the frequency of 500Hz. For position (a), the results for the sphere show a gradual convergence to that for the simple plane wave theory (Approx.1) and to the value for the approximation for an embedded sphere of infinite radius. For position (b), the results for the sphere also show a convergence, but fall well short of Approx.1. For the receiver at position (b), the sphere must have a significant radius for the results to approach the approximation. The results for the disk do not show a smooth convergence to that of Approx.1.

5.3 Summary

This chapter has been concerned with the numerical solution of the boundary integral equations derived in chapter 2, using a simple boundary element method, and the solution to both approaches were considered separately. It is seen that with careful choice of the shape of the scatterers, and with correct numbering of the elements on the scatterers, the resulting linear equations had a coefficient matrix that was shown to be *Block-Circulant*. This meant that solutions could be obtained using standard routines.

The scatterer shape chosen for the first approach was a *spheroid*, and for the second, a *circular* surface inhomogeneity. These choices gave scope for testing the theory with classical results. Such test were presented in section 5.2. The first test, which gave an indication of the size of elements to be used, involved comparing a boundary element method for calculating the field scattered by a sphere in an infinite absorbing medium, with values calculated by classical results. With the source for the boundary element method positioned sufficiently far from the sphere, such that the incident field at the sphere was effectively plane, such a comparison with the classical results, which involved plane wave incidence, could be made. It was seen that for the different receiver positions, there was convergence of the boundary element method with the classical results. A similar test was then carried out for a sphere embedded within a rigid porous medium and it was confirmed that an element size of $h = 0.2\lambda$ was sufficient for calculations.

With the element size determined, section 5.2.2 set out to validate the boundary element methods, involving a straightforward comparison with some simple plane wave theory approximations and an approximation for an integral equation for an embedded sphere of infinite radius. These limited tests demonstrated that the boundary element methods may be used with some confidence.

Chapter 6

Experimental method

In this and the following chapter, a description of the experimental part of this study is given. The actual experiments and their results together with the comparison with theory are left to chapter 5. In this chapter, the equipment, its specification, arrangement, and calibration are described.

6.1 Experimental procedure

The aim of the experiments was to investigate the accuracy of theoretical predictions of sound scattering by semi-oblate spheroids and circular disks embedded within various test media. The choice of the various experimental parameters was such as to allow direct comparison, as far as possible, with the theoretical predictions, whilst being constrained by the physical limits of the sample tray and anechoic chamber.

The experimental procedure used was to measure and then Fourier analyse, the instantaneous difference in sound pressure between two vertically separated microphones at a horizontal distance from a sound source over the surface of interest (see figure 6.1), thus obtaining a *level difference spectrum*. The level difference (L.D.) is defined as,

$$L.D. = 20log_{10}\left[\frac{\text{Sound pressure at upper receiver}}{\text{Sound pressure at lower receiver}}\right], \qquad (6.1)$$

and is determined, at any particular frequency, by calculating the difference in the sound pressure levels between the two microphones, *i.e.* the magni-

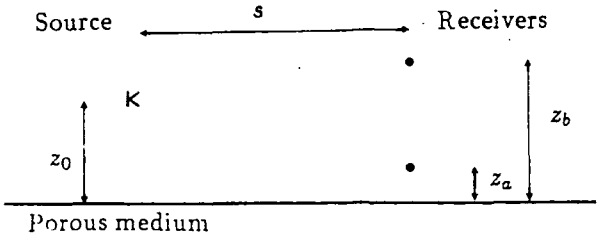

Figure 6.1 Source/receivers configuration for the measurement of level difference over a porous medium

tude of the *transfer function* between the two microphones. It is related to the excess attenuation (E.A.) from a point source, by,

$$L.D. = E.A._{\text{Top receiver}} - E.A._{\text{Bottom receiver}}, \tag{6.2}$$

excess attenuation being defined as,

$$E.A. = 20log_{10}\left[\frac{\text{Total sound pressure at receiver}}{\text{Direct sound pressure contribution at receiver}}\right]. \tag{6.3}$$

Figure 6.2 shows experimentally measured level difference spectra over a rigid (acoustically hard) surface using the configuration of figure 6.1. Two vertically separated microphones, with the top microphone at a fixed height of z_b =0.2m above the rigid surface were placed at a horizontal distance of s = 0.4m from a source of sound, also at a fixed height of z_0 =0.2m above the rigid surface, emitting a continuous broadband signal. It can be seen that increasing the height of the lower microphone, results in considerable changes in the spectra.

The observed maxima and minima are the result of interference between the direct and surface reflected path contributions, and so changes in the interference are due to the source or microphone heights. This becomes more clear by first considering excess attenuation spectra, where R_1 and R_2 are as defined in figure 6.3. At certain frequencies, the path length difference $R_2 - R_1$ will be such that there will be more or less complete destructive

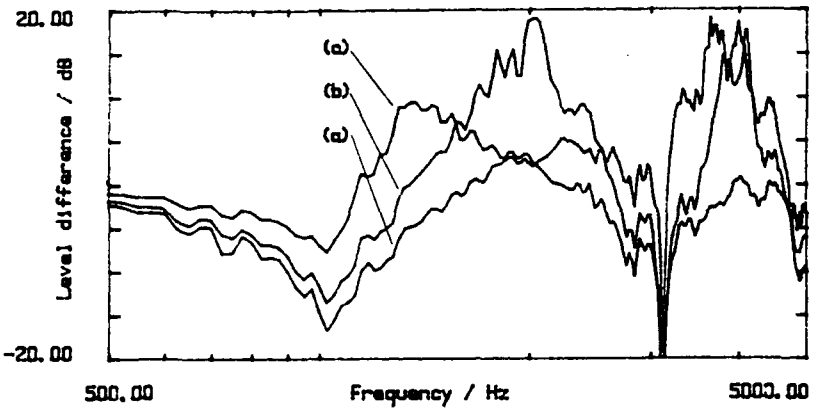

Figure 6.2 Variation of experimentally measured level difference spectra with the lower microphone height, z_a, for propagation over a rigid surface. Source/receivers configuration as for figure 6.1 with z_0 =0.2m, s =0.4m, z_b =0.2m, and z_a = (a) 0.05m, (b) 0.1m and (c)0.15m.

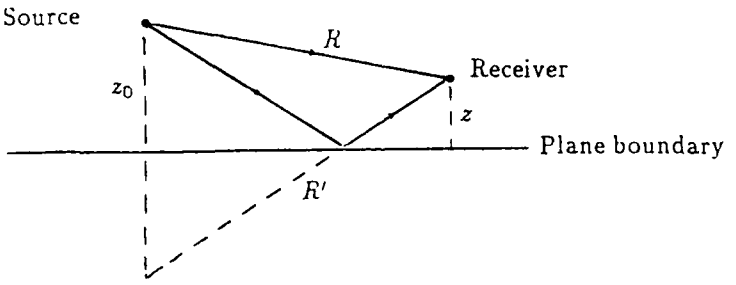

Figure 6.3 Direct and surface reflected ray paths.

interference; these frequencies, f, can be calculated using the expression, valid for a rigid reflecting surface,

$$\frac{2\pi f}{c}(R_2 - R_1) = n\pi, \tag{6.4}$$

for $n = 1, 2, \ldots$. If the surface is porous, a phase term $\phi(f)$ has to be added to the left hand side of equation (6.4). Depending on the position of the lower and upper receivers, it is clear that the level difference spectra will also give such minima and maxima.

Figure 6.4 shows what happens to the excess attenuation spectrum when the receiver height is varied. It can be seen from figure 6.3 and equation (6.4),that decreasing the receiver height reduces the path length difference between the direct and reflected paths, thus shifting the minima and maxima to higher frequencies, and this is what is shown in figure 6.4 (b) where decreasing the receiver height, reduces the path length difference. Also shown are the resultant level difference spectra calculated from subtracting the excess attenuation spectra at the lower receiver positions from that at the higher position; these level difference spectra can be compared directly with the experimental results in figure 6.2. For a very low receiver height, the first minimum in the excess attenuation spectrum is at a high frequency. This means that the level difference spectrum that most resembles the excess attenuation spectrum for the top receiver is when the lowest receiver is at its lowest position. This observation has been made previously by Embleton *et al* [98].

In the theoretical calculations, the source is assumed to be a perfect monopole source of sound, with no variation in directivity, and to emit a white noise spectrum. In contrast to this, the sound source used for the experiments will have some variation both in its directivity and in its frequency range. These effects cancel when measuring level difference but must be considered when measuring excess attenuation.

Using the same source/receivers configuration, the level difference spectra will vary for different ground types. Not only will the maxima and minima in the spectra for the absorbing ground shift in frequency, but the magnitudes of the maxima and minima will also vary compared to those

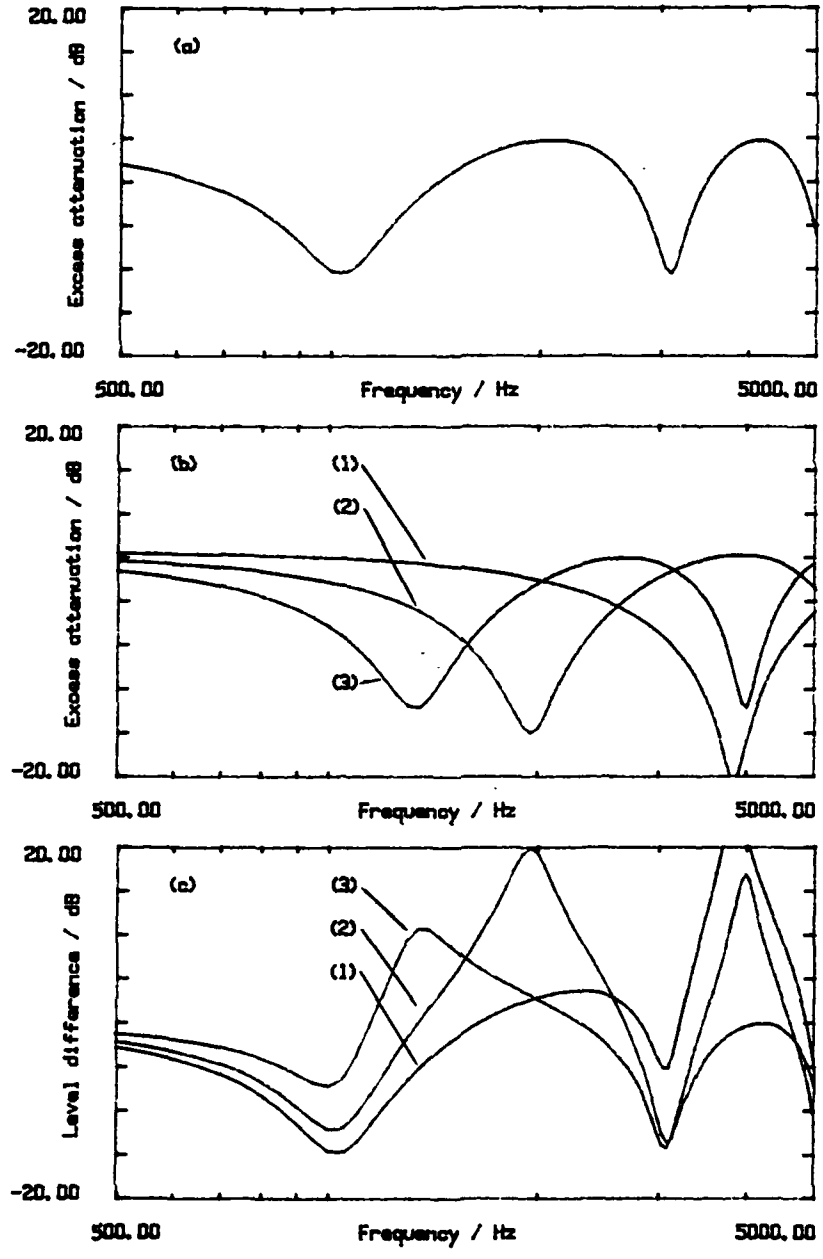

Figure 6.4 Variation of theoretical excess attenuation spectra with height of the receiver for propagation over a rigid surface. Source/receiver configuration as in figure 6.3. (a) z_0 =0.2m, s =0.4m and z =0.2m;(b) z_0 =0.2m, s =0.4m and z = (1)0.05m, (2)0.1m and (3)0.15m;(c)the resultant level difference spectra z_0 =0.2m, s =0.4m, z_b =0.2m and z_a = (1)0.05m, (2)0.1m and (3)0.15m

for a rigid surface. It will be seen in the following chapter that for given source/receiver configurations, the level difference spectra above the surfaces of the three different propagating media considered, vary quite considerably.

It has been argued that the level difference spectrum displays a series of maxima and minima, the frequency positions of which are dependent upon the source/receiver configurations and ground parameters. Further, it is the maxima and minima of the spectra that are most sensitive to variation in the ground parameters. For the purposes of the present study the first minimum was to occur at approximately 1kHz.

This imposed the first constraint on the source/receiver configuration. The next constraint was size. The size of the sample tray was designed so that it fitted snugly and centrally in the anechoic chamber, the plan dimensions of the sample tray being $1.8 \times 1.2\text{m}^2$, with a depth of 0.3 m. The maximum usable area, however, was much reduced to avoid spurious reflections from the tray edges. Thus, the test scatterers had to have a horizontal dimension of much less than 1.2m and a vertical dimension of much less than 0.3m. Furthermore, as noted in the last chapter, the source/receiver separation must be of a similar dimension as the test scatterers. Bearing these constraints in mind, a source/receiver configuration of z_0 =0.2m, s =0.4m, z_b =0.2m, and z_a =0.05m was chosen for the present study. Such a configuration has been used in the examples of this section.

6.2 Experimental apparatus

6.2.1 The sample tray and gantry

All experiments were performed in the Faculty of Technology anechoic chamber at the Open University. Figure 6.5 shows a floor plan of the anechoic chamber including the position of the sample tray. Figure 6.6 shows the experimental arrangement of source, microphones,sample tray and gantry arrangement within the anechoic chamber. Within the anechoic chamber was positioned a sample tray $1.8 \times 1.2\text{m}^2$, the depth being 0.3m. On two rails running the length of the tray was mounted a gantry. The gantry

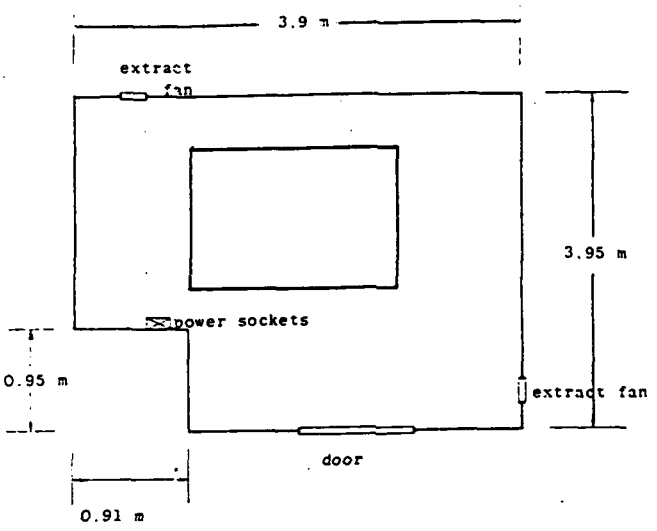

Figure 6.5 Floor plan of the Faculty of Technology anechoic chamber.

comprised two trolleys, one moving the length of the tray, and a second, mounted on the first, running the width of the tray. From this second trolley, a vertical shaft supported the speaker and from the first trolley, a vertical shaft supporting two microphones. This arrangement allowed the source and microphones considerable freedom for movement.

With the exception of the vertical motion, the position of the source and receivers was controlled by stepping motors instructed by computer. This allowed measurements to be made at numerous locations swiftly and accurately. The relative linear accuracy of the source/receiver position was 0.005m. Absolute accuracy was ensured by linear scales, positioned adjacent to the rails and by a mechanical stop. All supports for the source and microphones were designed so as to minimise reflective surfaces, whilst maintaining a rigid structure. Before any experiments with test media and scatterers were performed, measurements were carried out to check that the structure did not give spurious reflections.

The author was fortunate enough to inherit the main sections of the gantry system. Supports for the microphones and speaker were designed

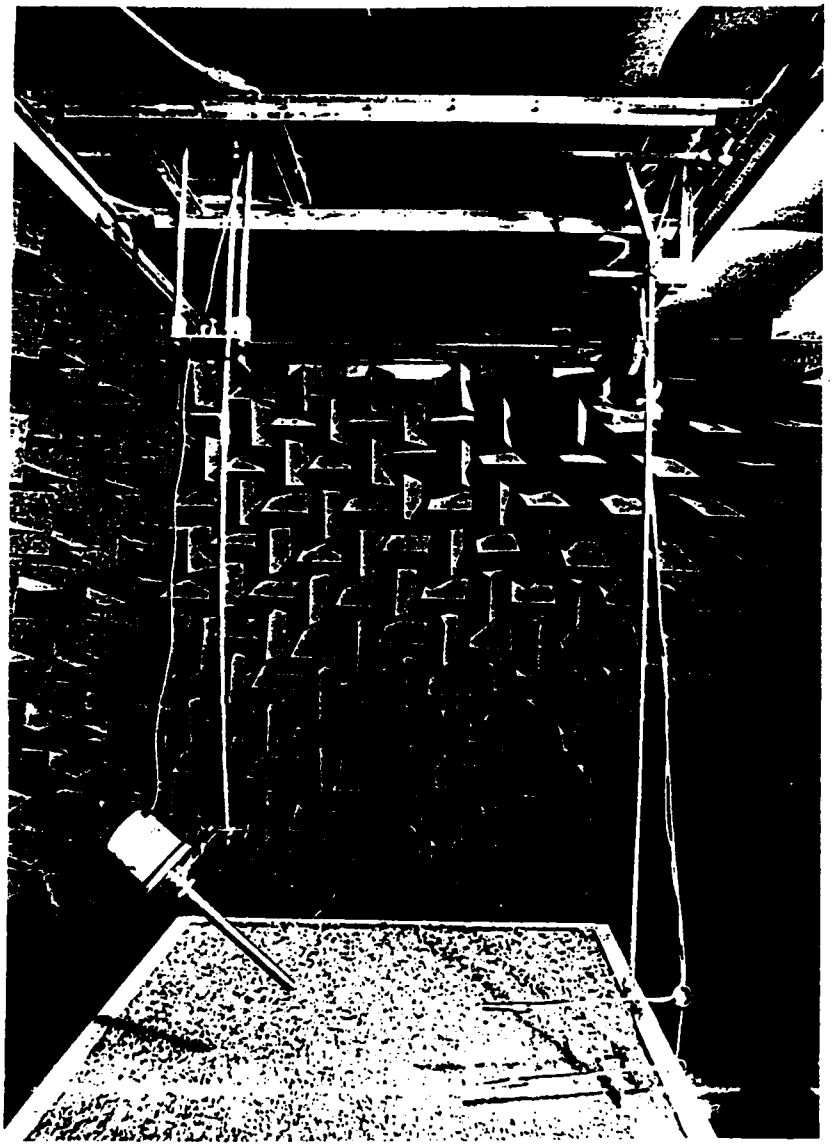

Figure 6.6 Photograph of the sample tray and gantry arrangement.

to the author's specification. Full details of the gantry and the anechoic chamber may be found in [108].

6.2.2 The transmission and reception system

A schematic diagram of the the transmission and reception system used for this study is shown in figure 6.7.

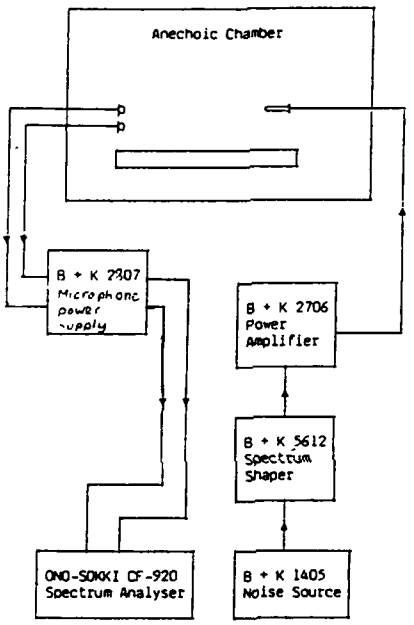

Figure 6.7 Schematic diagram of the transmission and reception system

The transmission system

For the measurement of level difference, the sound source had to emit an axisymmetric sound field, with a broad-band signal sufficiently above background and electronic noise.

For the purpose of this study, the white noise from a Brüel and Kjær type 1405 noise generator was used to generate this signal. This generator was able to produce a white noise output over the frequency range 20Hz to 100kHz, which was more than sufficient. The output from this generator

was then passed to a Brüel and Kjær type 5612 spectrum shaper set with a bandpass of 100Hz to 10kHz. Amplification of this signal was then provided directly by a 75 W, 0-40dB variable gain Brüel and Kjær power amplifier, having a flat transfer function over the frequency range 10Hz to 20kHz, which was again, more than sufficient. Finally, The sound source used, to which the amplified signal was passed, was a 40W Tannoy P4 driver unit with the exponential horn removed and replaced by an acoustically-damped hollow brass tube, as shown in figure 6.8. The tube consisted of a main shaft with an internal diameter 1.7cm, external diameter 1.9cm. For comparison

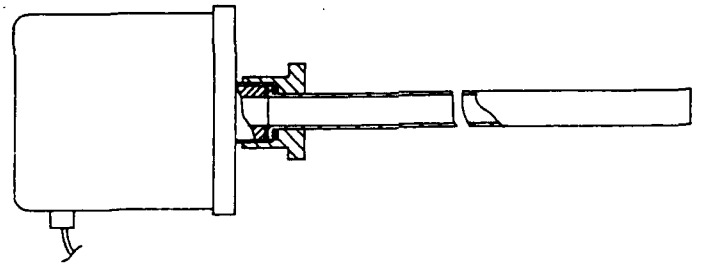

Figure 6.8 Section through the sound source and brass tube

of measured and theoretical level difference spectra, it is required that the field emitted by the source is spherical or omnidirectional. In practice, such perfect omnidirectional sources do not exist. The brass tube used here produced an axisymmetric field, and this property is used to minimise the distortion in the measured level difference due to departure from perfect sphericity.. Figure 6.9 shows the direct and reflected rays arriving at the two microphones in propagating over a homogeneous surface from the tube source. The angle the axis of symmetry subtended to the vertical, ϕ, was chosen so that γ_1 and γ_2 were approximately equal. For the configurations used, this angle was approximately 67.5 degrees.

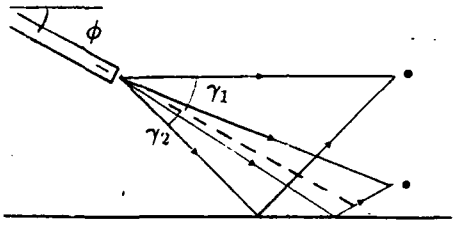

Figure 6.9 Source and axis of symmetry for the level difference technique

The reception system

For reception of signals in the frequency range 100Hz to 10kHz, Brüel and Kjær 4165 0.5 inch measuring microphones were used. The size refers to the nominal diaphragm diameter. This choice was made because the diaphragm size was small compared with the wavelength of the received sound wave (34.3 mm at 10kHz) to ensure omni-directional reception and that changes in the sound pressure field are small over the diaphragm area, but large enough to ensure good sensitivity. The Frequency response is quoted as ± 2 dB over 2.6Hz to 20kHz, more than adequate. The microphones were used in conjunction with Brüel and Kjær 2619 microphone preamplifiers having a frequency range 2Hz to 200 kHz.

The preamplifiers were connected to a Brüel and Kjær 2807 microphone power supply, which provided the necessary polarization voltage to the microphones. The amplified signals were then passed to the Ono Sokki 920 dual channel FFT analyser, which, at the frequency range 100Hz to 10kHz used in this study, samples the input voltage at 25.6 kHz. After reading in 1024 samples, (*i.e.* after about 0.04 seconds at this sampling rate) there is a pause in data collection while the fast fourier transform is calculated. The continuous nature of the analysed signal required the use of the Hanning window. A 400 line power spectrum is then calculated *i.e.* the voltage in adjacent 25Hz bands are calculated from 0 to 10kHz. The transfer function

is subsequently calculated from the two signals. For the experiments performed in this study, 64 consecutive transfer function spectra were averaged, to eliminate the effects of noise, such as source spectrum variations, receiver noise, etc.

The complete reception system was calibrated using a Brüel and Kjær 4230 calibrator, providing a 1kHz tone at a sound pressure level of 94dB.

6.3 The scatterers

The scatterers were designed and made to the author's specification.Two types of scatterers were made to enable direct comparison with the theory for scattering by embedded spheroids, and with that for scattering by disks.

Figure 6.10 shows an example of the semi-oblate spheroids constructed by the Engineering Mechanics Discipline workshop, from laminated wood. The photograph in figure 6.11 shows the laminated wood construction. All

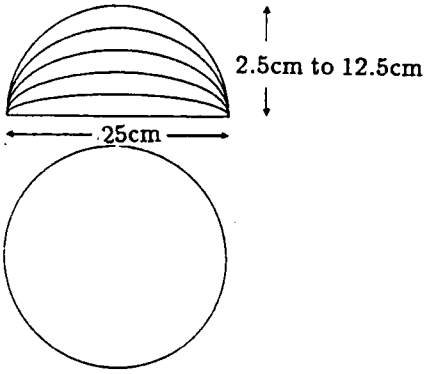

Figure 6.10 Dimensions of the semi-oblate spheroids used

the semi-oblate spheroids used had a fixed major radius of 12.5 cm with the minor radius varying from 2.5cm to 12.5cm in 2.5cm increments. The tolerance was quoted as 0.25cm either side of the 'true' shape.

The second type of scatterer was constructed from 1.25mm thick mild steel sheets cut into circular disks of radii 5cm to 12.5cm in 2.5cm increments. A photograph of a typical circular disk used is shown in figure 6.12.

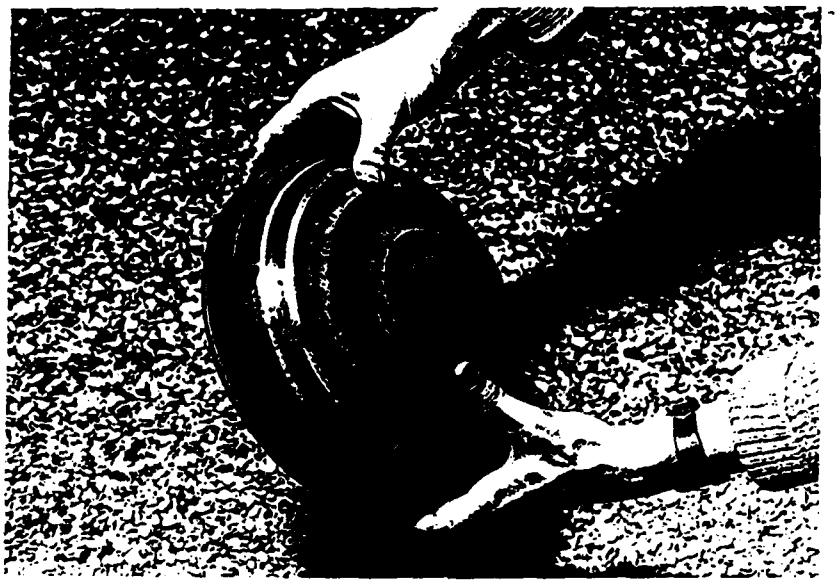

Figure 6.11 Photograph of an example semi-typical oblate spheroid used in this study

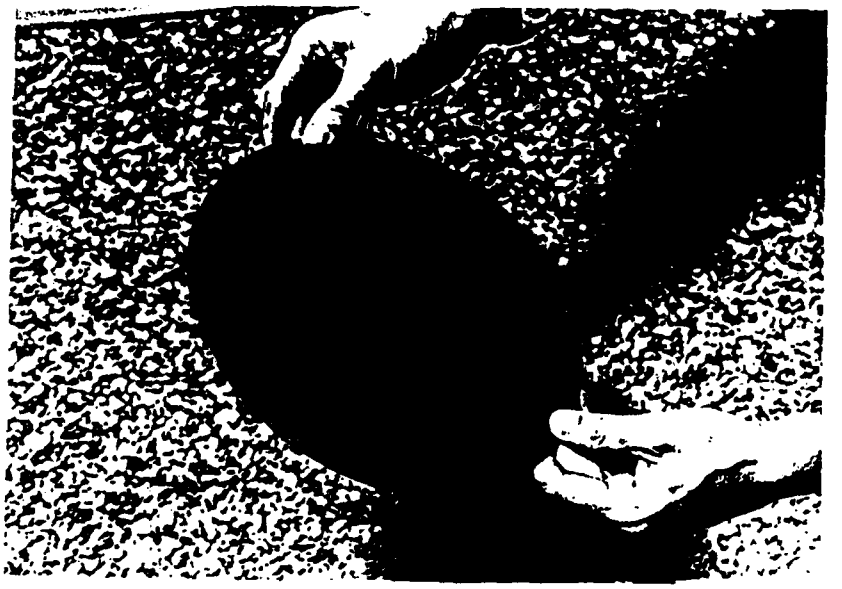

Figure 6.12 Photograph of an example mild steel circular disk used in this study.

6.4 The propagating media

Three different propagating media were used in this study, the physical properties of which are shown in table 6.1. The flow resistivity and porosity

	Gravel	Foam	Fibreglass
σ	9568.0	4090.0	28660.0
Ω	0.4	0.9 †	0.8 †
n'	0.5 †	1.0 †	1.0 †
s_f	1.0 †	1.0 †	1.0 †

Table 6.1 Measured and assumed constants of the propagating media. σ=flow resistivity, Ω = *porosity*, n'=grain shape factor, s_f=pore shape factor ratio†= predicted.

of each medium was measured using the methods described in Hess [13], and the results for these measurements are shown in table 6.1, along with the assumed values of grain shape factor and pore shape factor ratio.

The gravel used was supplied by Erith Building Supplies, Bletchley, Milton Keynes, and was a pea-gravel of nominal grain diameter 3/8 inch. This was found to be acoustically heterogeneous, a continual problem during the experiments being its uneven settling. To provide as uniform and consistent a gravel bed as possible, before all measurements were performed and each time the gravel was disturbed as a result of burying the test scatterers, the gravel in the vicinity of the test scatterers was loosened with a fork. Although tedious, this ensured that the gravel was gave consistent results for each set of measurements. The gravel was contained within and completely

filled the sample tray.

The fibreglass used in this study consisted of $1.2 \times 0.9\text{m}^2$, 0.05m thick Pilkington S300 Crown slabs. To give as homogeneous a propagating medium as possible, twelve slabs were placed adjacent to each other on two sheets of perspex on top of the sample tray, within the anechoic chamber, as shown in figure 6.13. The slabs were sufficiently uniform in shape that they could

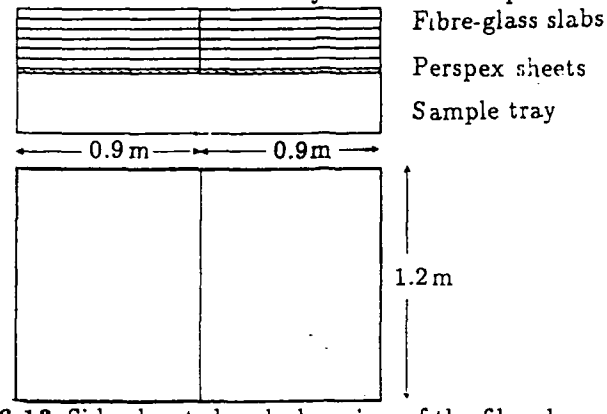

Figure 6.13 Side elevated and plan view of the fibreglass slabs

be placed adjacent to each other. Section 6.3 described the circular disks used; these were designed such that they could be inserted between the layers of fibreglass with ease, eliminating the necessity to modify the slabs to accommodate the disks. To bury the disks to a fraction of a slab thickness, grooves were cut into the slabs using a sharp knife, and the disks carefully inserted into these.

The polyurethane foam used in this study consisted of two $0.98 \times 0.67\text{m}^2$, 0.2m deep slabs, and were sufficiently uniform in shape that they could be placed on the perspex sheets on the top of the sample tray.

Again the circular disks were used in conjunction with the foam as the test scatterers. Here though, two semicircular shapes of radius 12.5 cm were cut out of the two adjacent slabs. The two semi-circular shapes were then cut into slices, the circular disks then being inserted between these foam slices.

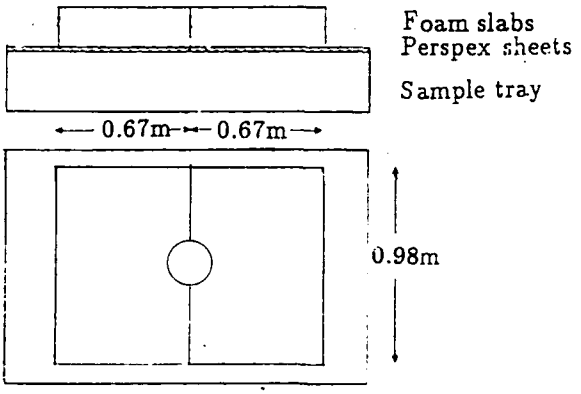

Figure 6.14 Side elevation and plan view of the polyurethane foam slabs

Chapter 7

Results

In this chapter, the experimental measurements of the field scattered by the scatterers embedded within the various media described in the previous chapter, are presented. The measurements were designed to test the validity of the theory in the light of the various approximations made.

Prior to these measurements, a series of numerical tests were conducted on the models, to assess their validity under various limits, in particular that:

1. the prediction of excess attenuation spectra above spheroids and disks in rigid porous media, with large values of radii converge to known results for a rigidly backed layer; and that for small values of radii, the predictions converge to that for the homogeneous case;
2. the prediction of excess attenuation spectra above spheroids and disks in rigid porous media converges to that for the homogeneous case as the depth of the upper scatterer surface is increased.

and section 7.1 considers these tests. This section is then followed by a description of experimental results with the chapter being concluded by a discussion and summary.

7.1 Theoretical results

Chapter 5 has shown that when the source is taken to a significant distance above the plane boundary, the ratio of scattered to direct pressure field is observed to converge to simple results using plane wave theory. The purpose of this section is to determine the influence of the near-surface scatterers when the source and receiver are *close* to the plane boundary, and figure 7.1 shows the source/receiver configuration that is going to be considered throughout this section. The source and receiver are at heights z_0 and z_b respectively above the plane boundary, separated by a distance, s. A spheroid is embedded within the rigid porous medium, centred on the origin, at a depth, D, beneath the plane boundary. Also shown, is the *depth*, d, which represents the closest point of the scatterer surface to the plane boundary. A rigid disk is also shown in the diagram.

Using the dependence of boundary properties given by the four parameter model, (equations (3.60),(3.61) and (3.62)), it has been shown [13], that the most important parameter on these equations is the flow resistivity, σ. In these initial tests of the models, a *standard* medium was given as: porosity $\Omega = 0.4$, flow resistivity, $\sigma = 10,000\text{N.s.m.}^{-4}$, grain shape factor, $n' = 1$ and pore shape factor ratio, $s_p = 0.75$. Attenborough [97], gives a value of $\sigma = 100,000\text{N.s.m.}^{-4}$ to be that typical of soils. This value, however, results in too high an attenuating medium for the present study; the scattered field is too weak for consideration.

Firstly consider the variation of the magnitude of the ratio of the scattered field to the total field with source/receiver separation, at a frequency of 1kHz, calculated by,

$$\text{Magnitude} = 20.0 log_{10} \left| \frac{P_{scat}}{P_{dir}} \right|. \tag{7.1}$$

It can be seen that when the separation is small, the ratio has a very small value, but as the separation is increased, this ratio increases, eventually tailing off with further increase in separation. This is straightforward to interpret. For small separations, the field at the receiver is dominated by the direct field, swamping any other contributions. With increasing separation,

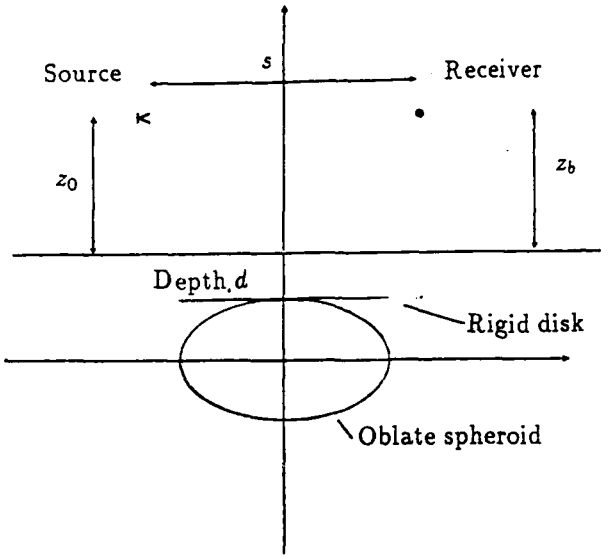

Figure 7.1 Theoretical source/receiver configuration for the prediction of excess attenuation

the direct field diminishes as -6dB per doubling of distance and other contributions including that from the scatterer become more important. With a source/receiver height of 0.2m, the greatest contributions occur when the source/receiver separation $s = 0.4$m. This probably corresponds to the geometry at which direct and ground reflected components interfere destructively. Consequently, this source/receiver configuration has been chosen for a series of numerical tests to determine the influence of near-surface inhomogeneities below a porous ground surface on the sound propagation from point source to receiver.

Consider first, the case of propagation over a rigidly backed layer. Figure 7.3 shows the variation of excess attenuation spectra as the layer thickness is varied, where the flow resistivity has a value of $10,000$N.s.m^{-4}. It can be seen that with increasing layer thickness, from 0.01m to 0.16m, the frequency of the first minimum decreases and becomes more shallow. It is also observed that the second minimum becomes less pronounced but increases in frequency. Eventually, with increasing depth, the excess atten-

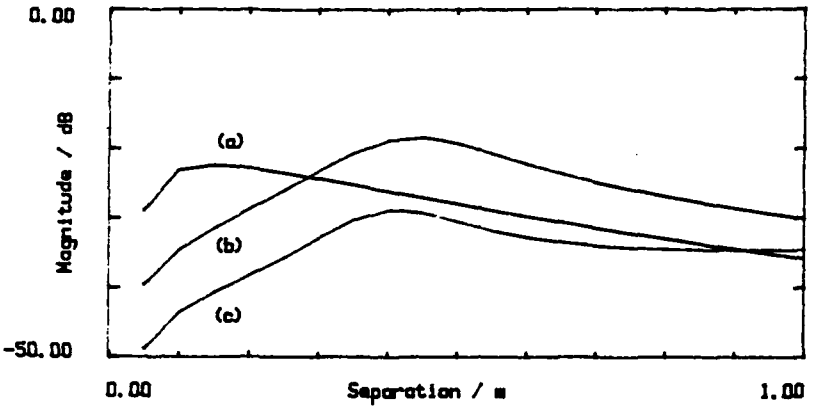

Figure 7.2 Variation of the scattered field to the direct field at 1kHz with source/receiver configuration. The medium is characterised by the four parameters, $\sigma = 10000\text{N.s.m}^{-4}$, $\Omega = 0.4$, $s_f = 0.75$ and $n' = 1$. (a) Source/receiver height=o.4m, (b) source/receiver height = 0.2m, and (c) source/receiver height = 0.1m

uation spectrum above the rigidly backed layer converges to the spectrum for the homogeneous case. In contrast to this, figure 7.4 shows similar results but for a medium in which the flow resistivity has been increased to a value of $100,000\text{N.s.m}^{-4}$. The higher attenuation associated with this higher flow resistivity, means that the excess attenuation spectrum above a layer thickness of 0.16m or greater is almost indistinguishable from that of the homogeneous case (and is not shown in the diagram). The greatest depth shown is $d = 0.04$m. The same trend as for the lower flow resistivity case occurs, but much more rapidly.

Under certain conditions, the excess attenuation spectra for for propagation above a rigid porous medium in which is embedded an oblate spheroid show similar results to those for the rigidly backed layer. Figure 7.5 shows the variation of excess attenuation spectra as the major axis radius of the spheroid is increased, from 0.05m to 0.2m, while keeping the minor axis radius constant at 0.05m and the depth d constant at 0.01m. This, in effect, is flattening the spheroid. Also shown are the spectra for propagation above a homogeneous medium and above a rigidly backed layer, with the layer thickness, d. When the major axis radius has its smallest value and

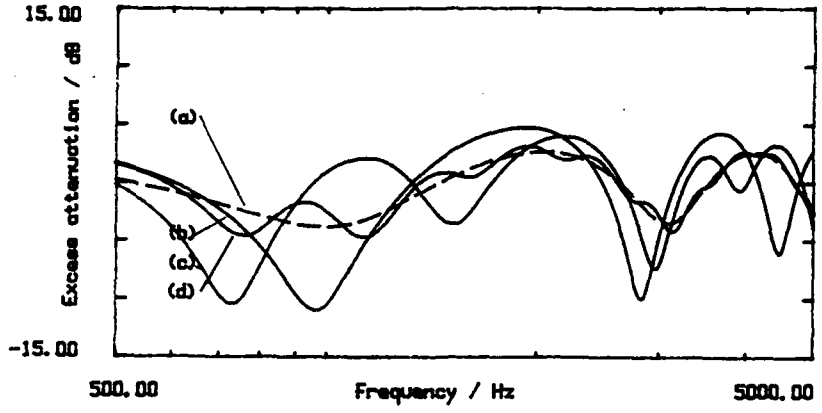

Figure 7.3 Variation of theoretical excess attenuation spectra with layer thickness for a rigidly backed layer. The coordinates, in metres, of the source and receiver are (-0.2,0.0,0.2) and (0.2,0.0,0.2), respectively. The medium is characterised by the four parameters, $\sigma = 10000\text{N.s.m}^{-4}$, $\Omega = 0.4$, $s_f = 0.75$ and $n' = 1$. (a) Homogeneous (dashed), (b) layer thickness=0.01m, (c) layer thickness=0.04m, and (d) layer thickness=0.16m.

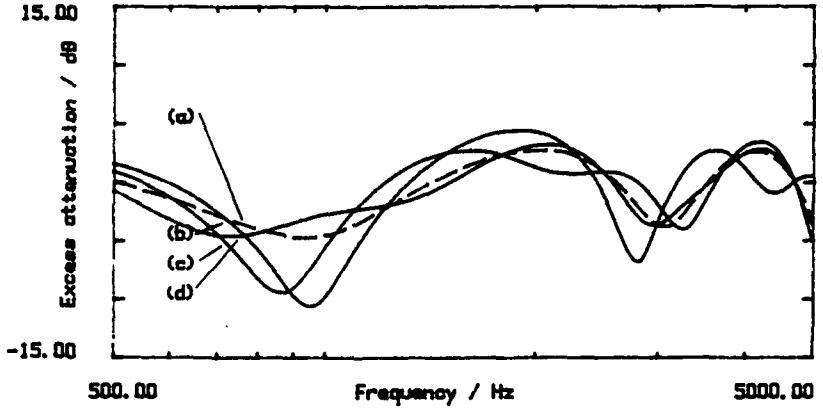

Figure 7.4 Variation of theoretical excess attenuation spectra with layer thickness for a rigidly backed layer. The coordinates, in metres, of the source and receiver are (-0.2,0.0,0.2) and (0.2,0.0,0.2), respectively. The medium is characterised by the four parameters, $\sigma = 100,000\text{N.s.m}^{-4}$, $\Omega = 0.4$; $s_f = 0.75$ and $n' = 1$. (a) Homogeneous (dashed), (b) layer thickness=0.01m, (c) layer thickness=0.02m, and (d) layer thickness=0.04m.

the the scatterer is spherical, the excess attenuation spectrum is almost indistinguishable from that of the spectrum above a homogeneous medium. However, as the radius of the oblate spheroid is increased, it can be seen that the first and subsequent minima in the excess attenuation spectra become deeper and converge to those predicted for propagation above a rigidly backed layer.

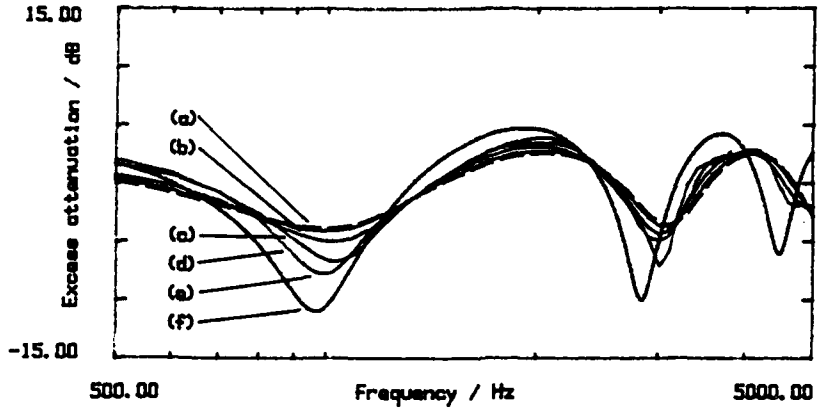

Figure 7.5 Variation of theoretical excess attenuation spectra with major axis radius for an oblate spheroid embedded within a rigid porous medium. The coordinates, in metres, of the source and receiver are (-0.2,0.0,0.2) and (0.2,0.0,0.2), respectively. The medium is characterised by the four parameters, $\sigma = 10,000\text{N.s.m}^{-4}$, $\Omega = 0.4$, $s_f = 0.75$ and $n' = 1$. Minor axis radius=0.05m.(a) Homogeneous (dashed), (b) major axis radius=0.05m (spherical), (c) major axis radius=0.1m, (d) major axis radius=0.15m, (e) major axis radius=0.2m and (f) rigidly backed layer. Depth, = 0.01m.

Figure 7.6 shows how the excess attenuation spectra vary as the oblate spheroid is flattened, *i.e.* the minor axis radius is reduced from 0.1m to 0.025m, while keeping the major axis radius constant at 0.125m, and the layer depth constant at 0.01m. This represents a different situation to the previous one. The major axis radius is kept constant, and so any effects in the resultant spectrum will be due purely to the sphericity of the scatterer rather than to change in cross-sectional aspect. For the source/receiver configuration used here (where the source/receiver separation is 0.4m, and the major axis radius is 0.125m), the oblate spheroid represents only a small fraction of the total separation. At large values of the minor axis radius,

where the oblate spheroid is least flattened (near-spheroidal), the excess attenuation spectra only differ slightly from that of the homogeneous case. Decreasing this radius does bring about a deepening of the first minimum, but only to a limited extent; the second minimum seems unaffected.An increase in the major axis radius, with the value of the smallest minor axis radius, would result in spectra being observed as in figure 7.5.

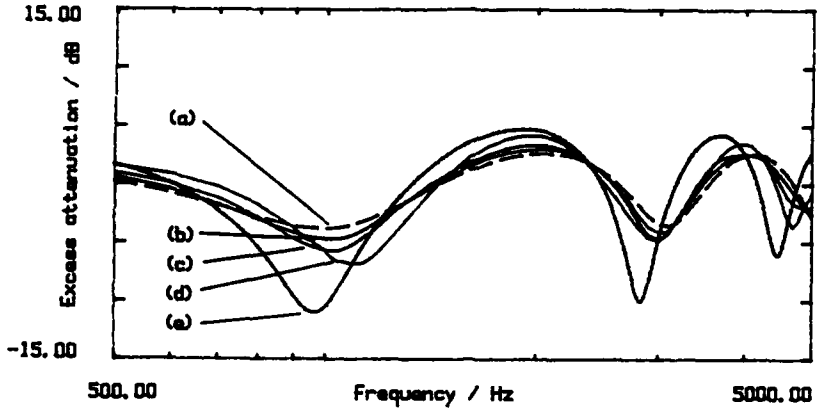

Figure 7.6 Variation of theoretical excess attenuation spectra with minor axis radius for an oblate spheroid embedded within a rigid porous medium. The coordinates, in metres, of the source and receiver are (-0.2,0.0,0.2) and (0.2,0.0,0.2), respectively. The medium is is characterised by the four parameters, $\sigma = 10,000\text{N.s.m}^{-4}$, $\Omega = 0.4$, $s_f = 0.75$ and $n' = 1$. Major axis radius = 0.125m. (a) Homogeneous (dashed), (b) minor axis radius=0.1m, (c) minor axis radius=0.05m, (d) minor axis radius=0.025m, and (e) rigidly backed layer. Depth, d= 0.01m.

Figure 7.7 shows the variation of theoretical excess attenuation spectra for an oblate spheroid of major axis radius 0.125m, and minor axis radius 0.025m, with depth,d. A similar trend in the excess attenuation spectra is observed to that for the rigidly backed layer case in figure 7.3. It can be seen that as the depth, d is varied, from 0.01m to 0.16m, the frequency of the first minimum decreases and becomes more shallow. It is also observed that the second minimum becomes more shallow and increases in frequency. At the depth d=0.16m, the excess attenuation spectrum varies only slightly from the spectrum of the homogeneous case.

If now the oblate spheroid is replaced with a circular disk, and the

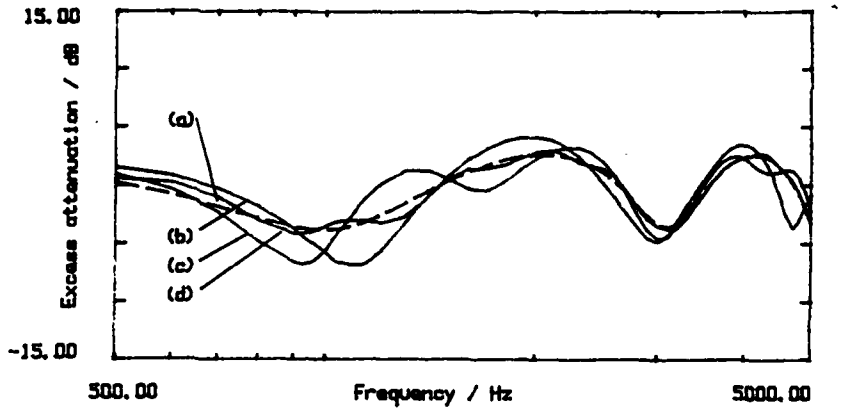

Figure 7.7 Variation of theoretical excess attenuation with layer thickness for an oblate spheroid embedded within a rigid porous medium. The coordinates, in metres, of the source and receiver are (-0.2,0.0,0.2) and (0.2,0.0,0.2), respectively. The medium is characterised by the four parameters, $\sigma = 10,000\text{N.s.m}^{-4}$, $\Omega = 0.4$, $s_f = 0.75$ and $n' = 1$. Major axis radius=0.125m, and minor axis radius=0.025m. (a) Homogeneous (dashed), (b) depth, d=0.01m, (c) depth, d=0.02m, and (d) depth, d=0.04m.

medium is assumed to be locally reacting, then similar graphs of excess attenuation spectra can be produced for comparison. Figure 7.8 shows how the excess attenuation spectra vary as the radius of the circular region is increased from 0.05m to 0.15m, while keeping the depth of the disk constant at d=0.01m. At small values of radius, the excess attenuation spectrum differs only slightly from that for propagation over a homogeneous medium. With increasing radius however, the first minimum becomes deeper and approaches that for the rigidly backed layer case. The subsequent minima, however, become deeper. With increased depths, these minima become shallower with eventual convergence to that for excess attenuation over a rigidly backed layer.

Figure 7.9 shows the variation of theoretical excess attenuation for a circular inhomogeneity of radius 0.125m, with depth, d. A similar trend in the excess attenuation spectra is observed to that for results for a rigidly backed layer in figure 7.3. It can be seen however, that with increasing depth, from 0.01m to 0.16m, the frequency of the first minimum decreases

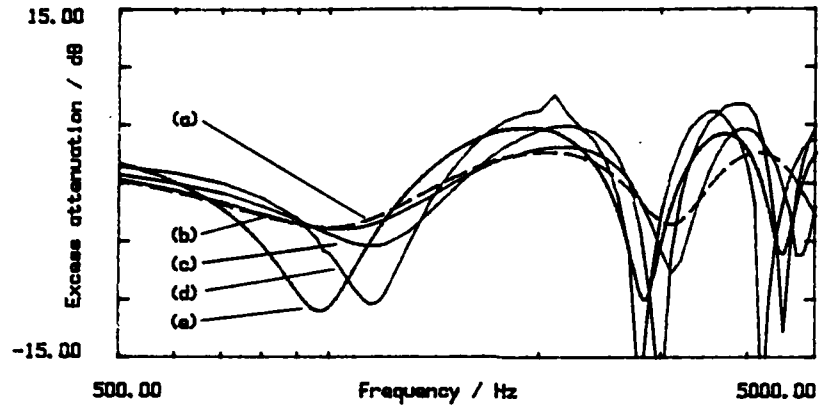

Figure 7.8 Variation of theoretical excess attenuation spectra with circular disk radius embedded within a rigid porous medium. The coordinates, in metres, of the source and receiver are (-0.2,0.0,0.2) and (0.2,0.0,0.2), respectively. The medium is is characterised by the four parameters, $\sigma = 10,000\text{N.s.m}^{-4}$, $\Omega = 0.4$, $s_f = 0.75$ and $n' = 1$. (a) Homogeneous (dashed), (b) radius=0.05m, (c) radius=0.1m, (d) radius=0.15m, and (e) rigidly backed layer. Depth, d= 0.01m

and becomes deeper before it becomes more shallow. It is also observed that the second minimum becomes more shallow and increases in frequency. At the depth d=0.16m, the excess attenuation spectrum varies only slightly from the excess attenuation spectrum for the homogeneous medium.

7.2 Experimental results

Using the experimental equipment and procedure described in chapter 6, level difference spectra were measured over the pea-gravel, fibreglass and polyurethane foam containing the different test scatterers. The source / receiver configuration of figure 6.1 was used to measure the level difference spectra.

Figure 7.10 shows both the experimental and predicted level difference spectra for the homogeneous media, the predictions being calculated by equation (3.33) for the low flow resistivity and high porosity polyurethane foam, and by equation (3.45) for the pea-gravel and fibreglass. It can be seen that the three media display quite different spectra, with the polyurethane

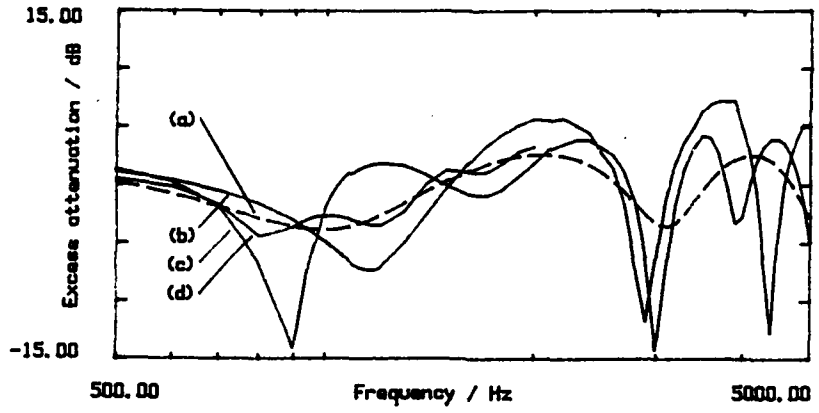

Figure 7.9 Variation of theoretical excess attenuation spectra with depth for a circular disk embedded within a rigid porous medium. The coordinates, in metres, are (-0.2,0.0,0.2) and (0.2,0.0,0.2), respectively. The medium is characterised by the four parameters, $\sigma = 10,000\text{N.s.m}^{-4}$, $\Omega = 0.4$, $s_f = 0.75$ and $n' = 1$. Major axis radius=0.125m, and minor axis radius=0.025m. (a) Homogeneous (dashed), (b) depth, d=0.01m, (c) depth, d=0.04m, and (d) depth, d=0.16m.

foam showing weak interference minima, with more defined minima for the pea-gravel. This variation of the spectra according to the type of medium being considered, has been used as the basis for the studies of soil type [13]. These spectra can now be compared with spectra measured over media containing the various scatterers.

Predictions have shown that the presence of oblate spheroids results in deepening of the first minimum of the excess attenuation spectra and that the more oblate the spheroid becomes, the deeper the minimum becomes. Figure 7.11 shows how experimental and predicted level difference spectra vary as a spheroid of major axis radius 0.125m, is flattened, *i.e.* the minor axis radius is reduced from 0.05m to 0.025m while keeping the depth constant at d=0.025m. It can be seen that the experimental results show that the first minimum becomes deeper with decreasing minor axis radius, but overall, the variations in the spectra associated with the spheroids are not predicted.

The comparison of predicted and experimental level difference spectra is

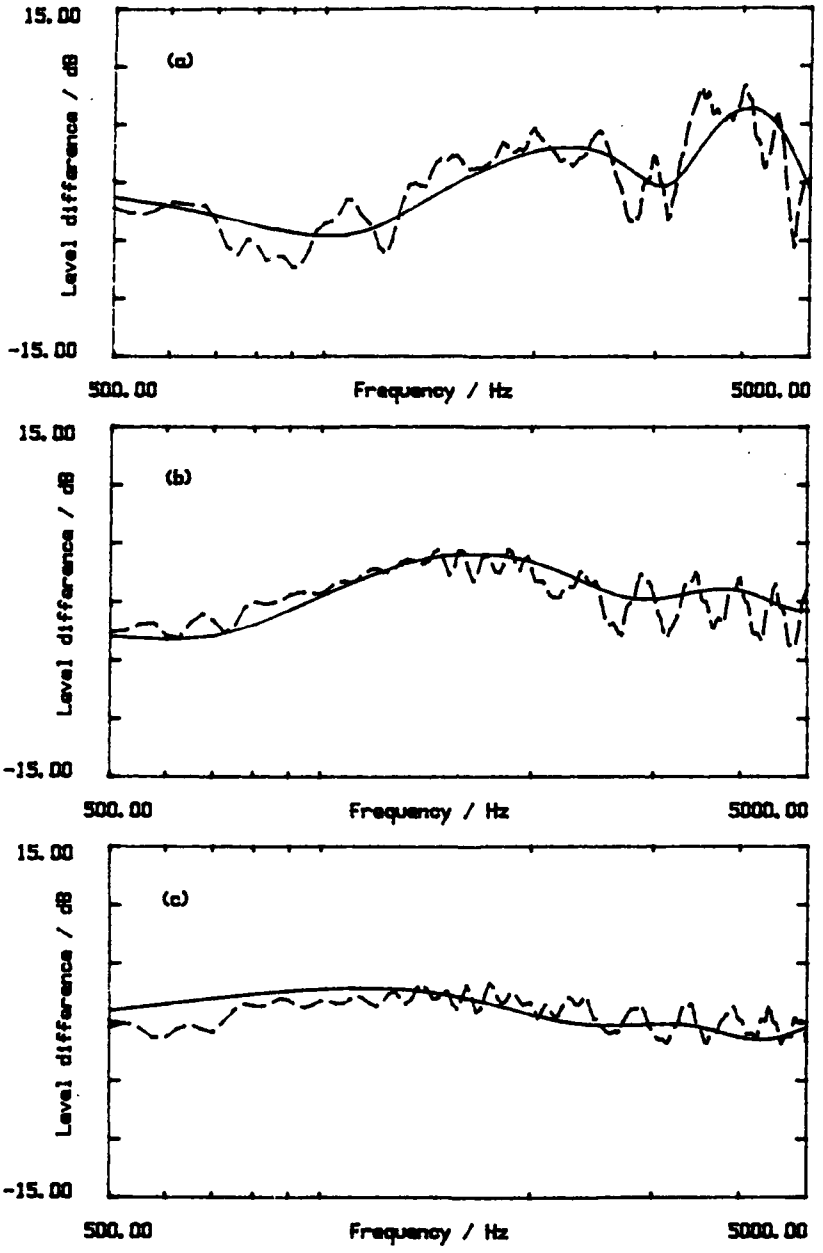

Figure 7.10 Experimental and predicted level difference spectra measured over pea-gravel, fibreglass and polyurethane foam. The coordinates, in metres, of the source and microphones are (-0.2,0.0,0.2), (0.2,0.0,0.05) and (0.2,0.0,0.2); solid line - predicted, dashed line - experimental. (a) Gravel, (b) glass-fibre, (c) polyurethane foam.

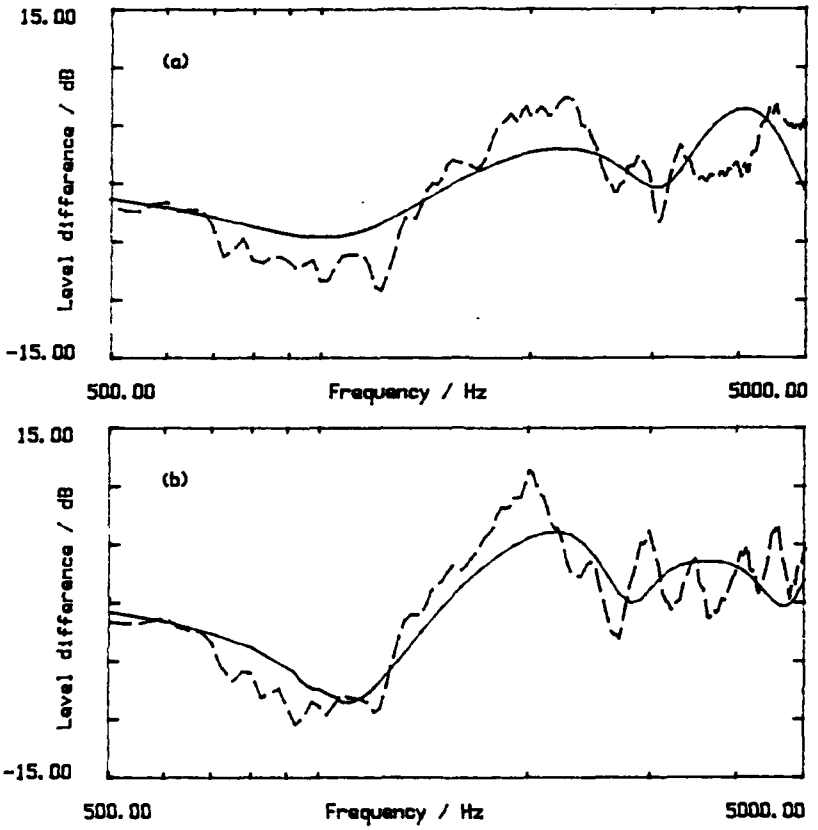

Figure 7.11 Variation of experimental and predicted level difference spectra with oblate spheroid minor axis radius in gravel. The coordinates, in metres, of the source and microphones are (-0.2,0.0,0.2), (0.2,0.0,0.05) and (0.2,0.0,0.2); solid line - predicted, dashed line - experimental; major axis radius = 0.125m; depth, d=0.015m. (a) Minor axis radius=0.05m, (b) minor axis radius=0.025m.

much better in figure 7.12 which shows the variation of spectra with radius of an embedded metal disk . Three different disk radii are considered, all at a layer depth of 0.015m within the gravel. The spectra display quite marked maxima and minima, in contrast to those observed in figure 7.11. Indeed, observable differences, compared to that of the homogeneous case, occur with a disk radius of 0.15m. Figure 7.13 shows similar results for fibreglass. Here, however, with the higher value of flow resistivity, the changes in the spectra compared to that of the homogeneous case are less marked and only results for disk radii of 0.25m and 0.2m are presented. Figure 7.14 shows again, similar results for polyurethane foam. The very low flow resistivity and porosity associated with this medium implies considerable extended reaction, and hence, due to the basic conditions set out in the boundary value problem, no predictions of these spectra will be valid. However, it is observed that the general trend of the spectra with decreasing disk radii is similar to that for the pea-gravel and fibreglass.

The previous figures have shown that the largest changes in the level difference spectra occur when, for a given depth, the radius of the disk is large, or, for the case of spheroids, when the major axis radius is large, and the minor axis radius is small. Figure 7.15 shows the variation of level difference spectra with position above an embedded oblate spheroid of major axis radius 0.125m, and minor axis radius 0.025m. As the point of specular reflection (for the upper microphone) moves progressively further away from the centre of the spheroid, the minima become less deep. Figure 7.16 shows a similar results above a disk of radius 0.125m embedded at a depth of 0.015m in gravel. The variation in the maxima and minima are adequately predicted by the theory. Finally, figure 7.17 shows results above a disk of radius 0.125m embedded at a depth, d=0.025m in foam.

7.3 Summary

The theoretical and experimental results of this study have been presented in this chapter, and the chapter first considered theoretical predictions in

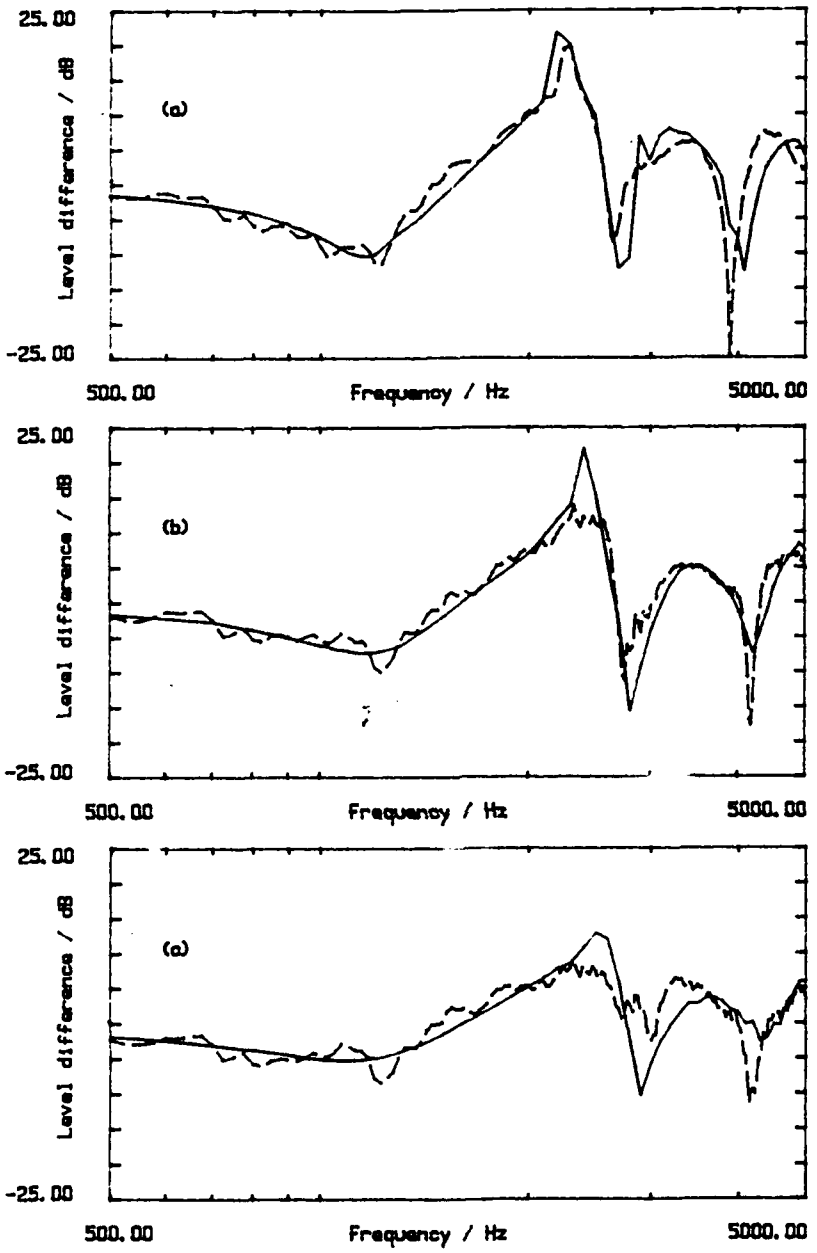

Figure 7.12 Variation of experimental and predicted level difference spectra with disk radius in gravel. The coordinates, in metres, of the source and microphones are (-0.2,0.0,0.2), (0.2,0.0,0.05) and (0.2,0.0,0.2); solid line - predicted, dashed line - experimental; depth d=0.015m. (a) Radius=0.25m, (b) radius=0.20m, and (c) radius=0.15m.

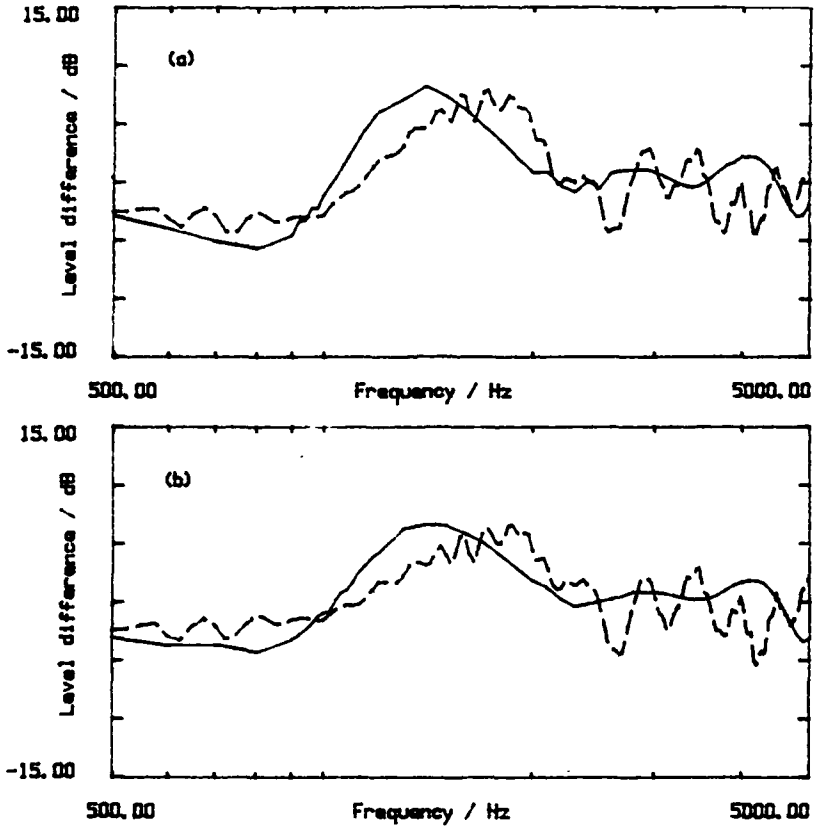

Figure 7.13 Variation of experimental and predicted level difference spectra with disk radius in fibreglass. The coordinates, in metres, of the source and microphones are (-0.2,0.0,0.2), (0.2,0.0,0.05) and (0.2,0.0,0.2); solid line - predicted, dashed line - experimental; depth, d=0.025m. (a) Radius=0.25m and (b) radius=0.20m.

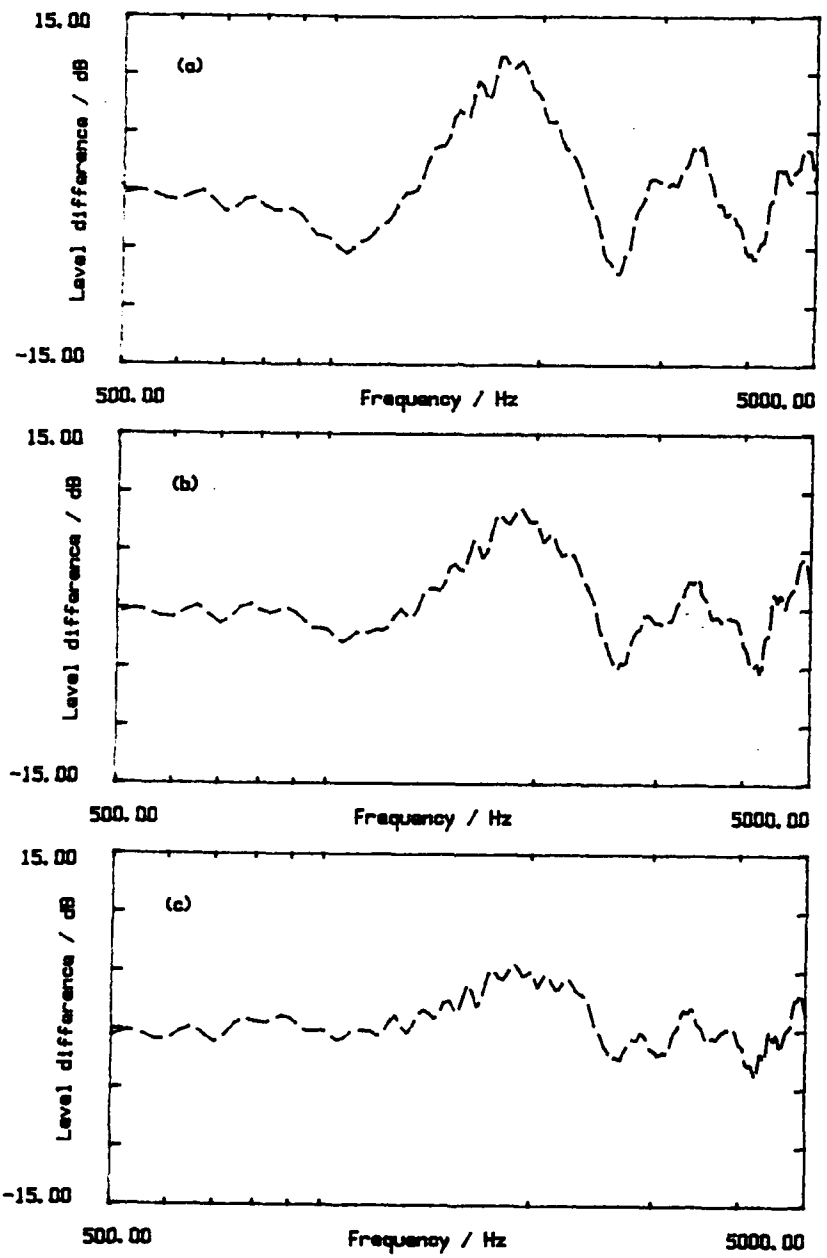

Figure 7.14 Variation of experimental and predicted level difference spectra with disk radius in polyurethane foam. The coordinates, in metres, of the source and microphones are (-0.2,0.0,0.2), (0.2,0.0,0.05) and (0.2,0.0,0.2); solid line - predicted, dashed line - experimental; depth, d=0.025m. (a) Radius=0.25m, (b) radius=0.20m and (c) radius=0.15m

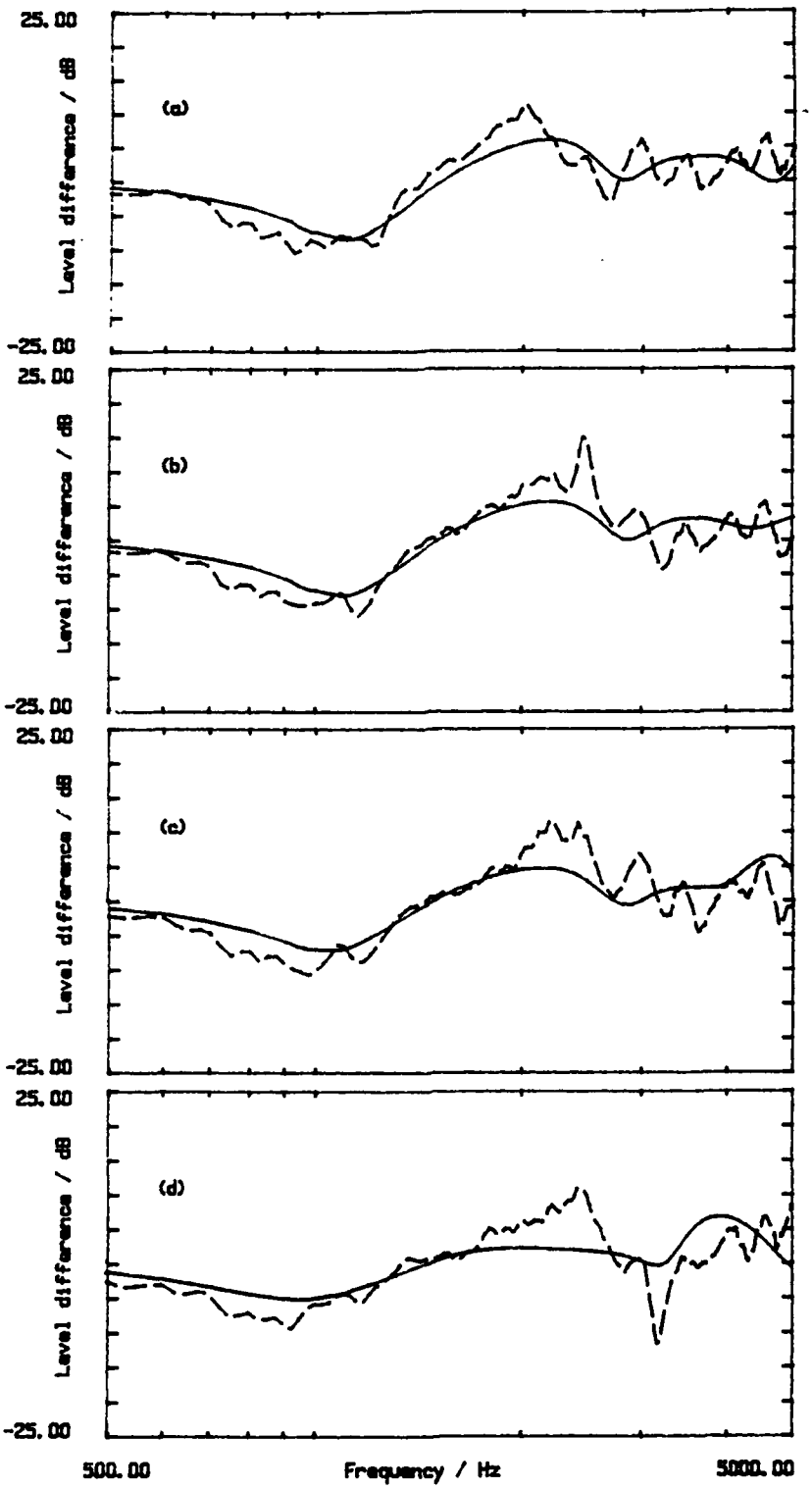

Figure 7.15 Variation of experimental and predicted level difference spectra with position above an oblate spheroid in gravel. Major axis radius=0.125m, minor axis radius=0.025m, layer depth=0.015m. The coordinates, in metres, of the source and microphones are (-0.2,Y,0.2), (0.2,Y,0.05) and (0.2,Y,0.2); solid line - predicted, dashed line - experimental. (a) Y=0.0, (b) Y=0.05, (c) Y=0.1 and (d) Y=0.2.

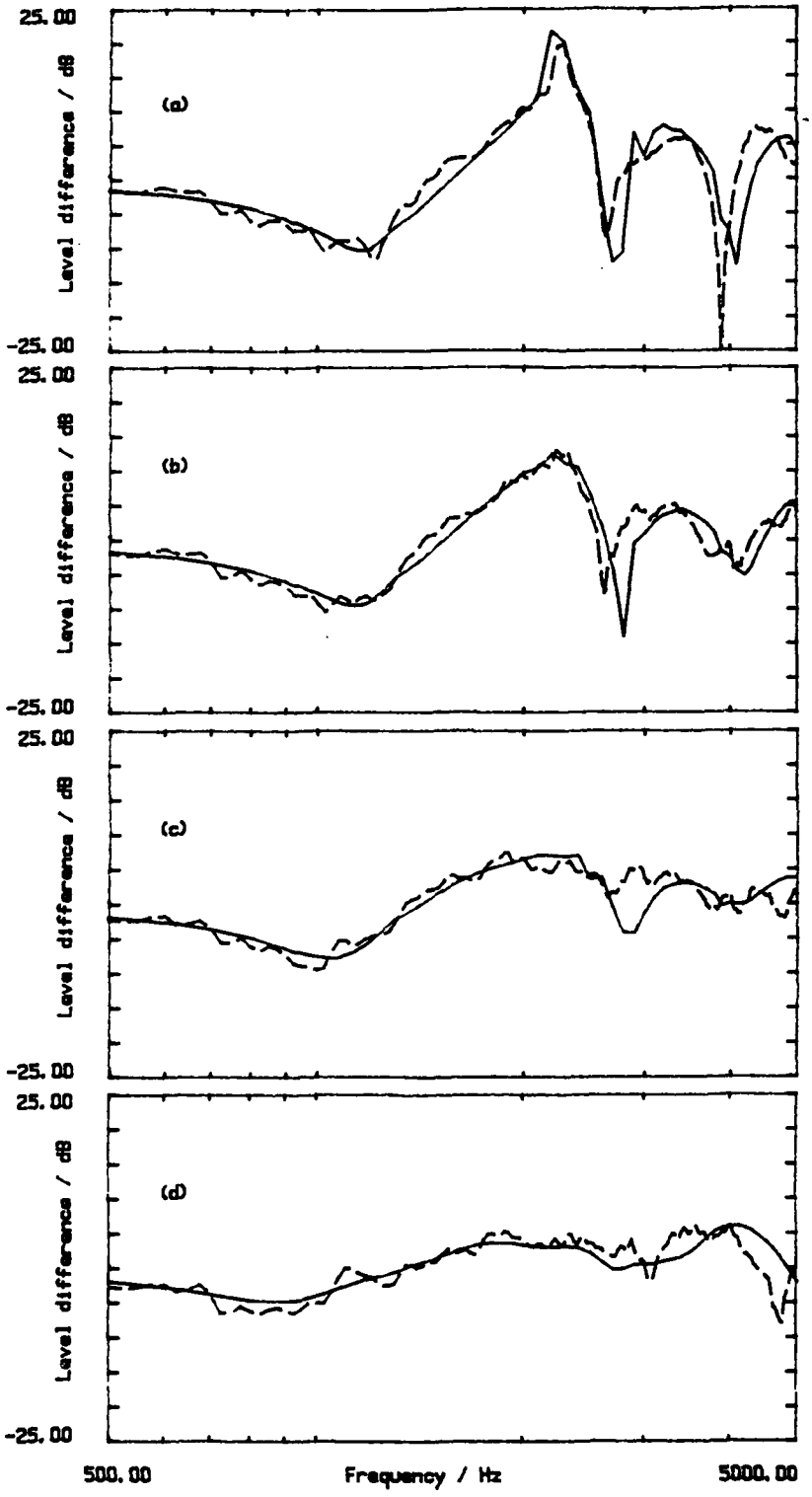

Figure 7.16 Variation of experimental and predicted level difference spectra with position above a disk in gravel. Radius=0.125m, layer depth=0.015m. The coordinates, in metres, of the source and microphones are (-0.2,Y,0.2), (0.2,Y,0.05) and (0.2,Y,0.2); solid line - predicted, dashed line - experimental. (a) Y=0.0, (b) Y=0.05, (c) Y=0.1 and (d) Y=0.2.

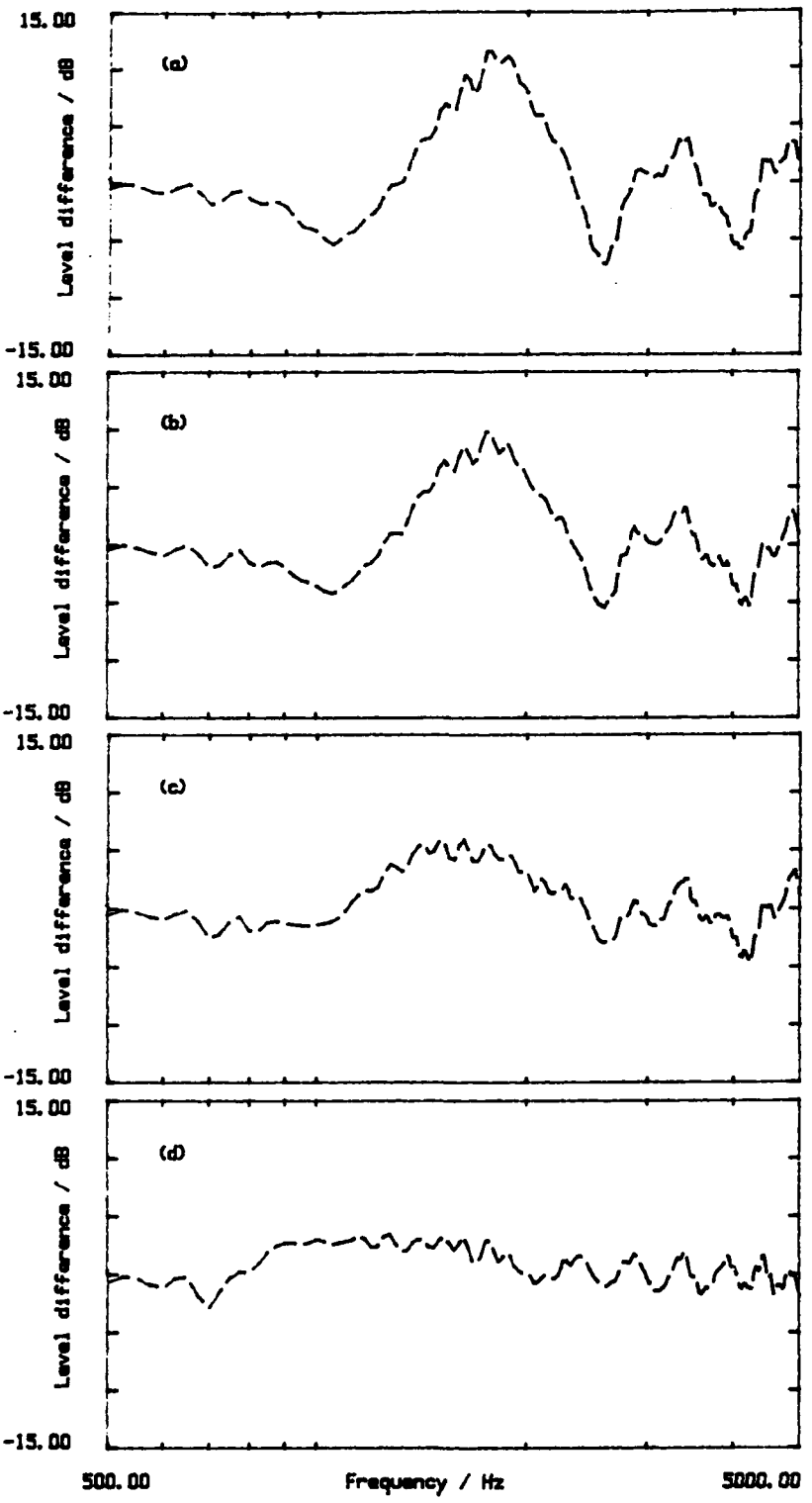

Figure 7.17 Variation of experimental level difference spectra with position above a disk in polyurethane foam. Radius=0.125m, layer depth=0.015m. The coordinates, in metres, of the source and microphones are (-0.2,Y,0.2), (0.2,Y,0.05) and (0.2,Y,0.2); solid line - predicted, dashed line - experimental. (a) Y=0.0, (b) Y=0.05, (c) Y=0.1 and (d) Y=0.2.

the form of excess attenuation spectra. These results showed that there was reasonable convergence of the methods with that for a rigidly backed layer, for varying disk and spheroid sizes and shapes. With the confidence in the theory gained by these tests, the theory was then compared with experimental data. Measurements were conducted with oblate spheroids and disks in gravel and disks in fibreglass and polyurethane foam, with theory being compared with all results apart from those for the polyurethane foam.

It was surprising that there was such good agreement of experimental results with the predictions of the theory, for the case of disk embedded within the gravel. The low value of flow resistivity of the gravel meant that the gravel was at the limit of the locally reacting condition. Agreement with predictions and experimental results for the oblate spheroids embedded within the gravel less good. Several reasons are proposed for this. Firstly, the transmission Green's functions used in the boundary element method were at the limit of their validity for the low flow resistivity of the gravel, which would result in slightly inaccurate predictions; the second reason is an experimental one *i.e.* the measurements were constrained practically by the dimensions of the tray containing the gravel, resulting in possible stray reflections its base and sides *i.e.* the gravel was not behaving as semi-infinite. This seems more likely in the case of the measurements over the spheroids, where their influence on the reflected field is much weaker than that from the disks, making the measurements more susceptible to stray reflections. A final reason is that the spheroids were made of wood, and were possibly not exhibiting the required rigid surface that was being modelled.

It is proposed that the poor agreement of the predictions with the results of the disks in fibreglass was due to the anisotropic nature of the medium. With the the thickness of fibreglass medium used ($\sim$ 30cm) it was assumed that the medium was behaving as semi-infinite. The layered nature of the medium, where it was made up of six separate sheets placed on top of each other, may have contributed to an unusual behaviour.

With the low flow resistivity of the polyurethane foam, no reasonable theoretical predictions could be made. However, similar trends in the ex-

perimental results to those of the gravel and fibreglass were observed.

Chapter 8

Discussions and conclusions

The various theoretical and experimental results were described in the previous chapter, and a discussion of their particular significance was given. In this concluding chapter, a review of these results, together with a discussion of the limitations and future extensions of the mathematical model and experimental investigation, are considered, and the chapter is completed with some general conclusions.

8.1 Review of present study

The aim of this study was twofold. Firstly, to provide a theoretical description of the influence of near-surface inhomogeneities on the reflection of acoustic fields at the surface of a porous medium. Secondly, to compare quantitively these theoretical predictions with measured acoustic fields across the surfaces of porous media containing embedded inhomogeneities so that the practical usefulness of the theory could be tested.

The theoretical development of the problem was straightforward, starting with its mathematical formulation in chapter 2. Two separate approaches were considered. The first approach, that of considering a scatterer within the rigid porous medium, was first stated in terms of a boundary value problem. The development here assumed that the scatterer was rigid, *i.e.* that the Neumann boundary condition applied on its surface. Two reformulations of this boundary value problem in terms of integral

equations via Green's second theorem were then presented, both reformulations requiring the Green's function solutions to much simpler problems; in the first, the problem involved the complicated calculation of Green's functions for propagation in the presence of a plane boundary separating two semi-infinite homogeneous media; in the second, the simpler calculation of Free-field Green's functions sufficed. The resultant integral equation for the first reformulation was conceptually simple, involving one integral term solely over the surface of the scatterer. In contrast, the second reformulation, involved a set of coupled integral equations with an integral having an infinite region of integration. Due to the difficulty of solving such a set of equations, the first integral equation was chosen for solution.

The second approach to the theoretical problem considered scattering by a small finite region in the plane boundary having a surface impedance different to that of the surrounding area. The boundary was assumed to be locally reacting, and as such, the details of the sound propagating in the lower medium could be ignored, and the sound propagating in the upper medium could be determined by the boundary's surface impedance. The reformulation of the boundary value problem in terms of an integral equation was similar to that of the first approach, requiring the Green's function solution of the much simpler problem of sound propagation in the upper medium only. The resultant integral equation involved a simple integral over the scattering surface.

The numerical solution of the integral equations requires Green's functions and their first derivatives for various source and receiver configurations and chapter 3 derived simple expressions for these. For the first approach, with the source and receiver configurations considered, approximations to the integral representations of the Green's functions involved just two terms, a direct component and a plane wave reflected component. Ignoring higher order terms, the first derivatives of these Green's functions were simple. The approximation to the transmitted Green's function used a simple expression combining the incident field at a point directly above the receiver point with an exponential term. This approximation required that the imaginary com-

ponent of the refractive index was large. For the second approach, where the boundary was assumed to be locally reacting, the Green's function for propagation from one point to another in the upper medium was given by the Weyl-Van der Pol equation.

In a sense, the second approach considers a more general problem than the first, in that the surface impedance within the finite region could take any form. The simplest situation that could have been considered was that of sound propagation over a finite region where the surface impedance within the region was modelled as homogeneous but different from the surrounding area. However, the impedance types considered in this study, were firstly, that due to a finite rigidly backed layer, *i.e.* in effect, a disk embedded within the porous medium; and secondly, that induced by an embedded rigid sphere. The expressions for these impedance types were considered in chapter 4. The derivation for the expressions for the induced surface impedance due to an embedded sphere were based on a number of assumptions:

1. that the incident waves on the plane boundary were the source of plane waves being transmitted normally in the lower medium;
2. that only one interaction with the spherical scatterer occured (*i.e.* that there was no multiple scattering);
3. that the interaction of the scattered wave with the plane boundary was expressed in terms of the plane wave reflection coefficient.

Other impedance functions within the region could have been considered such as that induced by a spheroid (which would have involved a spheroidal system). However, these expressions would have required further derivation, and were beyond the scope of this study.

Chapter 5 considered the numerical solution of the integral equations from both approaches, using a simple boundary element method. The solution method was straightforward: firstly, the values of complex pressure were determined on the scattering surface by letting the receiver point to be on the surface of the scatterer. This resulted in a set of simultaneous linear equations, efficient solution of which could only be carried out if the

scattering surfaces were axisymmetric about the vertical axis through their centres. With this condition, it was seen that the resultant matrices were block-circulant, a structure for which standard routines are available for solution. With these values of pressure on the surfaces of the integrating surfaces, the complex pressure at points away from the scatterers could be calculated by substitution back into the original equations.

A particular difficulty involved in the solution of the integral equation from the first approach was that the kernel function of the integral tended to infinity as the receiver point approached the source points on the surface of the scatterer, and a simple modification of the original integral equation was required. This resulted in a slightly more complex integral equation, but the block-circulant structure of the matrices is maintained.

In both approaches the scattering surfaces were divided into a number of boundary elements, and expressions for the normals, positions of the midpoints, and areas of the elements were derived. For the first approach, the scattering surfaces were restricted to spheroids, which meant that the basic shape of the scatterer could be varied from an oblate spheroid to a sphere without requiring extra subroutines. For the second approach, the scattering region, to satisfy axi-symmetry, was circular.

The experimental method for measuring level difference spectra over the scatterers embedded within the three different media was presented in chapter 6, describing in detail, the experimental procedure and apparatus, the scatterers and media. This chapter was then followed by a presentation of the results in chapter 7, with a discussion of the main conclusions to be drawn.

8.2 Limitations and future work

The major limitation of the surface inhomogeneity approach theory presented here is that it has not been possible to make any predictions when the medium is externally reacting. The initial boundary conditions of the boundary value problem involved the Robin boundary condition, thus im-

posing the condition of local reaction straight away. This is an omission of some importance for as might be expected, the greatest contribution of the scattered field occurs when the medium has a low flow resistivity, and hence is externally reacting. This problem is much more involved than those considered and is beyond the scope of this study.

However, an experimental investigation of the scattering from disks embedded in polyurethane foam was carried out, showing that the influence of the scatterer was quite dramatic and has a similar form to that observed in gravel.

The restriction on the lower frequency of interest to that of 500Hz has meant that the considerations have been made purely of rigid porous media, *i.e.* that the reflection of sound from a rigid porous half space is governed by the slow wave in the interconnected pores. No consideration of the seismic contributions has been considered.

Essential to the calculation of the boundary integral equation methods developed, is the ability to calculate, accurately and efficiently, the propagation of sound from a point source above and across a plane boundary. With the simple expressions for these Green's functions used, using just plane wave reflection coefficients and a large refractive index approximation (in the case of transmission), a certain amount of inaccuracy in the boundary integral equations methods will arise, but this has not been assessed in the study.

This study has not concerned itself with the prediction of acoustic fields in the lower medium in the presence of a near-surface scatterer. The study has been concerned purely with the influence of near-surface scatterers on the reflection of sound from the plane boundary. However, the the boundary element method lends itself just as easily to the analysis of fields in the lower medium as it does to the upper medium. It has not been pursued for the obvious reason that experimental comparison with the theoretical predictions would prove difficult.

With these limitations of the study in mind, the following suggestions for future work seem to be most appropriate:

1. further development of expressions for the Green's functions and their first derivatives for the propagation in the presence of an externally reacting medium and penetrable scatterers;
2. extension of the theory to predicting the influence of near-surface inhomogeneities on the reflection of acoustic fields from poro-elastic media;
3. further experimental investigation of the influence of near-surface *and* surface inhomogeneities on the reflection of acoustic fields from porous media, with a natural progression to measurements of seismic as well as acoustic influences.

8.3 Conclusions

The aim of this study was both to investigate theoretically and experimentally the influence of near-surface inhomogeneities on the reflection of acoustic fields at the surface of a porous medium. The majority of the study has been devoted to the development of the boundary integral equation method for the theoretical investigation. The boundary integral equation method has been shown by many authors, to be very effective for the calculation of acoustic fields over terrains of variable height and surface impedance. There is no doubt that application of the method to the problem of this study is appropriate. That there is an influence on the reflection of acoustic fields at the surface of a porous medium by a near-surface inhomogeneity is arguable intuitively. However, this study has shown both theoretically and experimentally that this influence is highly dependent on the medium characteristics and the shape and size of the scatterer. In particular, it has been shown that a near-surface embedded inhomogeneity with a spherical shape has a negligible influence on the level difference shape unless its radius is large. Furthermore, it has been shown that the more oblate the spheroid, the greater the influence on the level difference spectrum for a given cross sectional area of the spheroid.

The study can have wider implications. The theory could be adapted

to the problem of longer range sound propagation over inhomogeneous media. At present, models are only available for predicting sound propagation over infinite strips, as in the case of determining the noise from roads near grasslands [91]. For the case of architectural acoustics, the theory could be developed for determining the effect of absorbing patches in rooms. Finally, the use of this theory in non destructive testing can only be hinted at.

The results of this study should help to understand the behaviour of acoustic fields above inhomogeneous media containing near-surface scatterers, and to provide expressions for their prediction under certain restrictions. However, there is considerable scope, through a consideration of more accurate Green's functions, for providing a more accurate picture of the theoretical problem and to provide general rules to achieve certain specifications. With the high dependence of the scattered field on the medium properties, and the scatterer shape, it remains to be seen whether a successful application will be found.

Bibliography

[1] M.A. Biot. Theory of propagation of elastic waves in a fluid saturated porous solid. 1 low-frequency range. *Journal of the Acoustical Society of America*, 28(2):168–178, 1956.

[2] M.A. Biot. Theory of propagation of elastic waves in a fluid saturated porous solid. 2 higher frequency range. *Journal of the Acoustical Society of America*, 28(2):179–191, 1956.

[3] K. Attenborough. Acoustical characteristics of rigid fibrous absorbents and granular materials. *Journal of the Acoustical Society of America*, 73:785–799, 1983.

[4] J.M. Sabatier, H.E. Bass, and L.N. Bolen. Acoustically induced seismic waves. *Journal of the Acoustical Society of America*, 80(2):646–649, 1986.

[5] T.L. Richards, K. Attenborough, N.W. Heap, and A.P. Watson. Penetration of sound from a point source into a rigid porous medium. *Journal of the Acoustical Society of America*, 78:956 – 963, 1985.

[6] K. Attenborough. On the acoustic slow wave in air filled granular media. *Journal of the Acoustical Society of America*, 81(1):93–102, Jan. 1987.

[7] M.E. Delany and E.N. Bazley. Acoustical properties of fibrous absorbent materials. *Applied Acoustics*, 3:105 – 116, 1970.

[8] C.I. Chessel. Propagation of noise along a finite impedance boundary. *J.Acoust.Soc.Am.*, 62:825–834, 1977.

[9] K. Attenborough. Acoustical impedance models for outdoor ground surfaces. *Journal of sound and vibration*, 99:521–544, 1985.

[10] K. Attenborough, J.M. Sabatier, H.E. Bass, and L.N. Bolen. The acoustic transfer function at the surface of a layered poroelastic soil. *Journal of the Acoustical Society of America*, 79(5):1353–1358, 1986.

[11] K. Attenborough and H.M. Hess. Acoustical surveying of porous soils. In *14th International Symposium on Acoustical Imaging*, 1985.

[12] K. Attenborough, H. Bass, and L.N. Bolen. Sound transmission into plane porous ground surfaces. *Acoustics letters*, 6(6):87 – 90, 1982.

[13] H.M. Hess. *Acoustical determination of physical properties of porous grounds.* PhD thesis, Open University, 1988.

[14] J.M. Sabatier, H.E. Bass, L.M. Bolen, K. Attenborough, and V.V.S.S. Sastry. The interaction of airborne sound with the porous ground: the theoretical formulation. *Journal of the Acoustical Society of America*, 79(5):1345–1352, May 1986.

[15] G.A. Daigle and M.R. Stinson. Measurement of normal incidence impedence of outdoor ground surfaces in the frequency range 20-500hz. *Journal of the Acoustical Society of America*, Suppl.1 (78):586, 1985.

[16] J.J. Faran Jr. Sound scattering by thin elastic shells. *Journal of the Acoustical Society of America*, 23:405 – 418, 1951.

[17] M.C. Junger. Sound scattering by thin elasic shells. *Journal of the Acoustical Society of America*, 24:366 – 373, 1952.

[18] R. Hickling. Analysis of echoes from a hollow elastic sphere in water. *Journal of the Acoustical Society of America*, 34:1582, 1962.

[19] K. Yosioka and Y. Kawasima. Acoustic radiation pressure on a compressible sphere. *Acustica*, 5:167 – 173, 1955.

[20] T. Hasegawa and K. Yosioka. Acoustic radiation force on a solid elastic sphere. *Journal of the Acoustical Society of America*, 46:1139 – 1143, 1969.

[21] R. Hickling. Analysis of echoes for a hollow metallic sphere in water. *Journal of the Acoustical Society of America*, 36:1124 – 1137, 1964.

[22] R. Doolittle and H. Überall. Sound scattering by elastic cylindrical shells. *Journal of the Acoustical Society of America*, 39:272 – 275, 1966.

[23] A. Bostrom. Scattering of stationary acoustic waves by an elastic immersed in a fluid. *Journal of the Acoustical Society of America*, 67:390 – 398, 1980.

[24] B. Petersen, V.V. Varadan, and V.K. Varadan. Scattering of acoustic waves by layered elastic and viscoelastic obstacles in water. *Journal of the Acoustical Society of America*, 68:673 – 685, 1980.

[25] L. Flax, L.R. Dragonette, V.K. Varadan, and V.V. Varadan. Analysis and computation of the acoustic scattering by an elastic prolate spheroid obtained from the t-matrix formulation. *Journal of the Acoustical Society of America*, 71:1077 – 1082, 1982.

[26] T.A.K. Pillai, V.V. Varadan, and V.K. Varadan. Sound scattering by rigid and elastic infinite elliptical cylinders in water. *Journal of the Acoustical Society of America*, 72:1032 – 1037, 1982.

[27] T.A.K. Pillai, V.V. Varadan, V.K. Varadan, and R.P. Radlinski. Acoustic wave scattering by elastic cylindrical shells in water. *Journal of the Acoustical Society of America*, 74:619 – 624, 1983.

[28] A. Bostrom. Scattering of acoustic waves by a layered elastic obstacle in a fluid - an improved null field approach. *Journal of the Acoustical Society of America*, 76:588 – 593, 1984.

[29] J.D. Murphy, E.D. Breitenbach, and H. Überall. Resonance scattering of acoustic waves from cylindrical shells. *Journal of the Acoustical Society of America*, 64:677 – 683, 1978.

[30] J.D. Murphy, A. George, J. Nagl, and H. Überall. Isolation of the resonant component in acoustic scattering from fluid - loaded elastic spherical shells. *Journal of the Acoustical Society of America*, 65:368 – 373, 1979.

[31] L. Flax, L.R. Dragonette, and H. Überall. Theory of elastic resonance excitation by sound scattering. *Journal of the Acoustical Society of America*, 63:723 – 731, 1978.

[32] L. Flax, P.K. Raju, J. George, and H. Überall. Resonating fields inside elastic scattering objects. *Journal of the Acoustical Society of America*, 68:973 – 979, 1980.

[33] D. Brill and G.C. Gaunaurd. Acoustic resonance scattering by a penetrable cylinder. *Journal of the Acoustical Society of America*, 73:1448 – 1455, 1983.

[34] G. Gaunaurd and H. Überall. Rst analysis of monostatic and bistatic acoustic echoes from an elastic sphere. *Journal of the Acoustical Society of America*, 73:1 – 12, 1983.

[35] G. Chertock. Sound radiation from vibrating surfaces. *Journal of the Acoustical Society of America*, 36:1305 – 1313, 1964.

[36] H.A. Schenck. Improved integral formulation for acoustic radiation problems. *Journal of the Acoustical Society of America*, 44:41 – 58, 1968.

[37] G.H. Koopman and H. Benner. Method for computing the sound power of machines based on the helmholtz integral. *Journal of the Acoustical Society of America*, 71:78 – 89, 1982.

[38] A.F. Seybert, B. Soenarko, F.J. Rizzo, and D.J. Shippy. An advanced computational method for radiation and scattering of acoustic waves in three dimensions. *Journal of the Acoustical Society of America*, 77:362 – 368, 1985.

[39] W. Tobocman. Calculation of acoustic wave scattering by means of the helmholtz integral equation. *Journal of the Acoustical Society of America*, 76:599 – 607, 1984.

[40] W. Tobocman. Calculation of acoustic wave scattering by means of the helmholtz integral equation. ii. *Journal of the Acoustical Society of America*, 76:1549 – 1554, 1984.

[41] A.F. Seybert, B. Soenarko, F.J. Rizzo, and D.J. Shippy. A special integral equation formulation for acoustic radiation and scattering for axisymmetric bodies and boundary conditions. *Journal of the Acoustical Society of America*, 80:1241 – 1247, 1986.

[42] H.A. Schenck. Helmholtz integral equation formulation of the sonar equations. *Journal of the Acoustical Society of America*, 79:1423 – 1433, 1986.

[43] A.F. Seybert, T.W. Wu, and X.F. Wu. Radiation and scattering of acoustic waves from elastic solids and shells using the boundary element method. *Journal of the Acoustical Society of America*, 84(5):1906 – 1912, 1988.

[44] D. Colton and R. Kress. *Integral equation methods in scattering theory.* Wiley, 1983.

[45] P. Filippi, editor. *Theoretical acoustics and numerical techniques.* Springer-Verlag, 1983.

[46] R.P. Shaw. Boundary integral equation methods applied to wave problems 1. In P.K. Banerjee and R. Butterfield, editors, *Developments in boundary element methods*, Applied science publishers, 1979.

[47] A. Daumas. Etude de la diffraction par un écran mince disposé sur le sol. *Acustica*, 40:213–222, 1978.

[48] R. Seznec. Diffraction of sound around barriers: use of the boundary elements technique. *Journal of Sound and Vibration*, 73(2):195–209, 1980.

[49] S.N. Chandler-Wilde and D.C. Hothersall. The boundary integral equation method in outdoor sound propagation. In *Proceedings of the Institute of Acoustics Vol. 9*, 1987.

[50] D. Habault. Sound propagation above an inhomogeneous plane: boundary integral equation methods. *Journal of Sound and Vibration*, 100(1):55 – 67, 1985.

[51] S.N. Chandler-Wilde and D.C. Hothersall. Sound propagation over an inhomogeneous impedance plane. *Journal of Sound and Vibration*, 98:475 – 491, 1985.

[52] S.N. Chandler-Wilde and M.J.C. Gover. On the application of a generalization of toeplitz matrices to the numerical solution of integral equations with weakly singular convolution kernels. *Journal of Numerical Analysis*, 9:525–544, 1989.

[53] G. Kristensson and S. Ström. Scattering from buried inhomogeneities - a general three-dimensional formalism. *Journal of the Acoustical Society of America*, 64(3):917 – 936, 1978.

[54] H.E. Bass and G.E. Baird. Acoustic techniques for buried mine sensing. Physical Acoustics Research Laboratory, 1986.

[55] K.B. Rasmussen. Sound propagation over grass-covered ground. *Journal of Sound and Vibration*, 78(2):247–255, 1981.

[56] D. Habault and C. Corsain. Identification of acoustical properties of a ground surface. *Journal of Sound and Vibration*, 1985.

[57] A. Soom and R-R. Gu. Average excess attenuation during sound propagation from an isotropic source above grassland. *Journal of the Acoustical Society of America*, 70(4):1129–1139, 1981.

[58] C. Glaretas. *Acoustic Properties of the Ground.* Master's thesis, Pennsylvania State University, 1981.

[59] R.N. Foss. Effects of wind and ground plane attenuation on sound propagation near the ground. *Journal of the Acoustical Society of America*, 66(4):1088–1092, 1979.

[60] J. Nicolas, T. Embleton, and J. Piercy. Authors reply to 'comments on' precise model measurements versus theoretical prediction of barrier insertion loss in the presence of ground. *Journal of the Acoustical Society of America*, 74(4), Oct 1983.

[61] A. Sommerfeld. Uber die ausbreitung der wellen in der drahtlosen telegraphie. *Annalen der Physik*, 28:665–736, 1909.

[62] A. Sommerfeld. Uber die ausbreitung der wellen in der drahtlosen telegraphie. *Annalen der Physik*, 81:1135–1153, 1926.

[63] B. Van der Pol. Theory of the reflection of the light from a point source by a finitely conducting flat mirror with an applicatrion to radiotelegraphy. *Physica*, 2:843–853, 1935.

[64] K.A. Norton. The propagation of radio waves over the surface of the earth and in the upper atmosphere part 1. In *Proceedings of the institute of Radio Engineers*, pages 1367–1387, 1936.

[65] K.A. Norton. The propagation of radio waves over the surface of the earth and in the upper atmosphere part 2. In *Proceedings of the institute of Radio Engineers*, pages 1203–1236, 1937.

[66] I. Rudnick. The propagation of an acoustic wave along a boundary. *Journal of the Acoustical Society of America*, 19:348–356, 1947.

[67] M. Briquet and P. Filippi. Diffraction of a spherical wave by an absorbing plane. *Journal of the Acoustical Society of America*, 61:640–646, 1977.

[68] P. Filippi and D. Habault. Reflection of a spherical wave by the plane interface between a perfect fluid and a porous medium. *Journal of Sound and Vibration*, 56:97–103, 1978.

[69] D.I. Paul. Acoustical radiation from a point source in the presence of two media. *Journal of the Acoustical Society of America*, 29:1102–1109, 1957.

[70] D.I. Paul. Wave propagation in acoustics using the saddle-point method. *Journal of the Acoustical Society of America*, 38:1–15, 1959.

[71] K. Attenborough, S.I. Hayek, and J.M. Lawther. Propagation of sound above a porous half-space. *Journal of the Acoustical Society of America*, 68:1493–1501, 1980.

[72] U. Ingard. On the reflection of a spherical wave from an infinite plane. *Journal of the Acoustical Society of America*, 23:329–335, 1951.

[73] S.I. Thomasson. Reflection of waves from a point source by an impedance boundary. *Journal of the Acoustical Society of America*, 59:780–785, 1976.

[74] A.R. Wenzel. Propagation of waves along a finite impedance boundary. *Journal of the Acoustical Society of America*, 55:956–964, 1974.

[75] R.B. Lawhead and I. Rudnick. Acoustic wave propagation along a constant normal impedance boundary. *Journal of the Acoustical Society of America*, 23:546–549, 1951.

[76] S-I. Thomasson. A powerful asymptotic solution for sound propagation above an impedance boundary. *Acustica*, 45, 1980.

[77] C.F. Chien and W.W. Soroka. Sound propagation along an impedance plane. *Journal of Sound and Vibration*, 43:9–20, 1978.

[78] C.F. Chien and W.W. Soroka. A note on the calculation of sound propagation along an impedance surface. *Journal of Sound and Vibration*, 69:340–343, 1980.

[79] T. Kawai, T. Hidaki, and T. Nakajima. Sound propagation above an impedance boundary. *Journal of Sound and Vibration*, 83:125–138, 1982.

[80] R.J. Donato. Propagation of a spherical wave near a plane boundary with a complex impedance. *Journal of the Acoustical Society of America*, 60, 1976.

[81] R.J. Donato. Spherical wave reflection from a boundary of reactive impedance using a modification of Cagniard's method. *Journal of the Acoustical Society of America*, 60:999–1002, 1979.

[82] M.A. Nobile and S.I. Hayek. Acoustic propagation over an impedance plane. *Journal of the Acoustical Society of America*, 78, 1985.

[83] L.N. Brekhovskikh. *Waves in layered media.* Academic, 1960.

[84] P.M. Morse and K.U. Ingard. *Theoretical Acoustics.* Mc-Graw-Hill, 1968.

[85] K. Attenborough. Acoustical characteristics of porous materials. *Physics Reports*, 82(3):179–227, 1982.

[86] D.L. Berry, S.N. Chandler-Wilde, and K. Attenborough. Acoustic scattering by sub-surface inhomogeneities. In *Proceedings of the Institute of Acoustics*, pages 189 – 196, 1989.

[87] S.N. Chandler-Wilde. Private communication. Second integral equation formulation.

[88] I.N. Sneddon. *Special functions of mathematical physics and chemistry.* Oliver and Boyd, Edinburgh, 1962.

[89] L.R. Quartararo. *A theoretical investigation of sound propagation above a half-space of extended reaction.* PhD thesis, Pennsylvania State University, 1983.

[90] J. Stratton. *Electromagnetic theory.* Academic press, New York, 1941.

[91] S.N. Chandler-Wilde. *Ground effects in environmental sound propagation.* PhD thesis, University of Bradford, 1988.

[92] S.N. Chandler-Wilde and D.C. Hothersall. On the green function for two dimensional acoustic propagation above a homogeneous impedance plane. 1990. Submitted for publication.

[93] S.N. Chandler-Wilde and D.C. Hothersall. Proplib: a subroutine library for acoustic propagation: mark 1. Department of Civil Engineering, Bradford University, 1988.

[94] M.E. Delany and E.N. Bazley. Monopole radiation in the presence of an absorbing plane. *Journal of Sound and Vibration*, 13(3):269–279, 1970.

[95] C. Zwicker and C.W. Kosten. *Sound absorbing materials.* Elsevier, Amsterdam, 1949.

[96] M.E. Delany and E.N. Bazley. Acoustical characteristics of fibrous absorbent materials. National Physical Laboratory, 1979.

[97] K. Attenborough. Review of ground effects on outdoor sound propagation from continuous broadband sources. *Applied acoustics*, 24:289–319, 1988.

[98] T.F.W. Embleton and J.E. Piercy. Effective flow resistivity of ground surfaces determined by acoustical measurements. *Journal of the Acoustical Society of America*, 74:1239–1244, 1983.

[99] M. Abramowitz and I.A. Stegun, editors. *Handbook of mathematical functions.* Dover, New York, 1965.

[100] D.F. Mayers. Quadrature methods for fredholm equations of the second time. In L.M. Delves and J. Walsh, editors, *Numerical solution of integral equations*, Carendon Press, Oxford, 1974.

[101] H. Schippers. Multiple grid methods for equations of the second kind with applications in fluid mechanics. *Mathematical Centre Tracts*, 163, 1983.

[102] A.J. Burton. *Numerical solution of acoustic radiation problems.* Contract:OC5/535, National Physical Laboratory, 1976.

[103] A.B. Birtles, B.J. Mayo, and A.W. Bennett. Computer technique for solving three-dimensional electron-optics and capacitance problems. In *Proceedings 120*, pages 213 – 220, IEE, 1973.

[104] P.J. Davis. *Circulant Matrices.* John Wiley and Sons, 1979.

[105] O.B. Arushanian, M.K. Samarin, V.V. Voevodin, E.E. Tyrtyshnikov, B.S. Garbow, J.H. Boyle, W.R. Cowell, and K.K. Dritz. *The Toeplitz users' guide.* Argonne National Laboratory Report, ANL-83-16.

[106] L.E. Kinsler, A.R. Frey, A.B. Coppens, and J.V. Sanders. *Fundamentals of Acoustics.* John Wiley and Sons, third edition edition, 1982.

[107] S.N. Chandler-Wilde. Private communication. Integral equation solution.

[108] N.W. Heap. *Sound propagation over mixed impedances.* PhD thesis, Open University, 1982.

[109] V.V.S.S. Sastry. *Computation of Hankel/Bessel functions of complex argument and of integer order.* Internal report, School of Defence Management, Royal Military College of Science, Shrivenham, 1989.

[110] M.A. Price. *Sound propagation in woodland.* PhD thesis, Open University, 1986.

Appendix A

Formulation of a boundary integral equation for scattering by a sphere in an infinite homogeneous medium

A sphere, labelled S, with a rigid surface ∂S, is embedded in an infinite porous medium, characterised by a a complex wavenumber, k_1. The complex acoustic pressure is assumed to satisfy the following boundary value problem:
an inhomogeneous Helmholtz equation,

$$(\nabla^2 + k_1^2)p(\mathbf{r}, \mathbf{r}_0) = \delta(\mathbf{r} - \mathbf{r}_0); \tag{A.1}$$

the Neumann boundary condition for $\mathbf{r} \in \partial S$, for a rigid scatterer,

$$\frac{\partial p(\mathbf{r}, \mathbf{r}_0)}{\partial n(\mathbf{r})} = 0; \tag{A.2}$$

and Sommerfeld's radiation conditions,

$$\left.\begin{array}{rcl} \frac{\partial p(\mathbf{r},\mathbf{r}_0)}{\partial r} - ik_1 p(\mathbf{r}, \mathbf{r}_0) & = & o(r^{-\frac{1}{2}}), \\ p(\mathbf{r}, \mathbf{r}_0) & = & O(r^{-\frac{1}{2}}), \end{array}\right\} \tag{A.3}$$

uniformly in $\mathbf{r}$ as $r := |\mathbf{r}| \to \infty$ In the above, $n(\mathbf{r})$ denotes the normal to the surface ∂S at point $\mathbf{r}$.

To formulate the integral equation, let the Green's function $G(\mathbf{r}, \mathbf{r}_0)$, satisfy the following boundary value problem, for each $\mathbf{r}_0 \in \mathbf{R}^3 \backslash \Gamma$:
an inhomogeneous Helmholtz equation,

$$(\nabla^2 + k_1^2)G(\mathbf{r}, \mathbf{r}_0) = \delta(\mathbf{r} - \mathbf{r}_0); \tag{A.4}$$

and Sommerfeld's radiation conditions,

$$\left.\begin{array}{rcl} \frac{\partial G(\mathbf{r},\mathbf{r}_0)}{\partial r} - ik_1 G(\mathbf{r}, \mathbf{r}_0) & = & o(r^{-\frac{1}{2}}), \\ G(\mathbf{r}, \mathbf{r}_0) & = & O(r^{-\frac{1}{2}}), \end{array}\right\} \tag{A.5}$$

uniformly in $\mathbf{r}$ as $r := |\mathbf{r}| \to \infty$ Note that in the case when no obstacle is present,

$$p(\mathbf{r}, \mathbf{r}_0) = G(\mathbf{r}, \mathbf{r}_0), \tag{A.6}$$

for $\mathbf{r}, \mathbf{r}_0 \in \mathbf{R}^3$.

Now consider region V consisting of that part of U contained within a large sphere of surface, Σ and radius R, centred on the origin, but excluding small spheres, $\sigma_{\mathbf{r}}$ and $\sigma_{\mathbf{r}_0}$ of radii ϵ, centred on $\mathbf{r}$ and $\mathbf{r}_0$. The interiors of the spheres σ_r and σ_{r_0} are excluded so that the conditions of Green's second theorem are safisfied by p and G in the region V. Applying Green's second theorem to the region V, and noting that $p(\mathbf{r}_s, \mathbf{r}_0)$ and $G(\mathbf{r}_s, \mathbf{r})$ satisfy Helmholtz equation, the following equation is obtained for $\mathbf{r}, \mathbf{r}_0 \in \mathbf{R}^3$,

$$p(\mathbf{r}, \mathbf{r}_0) = G(\mathbf{r}_0, \mathbf{r}) + \int_{\partial S} p(\mathbf{r}_s, \mathbf{r}_0) \frac{\partial G(\mathbf{r}_s, \mathbf{r})}{\partial n(\mathbf{r}_s)} - G(\mathbf{r}_s, \mathbf{r}) \frac{\partial p(\mathbf{r}_s, \mathbf{r}_0)}{\partial n(\mathbf{r}_s)} ds(\mathbf{r}_s), \qquad \text{(A.7)}$$

for $\mathbf{r}, \mathbf{r}_0 \in U_+$.

The numerical solution of equation (A.7) is carried out using subroutines GEOSPHERE, FSURSPHIM and FRECSPHIM found in appendix D.

Appendix B

Analytical expression for the scattered field by a rigid sphere

Plane waves are travelling to along the the polar axis are incident on a rigid sphere centred on the origin. The incident acoustic pressure is given by,

$$p_i = \sum_{m=0}^{\infty} (2m+1) i^m P_m(cos\theta) j_m(kr), \tag{B.1}$$

where j_m denotes the spherical Bessel function of the first kind of order m, defined in terms of a Bessel function of fractional order by,

$$j_n(z) = \left(\frac{\pi}{2z}\right)^{\frac{1}{2}} J_{n+\frac{1}{2}}(z), \tag{B.2}$$

and $P_m(x)$ is the Legendre polynomial of degree m, defined for $m = 0, 1$, by $P_0(x) = 1$ and $P_1(x) = x$ and for $m > 1$ by the recurrence relation,

$$(n+1)P_{n+1}(x) = (2n+1)xP_n(x) - nP_{n-1}(x), \tag{B.3}$$

for $n = 1, 2$. It is assumed that the scattered wave has the form,

$$p_s = \sum_{0}^{\infty} a_m P_m(cos\theta) h_m^{(1)}(kr) \tag{B.4}$$

where the spherical Hankel functions of the first kind, $h_m^{(1)}$, are defined by,

$$h_m^{(1)}(z) = \left(\frac{\pi}{2z}\right)^{\frac{1}{2}} H_{m+\frac{1}{2}}^{(1)}(z). \tag{B.5}$$

Insisting that the normal velocity is zero on the surface of the sphere leads to expression for the coefficients a_m,

$$a_m = -(2m+1) i^m \frac{j_{m'}(kR)}{h_m^{(1)'}(kR)} \tag{B.6}$$

a_m and p_s given by equations (B.6) and (B.4) are calculated using subroutine PLNSCATCOE and complex function PLNSCATFLD found in appendix D.

Appendix C

Boundary integral equation formulation for sound propagation over a half-space containing an embedded sphere of infinite radius

A sphere, labelled S, with rigid surface ∂S, is embedded in a rigid porous (lower) half-space, with the upper-half space containing air. The boundary value problem of equations (2.34 to 2.40) which give the associated boundary integral equation (2.104), define this problem if the integrating surface is replaced by a sphere. With this modification, if the radius is now allowed to tend to infinity while keeping the depth, d, constant, and $\mathbf{r}$ and $\mathbf{r}_0$ directly above $\mathbf{r}_s^*$, the highest point on the surface ∂S, the integral equation becomes,

$$\alpha\kappa(\mathbf{r})p(\mathbf{r},\mathbf{r}_0) = \alpha G(\mathbf{r}_0,\mathbf{r}) - \int_{\partial S} p(\mathbf{r}_s,\mathbf{r}_0)\frac{\partial G(\mathbf{r}_s,\mathbf{r})}{\partial z_s}dA(\mathbf{r}_s) \qquad \text{(C.1)}$$

where ∂S is now a plane at a depth d beneath the ground surface Γ and S is the region below this plane; $\kappa(\mathbf{r}) := 1$, for $\mathbf{r} \in \Re^3\backslash\bar{S}$, $1/2$ for $\mathbf{r} \in \partial S$. Introducing polar coordinates in the surface ∂S, with the origin of the coordinates at $\mathbf{r}_s^*$ and R defined as $|\mathbf{r}_s - \mathbf{r}_s^*|$, this integral equation can be written,

$$\alpha\kappa(\mathbf{r})p(\mathbf{r},\mathbf{r}_0) = \alpha G(\mathbf{r}_0,\mathbf{r}) - 2\pi\int_0^\infty p(\mathbf{r}_s,\mathbf{r}_0)\frac{\partial G(\mathbf{r}_s,\mathbf{r})}{\partial z_s}RdR \qquad \text{(C.2)}$$

Now, letting $\mathbf{r}_0$ get further and further away from Γ, (*i.e.* letting $z_0 \to +\infty$), the pressure $p(\mathbf{r}_s,\mathbf{r}_0)$, assumes an almost constant value p_c in a larger and larger region surrounding the point $\mathbf{r}_s^*$. Putting $\mathbf{r} = \mathbf{r}_s^*$ in equation (C.1) gives a value for p_c as,

$$p_c = \alpha G(\mathbf{r}_0,\mathbf{r}_s^*)\left[\frac{\alpha}{2} + 2\pi\int_0^\infty \frac{\partial G(\mathbf{r}_s,\mathbf{r}_s^*)}{\partial z_s}RdR\right]^{-1}. \qquad \text{(C.3)}$$

The pressure at a point $\mathbf{r}$ above $\mathbf{r}_s^*$ in the upper half-space, is then given by,

$$\alpha p(\mathbf{r},\mathbf{r}_0) = \alpha G(\mathbf{r}_0,\mathbf{r}_+) - p_c 2\pi\int_0^\infty \frac{\partial G(\mathbf{r}_s,\mathbf{r}_+)}{\partial z_s}RdR. \qquad \text{(C.4)}$$

The integral in equation (C.3) can now be calculated numerically by standard techniques. The integral in equation (C.4) is a little more tricky to calculate , the problem being that the integrand tends to zero very slowly as R increases, being of the order $O(R^{-1})$. With reference to the notes of Chandler-Wilde [107], this problem is overcome by analysing the asymptotic behaviour of the integrand.

Letting $f(R) = -2\pi R\partial G(\mathbf{r}_s, \mathbf{r})/\partial z_s$ and replacing G by the approximations (3.51), $f(R)$ can be written,

$$f(R) = -\frac{ik_1\alpha R cos\theta\sqrt{n^2 - sin^2\theta}}{r(\alpha cos\theta + \sqrt{n^2 - sin^2\theta})} e^{ik_1(r+d\sqrt{n^2-sin^2\theta})}, \tag{C.5}$$

where $r = |\mathbf{r}_\Gamma - \mathbf{r}|$, and $\theta = cos^-(z/r)$, $\mathbf{r}_\Gamma$ being the point on the boundary Γ directly above $\mathbf{r}_s$. Now $Rcos\theta = z$ and if $n \neq 1$, then,

$$\sqrt{n^2 - sin^2\theta} = \sqrt{n^2 - 1}(1 + O(r^{-2})), \tag{C.6}$$

as $R \to \infty$, and also,

$$\alpha cos\theta + \sqrt{n^2 - sin^2\theta} = \sqrt{n^2 - 1} + O(r^{-1}). \tag{C.7}$$

Thus, making use of equations (C.6) and (C.7), equation (C.5) can be written,

$$f(\mathbf{r}_s) = g(\mathbf{r}_s) + O(r^{-2}), \tag{C.8}$$

where,

$$g(\mathbf{r}_s) = -\left[\frac{4\pi ik_1 z\alpha}{r} e^{ikd\sqrt{n^2-1}}\right] e^{ikr}. \tag{C.9}$$

Equation (C.4) may now be written,

$$\alpha p(\mathbf{r}, \mathbf{r}_0) = \alpha G(\mathbf{r}_0, \mathbf{r}) + p_c\left[\int_0^\infty g(R)dR + \int_0^\infty f(R) - g(R)dR\right], \tag{C.10}$$

where $f(\mathbf{r}_s) - g(\mathbf{r}_s) = O(r^{-2})$ as $r_s \to \infty$. $g(r_s)$ behaves as $O(r^{-1})$ but is straightforward to integrate:

$$\int_0^\infty g(R)dR = \frac{\pi k_1 z\alpha}{2} e^{ik_1 d\sqrt{n^2-1}} H_0^{(1)}(k_1 z), \tag{C.11}$$

Equation (C.4) has now thus been reduced to a form more amenable to numerical integration.

Appendix D

Listings of FORTRAN 77 subroutines referred to in the text

This appendix lists all of the FORTRAN 77 subroutines and functions that are mentioned in the text. Documentation is included for each.

D.1 Complex function CCOTH

CCOTH calculates the hyperbolic cotangent of a complex number. There are no subprograms referenced.

```
      COMPLEX FUNCTION CCOTH(Z)
      COMPLEX Z
C
C CALCULATES THE HYPERBOLIC COTANGENT OF A COMPLEX NUMBER
C IF THE REAL PART OF Z IS
C LARGE THEN CCOTH(Z) IS EQUAL TO 1 + IO
C
C ON ENTRY:
C
C Z   COMPLEX
      THE COMPLEX ARGUMENT
C
C INTERNAL VARIABLES
C
      REAL RZ2,AZ2,C1
      COMPLEX I
C
      I=CMPLX(0.0,1.0)
      IF (REAL(Z) .GT. 44.3) THEN
       CCOTH=(1.0,0.0)
       RETURN
      ELSE
       RZ2=2.*REAL(Z)
       AZ2=2.*AIMAG(Z)
       C1=COSH(RZ2)-COS(AZ2)
       CCOTH=(SINH(RZ2)-I*SIN(AZ2))/C1
      END IF
      RETURN
      END
```

D.2 Subroutine CD

CD calculates value of complex density using equation (3.62). Reference to other subprograms are:

- CMPBJ: a subroutine from Sastry [109].

```
      SUBROUTINE CD(F,MPR,SFR,SIGMA,POROS,CDENS)
      COMPLEX*8 CDENS
      REAL*4 F,MPR,SFR,SIGMA,POROS
C
C CD CALCULATES A SINGLE VALUE OF COMPLEX DENSITY
C USING THE FOUR PARAMETER MODEL.
C
C ON ENTRY
C
C    F       REAL
C            FREQUENCY
C
C    MPR     REAL
C            GRAIN SHAPE FACTOR
C
C    SFR     PORE SHAPE FACTOR RATIO
C
C    SIGMA   REAL
C            FLOW RESISTIVITY
C
C    POROS   REAL
C            POROSITY
C
C ON EXIT
C
C    CDENS   REAL
C            COMPLEX DENSITY
C
C THIS VERSION DATED 7TH DECEMBER, 1989.
C
C ROUTINE CMPBJ IS CALLED
C
C INTERNAL VARIABLES
C
      COMPLEX*8 I,YP,TP,J0,J1
      INTEGER*2 M1
      REAL*4 LAMBDAP,Q,PI,CF,GAMMA,PRANDTL,RHOF,AE,OMEGA
C
      Q=SQRT(POROS**-MPR)
      PI=4.0*ATAN(1.0)
      I=CMPLX(0.0,1.0)
      CF=343.0
      GAMMA=1.4
      PRANDTL=0.76
      RHOF=1.2
      AE=SQRT(8.0*(Q**2)/(POROS*SIGMA))
      OMEGA=2.0*PI*F
      LAMBDAP=(AE/SFR)*((OMEGA*RHOF)**0.5)
      YP=LAMBDAP*(I**0.5)
      M1=0
      CALL CMPBJ(YP,M1,J0)
      M1=1
      CALL CMPBJ(YP,M1,J1)
      TP=J1/J0
      CDENS=Q**2*RHOF/((1.0-(2.0/YP)*TP)*POROS)
      RETURN
      END
```

D.3 Complex function FFG

FFG calculates the free field G-een's function. There are no subprograms referenced.

```
      COMPLEX FUNCTION FFG(X,K)
      COMPLEX*8 K
      REAL*4    X
C
C FFG CALCULATES THE FREE-FIELD GREEN'S FUNCTION GIVEN THE MAGNITUDE
C OF THE VECTOR BETWEEN THE TWO POINTS, AND THE COMPLEX PROPAGATION
C CONSTANT.
C
C ON ENTRY:
C
C X   REAL
C     MAGNITUDE OF THE VECTOR BETWEEN THE TWO POINTS
C
C K   COMPLEX
C     COMPLEX PROPAGATION CONSTANT
C
      COMPLEX*8 I
      REAL*4 PI
C
      I=CMPLX(0.0,1.0)
      PI=3.141592653
      FFG=-CEXP(I*K*X)/(4.0*PI*X)
      RETURN
      END
```

D.4 Subroutine FRECCIR

FRECCIR calculates values of acoustic pressure at the receiver point in the upper medium using equation (5.44). Reference to other subprograms are:

- G11WVDP: see section D.14.

```
      SUBROUTINE FRECCIR(RCOOR,SCOOR,COOR,K1,K2,AREA,PRRO,N,M,
     &                   SCATT,GROR,PRRO,Z,ZC)
      PARAMETER(NMAX=200,MMAX=100,NMMAX=NMAX*MMAX,MMMAX=MMAX*MMAX)
      COMPLEX*8  PRRO(NMMAX),PRRO,Z(NMMAX),ZC,GROR,SCATT,K2
      INTEGER*2  N,M
      REAL*4     K1,RCOOR(3),SCOOR(3),COOR(3,NMMAX),AREA(NMMAX)
C
C  FRECCIR CALCULATES THE VALUES OF THE PRESSURE FIELD
C  AT THE RECEIVER POSITION IN THE UPPER MEDIUM.
C
C  ON ENTRY
C
C   RCOOR  REAL(3)
C          ARRAY  CONTAINING THE COORDINATES OF THE RECEIVER.
C          RCOOR IS UNCHANGED ON EXIT
C
C   SCOOR  REAL(3)
C          ARRAY  CONTAINING THE COORDINATES OF THE POINT SOURCE.
C          SCOOR IS UNCHANGED ON EXIT
C
C   COOR   REAL(3,N*M)
C          ARRAY  CONTAINING THE COORDINATES OF THE MIDPOINTS OF
C          THE BOUNDARY ELEMENTS.
C          COOR IS UNCHANGED ON EXIT
C
C   K1     REAL
C          PROPAGATION CONSTANT OF THE UPPER MEDIUM.
C          N.B. TIME DEPENDENCE EXP(-I*W*T) ASSUMED.
C          K1 IS UNCHANGED ON EXIT.
C
C   AREA   REAL(N*M)
C          VALUES OF THE AREA OF EACH BOUNDARY ELEMENT.
C          AREA IS UNCHANGED ON EXIT.
C
C   PRRO  COMPLEX(N*M)
C          ARRAY CONTAINING THE VALUES OF THE PRESSURE FIELD AT
C          THE MIDPOINTS OF THE ELEMENTS.
C          PRRO IS UNCHANGED ON EXIT.
C
C   N      INTEGER
C          THE CIRCULAR REGION IS DIVIDED INTO N SECTORS.
C          N IS UNCHANGED ON EXIT.
C
C   M      INTEGER
C          THE CIRCULAR REGION IS DIVIDED INTO M ANNULI.
C          M IS UNCHANGED ON EXIT.
C
C   Z(N*M) COMPLEX
C          INDUCED SURFACE IMPEDANCE AT THE MIDPOINTS OF THE BOUNDARY
C          ELEMENTS.
C          Z IS UNCHANGED ON EXIT.
C
C   ZC     COMPLEX
C          CHARACTERISTIC IMPEDANCE OF THE SURROUNDING AREA.
C          ZC IS UNCHANGED ON EXIT.
C
C  ON EXIT
C
C   SCATT  COMPLEX
```

```
C          THE SCATTERED FIELD.
C
C   GROR   COMPLEX
C          THE GREEN'S FUNCTION FOR A HOMOGENEOUS HALF SPACE.
C
C   PRRO   COMPLEX
C          THE CALCULATED PRESSURE VALUE.
C
C  THIS VERSION DATED 7TH DECEMBER, 1989.
C
C  ROUTINE G11WVDP IS CALLED.
C
C  INTERNAL VARIABLES
C
      COMPLEX*8  GRKR,I,RI
      INTEGER*2  NM,K
      REAL*4     AKCOOR(3),DEPTH
C
      NM=N*M
      I=(0.0,1.0)
      RI=K2/K1
      DEPTH=0.0
      CALL G11WVDP(RCOOR,SCOOR,K1,RI,ZC,GROR,DEPTH)
      SCATT=CMPLX(0.0,0.0)
      DO 010 K=1,NM
       AKCOOR(1)=COOR(1,K)
       AKCOOR(2)=COOR(2,K)
       AKCOOR(3)=COOR(3,K)
       CALL G11WVDP(AKCOOR,RCOOR,K1,RI,ZC,GRKR,DEPTH)
       SCATT=SCATT+PRKRO(K)*GRKR*AREA(K)*(1.0/Z(K)-1.0/ZC)
010   CONTINUE
      SCATT=I*K1*SCATT
      PRRO=GROR-SCATT
      RETURN
      END
```

D.5 Subroutine FRECSPH

FRECSPH calculates values of acoustic pressure at the receiver point in the upper medium using equation (5.11). Reference to other subprograms are:

- G11: see section D.10;
- G12DER: see section D.12.

```
      SUBROUTINE FRECSPH(L,RCOOR,SCOOR,COOR,NORM,PROP,AREA,PRKRO,N,M,
     &                   SCATT,GROR,PRRO,ZETA,RI,DEPTH)
      PARAMETER(NMAX=200,MMAX=100,NMMAX=NMAX*MMAX,MMMAX=MMAX*MMAX)
      INTEGER*4  N,M,L
      REAL*4     RCOOR(3),SCOOR(3),COOR(3,NMMAX),AREA(NMMAX)
      REAL*4     NORM(3,NMMAX),DEPTH
      COMPLEX*8  GROR,PROP,PRKRO(NMMAX),PRRO,ZETA,RI,SCATT
C
C  FRECSPH CALCULATES THE VALUES OF THE PRESSURE FIELD AT THE
C  RECEIVER POSITION.
C
C  ON ENTRY
C
C   RCOOR  REAL(3)
C          ARRAY  CONTAINING THE COORDINATES OF THE RECEIVER.
C          RCOOR IS UNCHANGED ON EXIT
C
C   SCOOR  REAL(3)
C          ARRAY  CONTAINING THE COORDINATES OF THE POINT SOURCE.
C          SCOOR IS UNCHANGED ON EXIT
C
C   COOR   REAL(NMMAX)
C          ARRAY  CONTAINING THE COORDINATES OF THE CENTROIDS
C          OF THE AREA ELEMENTS.
C          CCOOR IS UNCHANGED ON EXIT
C
C   NORM   REAL(3,NMMAX)
C          ARRAY CONTAINING THE NORMAL VECTORS AT THE CENTROIDS
C          NORM IS UNCHANGED ON EXIT
C
C   PROP   COMPLEX
C          PROPAGATION CONSTANT.
C          N.B. TIME DEPENDENCE EXP(-I*W*T) ASSUMED.
C          PROP IS UNCHANGED ON EXIT.
C
C   AREA   REAL(N*M)
C          ARRAY CONTAINING THE VALUES OF THE AREA OF EACH AREA ELEMENT
C          ON THE SPHERE.
C          AREA IS UNCHANGED ON EXIT
C
C   PRKRO  COMPLEX(N*M)
C          ARRAY CONTAINING THE VALUES OF THE PRESSURE FIELD ON THE
C          SURFACE OF THE SPHERE.
C          PRKRO IS UNCHANGED ON EXIT
C
C   N      INTEGER
C          THE SURFACE OF THE SPHERE IS DIVIDED INTO N LONGITUDINAL
C          BANDS.
C          N IS UNCHANGED ON EXIT
C
C   M      INTEGER
C          THE SURFACE OF THE SPHERE IS DIVIDED INTO M LATITUDINAL
C          BANDS.
C          M IS UNCHANGED ON EXIT
C
C   ZETA   COMPLEX
C          THE IMPEDANCE OF THE MEDIUM.
C          ZETA IS UNCHANGED ON EXIT
C
```

```
C   RI      COMPLEX
C           THE REFRACTIVE INDEX AT THE SURFACE GAMMA.
C           RI IS UNCHANGED ON EXIT
C
C   DEPTH   REAL
C           THE DISTANCE FROM THE CENTRE OF THE OBSTACLE TO
C           THE BOUNDARY GAMMA.
C           DEPTH IS UNCHANGED ON EXIT
C
C  ON EXIT
C
C   SCATT   COMPLEX
C           THE CALCULATED SCATTERED FIELD.
C
C   GROR    COMPLEX
C           THE GREEN'S FUNCTION FOR A HOMOGENE' S HALF SPACE.
C
C   PRRO    COMPLEX
C           THE CALCULATED PRESSURE VALUE.
C
C  THIS VERSION DATED 3RD DECEMBER, 1989.
C
C  SUBROUTINES G11 AND G12DER ARE CALLED.
C
C  INTERNAL VARIABLES
C
      REAL*4     AKCOOR(3),AKNORM(3),K1
      INTEGER*4  NM,K
      COMPLEX*8  NDG,ALPHA,GG,GX,GY,GZ
C
      K1=REAL(PROP/RI)
      ALPHA=ZETA*RI
      NM=N*M
      CALL G11(RCOOR,SCOOR,K1,RI,ZETA,GG,DEPTH)
      GROR=GG
      SCATT=CMPLX(0.0,0.0)
      DO 010 K=1,NM
       AKCOOR(1)=COOR(1,K)
       AKCOOR(2)=COOR(2,K)
       AKCOOR(3)=COOR(3,K)
       AKNORM(1)=NORM(1,K)
       AKNORM(2)=NORM(2,K)
       AKNORM(3)=NORM(3,K)
       CALL G12DER(AKCOOR,RCOOR,K1,RI,ZETA,GG,GX,GY,GZ,DEPTH)
       NDG=AKNORM(1)*GX+AKNORM(2)*GY+AKNORM(3)*GZ
       SCATT=SCATT+PRKRO(K)*NDG*AREA(K)
010   CONTINUE
      SCATT=SCATT/ALPHA
      PRRO=GROR+SCATT
      RETURN
      END
```

D.6 Subroutine FRECSPHIM

FRECSPHIM calculates values of acoustic pressure at the receiver point in the infinite medium for the numerical solution of equation (A.7). Reference to other subprograms are:

- FFG: see section D.3;
- NDFG: see section D.20;
- RMAG: see section D.24.

```
      SUBROUTINE FRECSPHIM(RCOOR,SCOOR,COOR,NORM,PROP,AREA,PRRO,N,M,
     &                     SCATT,GROR,PRRO)
      PARAMETER(NMAX=200,MMAX=100,NMMAX=NMAX*MMAX,MMMAX=MMAX*MMAX)
      INTEGER*2  N,M
      REAL*4     RCOOR(3),SCOOR(3),COOR(3,NMMAX),AREA(NMMAX)
      REAL*4     NORM(3,NMMAX)
      COMPLEX*8  PROP,PRRO(NMMAX),PRRO,SCATT
C
C  FRECSPHIM CALCULATES THE VALUES OF THE PRESSURE FIELD
C  AT THE RECEIVER POSITION.
C
C  ON ENTRY
C
C   RCOOR    REAL(NMMAX)
C            ARRAY CONTAINING THE RECEIVER CARTESIAN COORDINATES.
C            RCOOR IS UNCHANGED ON EXIT.
C
C   SCOOR    REAL(3)
C            ARRAY CONTAINING THE SOURCE CARTESIAN COORDINATES.
C            SCOOR IS UNCHANGED ON EXIT.
C
C   COOR     REAL(NMMAX)
C            ARRAY CONTAINING THE COORDINATES OF THE CENTROIDS.
C            COOR IS UNCHANGED ON EXIT.
C
C   NORM     REAL(NMMAX)
C            ARRAY CONTAINING THE NORMAL VECTORS AT THE CENTROIDS.
C            NORM IS UNCHANGED ON EXIT.
C
C   PROP     COMPLEX
C            PROPAGATION CONSTANT.
C            N.B. TIME DEPENDENCE EXP(-I*W*T) ASSUMED.
C            PROP IS UNCHANGED ON EXIT.
C
C   AREA     REAL(NMMAX)
C            ARRAY CONTAINING THE THE AREA OF EACH ELEMENT.
C            AREA IS UNCHANGED ON EXIT.
C
C   PRRO     COMPLEX(N*M)
C            ARRAY CONTAINING THE VALUES OF THE PRESSURE FIELD ON THE
C            SURFACE OF THE SPHERE.
C            PRRO IS UNCHANGED ON EXIT.
C
C   N        INTEGER
C            THE SURFACE OF THE OBSTACLE IS DIVIDED INTO N LONGITUDINAL
C            BANDS.
C            N IS UNCHANGED ON EXIT.
C
C   M        INTEGER
C            THE SURFACE OF THE OBSTACLE IS DIVIDED INTO M LATITUDINAL
C            BANDS.
C            M IS UNCHANGED ON EXIT.
C
C  ON EXIT
C
C     SCATT  COMPLEX
C            THE CALCULATED SCATTERED FIELD.
C
C     GROR   COMPLEX
```

```
C            THE CALCULATED FREE FIELD.
C
C     PRRO   COMPLEX
C            THE CALCULATED PRESSURE VALUE.
C
C  THIS VERSION DATED 11th MAY, 1989.
C
C  ROUTINES FFG, MDFG AND RMAG ARE CALLED.
C
C  FUNCTION TYPE DECLARATION
C
      REAL*4     RMAG,AKCOOR(3),AKNORM(3)
      COMPLEX*8  FFG,MDFG
C
C  INTERNAL VARIABLES
C
      REAL*4     X
      INTEGER*2  MM,K
      COMPLEX*8  GROR,MDFFG
C
      MM=M*M
      X=RMAG(SCOOR,RCOOR)
      GROR=FFG(X,PROP)
      PRRO=CMPLX(0.0,0.0)
      DO 010 K=1,MM
       AKCOOR(1)=COOR(1,K)
       AKCOOR(2)=COOR(2,K)
       AKCOOR(3)=COOR(3,K)
       AKNORM(1)=NORM(1,K)
       AKNORM(2)=NORM(2,K)
       AKNORM(3)=NORM(3,K)
       X=RMAG(AKCOOR,RCOOR)
       MDFFG=MDFG(X,PROP,AKCOOR,RCOOR,AKNORM)
       PRRO=PRRO+PRKRO(K)*MDFFG*AREA(K)
010   CONTINUE
      SCATT=PRRO
      PRRO=GROR+SCATT
      RETURN
      END
```

D.7 Subroutine FSURCIR

FSURCIR calculates values of pressure at the midpoints of the boundary elements of a circular surface inhomogeneity, using the theory of section 5.1.2. Reference to other subprograms are:

- CGSLC: a subroutine from Argonne National Laboratory's Toeplitz package [105];
- G11WVDP: see section D.14;
- PBETA3: a subroutine from the PROPLIB package [93];
- RMAG: see section D.24.

```
      SUBROUTINE FSURCIR(K1,K2,N,M,G,AREA,SCOOR,COOR,Z,ZC)
      PARAMETER(NMAX=200,MMAX=100,NMMAX=NMAX*MMAX,MMMAX=MMAX*MMAX)
      COMPLEX*8  Z(NMMAX),ZC,G(NMMAX),K2
      INTEGER*2  N,M
      REAL*4     SCOOR(3),COOR(3,NMMAX),AREA(NMMAX),K1
C
C  FSURCIR CALCULATES THE PRESSURE VALUES AT THE MIDPOINTS
C  OF THE BOUNDARY ELEMENTS OF A CIRCULAR SURFACE INHOMOGENEITY.
C
C  ON ENTRY
C
C     K1      REAL
C             PROPAGATION CONSTANT OF THE LOWER MEDIUM.
C             N.B. TIME DEPENDENCE EXP(-I*W*T) ASSUMED.
C             K1 IS UNCHANGED ON EXIT.
C
C     K2      COMPLEX
C             PROPAGATION CONSTANT OF THE UPPER MEDIUM.
C             N.B. TIME DEPENDENCE EXP(-I*W*T) ASSUMED.
C             K2 IS UNCHANGED ON EXIT.
C
C     N       INTEGER
C             THE CIRCULAR PATCH IS DIVIDED INTO N SECTORS.
C             N IS UNCHANGED ON EXIT.
C
C     M       INTEGER
C             THE CIRCULAR PATCH IS DIVIDED INTO M ANNULI.
C             M IS UNCHANGED ON EXIT.
C
C     AREA    REAL(M*N)
C             ARRAY CONTAINING VALUES OF THE AREA OF THE
C             M*N BOUNDARY ELEMENTS.
C             AREA IS UNCHANGED ON EXIT.
C
C     SCOOR   REAL(3)
C             THE CARTESIAN COORDINATES OF THE SOURCE
C             WITH THE ORIGIN AT THE CENTRE OF THE CIRCULAR
C             INHOMOGENEITY.
C             SCOOR IS UNCHANGED ON EXIT.
C
C     COOR    REAL(3)
C             THE CARTESIAN COORDINATES OF THE MIDPOINTS
C             OF THE BOUNDARY ELEMENTS.
C             COOR IS UNCHANGED ON EXIT.
C
C     Z       COMPLEX(M*N)
C             THE INDUCED SURFACE IMPEDANCE WITHIN THE
C             CIRCULAR PATCH.
C             Z IS UNCHANGED ON EXIT.
C
C     ZC      COMPLEX
C             THE CHARACTERISTIC IMPEDANCE OF THE SURROUNDING AREA.
C             ZC IS UNCHANGED ON EXIT.
C  ON EXIT
C
C     G       COMPLEX(NSTEP)
C             A VECTOR CONTAINING THE CALCULATED PRESSURE VALUES
C             AT THE MIDPOINTS OF THE BOUNDARY ELEMENTS.
C
```

```
C  THIS VERSION DATED 7TH DECEMBER, 1989.
C
C  ROUTINES CGSLC,G11WVDP, PBETA3 AND RMAG ARE CALLED.
C
C  FUNCTION TYPE DECLARATION
C
      REAL*4    RMAG
      COMPLEX*8 PBETA3
C
C  INTERNAL VARIABLES
C
      COMPLEX*8  AJK,R(MAX(MMAX,2*NMAX)),A(MMMAX,NMAX),GRKRJ,I,RI,GG
      INTEGER*2  K,J,KK,MMM,JJ,NM
      REAL*4     AJCOOR(3),AKCOOR(3),X,PI,DEPTH
C
      IF(N.GT.NMAX.OR.M.GT.MMAX)THEN
       WRITE(6,500)
500    FORMAT(' *ERROR* MAXIMUM ARRAY SIZE EXCEEDED')
       STOP
      ENDIF
      NM=N*M
      PI=4.0*ATAN(1.0)
      I=CMPLX(0.0,1.0)
      DO 010 K=1,NM
       DO 020 J=1,M
        AJCOOR(1)=COOR(1,J)
        AJCOOR(2)=COOR(2,J)
        AJCOOR(3)=COOR(3,J)
        AKCOOR(1)=COOR(1,K)
        AKCOOR(2)=COOR(2,K)
        AKCOOR(3)=COOR(3,K)
        IF(J.EQ.K)THEN
         AJK=1.0-I*K1*SQRT(AREA(K)/PI)*(1.0/Z(K)-1.0/ZC)
        ELSE
         X=RMAG(AKCOOR,AJCOOR)
         GRKRJ=PBETA3(X,K1,1.0/ZC)
         GRKRJ=GRKRJ-EXP(I*K1*X)/(2.0*PI*X)
         AJK=I*K1*GRKRJ*(1.0/Z(K)-1.0/ZC)*AREA(K)
        ENDIF
        JJ=J+((K-(INT((K-1)/M))*M)-1)*M
        KK=INT((K-1)/M)+1
        A(JJ,KK)=AJK
020    CONTINUE
       RI=K2/K1
       DEPTH=0.0
       CALL G11WVDP(AKCOOR,SCOOR,K1,RI,ZC,GG,DEPTH)
       G(K)=GG
010   CONTINUE
      MMM=M
      CALL CGSLC(A,G,R,MMM,N,MMMAX)
      RETURN
      END
```

D.8 Subroutine FSURSPH

FSURSPH calculates values of pressure at the midpoints of the boundary elements of a spheroid, using the theory of section 5.1.1. Reference to other subprograms are:

- CGSLC: a subroutine from Argonne National Laboratory's Toeplitz package [105];
- G12: see section D.11;
- G22DER: see section D.13;
- GDER: see section D.15.

```
      SUBROUTINE FSURSPH(PROP,N,M,G,AREA,SCOOR,COOR,NORM,ZETA,RI,
     &                   DEPTH)
      REAL*4     DEPTH
      INTEGER*4  N,M
      COMPLEX*8  PROP,ZETA,RI
C
C  FSURSPH CALCULATES PRESSURE VALUES ON THE SURFACE
C  OF A RIGID OBSTACLE, IN A RIGID POROUS MEDIUM.
C
C  ON ENTRY
C
C     PROP    COMPLEX
C             PROPAGATION CONSTANT OF THE LOWER MEDIUM.
C             N.B. TIME DEPENDENCE EXP(-I*W*T) ASSUMED.
C             PROP IS UNCHANGED ON EXIT.
C
C     N       INTEGER
C             THE SURFACE OF THE OBSTACLE IS DIVIDED INTO N LONGITUDINAL
C             BANDS.
C             N IS UNCHANGED ON EXIT.
C
C     M       INTEGER
C             THE SURFACE OF THE OBSTACLE IS DIVIDED INTO M LATITUDINAL
C             BANDS.
C             M IS UNCHANGED ON EXIT.
C
C     AREA    REAL(NMMAX)
C             THE SURFACE OF THE OBSTACLE IS DIVIDED INTO N*M
C             BOUNDARY ELEMENTS.
C             AREA IS UNCHANGED ON EXIT.
C
C     SCOOR   REAL(3)
C             ARRAY CONTAINING THE SOURCE COORDINATES.
C             SCOOR IS UNCHANGED ON EXIT.
C
C     COOR    REAL(NMMAX)
C             ARRAY CONTAINING THE COORDINATES OF THE CENTROIDS.
C             COOR IS UNCHANGED ON EXIT.
C
C     NORM    REAL(NMMAX)
C             ARRAY CONTAINING THE NORMAL VECTORS TO THE SURFACE AT THE
C             CENTROIDS.
C             NORM IS UNCHANGED ON EXIT.
C
C     ZETA    COMPLEX
C             THE IMPEDANCE OF THE MEDIUM.
C             ZETA IS UNCHANGED ON EXIT.
C
C     RI      COMPLEX
C             THE REFRACTIVE INDEX AT THE SURFACE.
C             RI IS UNCHANGED ON EXIT.
C
C     DEPTH   REAL
C             THE DISTANCE FROM THE SURFACE GAMMA TO THE CENTRE OF THE
C             OBSTACLE.
C             DEPTH IS UNCHANGED ON EXIT.
C
C  ON EXIT
C
```

```
C     G    COMPLEX(NSTEP)
C          A VECTOR CONTAINING THE CALCULATED PRESSURE VALUES.
C
C  THIS VERSION DATED 3RD DECEMBER, 1989.
C
C  ROUTINES GDER,G22DER,G12 ARE CALLED.
C          THE TOEPLITZ ROUTINE CGSLC IS ALSO CALLED.
C
C  INTERNAL VARIABLES
C
      PARAMETER(NMAX=200,MMAX=100,NMMAX=NMAX*MMAX,MMMAX=MMAX*MMAX)
      REAL*4      SCOOR(3),COOR(3,NMMAX)
      REAL*4      NORM(3,NMMAX),AREA(NMMAX),AKNORM(3)
      REAL*4      AJCOOR(3),AKCOOR(3),X,AICOOR(3),AINORM(3),K1
      INTEGER*4   J,NN,MM,K,JKL,KK,JJ,MMM
      COMPLEX*8   AJK,R(MAX(MMAX,2*NMAX)),NDG,GG,GX,GY,GZ
      COMPLEX*8   A(MMMAX,NMAX),G(NMAX*MMAX),ALPHA
C
      IF(N.GT.NMAX.OR.M.GT.MMAX)THEN
       WRITE(6,500)
500    FORMAT(' *ERROR* MAXIMUM ARRAY SIZE EXCEEDED')
       STOP
      ENDIF
      K1=REAL(PROP/RI)
      ALPHA=ZETA*RI
      NM=N*M
      MM=M*M
      DO 010 K=1,NM
       DO 020 J=1,M
        AJCOOR(1)=COOR(1,J)
        AJCOOR(2)=COOR(2,J)
        AJCOOR(3)=COOR(3,J)
        AKCOOR(1)=COOR(1,K)
        AKCOOR(2)=COOR(2,K)
        AKCOOR(3)=COOR(3,K)
        AKNORM(1)=NORM(1,K)
        AKNORM(2)=NORM(2,K)
        AKNORM(3)=NORM(3,K)
        IF(J.EQ.K)THEN
         AJK=(1.0,0.0)
         DO 600 I=1,NM
          IF(I.NE.J) THEN
           AICOOR(1)=COOR(1,I)
           AICOOR(2)=COOR(2,I)
           AICOOR(3)=COOR(3,I)
           AINORM(1)=NORM(1,I)
           AINORM(2)=NORM(2,I)
           AINORM(3)=NORM(3,I)
           CALL GDER(AICOOR,AJCOOR,GG,GX,GY,GZ)
           NDG=AINORM(1)*GX+AINORM(2)*GY+AINORM(3)*GZ
           AJK=AJK+AREA(I)*NDG
          ENDIF
600      CONTINUE
         AJK = AJK*ALPHA
        ELSE
         CALL G22DER(AKCOOR,AJCOOR,K1,RI,ZETA,GG,GX,GY,GZ,DEPTH)
         NDG=AKNORM(1)*GX+AKNORM(2)*GY+AKNORM(3)*GZ
         AJK=-NDG*AREA(K)
        ENDIF
```

```
      JJ=J+((K-(INT((K-1)/M))*M)-1)*M
      KK=INT((K-1)/M)+1
      A(JJ,KK)=AJK
020   CONTINUE
      CALL G12(AKCOOR,SCOOR,K1,RI,ZETA,GG,DEPTH)
      G(K)=GG
      G(K)=ALPHA*G(K)
010   CONTINUE
      MMM=M
      CALL CGSLC(A,G,R,MMM,N,MMMAX)
      RETURN
      END
```

D.9 Subroutine FSURSPHIM

FSURSPHIM calculates values of pressure at the midpoints of the boundary elements of a sphere, for the numerical solution of equation (A.7). Reference to other subprograms are:

- CGSLC: a subroutine from Argonne National Laboratory's Toeplitz package [105];
- FFG: see section D.3;
- NDFG: see section D.20;
- RMAG: see section D.24.

```
      SUBROUTINE FSURSPHIM(PROP,N,M,G,AREA,SCOOR,COOR,NORM)
      COMPLEX*8  PROP
      INTEGER*2  N,M
C
C  FSURSPHIM CALCULATES PRESSURE VALUES ON THE SURFACE
C  OF A RIGID OBSTACLE, IN A RIGID POROUS MEDIUM.
C
C  ON ENTRY
C
C     PROP   COMPLEX
C            PROPAGATION CONSTANT.
C            N.B. TIME DEPENDENCE EXP(-I*W*T) ASSUMED.
C            PROP IS UNCHANGED ON EXIT.
C
C     N      INTEGER
C            THE SURFACE OF THE OBSTACLE IS DIVIDED INTO N LONGITUDINAL
C            BANDS.
C            N IS UNCHANGED ON EXIT.
C
C     M      INTEGER
C            THE SURFACE OF THE OBSTACLE IS DIVIDED INTO M LATITUDINAL
C            BANDS.
C            M IS UNCHANGED ON EXIT.
C
C     AREA   REAL(NMMAX)
C            ARRAY CONTAINING THE THE AREA OF EACH ELEMENT.
C            AREA IS UNCHANGED ON EXIT.
C
C     SCOOR  REAL(3)
C            ARRAY CONTAINING THE SOURCE COORDINATES.
C            SCOOR IS UNCHANGED ON EXIT.
C
C     COOR   REAL(NMMAX)
C            ARRAY CONTAINING THE COORDINATES OF THE CENTROIDS.
C            COOR IS UNCHANGED ON EXIT.
C
C     NORM   REAL(NMMAX)
C            ARRAY CONTAINING THE NORMAL VECTORS AT THE CENTROIDS.
C            NORM IS UNCHANGED ON EXIT.
C
C  ON EXIT
C
C     G      COMPLEX(NMMAX)
C            A VECTOR CONTAINING THE CALCULATED PRESSURE VALUES.
C
C  THIS VERSION DATED 17th FEBRUARY, 1989.
C
C  ROUTINES FFG, NDFG AND RMAG ARE CALLED.
C          THE TOEPLITZ ROUTINE CGSLC IS ALSO CALLED.
C
C  FUNCTION TYPE DECLARATION
C
      REAL*4     RMAG
      COMPLEX*8  FFG,NDFG
C
C  INTERNAL VARIABLES
C
      PARAMETER(NMAX=200,MMAX=100,NMMAX=NMAX*MMAX,MMMAX=MMAX*MMAX)
      COMPLEX*8  G(NMAX*MMAX)
```

```
      REAL*4     AJCOOR(3),AKCOOR(3),X,AICOOR(3)
      REAL*4     SCOOR(3),COOR(3,NMMAX),AINORM(3),AKNORM(3)
      REAL*4     NORM(3,NMMAX),AREA(NMMAX)
      INTEGER*2  J,NN,MM,K,JKL,KK,JJ,MMM
      COMPLEX*8  A(MMMAX,NMAX),NDFFG,AJK,R(MAX(MMAX,2*NMAX))
      IF(N.GT.NMAX.OR.M.GT.MMAX)THEN
       WRITE(6,500)
500    FORMAT(' *ERROR* MAXIMUM ARRAY SIZE EXCEEDED')
       STOP
      ENDIF
      NM=N*M
      MM=M*M
      DO 010 K=1,NM
       DO 020 J=1,M
        AJCOOR(1)=COOR(1,J)
        AJCOOR(2)=COOR(2,J)
        AJCOOR(3)=COOR(3,J)
        AKCOOR(1)=COOR(1,K)
        AKCOOR(2)=COOR(2,K)
        AKCOOR(3)=COOR(3,K)
        AKNORM(1)=NORM(1,K)
        AKNORM(2)=NORM(2,K)
        AKNORM(3)=NORM(3,K)
        IF(J.EQ.K)THEN
         AJK=(1.0,0.0)
         DO 600 I=1,NM
          IF(I.NE.J) THEN
           AICOOR(1)=COOR(1,I)
           AICOOR(2)=COOR(2,I)
           AICOOR(3)=COOR(3,I)
           AINORM(1)=NORM(1,I)
           AINORM(2)=NORM(2,I)
           AINORM(3)=NORM(3,I)
           X=RMAG(AICOOR,AJCOOR)
           NDFFG=NDFG(X,(0.0,0.0),AICOOR,AJCOOR,AINORM)
           AJK=AJK+AREA(I)*NDFFG
          ENDIF
600      CONTINUE
        ELSE
         X=RMAG(AKCOOR,AJCOOR)
         NDFFG=NDFG(X,PROP,AKCOOR,AJCOOR,AKNORM)
         AJK=-NDFFG*AREA(K)
        ENDIF
        JJ=J+((K-(INT((K-1)/M))*M)-1)*M
        KK=INT((K-1)/M)+1
        A(JJ,KK)=AJK
020    CONTINUE
       X=RMAG(AKCOOR,SCOOR)
       G(K)=FFG(X,PROP)
010   CONTINUE
      MMM=M
      CALL CGSLC(A,G,R,MMM,N,MMMAX)
      RETURN
      END
```

D.10 Subroutine G11

G11 calculates the acoustic pressure at a receiver point in the upper medium due to a point source on the same side of the boundary, using equation (3.33). There are no subprograms referenced.

```
      SUBROUTINE G11(X2,X1,K1,N,ZETA,G,DEPTH)
C
C THIS SUBROUTINE CALCULATES AN APPROXIMATION FOR THE ACOUSTIC
C PRESSURE ON ONE SIDE OF AN INTERFACE DUE TO A POINT SOURCE ON
C THE SAME SIDE OF THE INTERFACE. CARTESIAN COORDINATES (X,Y,Z)
C ARE USED, THE INTERFACE HAS THE EQUATION Z=DEPTH, AND THE MEDIUM
C OCCUPYING Z > DEPTH IS CALLED MEDIUM 1, THE MEDIUM OCCUPYING
C Z < DEPTH IS CALLED MEDIUM 2. BOTH SOURCE AND RECEIVER ARE ASSUMED
C TO BE IN MEDIUM 2.
C
C LET K1, K2 DENOTE PROPAGATION CONSTANTS IN THE TWO MEDIUMS, AND
C LET Z1, Z2 DENOTE THE IMPEDANCES OF THE TWO MEDIUMS. NOTE THAT THE
C INCIDENT WAVE IS ASSUMED TO BE
C
C -EXP(I*K1*R)/(4*PI*R),
C
C WHERE R IS THE DISTANCE FROM THE SOURCE, AND
C       I = SQRT(-1).
C
C ON INPUT
C
C X2(I),    REAL(3)
C  I=1,2,3  ARE THE X,Y,Z CARTESIAN COORDINATES OF EITHER THE SOURCE
C           OR THE RECEIVER.
C           X2 IS UNCHANGED ON EXIT.
C
C X1(I),    REAL(3)
C  I=1,2,3  ARE THE X,Y,Z CARTESIAN COORDINATES OF EITHER THE SOURCE
C           OR THE RECEIVER. (EITHER X1 CONTAINS THE SOURCE COORDINATES
C           AND X2 THE RECEIVER COORDINATES OR VICE VERSA.)
C           X1 IS UNCHANGED ON EXIT.
C
C K1        REAL
C           IS THE PROPAGATION CONSTANT OF MEDIUM 1
C           K1 IS UNCHANGED ON EXIT.
C
C N         COMPLEX
C           N = K2/K1 IS THE REFRACTIVE INDEX.
C           N IS UNCHANGED ON EXIT.
C
C ZETA      COMPLEX
C           ZETA = Z2/Z1 IS THE IMPEDANCE RATIO.
C           ZETA IS UNCHANGED ON EXIT.
C
C DEPTH     REAL
C           IS THE Z-COORDINATE OF THE BOUNDARY BETWEEN MEDIA 1 AND 2.
C           DEPTH IS UNCHANGED ON EXIT.
C
C ON OUTPUT
C
C G         COMPLEX
C           IS THE ACOUSTIC PRESSURE AT THE RECEIVER.
C
C
      REAL X1(3),X2(3),K1,DEPTH
      COMPLEX N,ZETA,G
C
      COMPLEX ALPHA,Q,AC,RP
      COMPLEX FR,FRDASH
```

```
C
      PI = 4.0*ATAN(1.0)
      ALPHA = N*ZETA
      XD = X2(1)-X1(1)
      YD = X2(2)-X1(2)
      Z1 = X1(3)-DEPTH
      Z2 = X2(3)-DEPTH
      ZD = Z2-Z1
      ZSUM = Z2+Z1
      RSTS = XD*XD+YD*YD
      RST = SQRT(RSTS)
      R = SQRT(RSTS+ZD*ZD)
      RDASH = SQRT(RSTS+ZSUM*ZSUM)
      S = RST/RDASH
      C = ZSUM/RDASH
      Q = CSQRT(N*N-S*S)
      AC = ALPHA*C
      RP = (AC-Q)/(AC+Q)
      FR = CEXP(CMPLX(0.0,K1*R))/R
      FRDASH = CEXP(CMPLX(0.0,K1*RDASH))/RDASH
      G = (-1.0/(4.0*PI))*(FR + RP*FRDASH)
      RETURN
      END
```

D.11 Subroutine G12

G12 calculates the acoustic pressure transmitted across the plane boundary from a point source on the other side of the boundary, using equation (6.1). There are no subprograms referenced.

```
      SUBROUTINE G12(X2,X1,K1,N,ZETA,G,DEPTH)
C
C THIS SUBROUTINE CALCULATES AN APPROXIMATION FOR THE ACOUSTIC
C PRESSURE TRANSMITTED ACROSS AN INTERFACE FROM A POINT SOURCE ON
C THE OTHER SIDE OF THE INTERFACE. CARTESIAN COORDINATES (X,Y,Z)
C ARE USED, THE INTERFACE HAS THE EQUATION Z=DEPTH, AND THE MEDIUM
C OCCUPYING Z > 0 IS CALLED MEDIUM 1, THE MEDIUM OCCUPYING Z < 0
C IS CALLED MEDIUM 2.
C
C LET K1, K2 DENOTE PROPAGATION CONSTANTS IN THE TWO MEDIUMS, AND
C LET Z1, Z2 DENOTE THE IMPEDANCES OF THE TWO MEDIUMS. NOTE THAT THE
C INCIDENT WAVE IS ASSUMED TO BE
C
C -C*EXP(I*K*R)/(4*PI*R),
C
C WHERE K = K1 (K2) IF THE SOURCE IS IN MEDIUM 1 (2),
C       C = 1 (ALPHA) IF THE SOURCE IS IN MEDIUM 1 (2),
C       R IS THE DISTANCE FROM THE SOURCE, AND
C       I = SQRT(-1).
C
C ON INPUT
C
C X2(I),    REAL(3)
C  I=1,2,3  ARE THE X,Y,Z CARTESIAN COORDINATES OF WHICHEVER OF SOURCE/
C           RECEIVER IS IN MEDIUM 2.
C           X2 IS UNCHANGED ON EXIT
C
C X1(I),    REAL(3)
C  I=1,2,3  ARE THE X,Y,Z CARTESIAN COORDINATES OF WHICHEVER OF SOURCE/
C           RECEIVER IS IN MEDIUM 1.
C           X1 IS UNCHANGED ON EXIT
C
C K1        REAL
C           IS THE PROPAGATION CONSTANT OF MEDIUM 1.
C           K1 IS UNCHANGED ON EXIT
C
C N         COMPLEX
C           N = K2/K1 IS THE REFRACTIVE INDEX.
C           N IS UNCHANGED ON EXIT
C
C ZETA      COMPLEX
C           ZETA = Z2/Z1 IS THE IMPEDANCE RATIO.
C           ZETA IS UNCHANGED ON EXIT
C
C DEPTH     REAL
C           IS THE Z-COORDINATE OF THE BOUNDARY BETWEEN MEDIA 1 AND 2.
C           DEPTH IS UNCHANGED ON EXIT
C
C ON OUTPUT
C
C G         COMPLEX
C           IS THE ACOUSTIC PRESSURE AT THE RECEIVER.
C
      REAL X1(3),X2(3),K1
      COMPLEX N,ZETA,G
C
      COMPLEX ALPHA,Q,P
C
      PI = 4.0*ATAN(1.0)
```

```
ALPHA = M*ZETA
XD = X2(1)-X1(1)
YD = X2(2)-X1(2)
Z1 = X1(3)-DEPTH
Z2 = X2(3)-DEPTH
RST = SQRT(XD*XD+YD*YD)
R = SQRT(RST*RST+Z1*Z1)
S = RST/R
C = Z1/R
Q = CSQRT(M*M-S*S)
P = ALPHA*C+Q
G = (-C/(2.0*PI*R))*ALPHA*CEXP(CMPLX(0.0,K1)*(R-Z2*Q))/P
RETURN
END
```

D.12 Subroutine G12DER

G12DER calculates the components of the gradient of acoustic pressure transmitted across the plane boundary from a point source on the other side of the boundary, using equation (6.3). There are no subprograms referenced.

```
      SUBROUTINE G12DER(X2,X1,K1,N,ZETA,G,GX,GY,GZ,DEPTH)
      REAL DEPTH,X1(3),X2(3),K1
      COMPLEX N,ZETA,G,GX,GY,GZ
C
C THIS SUBROUTINE CALCULATES AN APPROXIMATION FOR THE COMPONENTS OF THE
C GRADIENT OF THE ACOUSTIC
C PRESSURE TRANSMITTED ACROSS AN INTERFACE FROM A POINT SOURCE ON
C THE OTHER SIDE OF THE INTERFACE. CARTESIAN COORDINATES (X,Y,Z)
C ARE USED, THE INTERFACE HAS THE EQUATION Z=DEPTH, AND THE MEDIUM
C OCCUPYING Z > 0 IS CALLED MEDIUM 1, THE MEDIUM OCCUPYING Z < 0
C IS CALLED MEDIUM 2. THE SPATIAL DERIVATIVES OF THE APPROXIMATION
C ARE ALSO CALCULATED.
C
C LET K1, K2 DENOTE PROPAGATION CONSTANTS IN THE TWO MEDIUMS, AND
C LET Z1, Z2 DENOTE THE IMPEDANCES OF THE TWO MEDIUMS. NOTE THAT THE
C INCIDENT WAVE IS ASSUMED TO BE
C
C -C*EXP(I*K*R)/(4*PI*R),
C
C WHERE K = K1 (K2) IF THE SOURCE IS IN MEDIUM 1 (2),
C       C = 1 (ALPHA) IF THE SOURCE IS IN MEDIUM 1 (2),
C       R IS THE DISTANCE FROM THE SOURCE, AND
C       I = SQRT(-1).
C
C ON INPUT
C
C X2(I),    REAL(3)
C  I=1,2,3  ARE THE X,Y,Z CARTESIAN COORDINATES OF WHICHEVER OF SOURCE/
C           RECEIVER IS IN MEDIUM 2.
C           X2 IS UNCHANGED ON EXIT.
C
C X1(I),    REAL(3)
C  I=1,2,3  ARE THE X,Y,Z CARTESIAN COORDINATES OF WHICHEVER OF SOURCE/
C           RECEIVER IS IN MEDIUM 1.
C           X1 IS UNCHANGED ON EXIT.
C
C K1        REAL
C           IS THE PROPAGATION CONSTANT OF MEDIUM 1.
C           K1 IS UNCHANGED ON EXIT.
C
C N         COMPLEX
C           N = K2/K1 IS THE REFRACTIVE INDEX.
C           N IS UNCHANGED ON EXIT.
C
C ZETA      COMPLEX
C           ZETA = Z2/Z1 IS THE IMPEDANCE RATIO.
C           ZETA IS UNCHANGED ON EXIT.
C
C DEPTH     REAL
C           IS THE Z-COORDINATE OF THE BOUNDARY BETWEEN MEDIA 1 AND 2.
C           DEPTH IS UNCHANGED ON EXIT.
C
C ON OUTPUT
C
C G         COMPLEX
C           IS THE ACOUSTIC PRESSURE AT THE RECEIVER.
C
C GX,GY,GZ  COMPLEX
C           ARE THE DERIVATIVES OF G WITH RESPECT TO X2(1),X2(2),X2(3).
```

```
C
C INTERNAL VARIABLES
C
      COMPLEX ALPHA,Q,P,DQDTH,DGDRST
C
      PI = 4.0*ATAN(1.0)
      ALPHA = M*ZETA
      XD = X2(1)-X1(1)
      YD = X2(2)-X1(2)
      Z1 = X1(3)-DEPTH
      Z2 = X2(3)-DEPTH
      RST = SQRT(XD*XD+YD*YD)
      R = SQRT(RST*RST+Z1*Z1)
      S = RST/R
      C = Z1/R
      S1 = S/R
      C1 = C/R
      Q = CSQRT(M*M-S*S)
      P = ALPHA*C+Q
      G = (-C/(2.0*PI*R))*ALPHA*CEXP(CMPLX(0.0,K1)*(R-Z2*Q))/P
      DQDTH = -S*C/Q
      DGDRST = G*(CMPLX(-S1,S1*K1*R)-(S1*Q+C1*DQDTH)/P
     +  -CMPLX(0.0,K1*Z2*C1)*DQDTH)
      IF(RST.GT.0.0) THEN
         GX = DGDRST*(XD/RST)
         GY = DGDRST*(YD/RST)
      ELSE
         GX = (0.0,0.0)
         GY = (0.0,0.0)
      ENDIF
      GZ = CMPLX(0.0,-K1)*Q*G
      RETURN
      END
```

D.13 Subroutine G22DER

G22DER calculates the components of the gradient of the acoustic pressure at a receiver point in the lower medium due to a point source on the same side as the medium, using equation (3.37). There are no subprograms referenced.

```
      SUBROUTINE G22DER(X2,X1,K1,N,ZETA,G,GX,GY,GZ,DEPTH)
      REAL X1(3),X2(3),K1
      COMPLEX N,ZETA,G,GX,GY,GZ
C
C THIS SUBROUTINE CALCULATES AN APPROXIMATION FOR THE GRADIENT OF
C THE ACOUSTIC PRESSURE ON ONE SIDE OF AN INTERFACE
C DUE TO A POINT SOURCE ON THE SAME SIDE OF THE INTERFACE.
C CARTESIAN COORDINATES (X,Y,Z)
C ARE USED, THE INTERFACE HAS THE EQUATION Z=DEPTH, AND THE MEDIUM
C OCCUPYING Z > DEPTH IS CALLED MEDIUM 1, THE MEDIUM OCCUPYING
C Z < DEPTH IS CALLED MEDIUM 2. THE SPATIAL DERIVATIVES OF THE
C APPROXIMATION ARE ALSO CALCULATED. NOTE THAT BOTH SOURCE AND
C RECEIVER ARE ASSUMED TO LIE IN MEDIUM 2.
C
C LET K1, K2 DENOTE PROPAGATION CONSTANTS IN THE TWO MEDIUMS, AND
C LET Z1, Z2 DENOTE THE IMPEDANCES OF THE TWO MEDIUMS. NOTE THAT THE
C INCIDENT WAVE IS ASSUMED TO BE
C
C -ALPHA*EXP(I*K2*R)/(4*PI*R),
C
C WHERE R IS THE DISTANCE FROM THE SOURCE, AND
C       I = SQRT(-1).
C
C ON INPUT
C
C X2(I),    REAL(3)
C  I=1,2,3  ARE THE X,Y,Z CARTESIAN COORDINATES OF EITHER THE SOURCE
C           OR THE RECEIVER.
C           X2 IS UNCHANGED ON EXIT
C
C X1(I),    REAL(3)
C  I=1,2,3  ARE THE X,Y,Z CARTESIAN COORDINATES OF EITHER THE SOURCE
C           OR THE RECEIVER. (EITHER X1 CONTAINS THE SOURCE COORDINATES
C           AND X2 THE RECEIVER COORDINATES OR VICE VERSA.)
C           X1 IS UNCHANGED ON EXIT
C
C K1        REAL
C           IS THE PROPAGATION CONSTANT OF MEDIUM 1.
C           K1 IS UNCHANGED ON EXIT
C
C N         COMPLEX
C           N = K2/K1 IS THE REFRACTIVE INDEX.
C           N IS UNCHANGED ON EXIT
C
C ZETA      COMPLEX
C           ZETA = Z2/Z1 IS THE IMPEDANCE RATIO.
C           ZETA IS UNCHANGED ON EXIT
C
C DEPTH     REAL
C           IS THE Z-COORDINATE OF THE BOUNDARY BETWEEN MEDIA 1 AND 2.
C           DEPTH IS UNCHANGED ON EXIT
C
C ON OUTPUT
C
C G         COMPLEX
C           IS THE ACOUSTIC PRESSURE AT THE RECEIVER.
C
C GX,GY,GZ  COMPLEX
C           ARE THE DERIVATIVES OF G WITH RESPECT TO X2(1),X2(2),X2(3).
```

```
C
      COMPLEX ALPHA,MINV,K2,Q,AQ,P,RP,CON,IRK2,IRDK2,EXP1,EXP2
      COMPLEX FR,FRDASH,GR,GRDASH,DRPDTH,A
C
      PI = 4.0*ATAN(1.0)
      ALPHA = M*ZETA
      MINV = (1.0,0.0)/M
      K2 = K1*M
      XD = X2(1)-X1(1)
      YD = X2(2)-X1(2)
      Z1 = X1(3)-DEPTH
      Z2 = X2(3)-DEPTH
      ZD = Z2-Z1
      ZSUM = Z2+Z1
      RSTS = XD*XD+YD*YD
      RST = SQRT(RSTS)
      R = SQRT(RSTS+ZD*ZD)
      RDASH = SQRT(RSTS+ZSUM*ZSUM)
      S = RST/RDASH
      C = -ZSUM/RDASH
      Q = CSQRT(MINV*MINV-S*S)
      AQ = ALPHA*Q
      P = C+AQ
      RP = (C-AQ)/P
      CON = (-1.0/(4.0*PI))*ALPHA
      IRK2 = CMPLX(0.0,R)*K2
      IRDK2 = CMPLX(0.0,RDASH)*K2
      EXP1 = CEXP(IRK2)
      EXP2 = CEXP(IRDK2)
      FR = EXP1/R
      FRDASH = EXP2/RDASH
      G = CON*(FR + RP*FRDASH)
      GR = (IRK2-(1.0,0.0))*FR/(R*R)
      GRDASH = (IRDK2-(1.0,0.0))*FRDASH/(RDASH*RDASH)
      DRPDTH = (-(S+S))*ALPHA*(Q-(C*C)/Q)/(P*P)
      IF(RST.GT.0.0) THEN
         A = CON*(GR + RP*GRDASH - (C/(RST*R))*FRDASH*DRPDTH)
      ELSE
         A = CON*(GR + RP*GRDASH)
      ENDIF
      GX = A*XD
      GY = A*YD
      GZ = CON*(GR*ZD +RP*GRDASH*ZSUM + (S/RDASH)*FRDASH*DRPDTH)
      RETURN
      END
```

D.14 Subroutine G11WVDP

G11WVDP calculates values of pressure at a receiver point due to a point source above an impedance boundary, using the equation (3.45). The subprogram that is referenced is:

- W: a subroutine to calculate the error function, $erfc$, see Price [110].

```
      SUBROUTINE G11WVDP(X2,X1,K1,N,ZETA,G,DEPTH)
C
C THIS SUBROUTINE CALCULATES AN APPROXIMATION FOR THE ACOUSTIC
C PRESSURE ON ONE SIDE OF AN INTERFACE DUE TO A POINT SOURCE ON
C THE SAME SIDE OF THE INTERFACE.
C CARTESIAN COORDINATES (X,Y,Z)
C ARE USED, THE INTERFACE HAS THE EQUATION Z=DEPTH, AND THE MEDIUM
C OCCUPYING Z > DEPTH IS CALLED MEDIUM 1, THE MEDIUM OCCUPYING
C Z < DEPTH IS CALLED MEDIUM 2. BOTH SOURCE AND RECEIVER ARE ASSUMED
C TO BE IN MEDIUM 1.
C
C LET K1, K2 DENOTE PROPAGATION CONSTANTS IN THE TWO MEDIA, AND
C LET Z1, Z2 DENOTE THE IMPEDANCES OF THE TWO MEDIA. NOTE THAT THE
C INCIDENT WAVE IS ASSUMED TO BE
C
C -EXP(I*K1*R)/(4*PI*R),
C
C WHERE R IS THE DISTANCE FROM THE SOURCE, AND I = SQRT(-1).
C
C ON INPUT
C
C X2(I),     REAL(3)
C  I=1,2,3   X2 ARE THE X,Y,Z CARTESIAN COORDINATES OF EITHER THE SOURCE
C            OR THE RECEIVER.
C            X2 IS UNCHANGED ON EXIT.
C
C X1(I),     REAL(3)
C  I=1,2,3   X1 ARE THE X,Y,Z CARTESIAN COORDINATES OF EITHER THE SOURCE
C            OR THE RECEIVER. (EITHER X1 CONTAINS THE SOURCE COORDINATES
C            AND X2 THE RECEIVER COORDINATES OR VICE VERSA.)
C            X1 IS UNCHANGED ON EXIT.
C
C K1         REAL
C            K1 IS THE PROPAGATION CONSTANT OF MEDIUM 1.
C            K1 IS UNCHANGED ON EXIT.
C
C N          COMPLEX
C            N = K2/K1 IS THE REFRACTIVE INDEX.
C            N IS UNCHANGED ON EXIT.
C
C ZETA       COMPLEX
C            ZETA = Z2/Z1 IS THE IMPEDANCE RATIO.
C            ZETA IS UNCHANGED ON EXIT.
C
C DEPTH      REAL
C            IS THE Z-COORDINATE OF THE BOUNDARY BETWEEN MEDIA 1 AND 2.
C            DEPTH IS UNCHANGED ON EXIT.
C
C ON OUTPUT
C
C G          COMPLEX
C            IS THE ACOUSTIC PRESSURE AT THE RECEIVER.
C
C THIS VERSION DATED 3RD DECEMBER, 1989
C
C ROUTINE W IS CALLED
C
      REAL X1(3),X2(3),K1,DEPTH
      COMPLEX N,ZETA,G,I,RP,BETA,PE,PE2,WIZ,F
```

```
C
      BETA=1.0/ZETA
      I=CMPLX(0.0,1.0)
      PI=4.0*ATAN(1.0)
      XD=X2(1)-X1(1)
      YD=X2(2)-X1(2)
      Z1=X1(3)-DEPTH
      Z2=X2(3)-DEPTH
      ZD=Z2-Z1
      ZSUM=Z2+Z1
      RSTS=XD*XD+YD*YD
      RST=SQRT(RSTS)
      R=SQRT(RSTS+ZD*ZD)
      RDASH=SQRT(RSTS+ZSUM*ZSUM)
      CTH=ZSUM/RDASH
      RP=(CTH-BETA)/(CTH+BETA)
      G=-CEXP(I*K1*R)/(4.0*PI*R)-RP*CEXP(I*K1*RDASH)/(4.0*PI*RDASH)
      PE=CSQRT(I*K1*RDASH/2.0)*(CTH+BETA)
      PE2=-I*PE
      CALL W(PE2,WIZ)
      F=1.0+I*SQRT(PI)*PE*WIZ
      G=G-(1.0-RP)*F*CEXP(I*K1*RDASH)/(4.0*PI*RDASH)
      RETURN
      END
```

D.15 Subroutine GDER

GDER calculates the magnitude of the principal singularity of equation (5.1) and also the components of its gradient. There are no subprograms referenced.

```
      SUBROUTINE GDER(X2,X1,G,GX,GY,GZ)
      REAL X1(3),X2(3)
      COMPLEX G,GX,GY,GZ
C
C GDER CALCULATES THE MAGNITUDE AND THE COMPONENTS OF THE GRADIENT
C OF THE PRINCIPAL SINGULARITY, EXCLUDING THE FACTOR ALPHA.
C
C ON ENTRY
C
C X2(3) REAL
C       CARTESIAN COORDINATES OF THE RECEIVER POINT
C       X1 IS UNCHANGED ON EXIT.
C
C X1(3) REAL
C       CARTESIAN COORDINATES OF THE SOURCE POINT
C       X1 IS UNCHANGED ON EXIT.
C
C ON EXIT
C
C G     COMPLEX
C       THE MAGNITUDE OF THE PRINCIPAL SINGULARITY
C
C GX    COMPLEX
C       THE X COMPONENT OF THE GRADIENT OF THE
C       PRINCIPAL SINGULARITY
C
C GY    COMPLEX
C       THE Y COMPONENT OF THE GRADIENT OF THE
C       PRINCIPAL SINGULARITY
C
C GZ    COMPLEX
C       THE Z COMPONENT OF THE GRADIENT OF THE
C       PRINCIPAL SINGULARITY
C
C INTERNAL VARIABLES
C
      REAL CON,R,RINV,XD,YD,ZD,
C
      CON = -7.957747155E-02
C CON = -1/(4*PI)
      XD = X1(1)-X2(1)
      YD = X1(2)-X2(2)
      ZD = X1(3)-X2(3)
      R = SQRT(XD*XD+YD*YD+ZD*ZD)
      RINV = 1.0/R
      G = CON*RINV
      CON = CON*RINV*RINV*RINV
      GX = CON*XD
      GY = CON*YD
      GZ = CON*ZD
      RETURN
      END
```

D.16 Subroutine GEOCIRCLE

GEOCIRCLE calculates values of area and the coordinates of the midpoints of the boundary elements of a circular surface inhomogeneity using the theory of section 5.1.2. There are no subprograms referenced.

```
      SUBROUTINE GEOCIRCLE(RAD,M,N,A,COOR)
      PARAMETER(NMAX=200,MMAX=100,NMMAX=NMAX*MMAX)
      REAL*4    RAD,A(NMMAX),COOR(3,NMMAX)
      INTEGER*2 M,N
C
C GEOCIRCLE CALCULATES THE AREA OF ELEMENT J FOR A CIRCLE, THE
C COORDINATES OF THE MIDPOINTS.
C
C ON ENTRY
C
C     RAD     REAL
C             THE RADIUS OF THE CIRCLE.
C             RAD IS UNCHANGED ON EXIT.
C
C     M       INTEGER
C             THE CIRCULAR PATCH IS DIVIDED INTO M ANULI.
C             M IS UNCHANGED ON EXIT.
C
C     N       INTEGER
C             THE CIRCULAR PATCH IS DIVIDED INTO N SECTORS.
C             N IS UNCHANGED ON EXIT.
C
C ON EXIT
C
C     A       REAL
C             THE AREA OF ELEMENT J.
C
C     COOR    REAL
C             THE CARTESIAN COORDINATES OF THE MIDPOINT OF ELEMENT J.
C
C INTERNAL VARIABLES
C
      REAL*4    PI,THET,RFRAC
      INTEGER*2 I1,I2,J
C
      PI=3.141592653
      RFRAC=RAD/M
      THET=2.0*PI/N
      DO 030 I1=1,N
       DO 040 I2=1,M
        J=(I1-1)*M+I2
        COOR(1,J)=(I2-0.5)*RFRAC*COS((I1-0.5)*THET)
        COOR(2,J)=(I2-0.5)*RFRAC*SIN((I1-0.5)*THET)
        COOR(3,J)=0.0
        A(J)=0.5*THET*((I2*RFRAC)**2-((I2-1)*RFRAC)**2)
040    CONTINUE
030   CONTINUE
      RETURN
      END
```

D.17 Subroutine GEOSPHERE

GEOSPHERE calculates values of area, the coordinates of the midpoints and the normals of the boundary elements of a sphere for the numerical solution of equation (A.7). There are no subprograms referenced.

```
      SUBROUTINE GEOSPHERE(RAD,M,N,A,COOR,NORM)
      PARAMETER(NMAX=200,MMAX=100,NMMAX=NMAX*MMAX)
      REAL*4    RAD,A(NMMAX),COOR(3,NMMAX),NORM(3,NMMAX)
      INTEGER*2 M,N
C
C GEOSPHERE CALCULATES THE AREA OF ELEMENT J FOR A SPHERE, THE
C COORDINATES OF THE MIDPOINTS AND THE NORMAL VECTORS TO THE MIDPOINTS.
C
C ON ENTRY
C
C     RAD     REAL
C             THE RADIUS OF THE SPHERE.
C             RAD IS UNCHANGED ON EXIT.
C
C     M       INTEGER
C             THE SURFACE OF THE SPHERE IS DIVIDED INTO M LATITUDINAL
C             BANDS.
C             M IS UNCHANGED ON EXIT.
C
C     N       INTEGER
C             THE SURFACE OF THE SPHERE IS DIVIDED INTO N LONGITUDINAL
C             BANDS.
C             N IS UNCHANGED ON EXIT.
C
C ON EXIT
C
C     A       REAL
C             THE AREA OF ELEMENT J. ONLY THE FIRST M ELEMENTS ARE
C             CALCULATED.
C
C     COOR    REAL
C             THE CARTESIAN COORDINATES OF THE MIDPOINT OF ELEMENT J
C
C     NORM    REAL
C             THE NORMAL VECTOR AT THE MIDPOINT OF ELEMENT J DIRECTED
C             INTO THE SPHERE. ONLY THE FIRST M ELEMENTS ARE CALCULATED.
C
C INTERNAL VARIABLES
C
      REAL*4    COZ(NMMAX),PI,THET,ANG,A1,A2
      INTEGER*2 I1,I2,J
C
      PI=3.141592653
      ANG=2.0*PI/N
      THET=PI/M
      DO 030 I1=1,N
       DO 040 I2=1,M
        J=(I1-1)*M+I2
        AN1=(0.5+FLOAT(I2-1))*THET
        AN2=FLOAT(I1-1)*ANG
        COOR(1,J)=RAD*SIN(AN1)*COS(AN2)
        COOR(2,J)=RAD*SIN(AN1)*SIN(AN2)
        IF(I1.EQ.1)THEN
         A1=2*PI*RAD*RAD
         A2=COS(FLOAT(I2-1)*THET)-COS(FLOAT(I2)*THET)
         A(J)=A1*A2/N
         COZ(J)=RAD*COS((0.5+FLOAT(I2-1))*THET)
        ELSE
         A(J)=A(I2)
```

```
          COZ(J)=COZ(I2)
        ENDIF
        COOR(3,J)=COZ(J)
        NORM(1,J)=-COOR(1,J)/RAD
        NORM(2,J)=-COOR(2,J)/RAD
        NORM(3,J)=-COOR(3,J)/RAD
040    CONTINUE
030   CONTINUE
      RETURN
      END
```

D.18 Subroutine GEOSPHEROID

GEOSPHEROID calculates values of area, the coordinates of the midpoints and the normals of the boundary elements of a spheroid using the theory of section 5.1.1. There are no subprograms referenced.

```
      SUBROUTINE GEOSPHEROID(A,B,M,N,AREA,COOR,NORM,TESTRAD)
      PARAMETER(NMAX=200,MMAX=500,NMMAX=NMAX*MMAX)
      REAL*4    A,B,AREA(NMMAX),COOR(3,NMMAX),NORM(3,NMMAX)
      REAL*4    TESTRAD(NMMAX)
      INTEGER*4 M,N
C
C GEOSPHEROID CALCULATES THE AREA OF ELEMENT J FOR AN OBLATE SPHEROID,
C THE COORDINATES OF THE MIDPOINTS AND THE NORMAL VECTORS TO THE MIDPOINTS.
C
C ON ENTRY
C
C     A       REAL
C             THE MAJOR AXIS OF THE OBLATE SPHEROID.
C             A IS UNCHANGED ON EXIT.
C
C     B       REAL
C             THE MINOR AXIS OF THE OBLATE SPHEROID.
C             A IS UNCHANGED ON EXIT.
C
C     M       INTEGER
C             THE SURFACE OF THE SPHEROID IS DIVIDED INTO M LATITUDINAL
C             BANDS.
C             M IS UNCHANGED ON EXIT.
C
C     N       INTEGER
C             THE SURFACE OF THE SPHEROID IS DIVIDED INTO N LONGITUDINAL
C             BANDS.
C             N IS UNCHANGED ON EXIT.
C
C ON EXIT
C
C     AREA    REAL
C             THE AREA OF ELEMENT J. ONLY THE FIRST M ELEMENTS ARE
C             CALCULATED.
C
C     NORM    REAL
C             THE NORMAL VECTOR AT THE MIDPOINT OF ELEMENT J DIRECTED
C             INTO THE SPHERE. ONLY THE FIRST M ELEMENTS ARE CALCULATED.
C
C     COOR    REAL
C             THE CARTESIAN COORDINATES OF THE MIDPOINT OF ELEMENT J
C
C INTERNAL VARIABLES
C
      REAL*4    COZ(NMMAX),PI,THET,ANG,A1,A2,AM2,BM2,THBIG(MMAX),ARC
      REAL*4    ALBIG,RAD(MMAX),XHAT,ZHAT,XDASH,COOR1(3),COOR2(3)
      REAL*4    RAD1,RAD2
      INTEGER*4 I1,I2,J
C
      REAL*4    RMAG
      PI=3.141592653
      ANG=2.0*PI/N
      THET=PI/M
      AM2=1.0/(A*A)
      BM2=1.0/(B*B)
      DO 030 I1=1,N
       DO 040 I2=1,M
        J=(I1-1)*M+I2
        ALBIG=(FLOAT(I1-1))*ANG
```

```
      IF(I1.EQ.1)THEN
       THBIG(I2)=(0.5+FLOAT(I2-1))*THET
       RAD(I2)=1.0/SQRT(AM2*SIN(THBIG(I2))**2+
     &  BM2*COS(THBIG(I2))**2)
       RAD1=1.0/SQRT(AM2*SIN((FLOAT(I2-1))*THET)**2+
     &  BM2*COS((FLOAT(I2-1))*THET)**2)
       RAD2=1.0/SQRT(AM2*SIN((FLOAT(I2))*THET)**2+
     &  BM2*COS((FLOAT(I2))*THET)**2)
       COOR1(1)=RAD1*SIN(FLOAT(I2-1)*THET)
       COOR1(2)=0.0
       COOR1(3)=RAD1*COS(FLOAT(I2-1)*THET)
       COOR2(1)=RAD2*SIN(FLOAT(I2)*THET)
       COOR2(2)=0.0
       COOR2(3)=RAD2*COS(FLOAT(I2)*THET)
       ARC=RMAG(COOR2,COOR1)
       AREA(I2)=2*PI*RAD(I2)*SIN(THBIG(I2))*ARC/N
       COZ(I2)=RAD(I2)*COS(THBIG(I2))
      ELSE
       AREA(J)=AREA(I2)
       COZ(J)=COZ(I2)
      ENDIF
      COOR(1,J)=RAD(I2)*SIN(THBIG(I2))*COS(ALBIG)
      COOR(2,J)=RAD(I2)*SIN(THBIG(I2))*SIN(ALBIG)
      COOR(3,J)=COZ(J)
      XDASH=SQRT(COOR(1,J)**2+COOR(2,J)**2)
      IF ((XDASH*XDASH)/(A*A).GT.1.0) THEN
       AA=0.0
      ELSE
       AA=SQRT(1.0-(XDASH*XDASH)/(A*A))*A*A/(B*XDASH)
      ENDIF
      XHAT=SQRT(1.0/(1.0+AA*AA))
      ZHAT=SQRT(AA*AA/((AA*AA)+1.0))
      IF (COOR(1,J).GT.0.0) XHAT=-XHAT
      IF (COOR(3,J).GT.0.0) ZHAT=-ZHAT
      NORM(1,J)=XHAT*ABS(COS(ALBIG))
      NORM(2,J)=XHAT*ABS(SIN(ALBIG))
      IF((COOR(1,J).GT.0.0).AND.(COOR(2,J).LT.0.0))
     &   NORM(2,J)=-NORM(2,J)
      IF((COOR(1,J).LT.0.0).AND.(COOR(2,J).GT.0.0))
     &   NORM(2,J)=-NORM(2,J)
      NORM(3,J)=ZHAT
040    CONTINUE
030   CONTINUE
      RETURN
      END
```

D.19 Subroutine LEGNDR

LEGNDR calculates values of the Legendre polynomial and its derivative. There are no subprograms referenced.

```
      SUBROUTINE LEGNDR(X,N,P,PDER)
      INTEGER N
      REAL X, P(N+1),PDER(N+1)
C
C  THIS SUBROUTINE CALCULATES P(I,X) AND ITS DERIVATIVE,
C  FOR I = 0,1,...,N, WHERE P(I,X)
C  DENOTES THE LEGENDRE POLYNOMIAL OF DEGREE N AND ARGUMENT X, AS
C  DEFINED IN CHAPTER 22 OF [1]. THE METHOD OF CALCULATION USED IS
C  FORWARD RECURRENCE, WHICH IS STABLE IF X LIES BETWEEN -1 AND 1.
C
C  ON ENTRY:
C
C  X       REAL
C          X SHOULD LIE IN THE RANGE  0 .LE. X .LE. 1.
C
C  N       INTEGER
C          N IS THE ORDER OF THE LARGEST DEGREE LEGENDRE POLYNOMIAL WHICH
C          IS TO BE CALCULATED.  N MUST BE A POSITIVE INTEGER.
C
C  X, N    ARE UNCHANGED ON EXIT.
C
C  ON EXIT:
C
C  P       REAL(N+1)
C          P(I+1) IS EQUAL TO P(I,X), FOR I = 0,1,...,N.
C
C  PDER    REAL(N+1)
C          THE DERIVATIVE OF P
C
C THIS VERSION DATED 9TH JANUARY 1990
C
C  REFERENCE:
C
C  [1] M ABRAMOWITZ AND I A STEGUN 'HANDBOOK OF MATHEMATICAL FUNCTIONS'
C      NEW YORK: DOVER.
C
C  NOW CARRY OUT THE FORWARD RECURRENCE TO CALCULATE P.
C
      P(1) = 1.0
      P(2) = X
      PDER(1)=0.0
      PDER(2)=1.0
      DO 10 I = 2,N
C
C        THE FOLLOWING EQUATION, USED TO CARRY OUT THE FORWARD
C        RECURRENCE, IS A REARRANGEMENT OF EQN. (8.5.3) IN [1].
C
         P(I+1) = ((I+I-1)*X*P(I) - (I-1)*P(I-1))/I
         IF(X.EQ.1.0)THEN
          PDER(I+1)=I*(I+1.0)/2.0
         ELSEIF(X.EQ.-1.0)THEN
          PDER(I+1)=((-1)**(I+1))*I*(I+1.0)/2.0
         ELSE
          PDER(I+1)=I*(X*P(I+1)-P(I))/(X*X-1.0)
         ENDIF
 10   CONTINUE
      END
```

D.20 Complex function NDFG

NDFG calculates the normal derivative of the free field Green's fuction. There are no subprograms referenced.

```
      COMPLEX FUNCTION NDFG(X,K,BCOOR,ACOOR,NORM)
      COMPLEX*8 K
      REAL*4 X
C
C NDFG CALCULATES THE NORMAL COMPONENT OF THE FIRST DERIVATIVE OF THE
C FREE-FIELD GREEN'S FUNCTION GIVEN THE MAGNITUDE OF THE VECTOR
C BETWEEN THE TWO POINTS AND THE COMPLEX PROPAGATION CONSTANT.
C
C ON ENTRY:
C
C X   REAL
C     MAGNITUDE OF THE VECTOR BETWEEN THE TWO POINTS
C
C K   COMPLEX
C     COMPLEX PROPAGATION CONSTANT
C
      COMPLEX*8 I,DFG
      REAL*4    PI,MGI,MGJ,MGK,BCOOR(3),ACOOR(3),NORM(3)
C
      I=CMPLX(0.0,1.0)
      PI=3.141592653
      DFG=(1.0-(I*K*X))*CEXP(I*K*X)/(4.0*PI*X*X)
      MGI=(BCOOR(1)-ACOOR(1))*NORM(1)
      MGJ=(BCOOR(2)-ACOOR(2))*NORM(2)
      MGK=(BCOOR(3)-ACOOR(3))*NORM(3)
      NDFG=DFG*((MGI+MGJ+MGK)/X)
      RETURN
      END
```

D.21 Subroutine PC

PC calculates value of complex propagation constant for the lower medium using equation (3.60). Reference to other subprograms are:

- CMPBJ: a subroutine from Sastry [109].

```
      SUBROUTINE PC(F,MPR,SFR,SIGMA,POROS,PROPC)
      REAL*4 F,MPR,SFR,SIGMA,POROS
      COMPLEX*8 PROPC
C
C PC CALCULATES A SINGLE VALUE OF COMPLEX PROPAGATION CONSTANT
C
C ON ENTRY
C
C     F       REAL
C             FREQUENCY
C
C     MPR     REAL
C             GRAIN SHAPE FACTOR
C
C     SFR     REAL
C             PORE SHAPE FACTOR RATIO. N.B. THIS IS DOUBLE
C             THE VALUE USED IN THE OLD PREDICTION ROUTINES.
C
C     SIGMA   REAL
C             FLOW RESISTIVITY
C
C     POROS   REAL
C             POROSITY
C
C ON EXIT
C
C     PROPC   REAL
C             UN-NORMALISED PROPAGATION CONSTANT
C
C ROUTINE CMPBJ IS CALLED
C
C THIS VERSION DATED 8TH JANUARY, 1990.
C
C INTERNAL VARIABLES
C
      REAL*4 LAMBDAP,PI,CF,GAMMA,PRANDTL,Q,SQRTNP,RHOF,AE,OMEGA
      COMPLEX*8 I,Y,T,YP,TP,ZKKB,J0,J1
      INTEGER*2 N1
C
      PI=4.0*ATAN(1.0)
      I=CMPLX(0.0,1.0)
      CF=343.0
      GAMMA=1.4
      PRANDTL=0.76
      Q=SQRT(POROS**-MPR)
      SQRTNP=SQRT(PRANDTL)
      RHOF=1.2
      AE=SQRT(8.0*(Q**2)/(POROS*SIGMA))
      OMEGA=2.0*PI*F
      LAMBDAP=(AE/SFR)*((OMEGA*RHOF)**0.5)
      Y=SQRTNP*LAMBDAP*(I**0.5)
      N1=0
      CALL CMPBJ(Y,N1,J0)
      N1=1
      CALL CMPBJ(Y,N1,J1)
      T=J1/J0
      YP=LAMBDAP*(I**0.5)
      N1=0
      CALL CMPBJ(YP,N1,J0)
```

```
      M1=1
      CALL CMPBJ(YP,M1,J1)
      TP=J1/J0
      PROPC=((1.0+2.0*((GAMMA-1.0)/Y)*T)/(1.0-(2.0/YP)*TP)
     & *(Q*OMEGA/CF)**2)**0.5
      RETURN
      END
```

D.22 Subroutine PLNSCATCOE

PLNSCATCOE calculates values of the complex coefficients using equation (B.6). Reference to other subprograms are:

- SPHBES: see section D.25;
- SPHHNK: see section D.26.

```
      SUBROUTINE PLNSCATCOE(X,A,N)
      INTEGER N
      COMPLEX X,A(N+1)
C
C PLNSCATCOE CALCULATES THE COEFFICIENTS FOR CALCULATION
C OF THE SCATTERED FIELD BY A RIGID SPHERE IN AN INFINITE
C HOMOGENEOUS MEDIUM.
C
C ON ENTRY:
C
C X   COMPLEX
C     THE ARGUMENT K*R
X     X IS UNCHANGED ON EXIT.
C
C N   INTEGER
C     N IS THE ORDER OF THE LARGEST ORDER AND MUST BE
C     A POSITIVE INTEGER.
C     N IS UNCHANGED ON EXIT.
C
C ON EXIT:
C
C A   COMPLEX
C     THE COEFFICIENTS AM.
C
C ROUTINES SPHBES AND SPHHNK ARE CALLED.
C
C INTERNAL VARIABLES
C
      COMPLEX IM,H(1000),HDER(1000),J(1000),JDER(1000)
      INTEGER L,M
C
      M=10
      CALL SPHBES(X,N,M,J,JDER)
      CALL SPHHNK(X,N,H,HDER)
      IM = (0.0,1.0)
      A(1)=-JDER(1)/HDER(1)
      A(2)=(0.0,-3.0)*JDER(2)/HDER(2)
      DO 010 L=3,N+1
       M=L-1
       IM=CMPLX(-AIMAG(IM),REAL(IM))
       A(L)=-(M+M+1)*IM*JDER(L)/HDER(L)
010   CONTINUE
      END
```

D.23 Complex function PLNSCATFLD

PLNSCATFLD calculates value of pressure field using equation (B.4). Reference to other subprograms are:

- LEGNDR: see section D.19;
- SPHHNK: see section D.26.

```
      COMPLEX FUNCTION PLNSCATFLD(Z,THETA,A,N)
      INTEGER N
      COMPLEX A(N+1),Z
      REAL THETA
C
C PLNSCATFLD CALCULATES THE SCATTERED FIELD AT THE RECEIVER BY A
C RIGID SPHERE IN AN INFINITE HOMOGENEOUS MEDIUM.
C
C ON ENTRY:
C
C Z      COMPLEX
C        VALUE OF K*R.
C        Z IS UNCHANGED ON EXIT.
C
C THETA REAL
C        ANGLE OF THE RECEIVER POINT.
C        THETA IS UNCHANGED ON EXIT.
C
C A      COMPLEX
C        THE ARRAY CONTAINING THE COEFFICIENTS CALCULATED BY
C        SUBROUTINE PLNSCATCOE.
C        A IS UNCHANGED ON EXIT.
C
C N      INTEGER
C        N IS THE ORDER OF THE LARGEST ORDER.
C        N MUST BE A POSITIVE INTEGER.
C        N IS UNCHANGED ON EXIT.
C
C ROUTINES LEGNDR AND SPHNNK ARE CALLED.
C
C INTERNAL VARIABLES
C
      COMPLEX H(1000),HDER(1000),SUM
      REAL X,P(1000)
C
      X = COS(THETA)
      CALL LEGNDR(X,N,P)
      CALL SPHNNK(Z,N,H,HDER)
      SUM=(0.0,0.0)
      DO 010 M = 1,N+1
       SUM=SUM+A(M)*P(M)*H(M)
 010  CONTINUE
      PLNSCATFLD=SUM
      END
```

D.24 Function RMAG

RMAG calculates the distance between two points, both in cartesian coordinates. There are no subprograms referenced.

```
      FUNCTION RMAG(RA,RB)
      REAL*4 RA(3),RB(3)
C
C RMAG CALCULATES THE MAGNITUDE OF THE VECTOR (RB - RA)
C
C ON ENTRY
C
C RA(3) REAL
C       CARTESIAN COORDINATES OF THE FIRST VECTOR
C
C RB(3) REAL
C       CARTESIAN COORDINATES OF THE SECOND VECTOR
C
      REAL*4 R1,R2,R3
C
      R1=(RB(1)-RA(1))**2
      R2=(RB(2)-RA(2))**2
      R3=(RB(3)-RA(3))**2
      RMAG=SQRT(R1+R2+R3)
      RETURN
      END
```

D.25 Subroutine SPHBES

SPHBES calculates values of the spherical Bessel function and its derivative. There are no subprograms referenced.

```
      SUBROUTINE SPHBES(Z,N,M,BES,BESDER)
      INTEGER N, M
      COMPLEX Z, BES(N+1), BESDER(N+1)
C
C  THIS SUBROUTINE CALCULATES AN APPROXIMATION TO J(I,Z) AND JD(I,Z),
C  FOR I = 0,1,...,N, WHERE J(I,Z) DENOTES THE SPHERICAL BESSEL
C  FUNCTION OF THE FIRST KIND OF ORDER I AND ARGUMENT Z, AS DEFINED
C  IN 10.1.1 OF [1], AND JD(I,Z) DENOTES ITS FIRST DERIVATIVE
C  WITH RESPECT TO Z.  THE METHOD OF CALCULATION OF J(I,Z) IS BACKWARD
C  RECURRENCE.  THE RECURRENCE IS STARTED FROM I = N2 := ABS(Z)+M+10,
C  USING THE STANDARD LARGE ORDER APPROXIMATION FOR J(N2,Z) AND
C  J(N2-1,Z) ([1], EQUATION (9.3.1)).
C
C  ON ENTRY:
C
C  Z       COMPLEX
C          Z SHOULD LIE IN THE HALF-PLANE  RE Z .GE. 0, AND THE ALGORITHM
C          WILL CALCULATE MORE ACCURATELY THE NEARER Z IS TO THE REAL AXIS.
C
C  N       INTEGER
C          N IS THE ORDER OF THE LARGEST ORDER BESSEL FUNCTION WHICH IS TO
C          BE CALCULATED.  N MUST BE A POSITIVE INTEGER.
C
C  M       INTEGER
C          THE LARGER M IS, THE MORE ACCURATE ARE THE APPROXIMATIONS TO
C          THE BESSEL FUNCTIONS CALCULATED, BUT TOO LARGE A VALUE WILL
C          INCREASE THE COMPUTER TIME USED UNNECESSARILY, AND MAY
C          LEAD TO UNDERFLOW.  A VALUE IN THE RANGE 0-10 IS SUGGESTED.
C
C  Z, N, M  ARE UNCHANGED ON EXIT.
C
C  ON EXIT:
C
C  BES     COMPLEX(N+1)
C          BES(I+1) IS AN APPROXIMATION TO J(I,Z), FOR I = 0,1,...,N.
C
C  BESDER  COMPLEX(N+1)
C          BESDER(I+1) IS AN APPROXIMATION TO JD(I,Z), FOR I = 0,1,...,N.
C
C  REFERENCE:
C
C  [1] M ABRAMOWITZ AND I A STEGUN 'HANDBOOK OF MATHEMATICAL FUNCTIONS'
C      NEW YORK: DOVER.
C
C  INTERNAL VARIABLE DECLARATIONS
C
      REAL E
      INTEGER NN,N2,I,I1
      COMPLEX ZZ,J1,J0,JTEMP,ALPHA
C
C  THE FUNCTION JAPPRX(NN,ZZ) DEFINED BELOW IS THE LARGE ORDER
C  APPROXIMATION TO J(NN,ZZ), GIVEN AS EQUATION (9.3.1) IN [1].
C
      COMPLEX JAPPRX
      JAPPRX(NN,ZZ) = 0.5*(ZZ*(E/(NN+NN+1)))**(NN+0.5)/SQRT(NN*ZZ)
      E = EXP(1.0)
C
C  NOW START THE BACKWARD RECURRENCE WITH THE APPROXIMATE CALCULATION
C  OF  J(N2,Z).
```

```
C
C
      M2=MAX(MINT(1.5*ABS(Z)),M)+5

C     M2 = 1.5*ABS(Z)+M+10
      J1 = JAPPRX(M2,Z)
      J0 = JAPPRX(M2-1,Z)
      DO 10 I = M2-2,M-1,-1
C
C        THE FOLLOWING EQUATION, USED TO CARRY OUT THE BACKWARD
C        RECURRENCE, IS A REARRANGEMENT OF EQN. (10.1.19) IN [1].
C
         JTEMP = (I+I+3)*J0/Z - J1
         J1 = J0
         J0 = JTEMP
C
C        AT THIS POINT J0 AND J1 APPROXIMATE J(I,Z) AND J(I+1,Z),
C        RESPECTIVELY.
C
 10   CONTINUE
      BES(M+1) = J1
      BES(M) = J0
      DO 20 I = M-2,0,-1
C
C        THE FOLLOWING EQUATION, USED TO CARRY OUT THE BACKWARD
C        RECURRENCE, IS A REARRANGEMENT OF EQN. (10.1.19) IN [1].
C
         BES(I+1) = (I+I+3)*BES(I+2)/Z - BES(I+3)
 20   CONTINUE
C
C  TO CORRECT ERRORS IN BES(I) CAUSED BY USING AN APPROXIMATION TO
C  START THE BACKWARDS RECURRENCE, THE VALUES BES(I), I = 1,2,...,M+1,
C  ARE NOW NORMALISED.
C
      J0 = SIN(Z)/Z
C
C  THIS IS THE EXACT VALUE OF J(0,Z).
C
      ALPHA = J0/BES(1)
      BES(1) = J0
      DO 30 I = 2,M+1
         BES(I) = ALPHA*BES(I)
 30   CONTINUE
C
C  THE EVALUATION OF THE ARRAY BES IS NOW COMPLETED.  THE DERIVATIVES
C  OF THE BESSEL FUNCTIONS ARE NOW CALCULATED, USING EQUATION (10.1.20)
C  IN [1].
C
      BESDER(1) = -BES(2)
      DO 40 I = 1,M
         I1 = I+1
         BESDER(I1) = BES(I) - I1*BES(I1)/Z
 40   CONTINUE
      END
```

D.26 Subroutine SPHHNK

SPHHNK calculates values of the spherical Hankel function and its derivative. There are no subprograms referenced.

```
      SUBROUTINE SPHHNK(Z,N,HNK,HNKDER)
      INTEGER N
      COMPLEX Z, HNK(N+1), HNKDER(N+1)
C
C  THIS SUBROUTINE CALCULATES AN APPROXIMATION TO H(I,Z) AND HD(I,Z),
C  FOR I = 0,1,...,N, WHERE H(I,Z) DENOTES THE SPHERICAL BESSEL
C  FUNCTION OF THE THIRD KIND OF ORDER I AND ARGUMENT Z, AS DEFINED
C  IN 10.1.1 OF [1] (H(I,Z) := J(I,Z) + II*Y(I,Z), WHERE J(I,Z) AND
C  Y(I,Z) DENOTE THE SPHERICAL BESSEL FUNCTIONS OF FIRST AND SECOND
C  KINDS RESPECTIVELY, AND II = SQRT(-1)).  HD(I,Z) DENOTES THE FIRST
C  DERIVATIVE OF H(I,Z) WITH RESPECT TO Z.  THE METHOD OF CALCULATION
C  OF H(I,Z) IS FORWARD RECURRENCE, WHICH IS STABLE AT LEAST PROVIDED
C  Z IS NOT TOO FAR FROM THE POSITIVE REAL AXIS.
C
C  ON ENTRY:
C
C  Z       COMPLEX
C          Z SHOULD LIE IN THE HALF-PLANE  RE Z .GE. 0, AND THE ALGORITHM
C          WILL CALCULATE MORE ACCURATELY THE NEARER Z IS TO THE REAL AXIS.
C
C  N       INTEGER
C          N IS THE ORDER OF THE LARGEST ORDER BESSEL FUNCTION WHICH IS TO
C          BE CALCULATED.  N MUST BE A POSITIVE INTEGER.
C
C  Z, N    ARE UNCHANGED ON EXIT.
C
C  ON EXIT:
C
C  HNK     COMPLEX(N+1)
C          HNK(I+1) IS AN APPROXIMATION TO H(I,Z), FOR I = 0,1,...,N.
C
C  HNKDER  COMPLEX(N+1)
C          HNKDER(I+1) IS AN APPROXIMATION TO HD(I,Z), FOR I = 0,1,...,N.
C
C  REFERENCE:
C
C  [1] M ABRAMOWITZ AND I A STEGUN 'HANDBOOK OF MATHEMATICAL FUNCTIONS'
C      NEW YORK: DOVER.
C
C  INTERNAL VARIABLE DECLARATIONS
C
      INTEGER I,I1
C
C  NOW CARRY OUT THE FORWARD RECURRENCE TO CALCULATE HNK.
C
      HNK(1) = (0.0,-1.0)*EXP((0.0,1.0)*Z)/Z
      HNK(2) = HNK(1)*((1.0,0.0)/Z-(0.0,1.0))
      DO 10 I = 2,N
C
C        THE FOLLOWING EQUATION, USED TO CARRY OUT THE FORWARD
C        RECURRENCE, IS A REARRANGEMENT OF EQN. (10.1.19) IN [1].
C
         HNK(I+1) = (I+I-1)*HNK(I)/Z - HNK(I-1)
 10   CONTINUE
C
C  THE EVALUATION OF THE ARRAY HNK IS NOW COMPLETED.  THE DERIVATIVES
C  OF THE BESSEL FUNCTIONS ARE NOW CALCULATED, USING EQUATION (10.1.20)
C  IN [1].
C
```

```
      HNKDER(1) = -HNK(2)
      DO 20 I = 1,N
         I1 = I+1
         HNKDER(I1) = HNK(I) - I1*HNK(I1)/Z
20    CONTINUE
      END
```

D.27 Subroutine ZC

ZC calculates value of characteristic impedance as given by equation (3.60). There are no subprograms referenced.

```
      SUBROUTINE ZC(F,PROPC,CDENS,ZR)
      REAL*4 F
      COMPLEX*8 PROPC,CDENS,ZR
C
C
C ZC CALCULATES A SINGLE VALUE OF CHARACTERISTIC IMPEDANCE.
C
C ON ENTRY
C
C    F       REAL
C            FREQUENCY
C
C    PROPC   COMPLEX
C            COMPLEX PROPAGATION CONSTANT
C
C    CDENS   COMPLEX
C            COMPLEX DENSITY
C
C ON EXIT
C
C    ZR      COMPLEX
C            RELATIVE (I.E. NORMALISED WRT AIR) CHARACTERISTIC IMPEDANCE
C
C THIS VERSION DATED 8TH JANUARY, 1990.
C
C INTERNAL VARIABLES
C
      COMPLEX*8 I
      REAL*4 PI,RHOF,OMEGA,CF
C
      PI=4.0*ATAN(1.0)
      I=CMPLX(0.0,1.0)
      RHOF=1.2
      OMEGA=2.0*PI*F
      CF=343.
      ZR=(CDENS*OMEGA)/(PROPC*RHOF*CF)
      RETURN
      END
```

D.28 Subroutine ZL

ZL calculates value of the surface impedance of a rigid-backed layer as given by equation (4.1), with Z_2 given by equation (3.61). Reference to other subprograms are:

- CCOTH: see section D.1

```
      SUBROUTINE ZL(F,PROPC,CDENS,D,ZR)
      COMPLEX*8 PROPC,CDENS,ZR
      REAL*4 F,D
C
C ZL CALCULATES A SINGLE VALUE OF THE SURFACE IMPEDANCE OF A
C RIGIDLY-BACKED LAYER.
C
C ON ENTRY
C
C    F       REAL
C            FREQUENCY
C
C    PROPC   COMPLEX
C            COMPLEX PROPAGATION CONSTANT
C
C    CDENS   COMPLEX
C            COMPLEX DENSITY
C
C    D       REAL
C            LAYER DEPTH
C
C ON EXIT
C
C    ZL      COMPLEX
C            SURFACE IMPEDANCE
C
C THIS VERSION DATED 5TH DECEMBER, 1989.
C
C SUBROUTINE CCOTH IS CALLED.
C
C INTERNAL VARIABLES
C
      COMPLEX*8 I,IKD,IKD1,ZC,CCOTH
      REAL*4 PI,RHOF,OMEGA,CF
      PI=4.0*ATAN(1.0)
      I=CMPLX(0.0,1.0)
      RHOF=1.2
      OMEGA=2.0*PI*F
      CF=343.0
      ZC=(CDENS*OMEGA)/(PROPC*RHOF*CF)
      IKD=-I*PROPC*D
      IKD1=CCOTH(IKD)
      ZR=IKD1*ZC
      RETURN
      END
```

D.29 Subroutine ZSPHERE

ZSPHERE calculates value of the surface impedance induced by a rigid sphere embedded within a rigid porous medium as given by equation (4.11). Reference to other subprograms are:

- LEGNDR: see section D.19;
- SPHBES: see section D.25;
- SPHHNK: see section D.26.

```
      SUBROUTINE ZSPHERE(K1,K2,R,Z1,Z2,THETA,A,N,RADIUS,Z)
      INTEGER N
      COMPLEX A(N+1),K2,Z2,Z
      REAL K1,THETA,R,RADIUS,Z1
C
C ZSPHERE CALCULATES VALUES OF INDUCED SURFACE IMPEDANCE DUE TO AN EMBEDDED
C SPHERE.
C
C ON ENTRY:
C
C K1     REAL
C        PROPAGATION CONSTANT OF THE UPPER MEDIUM
C        K1 IS UNCHANGED ON EXIT.
C
C K2     COMPLEX
C        PROPAGATION CONSTANT OF THE LOWER MEDIUM
C        K2 IS UNCHANGED ON EXIT.
C
C R      REAL
C        DISTANCE TO THE MEASUREMENT POINT
C        R IS UNCHANGED ON EXIT.
C
C Z1     REAL
C        IMPEDANCE OF THE UPPER MEDIUM
C        Z1 IS UNCHANGED ON EXIT.
C
C Z2     COMPLEX
C        IMPEDANCE OF THE LOWER MEDIUM
C        Z2 IS UNCHANGED ON EXIT.
C
C THETA  REAL
C        ANGLE
C        THETA IS UNCHANGED ON EXIT.
C
C A      COMPLEX
C        COEFFICIENT ARRAY
C        A IS UNCHANGED ON EXIT.
C
C N      INTEGER
C        N IS THE ORDER OF THE LARGEST ORDER.
C        N MUST BE A POSITIVE INTEGER.
C        N IS UNCHANGED ON EXIT.
C
C RADIUS REAL
C        RADIUS OF THE SPHERE
C        RADIUS IS UNCHANGED ON EXIT.
C
C Z      COMPLEX
C        INDUCED RELATIVE SURFACE IMPEDANCE
C        Z IS UNCHANGED ON EXIT.
C
C THIS VERSION DATED 16TH JANUARY, 1989.
C
C CALLS SUBROUTINES LEGNDR, SPHBES, SPHHNK.
C
C INTERNAL VARIABLES
C
      COMPLEX ALPHA,ALPHAINV,DRPDZ,H(1000),HDER(1000),I,IM,J(1000)
      COMPLEX JDER(1000),PRS,RI,RI2INV,RP,RP1M,RP1P,PP,QQ
```

```
      COMPLEX VRSA,VRSB,VRSCX,VRSCM,VRSCZ,VRS,ZK2R
      REAL C,CT,P(1000),PDER(1000),PI,S,ST,ST2
C
      M=10
      PI=4.0*ATAN(1.0)
      CT=COS(THETA)
      ST=SIN(THETA)
      C=COS(PI-THETA)
      S=SIN(PI-THETA)
      I=(0.0,1.0)
      RI=K2/K1
      THETAC=ASIN(ABS(K1/K2))
      RI2INV=1.0/(RI*RI)
      ZK2R=K2*R
      ALPHA=(Z2*K2)/(Z1*K1)
      ALPHAINV=1.0/ALPHA
      RP=(ALPHAINV*C-SQRT(RI2INV-S**2))/(ALPHAINV*C+SQRT(RI2INV-S**2))
      RP1M=1.0-RP
      RP1P=1.0+RP
      QQ=CSQRT(RI2INV-S*S)
      PP=C+ALPHA*QQ
      DRPDZ=-((S+S)*ALPHA*(QQ-(C*C)/QQ)/(PP*PP))*S/R
      CALL LEGNDR(CT,N,P,PDER)
      CALL SPHBES(ZK2R,N,M,J,JDER)
      CALL SPHHNK(ZK2R,N,H,HDER)
      VRSA=P(1)*K2*(JDER(1)+A(1)*HDER(1)*RP1M)
      VRSA=VRSA+P(2)*K2*(3.0*I*JDER(2)+A(2)*HDER(2)*RP1M)
      VRSB=PDER(1)*ST*(J(1)+A(1)*H(1)*RP1M)/R
      VRSB=VRSB+PDER(2)*ST*(3.0*I*J(2)+A(2)*H(2)*RP1M)/R
      VRSCZ=A(1)*P(1)*H(1)+A(2)*P(2)*H(2)
      PRS=P(1)*(J(1)+A(1)*H(1)*RP1P)
      PRS=PRS+P(2)*(3.0*I*J(2)+A(2)*H(2)*RP1P)
      IM=(0.0,1.0)
      DO 010 M = 3,N+1
       IM=CMPLX(-AIMAG(IM),REAL(IM))
       VRSA=VRSA+P(M)*K2*((2*M+1.0)*IM*JDER(M)+A(M)*HDER(M)*RP1M)
       VRSB=VRSB+PDER(M)*ST*((2*M+1)*IM*J(M)+A(M)*H(M)*RP1M)/R
       VRSCZ=VRSCZ+A(M)*P(M)*H(M)
       PRS=PRS+P(M)*((2.0*M+1.0)*IM*J(M)+A(M)*H(M)*RP1P)
010   CONTINUE
      VRSCZ=VRSCZ*DRPDZ
      VRS=-I*(-VRSA*C+VRSB*S+VRSCZ)/(Z2*K2)
      Z=PRS/VRS
      Z=Z/Z1
      END
```

Appendix E

Surface waves at an interface between air and a poroelastic medium

ABSTRACT

Using a modified Biot theory dispersion equations are derived both for a rigid porous half space and for a poroelastic half space. That for the former case has a single solution corresponding to the surface wave excited by a point source over rigid porous ground. Numerical search shows that, for parameter values characteristic of a dry soil, the dispersion equation for the interface between air and air-filled poroelastic half space has three possible solutions corresponding to the rigid porous case, an air-coupled pseudo-Rayleigh mode and a new fast surface mode with a speed slightly less than the bulk P-wave speed. The sensitivities of these three modes to porosity, and elastic parameters are investigated.

1 INTRODUCTION

Considerable effort has been devoted in the literature on the surface wave component that emerges from analysis of the field due to a point source above an absorbing plane [1,2] whose acoustical properties are provided, either by a rigid-framed porous ground model or by empirical relationships. A relatively straightforward deduction of the existence of such a surface wave type solution at a plane interface in air has been restricted to that over a rigid comb-like structure [3]. Most ground surfaces are both porous and elastic. Indeed a simple double layer poroelastic model of the ground structure has been used successfully to account for the magnitude and frequency dependence of acoustic-to-seismic coupling [4]. The possibility of an air-coupled elastic Rayleigh-type wave at the ground surface has been admitted by seismologists for several decades [5-7].

It should be straightforward to show the possibility of both types of surface wave at an air/air-filled poroelastic granular interface corresponding to a soil surface. It is the purpose of this paper to provide such a demonstration where the lower medium is simply a poroelastic half space and where the roots of the appropriate dispersion equation are found by numerical search.

Surface waves on a poroelastic half space have been studied theoretically for many years. A frequent starting point has been Biot's phenomenological theory for wave propagation in a fluid-saturated poroelastic medium [9]. This predicts the existence of two longitudinal wave types and one transverse wave type. All the waves represent inertial and viscous coupled motion of the fluid and solid constituents. An early study was presented by Jones [8]. He examined surface waves in a poroelastic half space in contact with a vacuum by considering the coupled transverse wave and only one of the two possible longitudinal waves. It is well known that in general the slower longitudinal wave is highly attenuated, so a surface wave containing only the transverse wave and the faster longitudinal wave can be regarded as a far field approximation. Under such an approximation Jones showed the existences of Rayleigh type waves on a poroelastic half space.

Later, Tajuddin [10] presented a study of poroelastic Rayleigh waves containing all three types of bulk waves, ie the transverse wave, the slow and fast longitudinal waves. But in his study, he neglected the damping terms in the Biot's equations of motion [6] for poroelastic media. With this assumption, Tajuddin found that only one surface wave type, again a Rayleigh type wave, is possible on a poroelastic half space.

More recently, Feng and Johnson [11] have predicted that three surface modes are possible when the effect of a fluid above a fluid-saturated poroelastic half space is considered. They examined the high frequency case so that the frequency correction function for viscosity is assumed to be a constant. According to Feng and Johnson, the three possible modes may be identified as a true surface mode, a pseudo-Stoneley mode and a pseudo-Rayleigh mode respectively. The true surface mode always has a speed less than that of the slowest bulk wave speed, ie that of the slow longitudinal wave. The speed of the pseudo-Stoneley mode is predicted to be faster than that of the slowest bulk mode but slower than the rest of the bulk modes. The predicted pseudo-Rayleigh mode at a fluid/porous medium boundary has a speed faster than those of the slowest bulk poroelastic mode and the bulk fluid mode, but slower than the bulk shear mode.

A subsequent experimental study by Mayes et al [12] of waves at a water/water-saturated glass beads interface at ultrasonic frequencies (of the order of MHz) has validated the prediction of these three surface modes. However, they find that the fastest surface wave mode, corresponding to the mode identified as a pseudo-Rayleigh mode by Feng and Johnson [11] consistently has a higher speed than that of the bulk shear mode.

Through a study of the incidence of a spherical surface wave on a poroelastic half space, Attenborough et al [12] predicted that in the light fluid limit, such that the density and stiffness of the entrained fluid are considerably less than those of the sound, there are two surface modes. One corresponds to Rayleigh waves in an equivalent elastic medium. The other corresponds to the surface wave predicted above a rigid porous half space.

In this paper, we shall begin with a brief derivation of the dispersion equation for the surface waves at an interface between air and a semi-infinite rigid porous medium. This is followed by a similar derivation for a poroelastic half space. Modified Biot's equations of motion are used for the latter problem and we shall not confine our considerations to either the low or high frequency case where the frequency correction function is a constant. An explicit expression of the dispersion equation is presented. This expression and its high frequency limit can be found in [11] and [12] respectively in implicit forms. Finally, some numerical results are given appropriate to parameters typical of a dry soil. Three surface modes are predicted. In addition to the expected two modes described by Attenborough et al [12], a third surface mode with a speed which is slightly slower than that of the fast longitudinal wave is predicted. For an air/dry soil boundary the slowest surface mode is a true surface mode defined according to [10]. The speeds of the surface modes are predicted to be almost independent of frequency while the attenuations along the propagation direction are predicted to increase with the increasing frequency, the attenuation of the slowest surface wave being the highest.

2 THEORY

For the modified Biot's theory [14], the properties of a poroelastic medium are specified by ten parameters. These are the bulk modulus of individual grains K_r, the bulk modulus of the fluid filling the pores, which we assume to be air, K_f^*, the shear modulus G_b, the bulk modulus of the assemblage of particles K_b, the average bulk density ρ, the fluid density ρ_f, the porosity Ω, the flow resistivity σ, the tortuosity q and the pore shape factor ratio S_p.

A rectangular coordinate system is used. The origin is set on the interface between the two media. The positive z-axis points upwards into the air. We assume that the wave propagates in the positive x-direction.

2.1 Surface Waves on Rigid Porous Half Space

In air, the equation of motion is given by

$$\nabla^2\phi_1 = \frac{1}{C_1^2}\frac{\partial^2\phi_1}{\partial t^2} \qquad (1)$$

where $C_1 = \sqrt{K_f/\rho_1}$ and ϕ_1 is a potential function of displacement field in air such that the displacement is given by

$$\bar{u}_1 = \nabla\phi_1 \qquad (2).$$

In a rigid porous medium, when the time harmonic motion ($\exp(-i\omega t)$) is assumed, the equations of motion may be written [14]

$$\nabla^2\phi_2 = \frac{1}{C_2^2}\frac{\partial^2\phi_2}{\partial t^2} \qquad (3)$$

where ϕ_2 is a potential function of displacement field and

C_2	$= \sqrt{K_f^*/\rho_c}$
ρ_c	$= q^2\rho_f/[\Omega(1 - 2T(\lambda)/\lambda)]$
λ	$= (2q^2\omega\rho_f i/\Omega\sigma)^{1/2}/S_p$
$T(\lambda)$	$= J_1(\lambda)/J_0(\lambda)$
K_f^*	$= K_f/[1 + 2(\gamma - 1)T(\lambda\sqrt{iN_{pr}})/(\lambda\sqrt{iN_{pr}})]$
K_f	= the adiabatic bulk modulus for air
γ	= the ratio of specific heats for air
N_{pr}	= the Prandtl Number for air
ω	= angular frequency.

The displacement vector of fluid particles in the rigid porous solid, in terms of the potential functions, is given by

$$\bar{u}_2 = \nabla\phi_2 \qquad (4)$$

In Air, the expression of pressure in terms of the potential function is given by

$$P_1 = -K_f \nabla^2 \phi_1 \qquad (5)$$

The pressure in the pores is given by

$$P_2 = -K_f^* \nabla^2 \phi_2 \qquad (6)$$

On the interface between the air and the porous medium pressure continuity requires

$$P_1 = P_2 \qquad (7).$$

Continuity of the z-component displacement requires

$$u_{1z} = u_{2z} \qquad (8).$$

We seek a general solution of the equations of motion in air of the form

$$\phi_1 = Ae^{-kq_1 z}\, e^{(ikx - i\omega t)} \qquad (9)$$

where A is arbitrary constant independent of time and position, $q_1 = \sqrt{1 - (V/C_1)^2}$, the complex phase velocity $V = \omega/k$ and k is the complex wavenumber.

In the rigid porous half space, the potential function of the wave field may be written

$$\phi_2 = Be^{kq_2 z}\, e^{ikx - i\omega t} \qquad (10)$$

where B is constant and

$$q_2 = \sqrt{1 - (V/C_2^2)}$$

After substituting the general solutions into the boundary conditions and using the constitutive equations, we can obtain a system of two homogeneous equations in unknowns A and B. The

condition for existence of non-trivial solution requires that the coefficient determinant is zero which gives the relationship between the frequency and the complex wavenumber

$$q_1\rho_c + q_2\rho_1 = 0 \qquad (11)$$

Eq (11) represents the dispersion equation for surface waves at a boundary between air and a rigid porous half space.

For the parameters values (in MKS units)

$K_f = 1.4 \times 10^5$	$\rho_a = 1.2$	$\gamma = 1.4$
$\rho_f = 1.2$	$\Omega = 0.4$	$N_{pr} = 0.7$
$\sigma = 3 \times 10^5$	$S_p = 0.5$	
$q = \sqrt{2.5}$	$\omega = 2\pi 500,$	

the surface wave speed (m/s) is given by

$$V_{surf} = \omega/\mathrm{Re}(k)$$

and the corresponding attenuation constant (nepers/m) is given by Im(k) The frequency dependence of these quantities is shown in Figure 1.

We note that below 400 Hz the surface wave speed for the above parameter values somewhat higher than the sound speed in air which is

$$C_a = 341.57$$

2.2 Surface Waves on a Poroelastic Half Space

In a poroelastic medium, when the time harmonic motion ($\exp(-i\omega t)$) is assumed and there is no displacement in the y direction, the equations of motion may be written

$$\nabla^2(H\phi_3 + \alpha M\phi_2) = \frac{\partial^2}{\partial t^2}(\rho\phi_3 + \rho_f\phi_2)$$

$$\nabla_2(\alpha M\phi_3 + M\phi_2) = \frac{\partial^2}{\partial t^2}(\rho_f \phi_3 + \rho_c \phi_2) \tag{12}$$

$$\nabla_2\phi_4 = \frac{1}{C_4{}^2}\frac{\partial^2\phi_4}{\partial t^2}$$

where ϕ_2, ϕ_3, ϕ_4 are potential functions of displacement field and

$$H = (K_r - K_b)^2/(D - K_b) + K_b + 4G_b/3$$
$$\alpha M = K_r(K_r - K_b)/(D - K_b)$$
$$M = K_r{}^2/(D - K_b)$$
$$D = K_r(1 + \Omega(K_r/K_f - 1))$$
$$C_4 = (G_b/(\rho - \rho_f{}^2/\rho_c))^{\frac{1}{2}}$$

The displacement vector for particles in solid, in terms of the potential functions, is given by

$$\bar{u}_s = \nabla\phi_3 + \nabla x\bar{X}_3 \tag{13}$$

and $\bar{X}_3 = \phi_4\hat{y}$. The relative displacement of fluid and solid is defined as

$$\bar{W} = \Omega(\bar{u}_s - \bar{U}_f) \tag{14}$$

In terms of the potential functions, $\bar{W}$ can be written as

$$\bar{W} = \nabla\phi_2 + \nabla x\bar{X}_2 \tag{15}$$

where $\bar{X} = -\frac{\rho_f}{\rho_c}\bar{X}_3$.

In terms of the potential function the pressure in air is given by equation (5). Stresses in the poroelastic half space are obtained in

terms of displacements from the constitutive equations. The constitutive equations are given by [13]

$$t_{ii} = He - \alpha M\zeta - 2G_b(e_{jj} + e_{kk})$$

$$t_{ij} = G_b e_{ij} \qquad (16)$$

$$P_f = M\zeta - \alpha Me$$

where t_{ij} are total stresses, P_f is pressure in the pores, and e_{ij} are strain components, given by

$e = \nabla \bar{u}_s$ and $\zeta = \nabla \bar{W}$.

On the interface between the air and the poroelastic medium as with the rigid porous case, the pressures in the air and in the pores are equal (equation (7)). This is equivalent to the open pore condition used by Feng and Johnson [11].

The total stress in the z-direction is equal to the pressure of air.

$$t_{zz} = P_1 \qquad (17)$$

The shear stress t_{zr} vanishes since air cannot sustain shear stress. Hence

$$t_{zx} = 0 \qquad (18)$$

The condition of the z-component displacement continuity requires [7]

$$u_{z1} = u_{z2} - W_{z2} \qquad (19).$$

We seek a general solution of the equations of motion in air in the form given by equation (9).

In the half space, the potential functions of wave field are written as

$$\phi_2 = (A_2 e^{kq_+ z} + A_3 Q_- e^{kq_- z}) e^{(ikx - i\omega t)}$$

$$\phi_3 = (A_3 e^{kq_- z} + A_2 Q_+ e^{kq_+ z}) e^{(ikx - i\omega t)} \qquad (20)$$

$$\phi_4 = iA_4 e^{kq_4 z}\, e^{(ikx - i\omega t)}$$

where A_2, A_3, A_4 are constants and

$$q_+ = \sqrt{1 - (V/V_+)^2}$$
$$q_- = \sqrt{1 - (V/V_-)^2}$$
$$q_4 = \sqrt{1-(V/C_4)^2}$$
$$\frac{V_\pm}{V_-} = [2A/(-B \pm \sqrt{(B^2 - 4AC)})] \qquad (21)$$
$$A = (\alpha M)^2 - HM$$
$$B = P\rho_c + M\rho_s - 2\alpha M \rho_f$$
$$C = \rho_f^2 - \rho\rho_c$$
$$Q_+ = (\alpha M/V_+^2 - \rho_f)/(\rho - H/V_+^2)$$
$$Q_- = (H/V_-^2 - \rho)/(\rho_f - \alpha M/V_-^2)$$

In the present problem, the wavenumber is always complex valued, so a surface speed is given by $V_{surf} = \omega/\mathrm{Re}(k)$ rather than the real part of the complex phase velocity V. The condition for exponential decay in the direction of the negative z axis requires that $\mathrm{Re}(kq_j) > 0$. For attenuation in the positive x direction, we require also that Im(k) must be greater than zero. These are different conditions to those imposed by Feng and Johnson [11] who require only that $\mathrm{Re}(kq_j) \geq \mathrm{Im}(kq_i)$.

After substituting the general solutions into the boundary conditions by means of the constitutive equations, we obtain a system of 4 homogeneous equations in unknowns A_1, A_2, A_3 and A_4. The condition for existence of non-trivial solution requires that he coefficient determinant is zero which gives the relationship between the frequency and the complex wavenumber as follows:

$$\begin{vmatrix} q_1 & q_+(Q_+ - 1) & q_-(1 - Q_-) & (R + 1) \\ K_f\left(\frac{V}{C_a}\right)^2/G & ((HQ_+ - \alpha M)\left(\frac{V}{V_+}\right)^2 - 2GQ_+)/G & ((H - \alpha M_-)\left(\frac{V}{V_-}\right)^2 - 2G)/G & 2q_4 \\ 0 & -2q_+Q_+ & -2q_- & (1 + q_4^2) \\ K_f\left(\frac{V}{C_a}\right)^2/G & \left(\frac{V}{V_+}\right)^2(M - Q_+\alpha M)/G & \left(\frac{V}{V_-}\right)^2(MQ_- - \alpha M)/G & 0 \end{vmatrix} = 0 \quad (22)$$

where $R = \rho_f/\rho_c$. Eq (22) represents the dispersion equation for interface waves between air and a poroelastic half space.

For given material constants, we can solve the dispersion equation (22) numerically. As Eq (22) is a complex equation, the equating of the real part and the imaginary part of the equation to zero respectively gives two simultaneous equations. We fix ω and solve the simultaneous equations to obtain the corresponding values of Re(k) and Im(k).

The parameter values chosen correspond to an acoustically-hard (high flow resistivity, high p-wave speed) soil or sand [4,14]. In mks units the values for the poroelastic half space may be written as follows:-

$K_r = 3 \times 10^{10}$ $\quad K_b = 8 \times 10^8$
$G_b = K_b$ $\quad \rho = 1 \times 10^3$

and other parameter values are as stated previously for the rigid porous half space example.

We consider the frequency range from 100 Hz to 500 Hz.

For the parameters we have chosen, the bulk speeds are given by

$C_+ = \omega/\mathrm{Re}(k_+) = 1366$ ----- *Fast longitudinal speed*
$C_s = \omega/\mathrm{Re}(k_4) = 894$ ----- *Transverse speed*

$C_a = 341$ ----- *Sound speed in air*
$C_- = \omega/\mathrm{Re}(k_-) = 38\text{-}81$ ----- *Slow longitudinal speed*

Over the whole frequency range, three surface modes can be found (Figure 2). One mode which may be called a pseudo-Rayleigh mode has a speed just slower than the transverse bulk wave speed and is very close to the Rayleigh wave speed predicted for the poroelastic solid. The other mode has a speed approximately equal to the sound speed of air and may be called a pseudo-Stoneley mode. Although it is numerically similar to the surface wave predicted on a rigid porous surface, there are significant differences in the predicted frequency dependences of the phase speed sand attenuation constants.The third surface wave mode has a speed just smaller than that of the fast bulk mode. It is similar to the fastest mode found experimentally by Mayes et al [12]. Strictly, since the speed is greater than that of the bulk shear wave, the fast surface mode may not be called a pseudo-Rayleigh wave. The three speeds are predicted to be almost independent of the frequency, and the attenuation of the fast surface mode is negligible. However the attenuations of the other two surface modes change from the order of 10^{-4} to 10^{-2} nepers
m^{-1} over the frequency range 100-500 Hz.

For this half space model and for these parameters, it is not possible to find a 'true' surface mode with a speed slower than any of the body wave speeds.

We investigate also the sensitivity of the results to change in material constants. Change in the pore shape factor has negligible effect on the surface modes. But the attenuation of the pseudo-Stoneley mode is dependent on porosity (and flow resistivity). High porosity results in rapid attenuation and a strong dependence on frequency. Change in G_b effects the pseudo-Rayleigh mode but has little influence on the pseudo-Stoneley mode. The results are shown in Figures (3) to (5).

4 CONCLUDING REMARKS

A slow surface wave mode has been predicted on both a rigid porous and a poroelastic half space using parameter values typical of an acoustically hard soil. Even with such a relatively stiff solid frame, its elasticity is predicted to have a significant effect on this surface mode. It should be noted that since the rigid porous boundary model predicts an impedance such that the resistance exceeds the reactance at all frequencies, this slow mode would not be excited by a point source [1,2]. Further research is required to confirm whether the corresponding wave would be excited by a point source over a poroelastic half space as predicted elsewhere after various approximations [13].

The main result of this paper is the prediction of the possibility of two additional types of surface wave at such an air/air-filled poroelastic half space. As explained in the introduction, this is not the first such prediction for a fluid/poroelastic interface, but the results for the parameter range considered here have potentially a wide significance for studies of outdoor sound propagation. Two of the surface modes are well known as the surface wave over a rigid porous half space and as the air-coupled Rayleigh wave respectively. Particularly interesting is the prediction of a fast surface mode with a speed slightly less than that of the highest speed bulk mode. This represents a surface wave possibility that has not been suspected before.

The predicted high attenuation of the pseudo-Stoneley mode makes its existence difficult to verify experimentally. The fast surface mode, if excited significantly, is predicted to travel with little attenuation, but will lose energy by radiating into the air. Further work is required to determine the extent to which it may be excited by an airborne source. On the other hand the experimental evidence for the existence of an air-coupled pseudo-Rayleigh wave is overwhelming, albeit for rather more complicated ground structures than a half-space.

5 ACKNOWLEDGEMENTS

This work was supported in part by the European Research Office of the US Army. The second author would like also to express gratitude to Prof K Fidler for support through Open University Research Funds.

REFERENCES

1 K Attenborough, S I Hayek and J M Lawther, 'Propagation of sound above a porous half-space', J Acoust Soc Am 68 1493-1501 (1980).

2 R Raspet and G E Baird, 'The acoustic surface wave above a complex impedance ground surface', manuscript submitted to J Acoust Soc Am (1988).

3 L M Brekhovskikh, 'Surface waves in acoustics', Soviet-Physics-Acoustics 5, 3-12 (1959).

4 J M Sabatier, H E Bass, L N Bolen and K Attenborough, 'Acoustically-induced seismic waves', J Acoust Soc Am 80 (2) 646-649 (1986).

5 F Press and M Ewing, 'Ground roll coupling to atmospheric compressional waves', Geophysics 16 416-430 (1951).

6 W S Jardetzky and F Press, 'Rayleigh wave coupling to atmospheric compressional waves', Bull Seis Soc Am 42 135-144 (1952).

7 F Press and M Ewing, 'Theory of air-coupled flexural waves', J Appl Phys 22 892-899 (1951 b).

8 J P Jones, 'Rayleigh waves in a porous elastic saturated solid', J Acoust Soc Am 33, 959-962 (1961); Appl Mech Rev 15 1381 (1962).

9 M A Biot, 'Mechanics of deformation and acoustic propagation in porous media', J Appl Phys 33, 1482-1498 (1962).

10 M Tajuddin, 'Rayleigh waves in a poroelastic half-space', J Acoust Soc Am 75 (3) 682-684 (1984).

11 S Feng and D L Johnson. 'High-frequency acoustic properties of a fluid/porous solid interface I New surface mode', J Acoust Soc Am 74 (3) 906-914 (1983).

12 M J Mayes, P B Nagy, L Adler, B P Bonner and R Streit, 'Excitation of surface waves of different modes at fluid-porous solid interface', J Acoust Soc Am 79 (2) 249-252 (1986).

13 K Attenborough, N W Heap, T L Richards and V V S S Sastry, 'Acoustic-to-seismic coupling over porous ground surfaces', Final Tech Report on Contract DAJA 37-81-C-0210 (1984).

14 K Attenborough, 'On the acoustic slow wave in air-filled granular media', J Acoust Soc Am 81 (1) 93-102 (1987).

15 J M Sabatier, H E Bass, L N Bolen, K Attenborough and V V S S Sastry, 'The interaction of airborne sound with the porous ground: The theoretical formulation', J Acoust Soc Am 79 (5) 1345-1352 (1986).

LIST OF FIGURES AND CAPTIONS

Figure 1 (a) phase speed and (b) attenuation constant of the surface wave mode at the interface of air and an air-filled rigid porous half space for the parameter values given in the text.

Figure 2 (a) phase speeds and (b) attenuation constant as a function of frequency for the three interface waves predicted at an air/air-filled poroelastic half space boundary given the parameter values stated in the text.

Figure 3 Sensitivity of slow surface wave mode to porosity (a) phase speed, (b) attenuation constant. Parameters are as given in the text except for the porosity values which are indicated on the figure.

Figure 4 Sensitivity of the attenuation constant of the pseudo-Rayleigh mode to bulk rigidity modulus. Parameters are as given in the text except for rigidity moduli indicated on the Figure. The phase speed is approximately constant at 1269 m s^{-1} over the given frequency range for $G_b = 2 \times 10^9$ mks units.

Figure 5 Sensitivity of the attenuation constant of the fast surface mode to rigidity modulus. Parameters are as given in the text except for those indicated on the Figure. The phase speed is approximately constant at 2160 m s^{-1} for $G_b = 2 \times 10^9$ mks units.

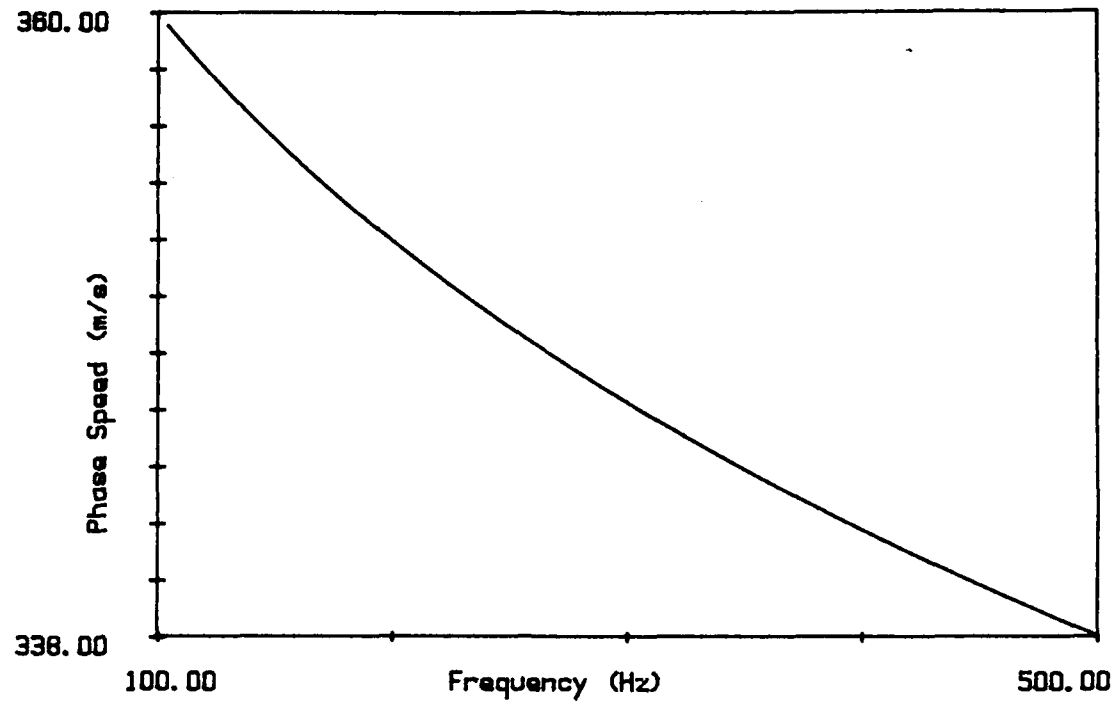
360.00
338.00
Phase Speed (m/s)
100.00
Frequency (Hz)
500.00

(a)

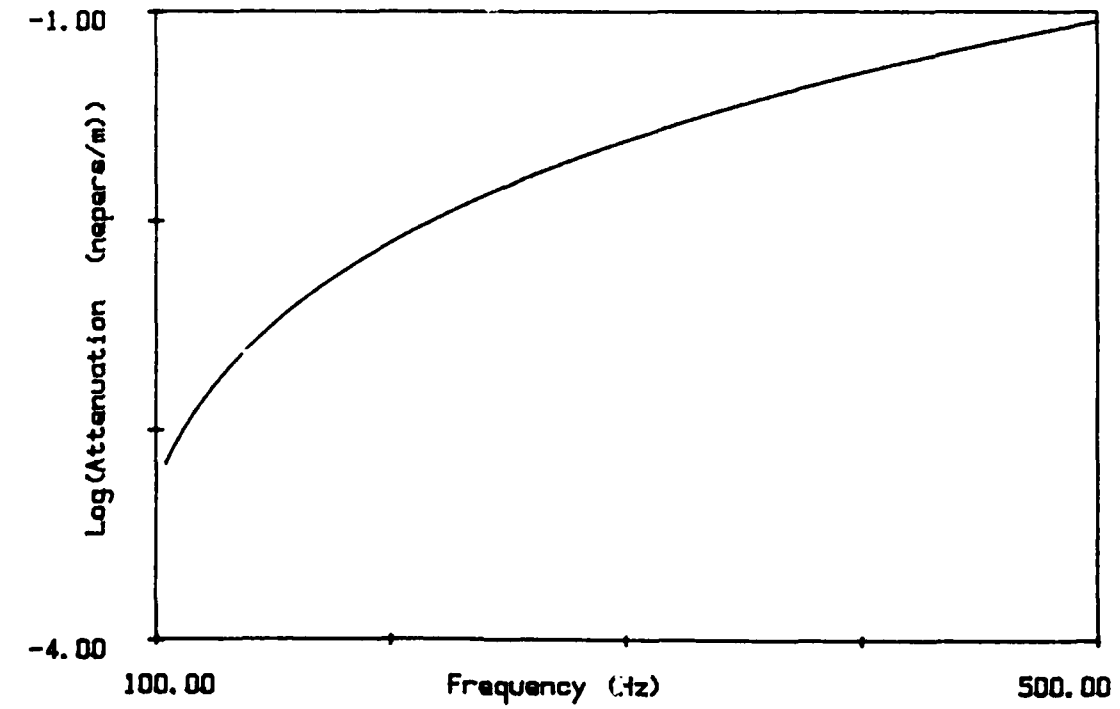
-1.00
-4.00
Log(Attenuation (nepers/m))
100.00
Frequency (Hz)
500.00

Figure 1 (b)

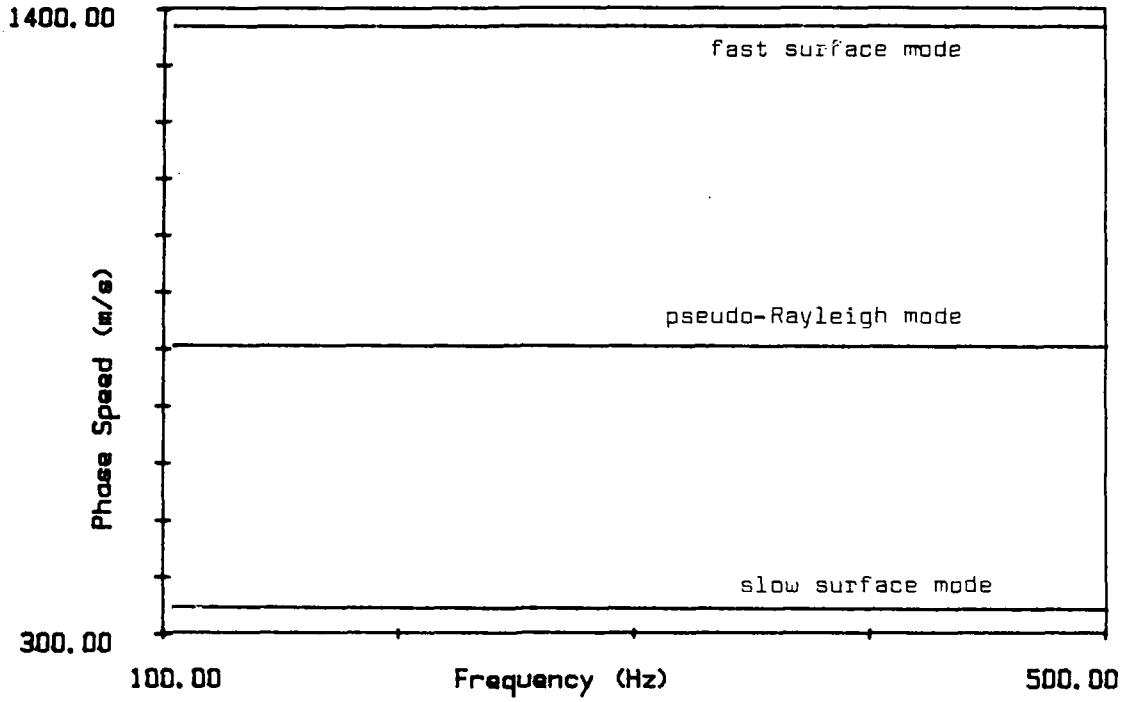
1400.00
fast surface mode
pseudo-Rayleigh mode
Phase Speed (m/s)
slow surface mode
300.00
100.00
Frequency (Hz)
500.00

Figure 2 (a)

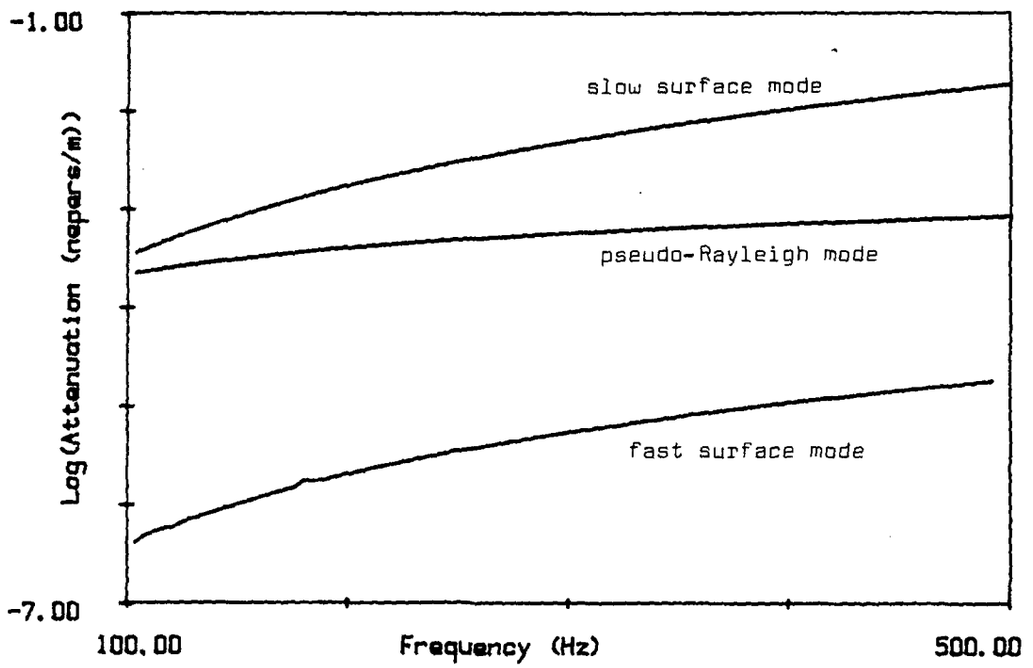
-1.00
-7.00
Log(Attenuation (nepers/m))
slow surface mode
pseudo-Rayleigh mode
fast surface mode
100.00
Frequency (Hz)
500.00

Figure 2 (b)

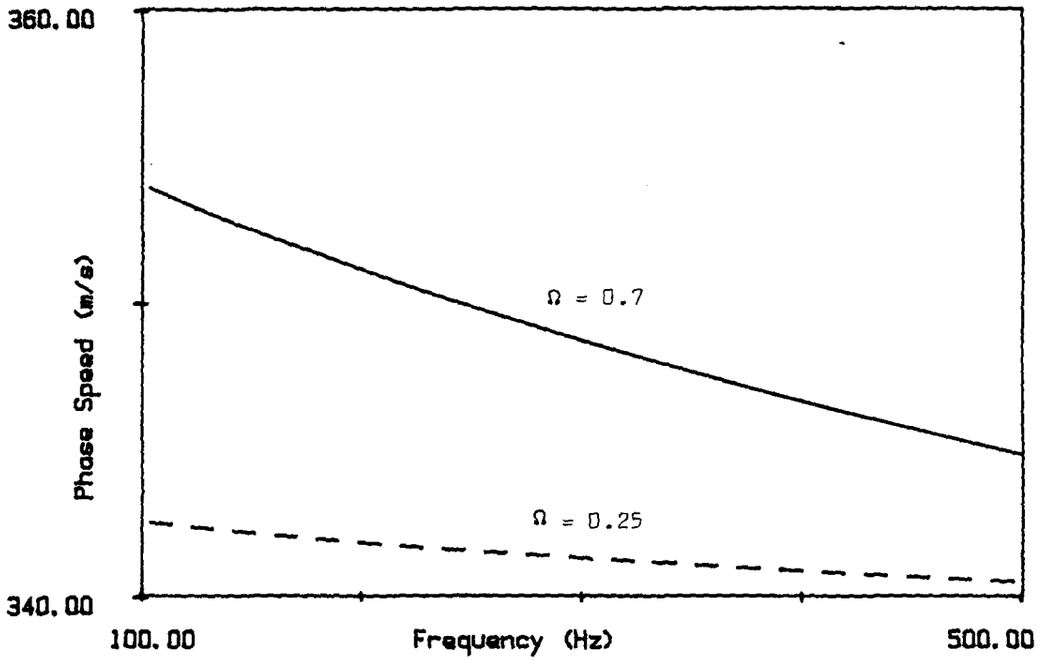
360.00
340.00
Phase Speed (m/s)
Ω = 0.7
Ω = 0.25
100.00
Frequency (Hz)
500.00

(a)

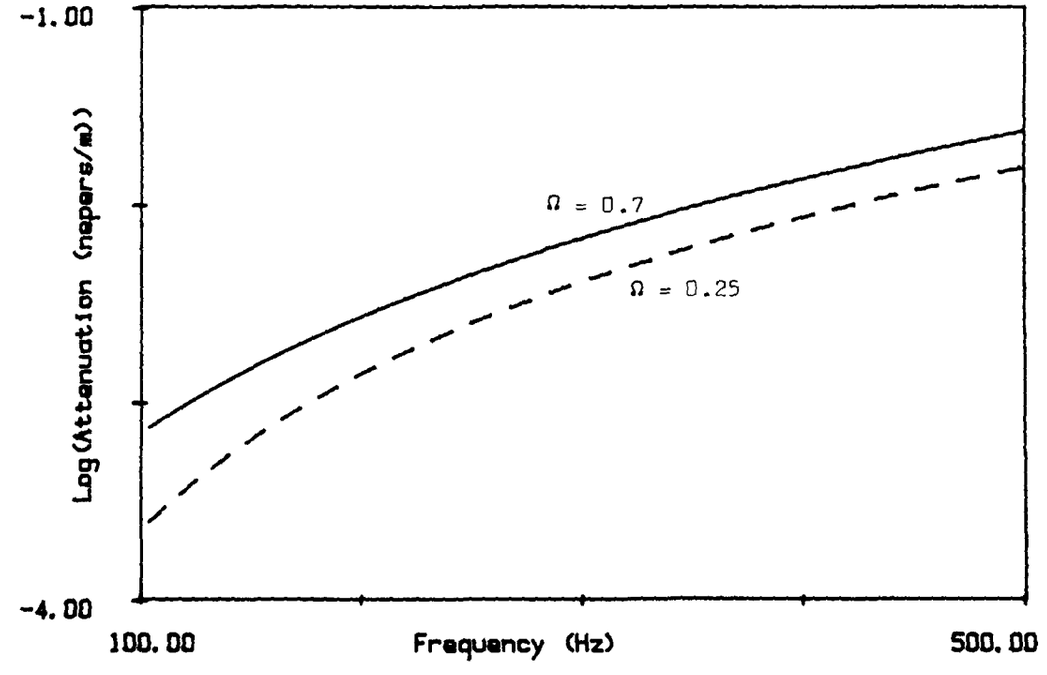
-1.00
-4.00
Log(Attenuation (nepers/m))
Ω = 0.7
Ω = 0.25
100.00
Frequency (Hz)
500.00

Figure 3 (b)

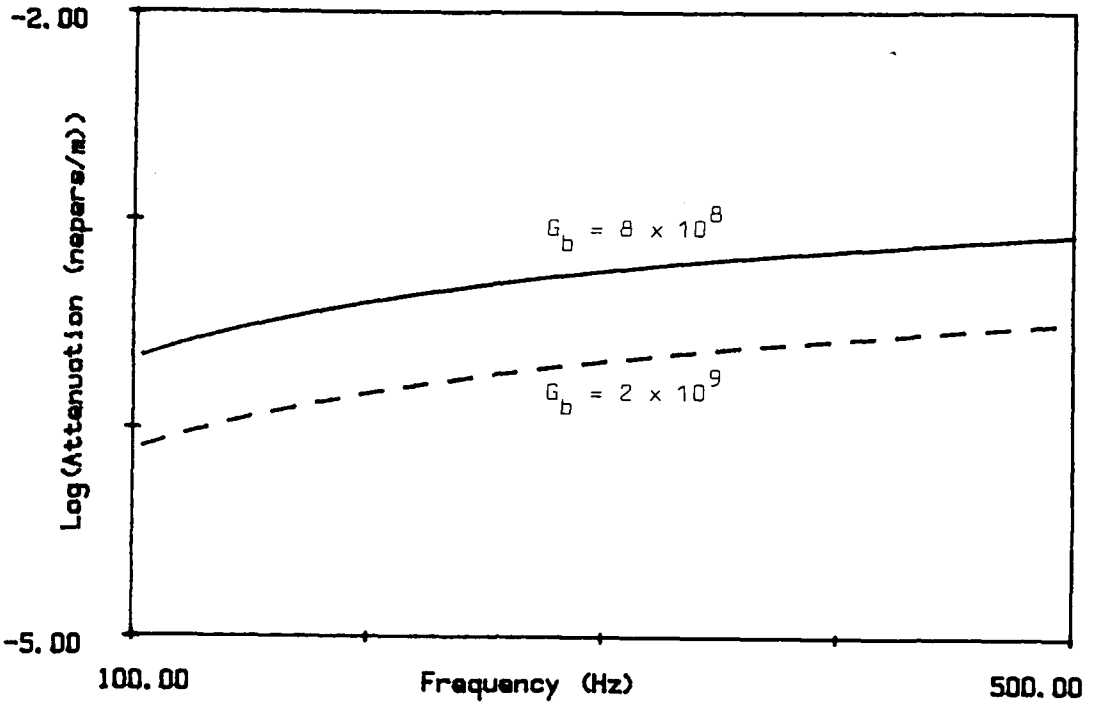
-2.00
-5.00
Log(Attenuation (nepers/m))
$G_b = 8 \times 10^8$
$G_b = 2 \times 10^9$
100.00
Frequency (Hz)
500.00

Figure 4

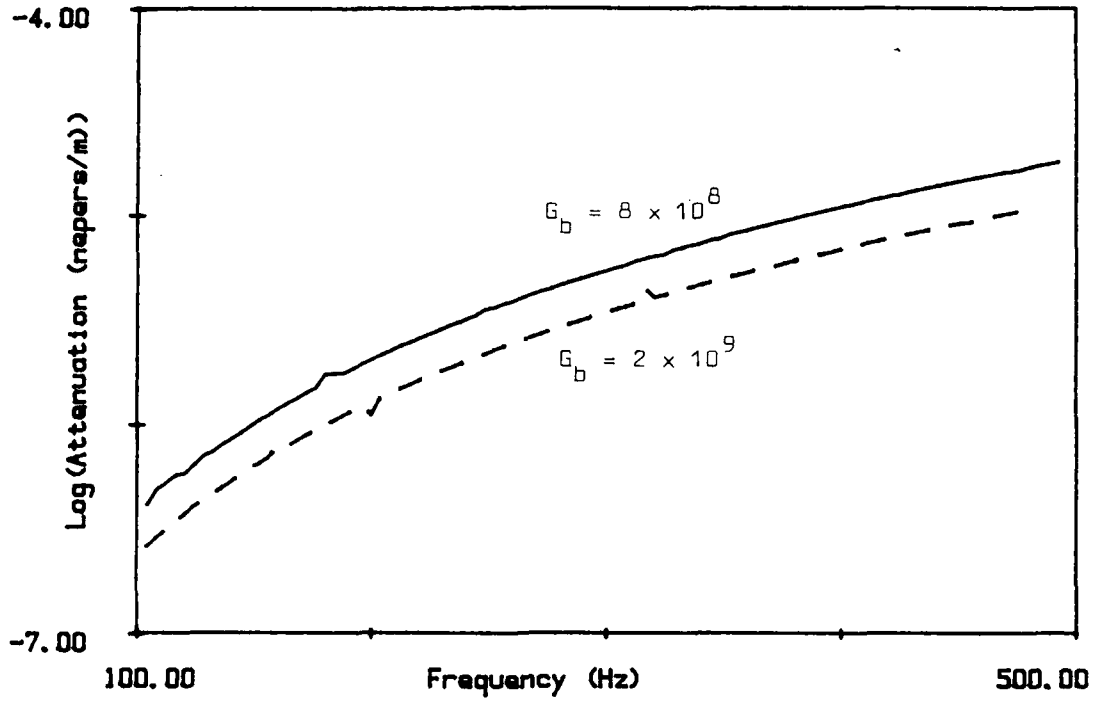
-4.00
-7.00
Log(Attenuation (nepers/m))
$G_b = 8 \times 10^8$
$G_b = 2 \times 10^9$
100.00
Frequency (Hz)
500.00

Figure 5